AN ABSTRACT OF THE THESIS OF

Thamir Rauf Al-Alusi for the degree of Doctor of Philosophy in Mechanical Engineering Presented on October 3, 1989.

Tiltle: An Experimental Study of Natural Convection Heat Transfer From a Horizontal Cylinder Array Vertically Aligned to and Confined by a Single Wall and Two Walls

Abstract approved:

Redacted for privacy

Dwight J. Bushnell

Convection heat transfer was experimentally investigated for two different geometries. One case had three horizontal cylinders in a vertical plane placed between two vertical walls. The second case had three horizontal cylinders in a vertical plane with only one vertical wall. Several different cylinder center-to-center spacings were investigated. The wall spacings for the two wall and single wall cases were also varied.

The cylinders were placed in a still air medium at atmospheric pressure and were maintained at a constant heat flux. The modified Rayleigh number, based on the diameter of the cylinders, ranged from 6.2×10^4 to 1.2×10^6. A scale analysis was performed to predict the relationship between the Nusselt number and the modified Rayleigh number. A standard finite-difference code was employed to show the temperature

distribution and velocity vectors distribution around the cylinders.

The results showed that there was a maximum heat transfer from each cylinder at a specific wall-array spacing and a specific center-to-center spacing. Comparisons of heat transfer results with a single free cylinder and a free array of horizontal cylinders were made and discussed. Empirical equations were proposed to predict the effects of the experimental parameters on the heat transfer as expressed by the average Nusselt number of each cylinder or the average Nusselt number of the whole array.

Flow visualization was accomplished using laser sheets. The resulting studies showed that the presence of a single wall or the asymmetrical placement of the array between the two walls eliminated the presence of the vortices in the spaces between the cylinders and displaced the stagnation points. The asymmetrical placement of the array between two walls created a reversed current between the two walls.

An Experimental Study of Natural Convection Heat Transfer From a Horizontal Cylinder Array Vertically Aligned to and Confined by a Single Wall and Two Walls

by

Thamir R. Al-Alusi

A THESIS

submitted to

Oregon State University

in partial fulfillment of
the requirements for the
degree of

Doctor of Philosophy

Completed October 3, 1989

Commencement June 1990

APPROVED:

Redacted for privacy

Professor of Mechanical Engineering in charge of major

Redacted for privacy

Head of Department of Mechanical Engineering

Redacted for privacy

Dean of Graduate School

Date thesis is presented October 3, 1989.

Typed by Cathryn Westbrook for Thamir R. Al-Alusi .

ACKNOWLEDGEMENTS

I wish to thank my major advisor, Professor Dwight Bushnell, for his guidance and encouragement throughout my graduate studies. His patience and support over the past five years have been greatly appreciated. I would also like to express my appreciation to each member of my committee, Professor Jonathan Istok, Professor Milton Larson, Professor Alan Robinson, and Professor Charles Smith, for their time and assistance.

I would like to thank Dr. Donald Trent, visiting faculty from Battelle Laboratories, for his guidance and input in the use of Tempest, a computer software program which he co-authored.

Finally, I would like to thank the members of my family for their unflagging moral support and encouragement. First, I wish to thank my father, Rauf Al-Alusi, for making it possible for me to pursue my graduate studies. Secondly, I wish to thank my aunts, Sabriah and Fatima Al-Alusi, and my brothers and sisters, for their ongoing support over the past several years. And last, my love and appreciation to my wife, Cathryn Westbrook, for her time and assistance throughout the preparation of my thesis.

TABLE OF CONTENTS

LIST OF FIGURES

LIST OF TABLES

LIST OF APPENDIX FIGURES

LIST OF APPENDIX TABLES

NOMENCLATURE

A	= Surface area of the cylinder , =(Π D L), m^2 .
A_c	= End cap cross section area, m^2
CC	= Cylinder center-to-center spacing, m.
C_p	= Specific heat, W Hr/(Kg K).
D	= Cylinder diameter, m.
e	= Emissivity.
Gr^*	= Modified Grashof number, equation 3.3 .
g	= Acceleration of gravity, m/s^2 .
h	= Average heat transfer coefficient, W/m^2 K.
I	= Electrical current, amp.
K	= Thermal conductivity, W/m K.
L	= Cylinder length.
Nu	= Average Nusselt number of the cylinder,=((h D)/K)
Nu_{av}	= Average Nusselt number of the whole array for single wall cases, equation 4.4 .
$Nu_{av/f}$	= Nusselt number ratio for single wall cases, equation 4.5 .
$Nu_{av,RW}$	= Average Nusselt number of the whole array for two walls cases, equation 5.2 .
$Nu_{av,RW/f}$	= Nusselt number ratio for two walls cases, equation 5.3 .
$Nu_{av/s}$	= Nusselt number ratio for single wall cases, equation 4.6.

Nu_i = Average Nusselt number for cylinder #i .

$Nu_{i,f}$ = Average Nusselt number for cylinder #i in a free array .

$Nu_{i,Rw}$ = Average Nusselt number for cylinder #i for two walls cases.

Nu_s = Average Nusselt number for a free single cylinder.

p = Pressure, N/m^2 .

P = Electrical power, W.

Pr = Prandtl number.

Q = Total power input, W.

Q_{cv} = Heat flux by convection, W.

Q_{cd} = Heat flux by conduction, W.

Q_r = Heat flux by radiation, W.

q = Heat flux per unit area, W/m^2 .

R = Electrical resistance, ohm .

Ra^* = Modified Rayleigh number, equation 3.4 .

Ra_i^* = Modified Rayleigh number for cylinder #i for single wall cases.

$Ra_{i,f}^*$ = Modified Rayleigh number for cylinder #i for free array cases.

$Ra_{i,RW}^*$ = Modified Rayleigh number for cylinder #i for two walls cases.

$R1$ = One ohm electrical resistance.

S = Spacing between the array and the wall, m .

Sb = Stefan-Boltzmann constant = 5.6696×10^{-8} $w/m^2.K^4$

S/D = Array to left wall spacing for single wall cases.

$(S/D)_R$ = Array to right wall spacing for two walls caces.

T = Temperature, ^oC .

T_w = Surface temperature of the cylinder, ^oC.

$T_{w,i}$ = Surface temperature of cylinder #i , ^oC.

T_{inf} = Ambient temperature, ^oC.

U = Fluid velocity in Y-direction, m/s.

V = Voltage, Volt.

v = Fluid velocity in Y- direction, m/s.

X = X- coordinate, m.

Y = Y- Coordinate, m.

Y_i = Distance from the center of the lowest cylinder to the center of cylinder #i .

α = Themal diffusivity, m^2/Hr .

β = Coefficient of thermal expansion, K^{-1}.

δ_T = Thermal boundary layer thickness, m.

μ = Dynamic viscosity, Kg/m Hr.

υ = Kinematic viscosity, m^2/Hr.

ρ = Density, Kg/ m^3.

θ = Angular location measured from 6 o'clock position, radians.

ϕ = Normalized temperature, equation 4.3.

An Experimental Study of Natural Convection Heat Transfer From a Horizontal Cylinder Array Vertically Aligned to and Confined by a Single Wall or Two Walls

CHAPTER 1

INTRODUCTION AND THEORETICAL ANALYSIS

1.1 Introduction

Natural convection processes occur both in natural and technological applications when the fluid flow is driven by buoyancy forces resulting from inhomogeneities in fluid density. These gravitational forces arise when a body is placed in an otherwise motionless medium having a higher or a lower temperature than that of the body.

Establishment of heat transfer by natural convection takes place in three stages [1, 2]. During these stages, the temperature and velocity changes are assumed to be confined to a small boundary layer next to the body's surface. In the first stage, the heat is transferred by pure conduction from the body to the adjacent fluid particles. During the second stage, the heat is transferred by a combination of pure conduction and convection. Finally, in the third stage, the velocity and temperature profiles are independent of time and the steady convection flow is fully established. Parsons and Arey [2, 3] show Mach-Zehnder

photographs of these stages for natural convection heat transfer for a single horizontal wire and for two horizontal wires vertically aligned.

Although natural convection has a lower heat transfer coefficient than forced convection, heat transfer engineering designers prefer the natural convection mode because it is more reliable due to the elimination of the cooling/heating fluid circulation parts [4]. The convection heat transfer coefficient is a function of the fluid flow, the thermal properties of the fluid medium, and the geometry of the system. Many industrial heat components have horizontal cylinders stacked vertically near a wall or positioned asymmetrically between two walls. These components are found in electronic equipment (i.e., computers and power supply equipment), heat exchangers, nuclear power equipment, and power transmission cables which are aligned next to a wall.

When horizontal cylinders are stacked vertically near a wall, the heat transfer from the lower cylinder behaves much like free natural convection from a single cylinder. Due to the plume rising from the lower cylinder and the boundary layer buildup by the wall, the flow around the upper cylinders is no longer a free convection flow. For a steady state case, the temperatures of the cylinders above the lower cylinder are a result of the balance between the surrounding fluid temperature increases (due to the lower cylinder(s)) and the velocity of fluid which is induced by

the raised plume [5].

The exact solution for natural convection for such an arrangement is complicated by complex geometries and by the nonlinear nature of the problem. The nonlinearities arise from the fluid acceleration terms and the coupling of the momentum and energy equations. Due to the wake effect(s), the cylinder spacing is a critical and not fully understood variable [3]. Consequently, cylinder spacing has begun to receive more attention [3]. The lack of quantitative information concerning cylinder and wall spacing and the need to have more understanding of the flow around the cylinders has prompted this study.

1.2 Scope of the Study

The objective of this study is to investigate heat transfer by natural convection from three horizontal cylinders, at constant heat flux, aligned vertically parallel to a vertical wall(s). During the course of the experiment, the effect of the wall spacing on natural convection from the cylinders was studied. The effect of cylinder-to-cylinder spacing on natural convection was also investigated. Increased understanding of the fluid flow around the cylinders was accomplished by videotaping and taking photographs of the flow field. Laser sheets were used to illuminate smoke particles in the testing section. The

temperature and velocity fields were studied (for some cases) by using Tempest (computer software from Battelle Laboratories) on the Floating Point system super computer at O.S.U.

Pilot experiments were conducted with a single isolated cylinder in order to compare readings with the results of previous studies where the average Nusselt number from a horizontal cylinder at constant heat flux was expressed as a function of modified Rayleigh number, Ra^*. The results of the pilot experiments were also compared to the scale analysis which will be shown in the next section of this chapter.

1.3 Governing Equations and Scale Analysis

In the cases of steady state, two-dimensional flow and laminar free convection, the boundary layer theory concepts were employed. These concepts are governed by the conservation of mass, momentum, and energy equations. With the assumption of constant fluid properties, except in the case of the density in the buoyancy force term, the governing differential equations appear [6] as follows:

$$\frac{\partial U}{\partial X} + \frac{\partial V}{\partial Y} = 0. \tag{1.1}$$

$$U\frac{\partial U}{\partial X} + V\frac{\partial U}{\partial Y} = g\,\beta\,(T - T_{inf})\sin\theta + \upsilon\left(\frac{\partial^2 U}{\partial X^2} + \frac{\partial^2 U}{\partial Y^2}\right) \tag{1.2}$$

$$U\frac{\partial V}{\partial X}+V\frac{\partial V}{\partial Y}=-g\beta(T-T_{inf})\cos\theta+\upsilon\left(\frac{\partial^2 V}{\partial X^2}+\frac{\partial^2 V}{\partial Y^2}\right) \qquad (1.2b)$$

$$U\frac{\partial T}{\partial X}+V\frac{\partial T}{\partial Y}=\alpha\left(\frac{\partial^2 T}{\partial X^2}+\frac{\partial^2 T}{\partial Y^2}\right) \qquad (1.3)$$

The system of coordinates is shown in figure 1.1 .

Following the scale analysis rules as outlined by Bejan [7], y is of the same order of magnitude as the thermal boundary layer, δ_T. This will be written as $Y \sim \delta_T$. Since x=f (D, θ),

$$X \sim D$$

$$\delta_T^2 \ll D^2$$

$$\frac{\partial^2}{\partial Y^2} \gg \frac{\partial^2}{\partial X^2}$$

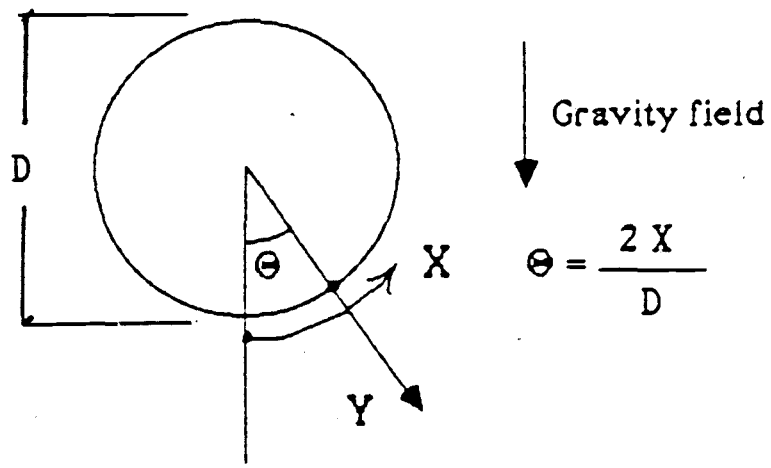

Figure 1.1 System of coordinates.

Thus the $\frac{\partial^2}{\partial X^2}$ terms in the momentum and energy equations (equations 1.2a, 1.2b and 1.3, respectively) are neglected. The scaling of the continuity equation, equation 1.1, gives

$$V \sim U \frac{\delta_T}{D} \tag{1.4}$$

and the scaling of the energy equation gives

$$U \frac{\Delta T}{D} \text{ , } V \frac{\Delta T}{\delta_T} \sim \alpha \frac{\Delta T}{\delta_T^2}$$

|____ convection ____| |___ conduction __|

By substituting for V from equation 1.4 in the last equation, both convection terms are of the order $U \frac{\Delta T}{D}$. Therefore,

$$U \sim \alpha \frac{D}{\delta_T^2} \tag{1.5}$$

The momentum equations, equation (1.2a) and (1.2b), give the following scale balance:

$$\frac{U^2}{D} \text{ , } V \frac{U}{\delta_T} \quad \text{or} \quad \upsilon \frac{U}{\delta_T^2} \sim g \beta \Delta T \sin\theta$$

|__ inertia _____| |__ friction __| |__ buoyancy __|

$$U\frac{V}{D} \text{ , } \frac{V^2}{\delta_T} \quad \text{or} \quad \upsilon \frac{V}{\delta_T^2} \sim g \beta \Delta T \cos\theta$$

|__ inertia _____| |__ friction __| |__ buoyancy __|

Hence the δ_T is ruled by an Inertia - Buoyancy balance or by a Friction - Buoyancy balance. For Pr greater than one, the thermal boundary layer thickness, δ_T, is much smaller than the velocity boundary layer thickness and δ_T is ruled by the Friction - Buoyancy balance.

By adding the square of the friction terms and the square of the bouyancy terms in the above equations, the following relationship is obtained:

$$\upsilon^2 \left(\frac{U^2}{\delta_T^4} + \frac{V^2}{\delta_T^4} \right) \sim g^2 \beta^2 \Delta T^2 (\sin^2\theta + \cos^2\theta)$$

Equation (1.4) implies that $V^2 << U^2$. Therefore, V^2 can be neglected. By substituting for $(\sin^2\theta + \cos^2\theta) = 1$ and rearranging the terms, the above relationship can be written as,

$$\frac{\upsilon U}{g \beta \Delta T \delta_T^2} \sim 1$$

By substituting for (U) from equation 1.5,

$$\frac{\upsilon \alpha D}{g \beta \Delta T \delta_T^4} \sim 1 \qquad (1.6)$$

The no-slip condition implies that the heat transfer adjacent to the wall at $0< Y <0^+$ is by pure conduction and governed by Fourier's law [8].

$$q = K \left.\frac{\partial T}{\partial Y}\right)_{Y=o} \tag{1.7}$$

Therefore, $q \sim K \frac{\Delta T}{\delta_T}$ gives $\Delta T \sim q \frac{\delta_T}{K}$.

Sustituting for this value of ΔT and for $\alpha = \frac{K}{\rho C_P}$ and $\upsilon = \frac{\mu}{\rho}$ equation (1.6) becomes

$$\left(\frac{\mu K^2}{\rho^2 g \beta C_p q D^4}\right)\left(\frac{D^5}{\delta_T^5}\right) \sim 1$$

Thus $\delta_T \sim Ra^{*-1/5} D$ (1.8)

where Ra^* is modified Rayliegh number. The wall-heat flux equation, $q=h(T-T_{inf}) = h \Delta T$, and equation (1.7) give

$$q \sim K \frac{\Delta T}{\delta_T} \sim h \Delta T$$

hence $h \sim \frac{K}{\delta_T}$

Using equation (1.8) and rearranging the terms

$$Nu = \frac{hD}{K} \sim Ra^{*1/5} \tag{1.9}$$

Therefore, the Nusselt number for free natural convection heat transfer from a single isolated horizontal cylinder is a function of the modified Rayleigh number to the 1/5th power. Further, the

modified Rayleigh number, shown by equation 1.8, is of the same order of magnitude as the ratio of D to the thermal boundary layer thickness, δ_T.

CHAPTER 2

LITERATURE REVIEW

2.1 Single Cylinder without confining walls(s)

Numerous studies on natural convection heat transfer from a horizontal cylinder have been published. Morgan [9] tabulated sixty-four references which presented the natural convection heat transfer results from an isolated cylinder or array of horizontal heated cylinders (wires). The ratios of cylinder length to diameter in these studies ranged from 2.8 to 9000. The Rayleigh number, Ra, based on the cylinder diameter and on the film temperature, $T_f = (T_w + T_{inf})/2$, ranged from 7 x 10 to 10 . Only one of these studies, Dyer [10], was conducted at uniform heat flux. Based on the data from these references and on their correlation equations, Morgan [9] proposed the correlation for natural convection from a horizontal cylinder as

$$Nu = B\,(R_a)^M$$

where B and M are constants depending on the range of Ra. Ra is based on the cylinder diameter and the fluid properties at the film temperature, T_f .

In a theoretical and experimental study, Kim, Pontikes, and Wollersheim [11] studied the local and the average Nusselt number, Nu, from a horizontal cylinder to a Newtonian fluid

(mineral oil). They obtained the following relations for the average Nusselt number:

Isothermal cylinder, $Nu_i = 0.89\ (Gr_i \cdot Pr)^{.19}$

Constant heat flux, $Nu_c = 0.57\ (Gr_c \cdot Pr)^{.2}$

where Gr is the Grashof number and Pr is the Prandtl number. The subscripts i and c mean Gr based on temperature difference or uniform heat flux, respectively.

2.2 Array of cylinders without confining wall(s):

Lieberman and Gebhart [12] investigated the heat transfer from an array of heated wires. The wires had a length to diameter ratio equal to 1450. (The Rayleigh number was of order 10 and the array took different angle positions. The results were inferred from interferograms of the temperature field and the rising plume. They found that the temperatures of the wires increased up the array when the spacing between the wires was 37.5 diameter (the closest spacing). But, for higher spacing (75 diameter), the temperatures decreased as the position of the wire ascended the array. This was due to the increase of the air velocity in the plume, which resulted in lowering the plume temperature while the plume rose up in the array.

Marsters [13] studied the natural convection for vertical

arrays of heated horizontal cylinders. In his work the effect of cylinder-to-cylinder spacing was experimentally studied for three, five, and nine-cylinder arrays. The spacing took values from 2 to 20 cylinder diameters. Air was the working medium and the Grashof number, based on cylinder diameter and temperature difference, ranged from 750 to 2000. He found that the Nusselt numbers for narrow spacing are smaller than the Nusselt numbers for a single cylinder (about 50% smaller), while for wide spacing, the Nusselt numbers are about 30% higher than for a single cylinder. The temperature distribution along the array agreed with the results of Lieberman and Gebhart [12]. Furthermore, the lower cylinder in any array behaves much like a single cylinder. Marsters suggested that the Grashof number should be based on the characteristic length of the distance from the lower cylinder rather than on the cylinder diameter to explain the temperature distribution along an array.

The effect of vertical separation distance and cylinder-to-cylinder temperature imbalance on natural convection for a pair of horizontal cylinders was examined by Sparrow and Niethammer [5]. In these experiments, the lower cylinder wall-to-ambient temperature difference ranged from zero to three times the upper cylinder wall-to-ambient temperature difference. The values of Rayleigh numbers, based on the cylinder diameter, for the upper cylinder were from 20,000 to 200,000.

The results were presented as the Nusselt number ratios and the temperature ratios. The Nusselt number ratio was the Nusselt number of the upper cylinder divided by the Nusselt number of an isolated cylinder of the same Rayleigh number, while the temperature ratio was the ratio of the wall-to-ambient temperature difference of the upper cylinder divided by that of the lower cylinder. At a specified temperature ratio and Rayleigh number, the Nusselt number ratio increases sharply at a small separation distance, S. The slope of the Nusselt number ratio becomes flatter at larger spacing and the ratio takes a maximum value in the range of S/D between seven and nine. At low spacing ratio the increase of the temperature ratio degrades the Nusselt number ratio.

Sparrow and Boessneck [14] studied the effects of transverse misalignment on natural convection from a pair of parallel, vertically stacked, horizontal cylinders. At several fixed separation distances (cylinder-to-cylinder distance) the transverse offset was varied. The transverse misalignment had eight values ranging from zero to three cylinder diameters. The separation distance took several values between 2 and 9 cylinder diameters. The cylinder diameter was 1.49 inches and its length/diameter ratio was 20. Rayleigh numbers were based on the cylinder diameter and the cylinder-to-ambient temperature difference. During the course of the experiment, Rayleigh numbers ranged from 20,000 to 200,000 and the testing fluid

was air.

Since the lower cylinder is not affected by misalignment (i.e., it behaves like a single cylinder), the study focused on the upper cylinder Nusselt number ratio. This ratio was the misaligned upper cylinder Nusselt number to the perfectly aligned upper cylinder. The offsetting enhanced the Nusselt number ratio (up to 27%) at small cylinder-to-cylinder vertical separation. While at large separation distances the offsetting decreased the Nusselt number ratio (up to 22%). For specific offset, the Nusselt number enhanced at lower Rayleigh number. This enhancement decreased as the vertical separation increased. In all the cases the Nusselt number reached a single value, which was about 3% higher than that of a single cylinder when the offset was large. The results, when all the cylinders were aligned, agree with the results of [5], where the Nusselt number of the upper cylinder was enhanced as the vertical separation between the cylinders was increased.

2.3 Single cylinder confined by two parallel walls:

Marsters [15] studied the effects of adiabatic walls confinement on the heat transfer from a horizontal heated cylinder. During the course of the experiments, Rayleigh number values ranged from 10 to 500,000. This range was achieved by using air, water and freon 113 as working fluids and two

different cylinder diameters to give cylinder length-to-diameter ratios of 70 and 67.9. The wall spacing was varied between 2 to 20 cylinder diameters and the wall height-to-diameter ratio had values between 5 and 128. The study consisted of two parts. First, the cylinder was tested with no-wall (isolated cylinder) and a correlation equation for the average Nusselt number, Nu, was presented

$$Nu = 0.88\ Ra^{(0.14+0.013\ \log\ Ra)} \qquad \text{for } 10 < Ra < 500{,}000$$

where Ra was based on the cylinder diameter and the temperature difference. In the second part, the cylinder was confined by the walls. The results showed that the heat transfer characteristics were enhanced significantly by the presence of the walls. Even at large wall spacing (20 cylinder diameters), there was a 30% increase in the heat transfer over the no-wall case. On the other hand, Marsters found that there was no effect of the cylinder elevation (the distance from the bottom of the walls to the center of the cylinder) as long as the cylinder lay between the walls. Analysis of the data gave the following correlation equation for the Nusselt number:

$$Nu = 0.82\ \ Ra^{a}\ .\ 10^{b}$$

where $a = 0.17\ (1 + 0.05\ \text{Log Ra})$

$b = 0.02\ (H/w)\ \{1-0.018\ (H/t) - 9.2\ (d/H)\}$

H = height of the walls

w = spacing between the walls.

This equation indicates that the higher order of the geometry terms was unimportant. Also, it shows Nu decreased when H/w>28 for fixed values of w, D and Ra.

Sparrow and Pfeil [16] determined the heat transfer characteristics of a heated horizontal cylinder situated at the mid-height of a vertical channel with adiabatic channel walls. The cylinder length-to-diameter ratio was 20/1. The experiment was carried out in air with Rayleigh number, Ra (based on cylinder diameter and temperature difference), between 15,000 and 200,000. The effects of the channel height, the interwall spacing (the distance between the walls), and the wall materials on the heat transfer were studied. It was found that the Nusselt number, relative to the no-wall condition, was enhanced as the channel height increased. Thus, the vertical placement of the cylinder in the channel enhances the heat transfer. This enhancement can reach up to 40% at small interwall spacing, while lower at large interwall spacing.

Sparrow and Pfeil's [16] conclusion does not agree with that of Marsters [15], where the vertical placement of the cylinder does not affect the heat transfer characteristics. However, both studies agree that the Nusselt number was enhanced at the small interwall spacing. This enhancement decreases as the spacing increases. In Sparrow and Pfeil's [16] experiment, the spacing effect decreased as the height of the channel increased. They used three different shroud types (the walls parallel to the

cylinder axis) including: highly conducting, highly conducting with insulation on the back side, and non-conducting shrouds. The results revealed that the Nusselt number was insensitive to the various types of shrouds. They presented a correlation equation for the Nusselt number in the following form,

$$Nu = C\,Ra^{n}$$

where C and n are constants depending on the ratios of the channel height and interwall spacing to the cylinder diameter.

Karim et al. [17] investigated the effects of the interwall spacing and the vertical placement on the natural convection heat transfer from a horizontal isothermal cylinder symmetrically placed between two parallel adiabatic walls. Two different cylinder diameters were used with length-to-diameter ratios of 17.4 and 25.98. Average Nusselt numbers were determined for a Rayleigh number of 2,000 to 300,000. The results showed that the Nusselt number degraded with increasing Rayleigh number for all the wall spacing ratios (wall spacing to cylinder diameter). Their experiments agree with [15] , where the confinement enhances the Nusselt number and there is no significant effect from the cylinder's vertical placement on the heat transfer characteristics. But, their findings disagree with [15] when there is an optimal spacing for maximum heat transfer. A correlated equation to calculate the average Nusselt number was presented by Karim et. al. as

$$Nu = \{0.481 + 0.172 \exp(-0.258\,(W/D))\} \cdot Ra^{.25}$$

where W is the spacing between the walls and Ra is the Rayleigh number based on cylinder diameter, D, and on cylinder-ambient temperature difference.

2.4 Array of cylinders confined by two parallel walls:

Marsters and Paulus [18] examined the effects of confining walls on a vertical array of horizontal cylinders. The array consisted of nine heated cylinders with cylinder's length-to-diameter ratio equal to 70 and with cylinder-to-cylinder spacing equal to 6 cylinder diameters. They found that the walls influenced the heat transfer characteristics of an individual cylinder in the array, but the walls had less effect on the overall heat transfer of the array. They presented curves for normalized temperature (the cylinder-to-ambient temperature difference to the bottom cylinder-to-ambient temperature difference). The curves illustrate that the normalized temperature increased as the cylinder was elevated in the array and as the wall spacing decreased. The experiments were carried out with/without ventilating walls (the side walls perpendicular to the cylinder axes). They also examined the normalized temperature for a single wall spaced two cylinder diameters distance from the center of the array. Again, in this case, the temperature increased as the cylinders were elevated in the array.

Natural convection characteristics for a vertical array of

heated cylinders with/without confining walls were experimentally investigated by Tokura et. al. [17]. The experiments were carried out for 2, 3, and 5-cylinder arrays with cylinder lengths equal to 20.8 cylinder diameters. For non-confining arrays, their results agreed with [5 and 13] that the average heat transfer coefficients increase as the center-to-center distances increase. This enhancement reaches a maximum value when the spacings are approximately five times the cylinder's diameter. The following equations were predicted:

(1) The average Nusselt number for the second cylinder in an array as a function of Rayleigh number, Ra, and distance from the center of the bottom cylinder to the center of the second cylinder, CC, and the cylinder diameter, D.

$$Nu = 0.26\ (CC/D)^{3/4}\ \ [1-\exp\{-2.22/((CC/D)^{3/4}) -1)\}]\ \ Ra^{1/4}$$

This equation produced close results to those obtained in the case of a single cylinder when CC extends to infinity. The above equation can be used for the other cylinders in the down stream of the array when the spacing between the cylinders is large.

(2) The average Nusselt number for a whole array as a function of Ra and b/D where b is the diameter-to-diameter cylinder separation distance and N is the

number of the cylinders in the array.

$$Nu = 0.41\ Ra^{1/4}\ Ln\ \{[(b/D)/1.3]^{.055N}\}+0.434$$

The error in this equation is $\pm$10% for $[(b/d)/1.3]^{.055N} = 0.7$ to 1.2 and Gr = 40,000 to 400,000.

For an array between two parallel plates, they found that the Nusselt number for a whole array was enhanced. This enhancement reached its maximum when the spacing between the plates was three times the cylinder diameter, S/D = 3. When S/D = 30, the effects of parallel plates on the average Nusselt number was insignificant. The average Nusselt number for each cylinder was almost the same for all the cylinders above the bottom one when the spacing between the cylinders was 6D (i.e., b/D=6). But, when b=D, the average Nusselt number for the cylinder above the bottom one was much smaller than the average Nusselt number for the bottom cylinder. This difference decreases as the S/D increases. In general, the effect of the spacing between the cylinders is greater than the effect of the distance between the plates. Relative to an array without confining walls, the effect of the walls increased the heat transfer by 10 to 15% when the separation distance between the walls was 2 to 6 times the cylinder's diameter.

2.5 Cylinder(s) confined by a single wall:

Five references are cited under this category. Four of them were published with Sparrow as a co-author. The articles were published between 1981 and 1987. Three of these articles, as shown below, investigate the natural convection heat transfer from a horizontal cylinder(s) fixed perpendicularly on a vertical heated wall.

The natural convection heat transfer characteristics from an isothermal horizontal cylinder attached to an isothermal vertical plate at the same temperature were investigated experimentally by Sparrow and Chrysler [20]. During the course of the experiments, the cylinder axes were perpendicular to the plate surface. The effect of the cylinder position from the leading edge was studied by attaching the cylinder to one of the three positions along the height of the plate. Two cylinders with length-to-distance ratio, L/D, equal to 1 and 1/2 were used. The Rayleigh number, Ra (based on cylinder diameter, D), ranged from 14,000 to 140,000. Sparrow and Chrysler found that at a given Ra the Nusselt number was insensitive to the cylinder's vertical position. In addition, the Nusselt number was enhanced at the higher position and it was lower at the lower position for a given Ra. However, at the middle position the Nusselt number was lower than that at the lowest position. This demonstrated nonmonotonic variation of the Nusselt number with the elevation

of the cylinder. The presence of the vertical plate degraded the Nusselt number due to the boundary layer build-up by the plate. This effect was higher on the shorter cylinder than on the longer cylinder due to the plate-cylinder interaction. From the data obtained in these experiments, the following empirical equation was presented to find the average Nusselt number as a function of Ra:

$$Nu = C\ Ra^{1/4} \qquad \text{for} \qquad 14{,}000 < Ra < 140{,}000.$$

where C depends on the cylinder's length-diameter ratio and the cylinder position from the lower edge of the plate.

The above work, [20], was extended by Sparrow et. al. [21] to investigate the natural convection heat transfer for a vertical array of horizontal cylinders perpendicular to a vertical plate. Both the cylinders and the plate were at the same constant temperature. Two arrays comprised of two and three cylinders were used. Using a two-cylinder array allowed examination of the effects of wider cylinder-to-cylinder distance and two array elevations (distance from the leading edge of the plate to the lower cylinder). Four parameters were studied. These include the fin (cylinder) length-to-diameter ratio, the interfin spacing, the position at which the fin is attached to the host vertical plate, and the Rayleigh number, Ra.

For an individual cylinder in the array, the results showed that the presence of a cylinder (or cylinders) below it lower the

Nusselt number(s) at higher Rayleigh number. The lowest cylinder of the array was not affected by the presence of the cylinder(s) above it. For the two-cylinder array, the presence of the array at the lower part of the plate gave the upper cylinder a higher Nusselt number than the array at the higher part of the plate. Higher interfin spacing also produced higher Nusselt numbers for the upper cylinder. For the three-cylinder array, the Nusselt number degraded as the cylinder elevation increased at low Rayleigh number. While at higher Ra, the cylinder in the middle obtained the highest Nusselt number.

Sparrow et. al. [22] extended the investigation of natural convection heat transfer from an isothermal horizontal cylinder attached perpendicularly on a vertical plate at equi-temperature to include the duct-flow effects. The walls of the duct (except the vertical plate) were adiabatic. During the experimental work, the spacing, S, between the isothermal vertical plate and the opposite wall was changed from S/L = 1.4 to S/L = 5.4, where L = cylinder length. At large S/L the condition reached external flow mode. This also occurred in the cases discussed by Sparrow and Chrysler [20].

The enhancement or the degradation of heat transfer was compared as a percentage of the external flow mode (large S/L). The results showed that the heat transfer from the lower cylinder position was enhanced by 60% to 20% as the S/L changed from 1.43 to 5.4 This enhancement was lower for the middle cylinder

position (about 40 to 50%). In both cases (lower and middle cylinder positions) the effect of the Rayleigh number was insignificant. For the upper cylinder position, the results were sensitive to the Rayleigh number at a small S/L ratio. Conversely, the results were less sensitive for the Rayleigh number at a higher S/L ratio. At low S/L the enhancement decreased as the Rayleigh number increased. At high S/L the enhancement was zero. These results suggest that the external flow is more preferable for the upper cylinder position.

The effects of the radiation conditions of the unheated walls on the heat transfer were examined during these experiments by using black body walls and reflective walls. The reflective walls showed lower enhancement of the heat transfer than the black body walls. This was due to the temperature difference of the black body surfaces being higher than the temperature difference of the reflecting surfaces. The temperature difference was defined as the difference between the wall temperature and the ambient temperature. In the black body case, the higher temperature differences helped to induce more flow inside the duct in addition to the induced flow by the isothermal vertical plate. This higher velocity enhanced the heat transfer.

The characteristics of natural convection heat transfer from a heated isothermal horizontal cylinder parallel to an adiabatic wall(s) were examined by Sparrow and Ansari [23]. The experimental configurations included a single vertical wall

situated to the side of the cylinder, a horizontal wall beneath the cylinder, and a corner formed by a vertical and a horizontal wall. The cylinder length was equal to 20 times its diameter. The ratio of the distance between the cylinder and the wall(s), in one of the specified conditions, to the cylinder diameter, S/D, was changed systematically from S/D = 1/12 to S/D = 4/3. The results were presented as the ratio of the dissipated heat transfer from the cylinder in the presence of the wall(s) to the dissipated heat transfer with no-wall(s) (isolated cylinder). The experiments were carried out in air with Rayleigh numbers from 20,000 to 200,000.

In general, the presence of the wall(s) degraded the cylinder heat transfer relative to the isolated cylinder heat transfer. In the case of a vertical wall, there was a 20% reduction for S/D = 1/12. This reduction was negligible when S/D = 1/4 or greater. For a horizontal wall beneath the cylinder, the reduction in the heat transfer was 5% greater than the vertical wall case. The effect of the horizontal wall was eliminated when the spacing ratio, S/D, equalled 1.33 or greater.

The degradation in heat transfer for the corner case was 40% at the closest spacing and 20% for 1/4 cylinder diameter spacing or greater. The experiments also demonstrated that the adiabatic wall(s) experienced a temperature rise relative to the ambient temperature due to wall(s)-to-cylinder interaction. The highest temperature rise reported was approximately 86% of the

cylinder-ambient temperature difference, which occurred at the closest cylinder-wall spacing of the corner-cylinder interactions.

McCoy [24] studied the convection heat transfer behavior from an isothermal heated horizontal cylinder parallel to an isothermal vertical wall. The enhancement or degradation of the Nusselt number relative to the Nusselt number of an isolated cylidner, Nu/Nu_s, was examined with different cylinder positions. These positions included cylinder-wall spacings and the elevation of the cylinder from the leading edge of the vertical wall. Water was used as a working fluid and the Rayleigh number ranged from 400,000 to 10,000,000. It was found that Nu/Nu_s ratio increased slowly as the wall-cylinder distance was decreased. This enhancement reached its maximum at approximately S/D = 0.2. Then Nu/Nu_s dropped off sharply for closer spacings. This was due to the interaction between the cylinder and the wall boundary layer. This interaction was higher at low Rayleigh numbers where the boundary layer was thick.

CHAPTER 3

EXPERIMENTAL APPARATUS AND PROCEDURES

3.1 Introduction

The overall design of the experiments was devised in order to satisfy the following requirements:

1) Two dimensional heat transfer conditions. These were achieved by specifying proper cylinder dimensions and cylinder's end conditions.
2) Steady state heat transfer conditions. These were accomplished by allowing adequate time for the experimental set-ups and by providing stable environmental conditions.
3) Accurate data readings. Proper devices and computerized techniques to supply and collect data were used to satisfy this condition.
4) Rapid and efficient re-arrangement of the geometrical experimental set-up (especially wall(s) spacing). Figure 3.1 shows a pictorial view of the testing section.

The above requirements will be discussed in detail in the following sections, where the experimental components and instrumentation are discussed. At the end of this chapter the experimental procedure is presented.

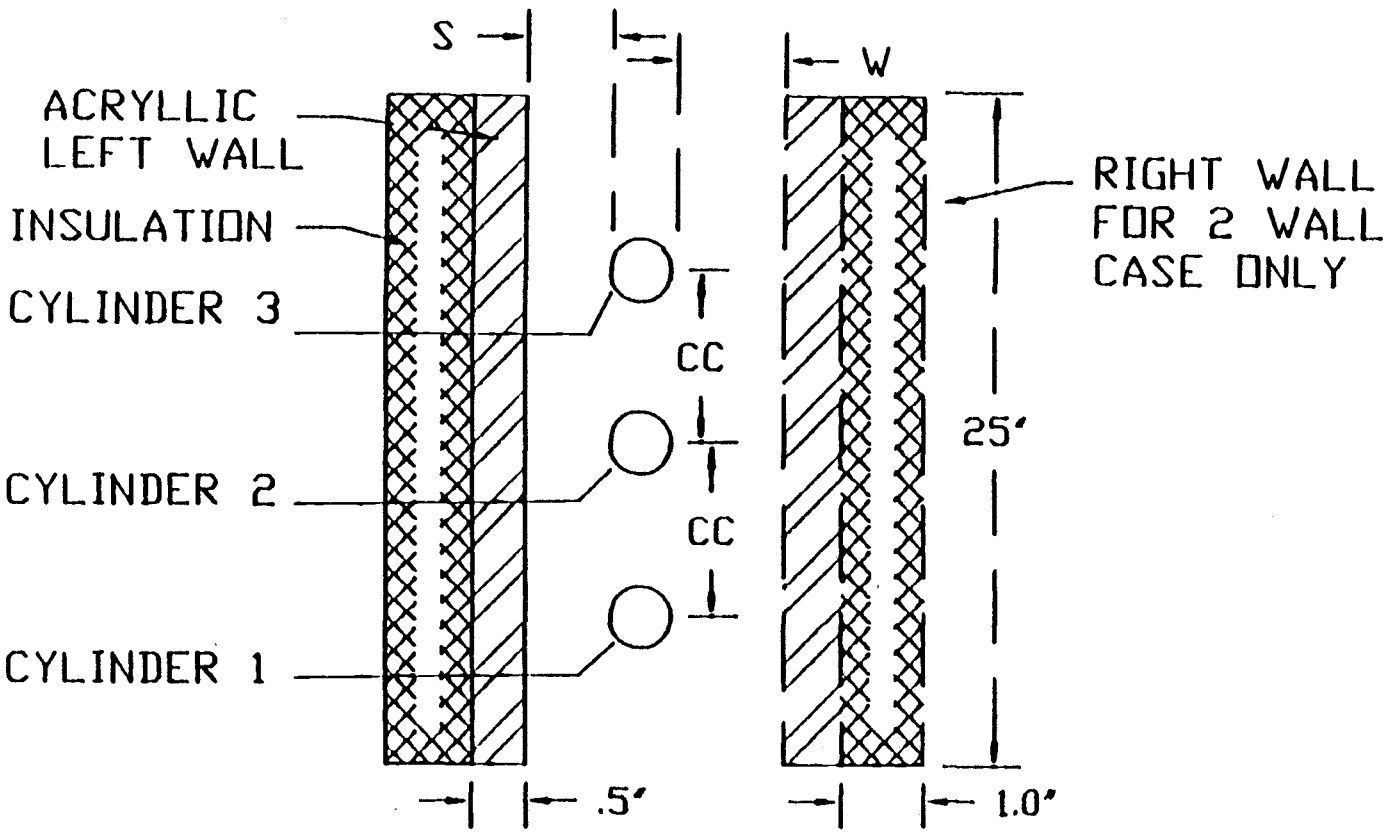

Figure 3.1 Pictorial view of the testing section.

3.2 Components

3.2.1 Heaters

Etched-foil heaters were used to provide a uniform surface heat flux and to ease the fabrication process of the testing cylinders. Two etched-foil heaters were used for each cylinder. The heaters were manufactured by MINCO Products, Inc. The heated foils were insulated by 0.2 mm (0.008 inch) glass reinforced silicone rubber. Their dimensions were 7.62 Cm X 12.7Cm (3 inches x 5 inches)with a 0.5mm (0.02 inch) maximum thickness. The working temperature range of the insulation was from -62 degrees Centigrade to 235 degrees Centigrade.

Each heater had 30.48 Cm (12-inch) teflon insulated wires, size 24 AWG. The unheated ends of the heaters were trimmed to give a final dimension of 7.42Cm x12.38Cm (2.92 inches x 4.875 inches). This allowed for a better fitting of the heaters inside the cylinders and reduced the unheated area of the heaters to supply uniform heat flux to the cylinder surfaces.

3.2.2 Thermocouples

Constantan and copper-nickel (type-T) thermocouples were employed in the experiments. Type-T was chosen because it has a low rate of error across the temperature range of the

experiments. This type of thermocouple has a temperature range from -200 degrees Centigrade to 350 degrees Centigrade with a limit of error of 1.0 degree Centigrade or 0.75%, whichever of these is greater [25].

Small thermocouple wires of .254mm (0.01 inch) in diameter were selected to reduce the conduction heat loss from the cylinders. The thermocouples were fabricated by using a Hot-Spot thermocouple welder from DCC corporation and following the instructions in [26]. After obtaining a spherical, homogeneous thermocouple bead, the bare lead wires close to the bead were insulated by thermocouple epoxy to prevent their contact. Then, the thermocouple resistance was measured and compared to the resistance of the lead wires to insure a good electrical contact in the junction (bead). All thermocouples were calibrated by using boiling water and ice water as reference temperatures. The calibration process also included measuring the voltage drop across the thermocouples and comparing it to the tables in reference [25]. Those thermocouples which passed the calibration test were selected for use in the experiment. A total of 26 thermocouples was employed in the experiments. The location and manner by which the thermocouples were attached to each component will be discussed in later sections.

3.2.3 Cylinders

Three cylinders comprised the main experimental apparatus. These cylinders were fabricated to be identical in all respects (i.e., dimensions and surface radiation conditons). The test section assembly for the cylinders is shown in Figure 3.2. The cylinders were fabricated from aluminum tube with a 2.54 Cm (1.0 inch) outside diameter and a 2.36Cm (0.93 inch) inside diameter.

Aluminum was chosen as the heat transfer surface because, when polished to a mirror-like finish, it reduces the radiative heat loss which competes with natural convection [14]. The high thermal conductivity of aluminum is another important factor as aluminum provides a more uniform heat flux surface.

Each cylinder had a length-to-diameter ratio equal to 10, allowing for suppression of the axial heat transfer effect. The cylinders were polished to a mirror-like finish by using a fine-metal polish in order to reduce the radiation effect.

Eight thermocouples were used for each cylinder. Two of them were used for the end-cap temperature gradient. The other six thermocouples were used to measure the temperature of the cylinder surface, Fig. 3.2. Two thermocouples were cemented to the interior surface of the cylinder by using thermocouple epoxy and placed 2.54 Cm (1.0 inch) from each cylinder's end, below the top stagnation point of the cylinder. The epoxy, which was manufactured by OMEGA Engineering, Inc., uses aluminum

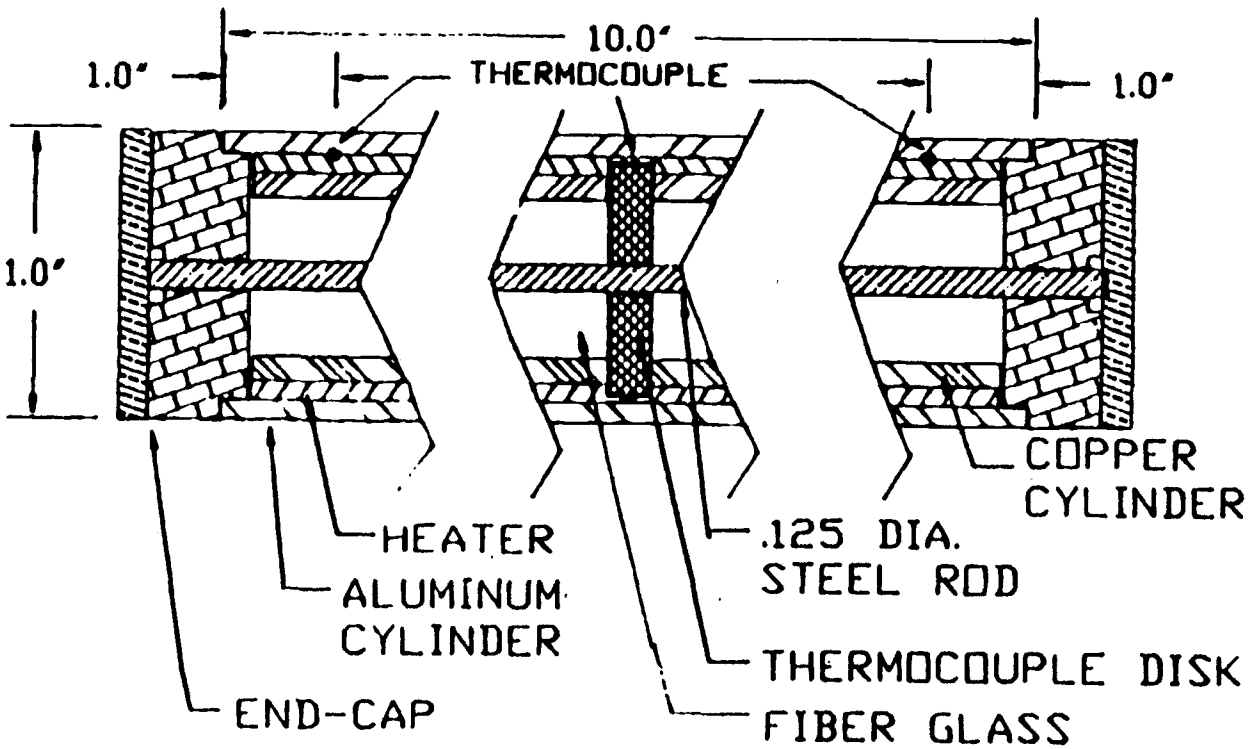

Figure 3.2 Test section assembly for the cylinders.

powder to enhance the thermal conductivity of the joint. The other four thermocouples were radially positioned at the mid-length of the cylinder at 90 degree intervals from the top stagnation point around the inner circumference of each cylinder. These thermocouples were hosted in a thermocouple disk.

Each disk, Figure 3.3, was made of 0.635 Cm (0.25 inch) aluminum plate. The disk's outer diameter was 2.286 cm (0.9 inch). This left enough clearance for the heaters to be inserted between the disk and the cylinder wall. Each disk had two axial holes, one located at the center and the other located off-center. The latter was used to pass the lead wires of the front heater and the front end thermocouple to the back end of the cylinder (the end through which all the lead wires were passed). The center hole was used to pass the steel support rod of the end-caps. The radial thermocouples were hosted in four radial holes, 90 degrees apart. Each radial hole was made by two drilling stages.

In the first stage, a 5 mm (0.2 inch) diameter with a 6.35 Cm (0.25 inch) depth hole was drilled. A thermocouple pin and a 3.17 mm (0.125 inch) outside diameter spring were hosted in this hole. The pin was made of 3.81 mm (0.15 inch) copper tube and was 4.57 mm (0.18 inch) in length. The pin was used to support the thermocouple bead, which was threaded through the pin and cemented to it by the epoxy. The thermocouple beads were also threaded through the spring, which pressed the pin and the bead against the cylinder's surface. The thermocouple beads were

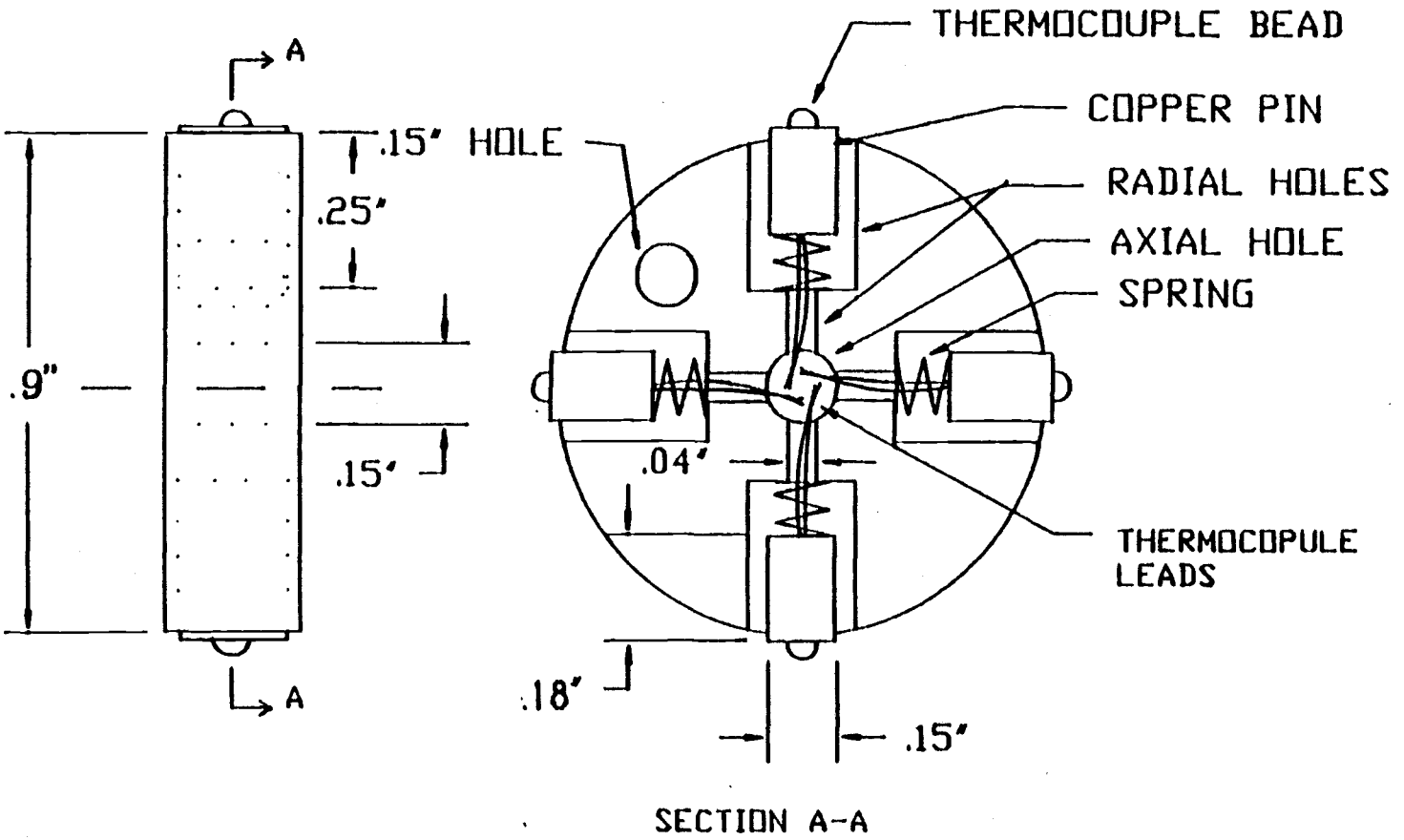

Figure 3.3 Thermocouple disk.

flattened at the point of contact with the cylinder to insure a larger contact area. To insure a safe passage for the radial thermocouple leads, a 1.02 mm (0.04 inch) diameter second-stage hole was drilled to connect the radial holes to the center hole of the disk.

The thermocouple disks were placed at the midpoint of each cylinder. Then, two foil heaters were inserted from each end of the cylinder. These heaters were backed up by 2.223 mm (0.875 inch) diameter copper cylinders with a length of 12.065 Cm (4.75 inches). The copper cylinders were used to support the heaters against the aluminum cylinders and to prevent hot spots on the heating foils due to loss of contact between the heaters and the cylinders. In order to prevent an internal natural convection in the cores of the cylinders, the cores were filled with pressed fiber glass insulation. End-caps were used to seal the cylinders.

Solid delrin and artificial cork were used to fabricate the end-caps. As shown in figure 3.4, each cap consisted of two disks. The first disk was made of delrin and hosted two thermocouples, one on each axial surface. The thermocouples were glued to the surfaces with thermocouple epoxy. A 3.81mm (0.15 inch) diameter hole was drilled at the center of each disk to allow insertion of a 3.175 mm (0.125 inch)diameter steel rod used to hold the caps at the ends of each cylinder. The rear end-caps had two extra holes drilled to thread the lead wires of the heaters and thermocouples through. This left the front ends free of lead

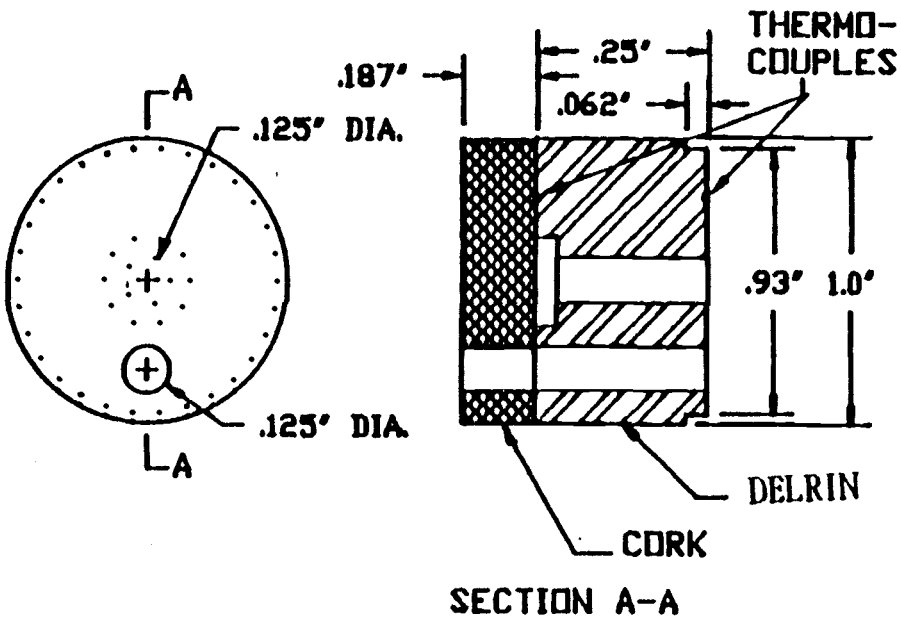

Figure 3.4 End-Caps.

wires to give clear flow visualization pictures. The second disk of the end-caps was made of artificial cork and was glued with silicone rubber onto the external surface of the delrain cap. After the cylinders were installed on the main supporting frame, the end-caps of the cylinders were hosted in a block of styrofoam with three holes. The thickness of the styrofoam blocks was 5.08 Cm (2.0 inches) and each block extended 2.54 Cm (1.0 inch) beyond the surfaces of the array, Figure 3.5

3.2.4 Wall(s)

Two types of walls were used in the experiment: the side wall(s), which were parallel to the cylinders and the end walls (the baffles), which were perpendicular to the cylinders' axes. The side walls were made from 1.27 Cm (0.5 inch) thick acryllic and were constructed with a height of 63.5 Cm (25 inches) and a width of 25.4 Cm (10 inches). They were backed with 2.54 Cm (1 inch) thick styrofoam insulation which was glued on the back surface of each wall. The surfaces of all the walls facing the cylinders were painted with a flat black paint in order to achieve a uniform radiation condition, [18].

Aluminum bars 1.27 Cm x 1.905 Cm x 35.56 Cm (0.5" x 0.75" x 14") were fixed at the top and the bottom of each wall. The 1.27 Cm x 35.56 Cm (0.5" x 14") surface of the bars lay on the same plane as the surface of the walls facing the cylinders. The

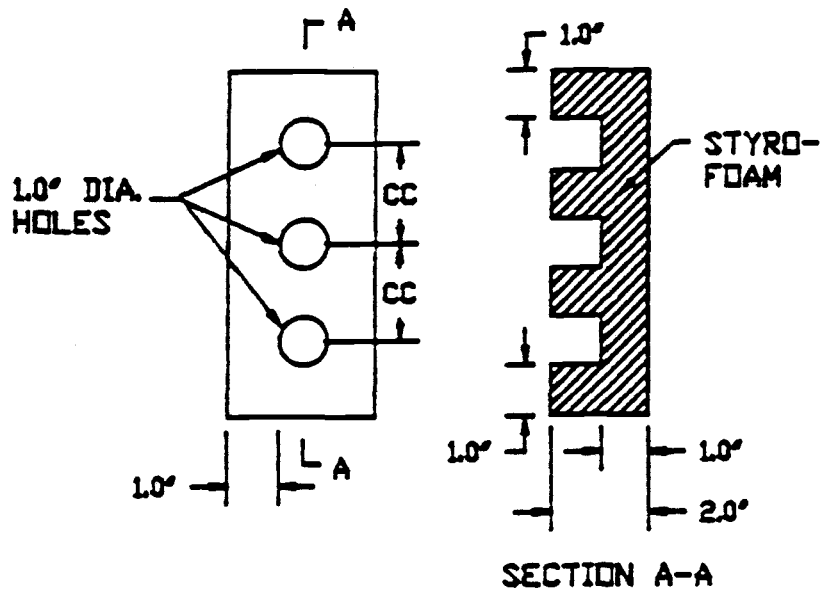

Figure 3.5 End-Block.

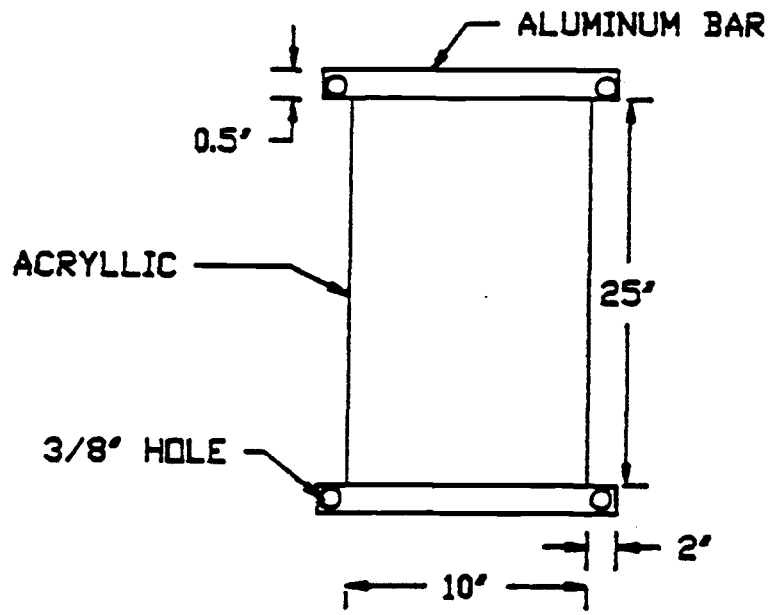

Figure 3.6 Side wall.

bars extended 5.08 Cm (2.0 inches) from the sides of the walls to form an "I" shape as shown in figure 3.6. To facilitate the wall-array spacing adjustments, each extension had a 1.27 Cm (0.5 inch) hole to host a 0.953 Cm (3/8")diameter adjusting screw. The adjusting screws were bolted on the main frame above and below the baffle supports. Each side wall was equipped with seven thermocouples. The thermocouples were led in from the back surface of each wall through 1/32" holes and their junctions lay in the same plane as the front surface of the walls.

In order to approximate the experimental conditions of two-dimensional cases [23], end walls made of 3.175 mm (1/8") thick acryllic were used. The end walls assisted in preventing the transverse inflow of air toward the cylinders. Three sets of end walls were fabricated to accommodate the three settings (CC = 4D, 2D and 1.5D). The positions of the top cylinder (cylinder #3) from the top end of the baffles were the same for all the sets. This left the positions of the lower cylinders (#2 and #1) dependent on the cylinder-to-cylinder spacings.

The surfaces of the baffles that faced the cylinders were painted with a flat black paint. There were three 2.54 Cm (one-inch) diameter holes on each baffle to host the ends of the cylinders. There was no direct contact between the cylinders' surfaces and the baffles, since the baffles supported the end-caps of the cylinders. For each set, two end walls were placed 25.4 Cm (10 inches) apart on the main frame to form a C-shape channel

for a single wall case and a closed vertical duct for a two-walls case.

3.2.5 Main Frame and Enclosure

An illustration of the main frame is shown in Figure 3.7. Angle-aluminum 2.54 Cm x 2.54 Cm (1" x 1") was used to make the 40.64 Cm x 50.8 Cm x 182.88 Cm (16" x 20" x 6') frame. The baffle supports were made of 1.905 Cm (3/4" x 3/4") wooden bars. The lower edges of the baffle supports (which were at the same level as the lower edges of the side walls) were three feet above the floor. The aluminum frame was mounted on the frame base, which was made of 5.08 Cm x 10,16 Cm (2" x 4") wooden bars. Four screws (1.27 Cm x 12.7 Cm) were used on the four corners of the base to support the main frame assembly. By changing the height of the screws below the base, the vertical plane and the horizontal level of the array could be adjusted.

To reduce the air movement around the testing section, the main frame was placed in a 1.1 m x .765 m x 2.134 m (3.5' x 2.5' x 7') enclosure. The enclosure was made of 1.27 Cm (1/2") plywood sheets. The top and bottom ends of the enclosure were open, Figure 3.8. To prevent air stratification in the enclosure, a 2.54 Cm (one-inch) gap between the floor and the bottom end of the enclosure was left. The test section was made accessible through a 91.44 Cm x 76.2 Cm (3' x 2.5') wooden door on one side

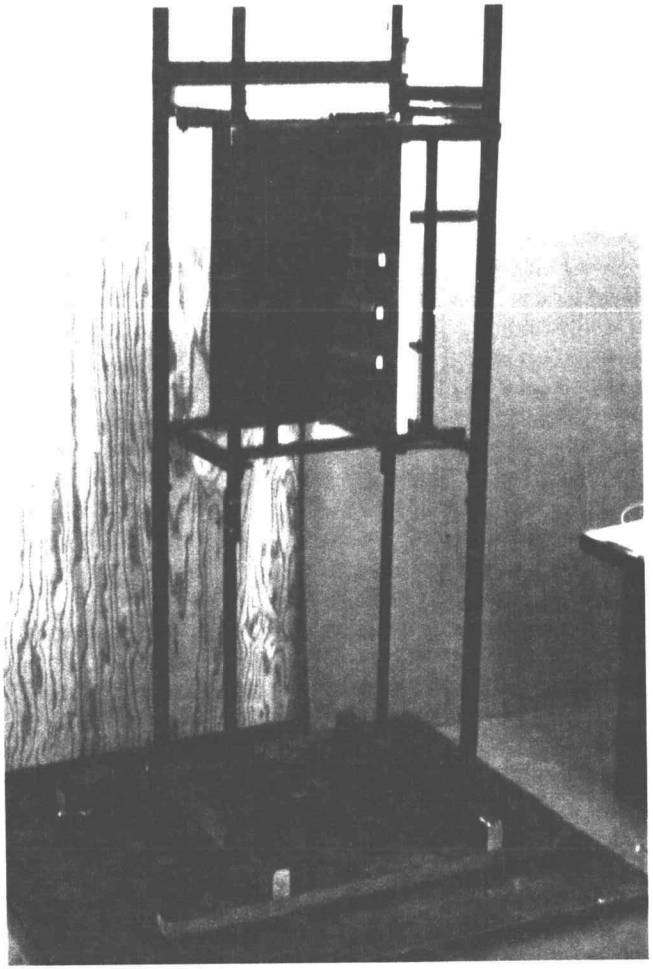

Figure 3.7 The main frame.

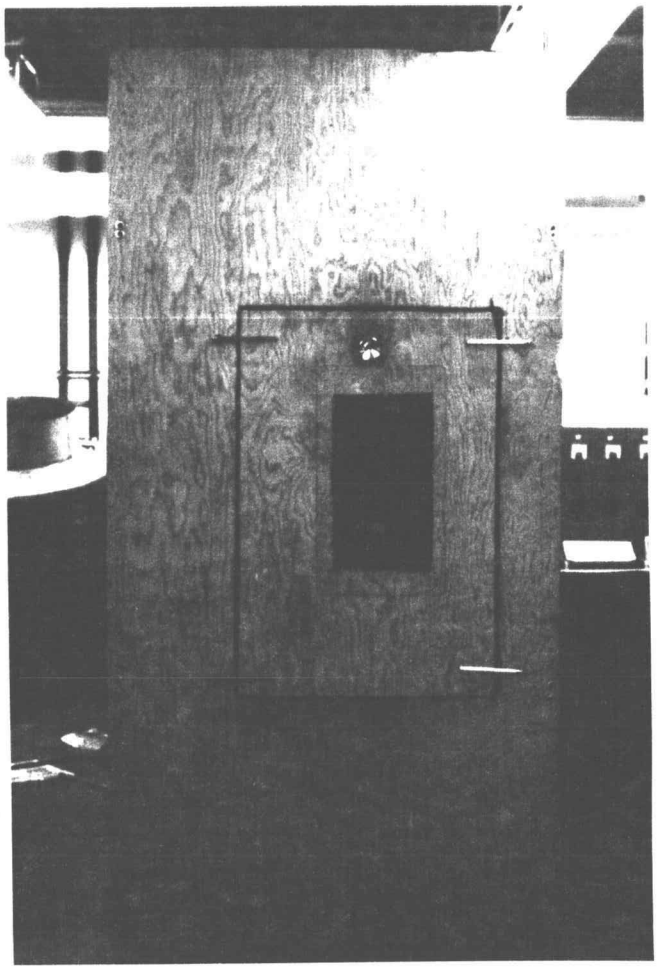

Figure 3.8 The enclosure.

of the enclosure. The door was fitted with a 40.64 Cm x 22.86 Cm (16" x 9") acryllic window. While the experiment was running, the window was covered from the inside with a black surface. The black window surface was removed during the flow visualization procedure.

The main frame was positioned in the middle of the enclosure where its 50.8 Cm x 182.88 Cm (20" x 6') side was parallel to the plane of the door. The array plane was placed perpendicular to the 50.8 Cm x 182.88 Cm (20" x 6') side of the main frame. In order to maintain a uniform radiation condition, the main frame and the inside surfaces of the enclosure were painted with a flat black paint.

3.2.6 Electrical Systems

There were two electrical systems used in this experiment, each having different functions. The purpose of the first system was to supply power to the heaters in the cylinders and to measure the power supply for each heater, Figure 3.9. The second system was used to monitor the output of the thermocouples, Figure 3.10. A regulated power supply, Model 62-121 manufactured by Dressen-Barnes Corporation, was used to supply a direct current to heat the cylinders.

Each heater was connected in a series with an ammeter, rheostate and one ohm resistance. The one ohm resistance was

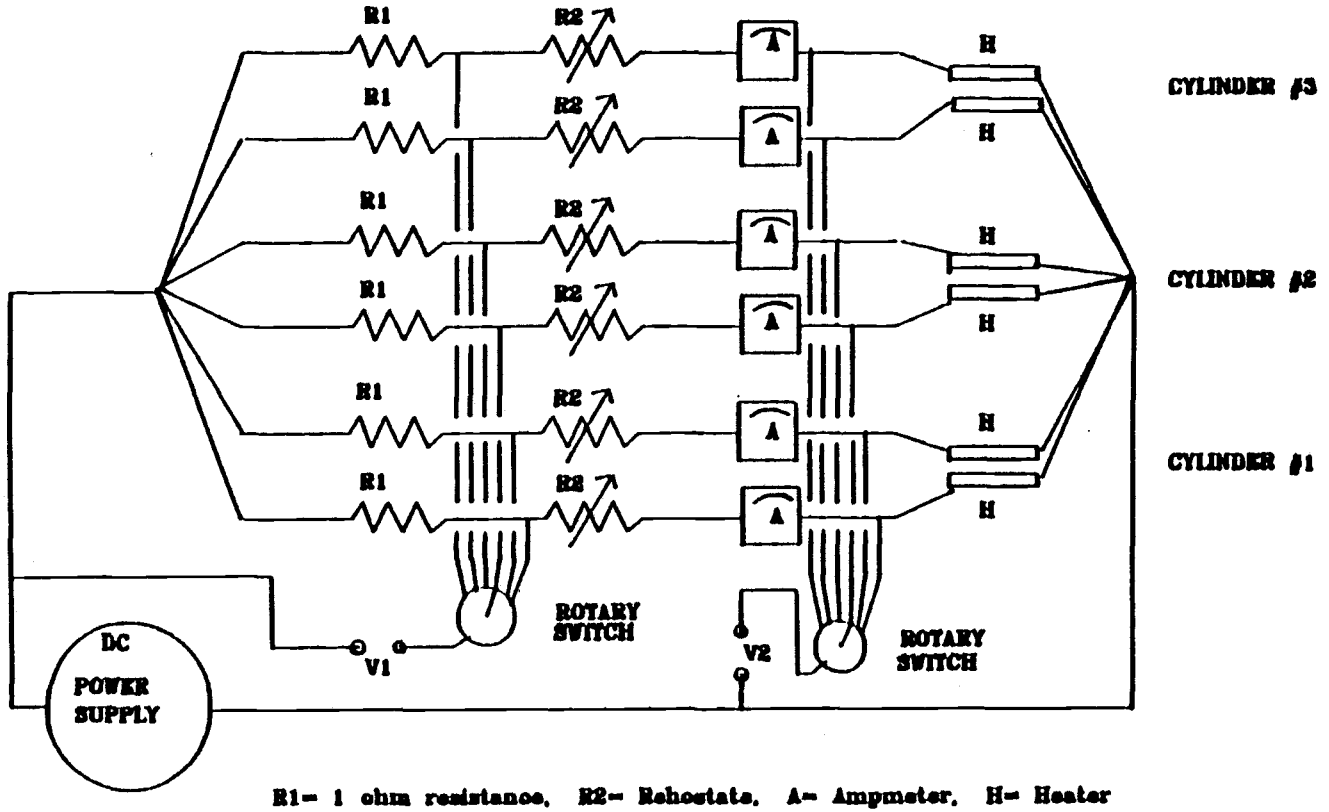

R1= 1 ohm resistance, R2= Rehostats, A= Ampmeter, H= Heater
V1= Voltage drop across R1, V2= Voltage drop across H

Figure 3.9 Power supply system.

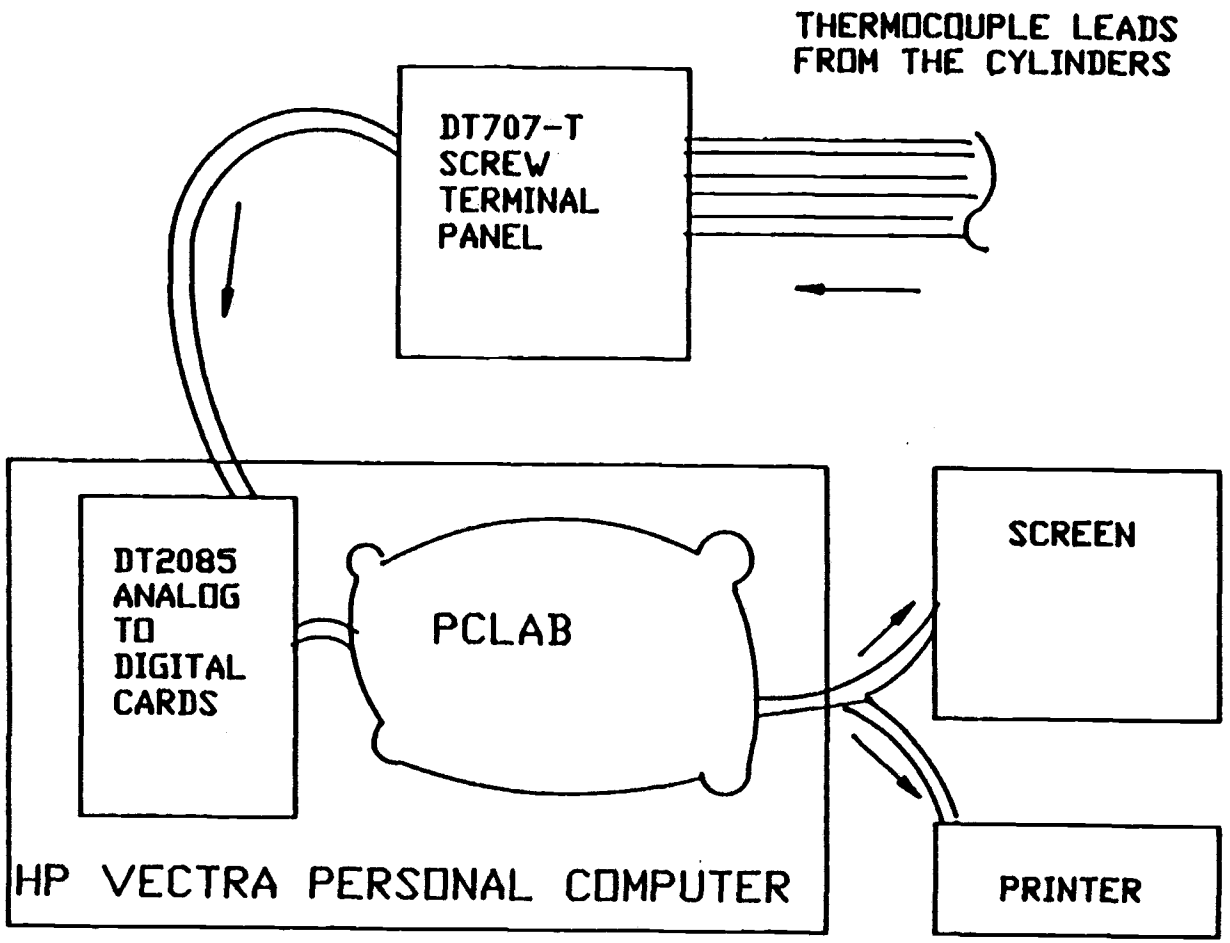

Figure 3.10 Temperature monitoring system.

used to measure the exact current through each heater by measuring the voltage drop across the resistance. Two rotary switchs with six channels for each of them, two channels for each heater, were used. At each position of the rotary switchs, two voltage terminals were activated. One terminal was used to measure the voltage drop across the one ohm resistance and the other terminal was used to measure the voltage drop across the heater. The voltage drops were measured by a Tektronix DM 5010 programmable digital multimeter and a Tektronix DM 502A autoranging DMM.

The temperature measurements were accomplished by using data acquisition boards from Data Translation, Inc., PCLab software and a Hewlett-Packard Vectra personal computer, as shown in Figure 3.10. The hardware and software were calibrated and adjusted according to the specifications in their manuals [27, 28]. The thermocouple leads were connected to DT707-T screw terminal with a cold junction compensation circuit board. When the voltage across the thermocouples were sensed by the DT707-T's barrier strip, a second cold junction thermocouple was formed. The cold junction thermocouple is the same type as the actual thermocouple, but with opposite electrical polarity, and is referenced to the ambient temperature of the DT707-T screw terminal panel. This panel has a thermocouple cold-junction compensation (CJC) circuit to determine the temperature of the DT707-T [27]. The output

signals from the DT707-T were fed into DT2085 analog-to-digital cards. These cards were installed in the Hewlett-Packard Vectra (IBM compatible) personal computer.

A computer program, as shown in Appendix A, was written to employ the PCLab subroutines. This program converts the digital voltage output from DT2085 into temperature centigrade. It prints out the average of sixteen readings for each thermocouple channel. Then it waits for twenty seconds and repeats the process.

3.3 Flow Visualization

Flow visualization was accomplished by illuminating smoke particles with laser sheets perpendicular to the cylinders' axes as shown in figure 3.11. The patterns of the flow fields were recorded on a video tape and on slides. Some modifications were made to accommodate this procedure. A 6.35 mm (1/4") wide strip of the back insulation along one of the 1.27 Cm (1/2") acryllic side walls was removed. This strip was extended vertically at the mid-width of the wall. A strip of the black paint, on the opposite side of the wall, was removed to provide a clear strip on the wall. This clear strip was used as an entrance for the horizontal laser sheet. The source of the horizontal laser sheet passed through a 6.35 mm x 5.08 Cm (1/4" x 2") slot on the 0.762 m x 2.134 m (2.5' x 7') side of the enclosure. A hole, on the same

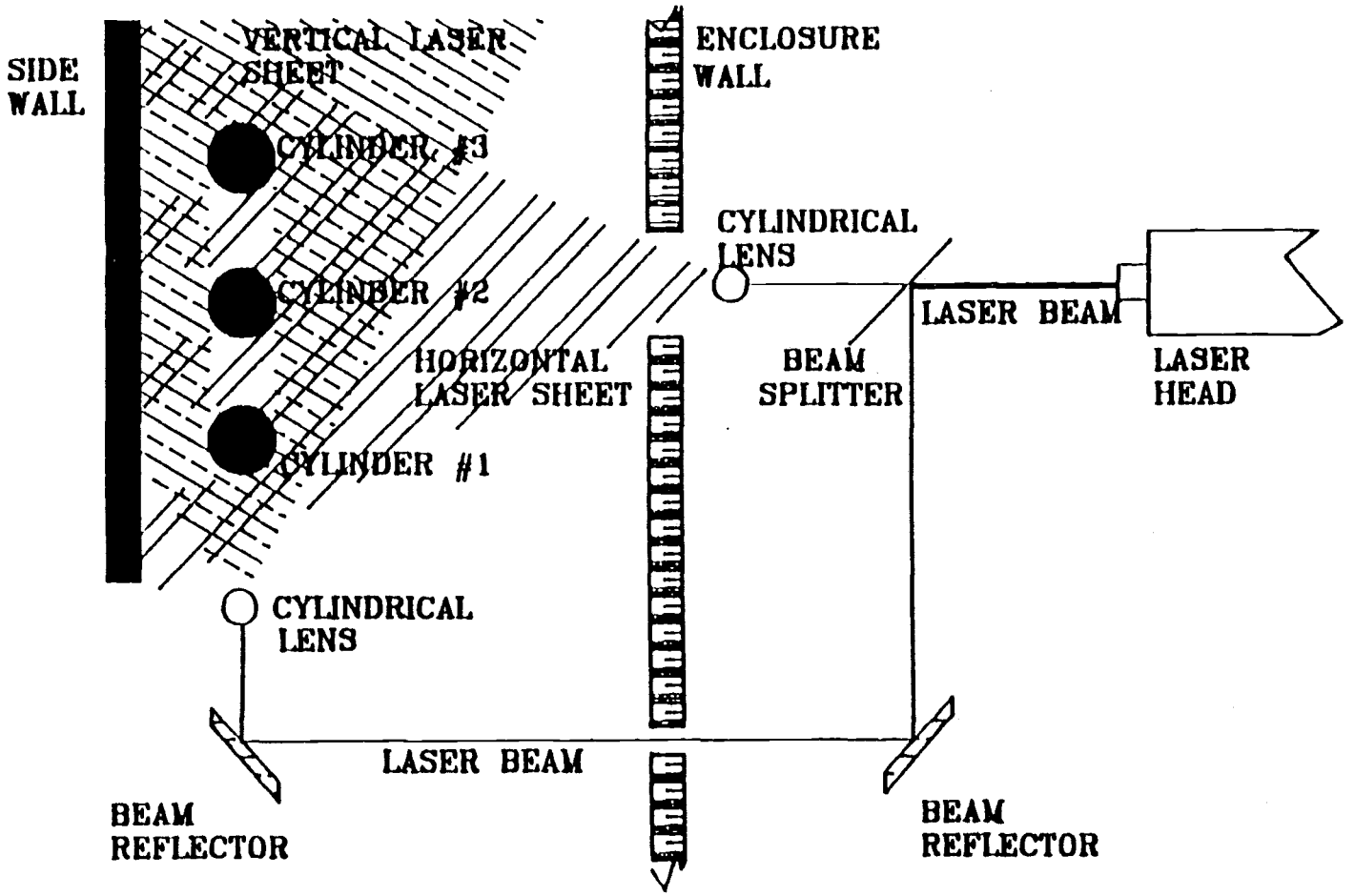

Figure 3.11 Laser illumination system.

side of the enclosure, with a 1.27Cm (1/2") diameter was made at a level 15.24 Cm (6.0 inches) below the bottom edge of the side walls of the main frame. This hole was used to pass the laser beam through to generate the vertical laser sheet.

A three-watt Argon and Krypton Ion Laser, Model 85, from Lexel Corporation, was utilized. A beam splitter, two beam reflectors and two cylindrical lenses were used to generate two laser sheets, Figure 3.11. These sheets illuminated one vertical plane at the mid-width of the array. The vertical plane, except those sections blocked out by the cylinders themselves, was illuminated by the horizontal sheet. The horizontal sheet was created from the horizontal laser beam. Therefore, a vertical laser sheet created from the vertical laser beam was used to illuminate an opaque area and to enhance the illumination of the other parts of the illuminated plane.

Figure 3.12 shows the fabricated smoke generation system designed to produce the smoke particles. This system consisted of two chambers. The core chamber was used as a burner, while the exterior chamber was employed to filter the large particles from the ashes. Tobacco was used to generate the smoke. First, the generated smoke passed through a 0.92 m (3') pipe of aluminum, which was cooled by wet cloth. This reduced the temperature of the smoke substantially. Then, the smoke was passed through a thirty-foot, thin-wall teflon hose with a 9.53 mm (3/8") diameter. At the end of this line the smoke was at

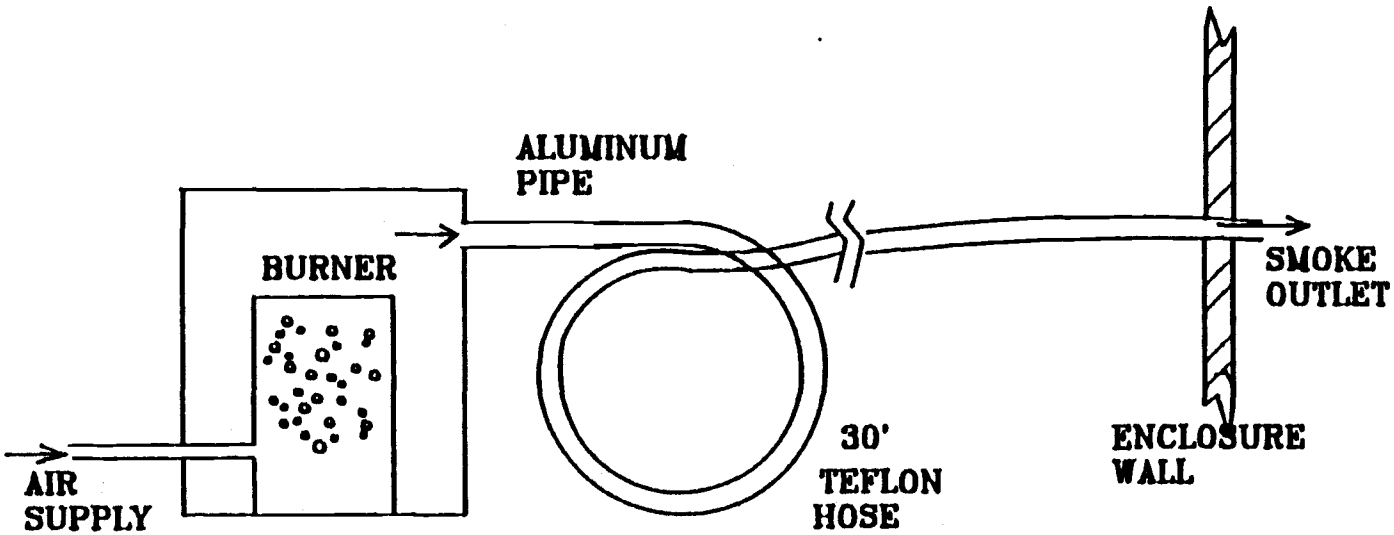

Figure 3.12 Smoke generation system.

room temperature. This system was placed outside the experimental room, but the teflon hose was passed into the room and through the wall of the enclosure.

3.4 Procedures

3.4.1 Data Collection

The aim of each experimental run was to establish a thermal equilibrium. For each set-up, the cylinders were aligned vertically by using a plumb bob. Then, the wall(s) was placed vertically at a specific wall spacing, S, by using feeler gauges and a plumb bob. This was achieved by using the adjusting screws on the main frame base. Next, the enclosure door and the testing room door were securely closed prior to beginning each experimental run and opened only at the end of each run. The power supply and rheostats were adjusted in order to supply the same power for each cylinder.

The power dissipation from each heater was calculated from

$$P = I\,V$$

where V is the voltage drop across the heater and I is the current measured from the voltage drop across the one ohm resistance. The manner in which I is measured overcomes the error in the power dissipation if it is calculated from $P = I^2 R$ or $P = V^2/R$ due to heater resistance changes when the temperature changes.

Once the power was adjusted, it was not changed until all the wall spacings results at fixed set-up (i.e., fixed center-to-center spacing, CC) were recorded. For all the set-ups, the power dissipation was adjusted to give the following heat flux: 49.338 W/m^2 , 149.014 W/m^2 , 493.38 W/m^2 , 986.762 W/m^2 , and 1480.143 W/m^2. The wall spacing settings were started from the smallest to the largest spacing. These values are shown in Table 3.1 for each case.

Table 3.1 Spacings of the cylinders and of the walls for the experiments

CC/D	Number of Cylinders	Walls	Variable wall spacing, S/D									Fixed wall spacing	Total
non	1	non	--	--	--	--	--	--	--	--	--	----	24
1.5, 2, & 4	3	1	.081	.155	.25	.50	.75	1.0	1.5	2.0	inf	----	135
1.5, 2, & 4	3	2	.50	.75	1.0	1.5	2.0	2.5	3.5	--	--	0.5	105

After the power was adjusted, the temperature monitoring program, shown in Appendix A, was started on the Hewlett-Packard computer. The program displayed the temperature readings on the screen every twenty seconds. When the variation in the average temperature was less than 0.2% for ten

minutes, steady-state conditions were considered to be established. The data were recorded one hour after the establishment of the steady-state conditions in order to accommodate the slow thermal response of the 1.27 Cm (1/2") thick acrylic wall. As shown in Table 3.1, a total of 264 experimental runs were recorded.

Since the wall thickness of the cylinder(s) is very small, 0.889 mm (0.035 inch), and the thermal conductivity of aluminum is much higher than the thermal conductivity of the air, the temperature readings of the thermocouples were considered to be the same as the temperatures of the cylinder surfaces. The difference between the two temperatures, the inner and the exterior cylinder surfaces, was found to be less than 0.0066 degrees Centigrade, as calculated from equation 3.1.

For a one-dimensional steady state heat conduction from a hollow cylinder, the total heat transfer, Q, can be represented as:

$$Q = \frac{2\,\Pi\,K_{Al}\,L\,(T_{in} - T_w)}{Ln(r_w - r_{in})} \qquad (3.1)$$

For the present case:

r_s =0.0127 m

r_{in}=0.011811m

L =0.254m

K_{AL}=204 W/m °C from [8].

Therfore, $T_w = T_{in}$- (0.000222 Q) where Q= total input power in watts.

3.4.2 Data Reduction

Once the average temperature of the cylinder(s) and the ambient temperature were recorded and the power supply was determined, the total heat transfer by convection, Q_{cv}, could be calculated from:

$$Q_{cv} = Q - Q_r - Q_{cd}$$

Q_{cd} is the conduction heat loss from the cylinders' end-caps. This heat loss was calculated from the Fourier's low as:

$$Q_{cd} = - K A \frac{dT}{dX}$$

Where dT is the temperature difference of the thermocouple readings between the inner and outer surface of the end-caps, dX is the end-caps' thickness, A_c is the end cap cross section area, and K is the thermal conductivity of the end-caps' material (K = 0.0023 w/m °C). The maximum heat loss by conduction was about .02 % of the total input power. This occurred when the total input power, Q, was equal to 30 watts at center-to-center spacing, CC = 1.5 D, and wall spacing ratio, S/D = 0.081 .

The radiation heat loss, Q_r, ranged from 6% to 8% of the total

input power for no wall cases and from 4% to 7% of the total input power for both single and double wall cases. Since the cylinders were polished to mirror-like surfaces, the emisivity was considered equal to 0.05, [8, 22, 5, 16]. Appendix B shows the methods that were used to calculate the view factors and the heat loss by radiation from a free cylinder (within an infinite medium), from an array of cylinders without walls, and from an array of cylinders with wall(s).

Once the convection heat transfer, Q_{cv}, was determined, the average heat transfer coefficient was obtained from:

$$h = \frac{Q_{cv}}{A\,(T_w - T_{inf})}$$

Then the average Nusselt number, Nu, was determined from:

$$Nu = \frac{h\,D}{K} = \frac{Q_{cv}\,D}{A\;K\;(T_w - T_{inf})} \qquad (3.2)$$

For correlating the data, the modified Grashof number was calculated from:

$$Gr^* = \frac{G\,\beta\,\rho^2 \left(\frac{Q_{cv}}{A}\right) D^4}{K^2\;\mu^2} \qquad (3.3)$$

The modified Rayleigh number was calculated from:

$$Ra^* = Gr^* Pr = \frac{G \beta \rho^2 C_P \left(\frac{Q_{cv}}{A}\right) D^4}{K^2 \mu} \qquad (3.4)$$

All the air properties were calculated at the film temperature, $T_f=(T_w+T_{inf})/2$ from the following equations:

(1) The density was calculated by considering the air as an ideal gas:

$$\rho = \frac{p}{R_g T} = () \text{ Kg/m3} \qquad (3.5)$$

where p is the atmospheric pressure and R_g is the gas constant.

(2) The thermal conductivity was calculated from the following equation which is recommended for temperatures up to 550 degrees C, [29]:

$$K = \frac{0.6325 \times 10^{-5} \; T^{0.5}}{\left[1.0 + \left(\frac{245.}{T}\right) \times 10^{-\left(\frac{12}{T}\right)}\right]} \left(\frac{360.}{0.86042}\right) \qquad (3.6)$$

K=() W/m.K

(3) The specific heat of the air was calculated from equation 3.7. This equation is valid for a temperature between 260 degrees K and 610 degrees K, [30]:

$$C_p=(0.249679-7.55179\times10^{-5}\ T+\ 1.69194\times10^{-7}\ T^2 - 6.46128\times10^{-11}\ T^3)\ \ 1.162\ \ =\ ()\ \ W\ Hr/(Kg\ K) \qquad (3.7)$$

(4) The coefficient of thermal expansion, β, was calculated as:

$$\beta = \frac{1}{T_{inf}} =() \quad K^{-1} \qquad (3.8)$$

(5) Hilsenrath et. al. [31] show that the viscosity of the air, μ , at atmospheric pressure can be calculated from:

$$\mu = \frac{145.8\ T^{(3/2)}}{(T+110.4)}\ (360.0\times10^{-7}) = ()\ Kg/m\ Hr \qquad (3.9)$$

Equations 3.5 through 3.9 were implemented as a subroutine in the data reduction program, shown in Appendix C.

3.4.3 Uncertainty

The uncertainty in the Nusselt number was calculated as shown in Appendix D. It was found that there is a maximum of 5.0% uncertainty in the calculated Nusselt number from the experimental results.

CHAPTER 4

SINGLE WALL: RESULTS AND DISCUSSION

The results of the heat transfer experiments and the correlation equation for the Nusselt number for an isolated single cylinder will be discussed at the beginning of this chapter. Following will be a discussion of the experimental results for a three cylinders array with a single wall. The correlation equation representing the heat transfer coefficient in a known dimensionless form (i.e. Nu) will be discussed for the three cylinders' array with a single wall case at the end of this chapter.

4.1 Free Single Cylinder

The three cylinders that were used in the array were tested separately as isolated single cylinders in an infinite expanded medium (the surrounding air). The data were collected for each cylinder for eight different heat flux conditions. These conditions were as follows: 49.338 w/m^2, 149.014 w/m^2, 197.352 w/m^2, 493.38 w/m^2, 789.41 w/m^2, 986.762 w/m^2, 1480.143 w/m^2, and 1973.525 w/m^2. There were two primary reasons to study the free single cylinder case. First, it was necessary to verify the data-taking process and to check the related equipment setup. This was accomplished by comparing the Nusselt number from

this experimnent with the available data in the literature. The second reason was to find a correlation equation to represent the average Nusselt number for a single free cylinder, Nu_S, as a function of the modified Rayleigh number, Ra^* . This equation would serve as the datum from which the heat transfer in the other cases would be considered enhanced or degraded.

Figure 4.1 shows the average Nusselt number for each cylinder versus the modified Rayleigh number for the eight heat flux values. The functional relationship between Nu_s and Ra^* for these data is shown in equation 4.1:

$$Nu_s = 0.571\ Ra^{*0.2027} \qquad 3x10^4 < Ra^* < 10^6 \qquad (4.1)$$

The r^2 , defined as the percentage of the variability in the dependent variable which is explained by the independent variable, for equation 4.1 is 99%. The solid line in figure 4.1 represents equation 4.1, while the dashed line represents equation 4.2 which is the correlation equation of Dyer [10].

$$Nu_s = 0.6\ Ra^{*0.2} \qquad 10^4 < Ra^* < 10^6 \qquad (4.2)$$

Equation 4.1 lies about 1.6% below Dyer's equation. Equation 4.1 also agrees with the scale analysis results in Chapter 1 where Nu is in the order of $Ra^{*0.2}$ as shown in equation 1.9.

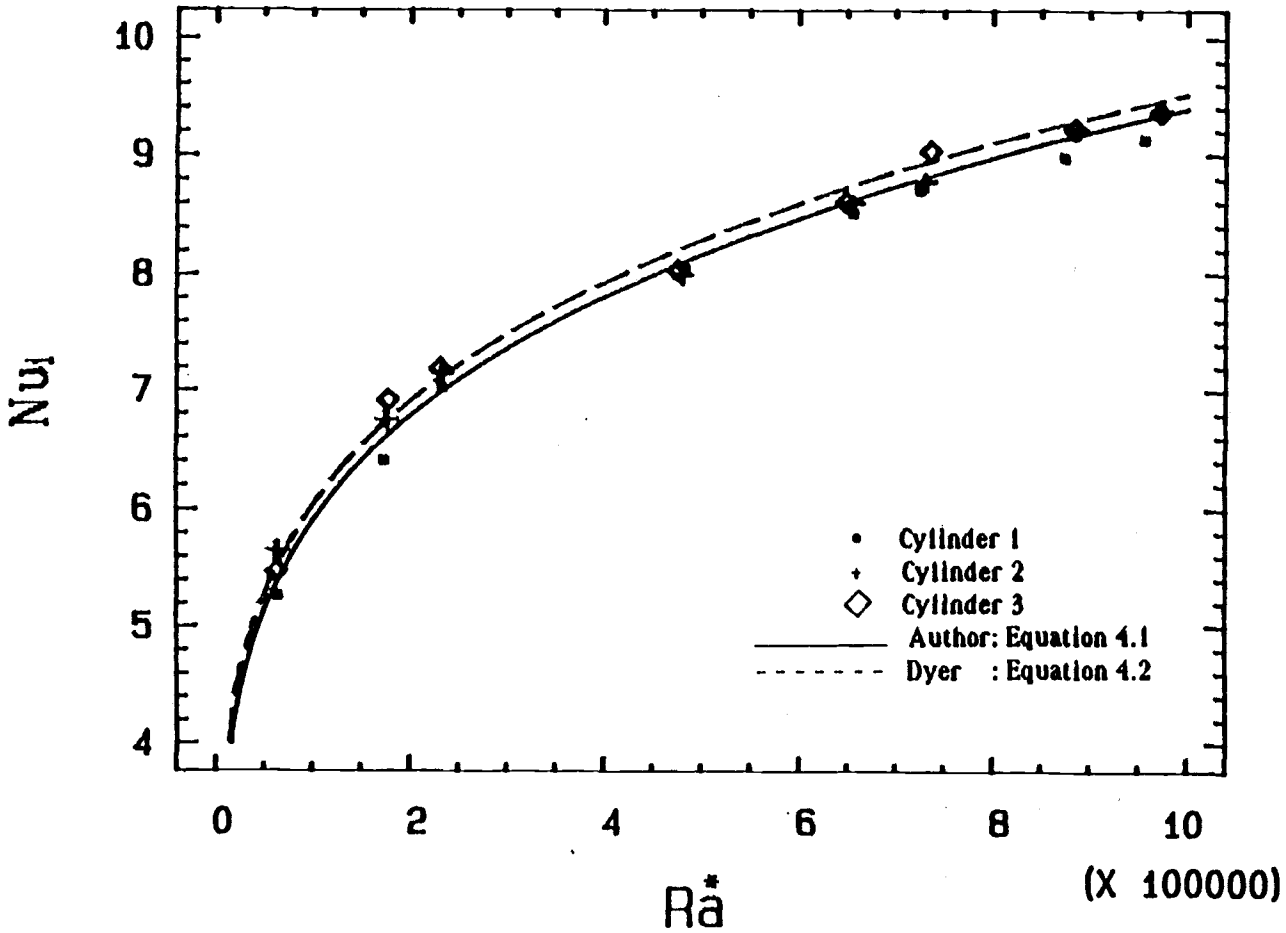

Figure 4.1 Nusselt number, Nu_i, versus Ra^* for a free single cylinder.

4.2 Temperature distribution along the array with various wall spacings:

The data are presented as the normalized temperature, ø, which is defined as the ratio of excess temperature from the ambient temperature for each cylinder divided by the excess temperature from the bottom temperature, as shown in equation 4.3 .

$$\phi = \frac{T_{w,i} - T_{inf}}{T_{w,1} - T_{inf}} \qquad (4.3)$$

These data are shown in Figures 4.2 through 4.6. Each figure shows the data for constant heat flux and for the three center-to-center spacings, CC, of the array. These values are shown in each figure.

In these figures the normalized temperatures, ø, for CC = 1.5D and CC = 2D have a fixed pattern where the highest cylinder always has a higher normalized temperature than the second cylinder. In both cases the normalized temperatures are greater than one. This indicates that the upper cylinders, numbers 2 and 3, are at a temperature higher than that of the lowest cylinder in the array. This increase in cylinder temperature for cylinders higher in the array is attributed to the balance between the temperature increase of the surrounding air of the upper cylinders and the increase of the plume velocity due to the density change from adding heat from the lower cylinders to the

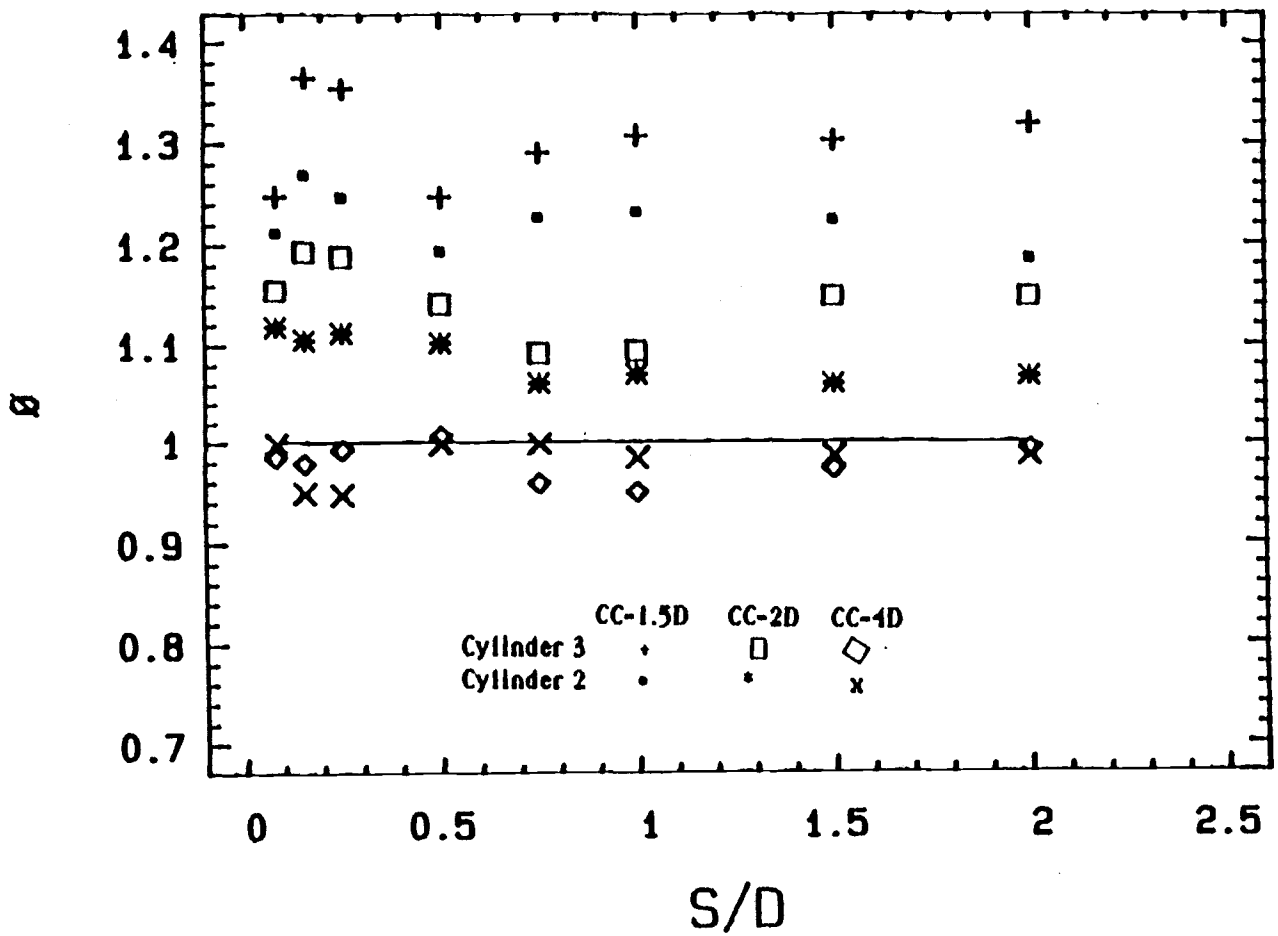

Figure 4.2 The effect of wall spacing on the normalized temperature at q= 49.338W/m^2.

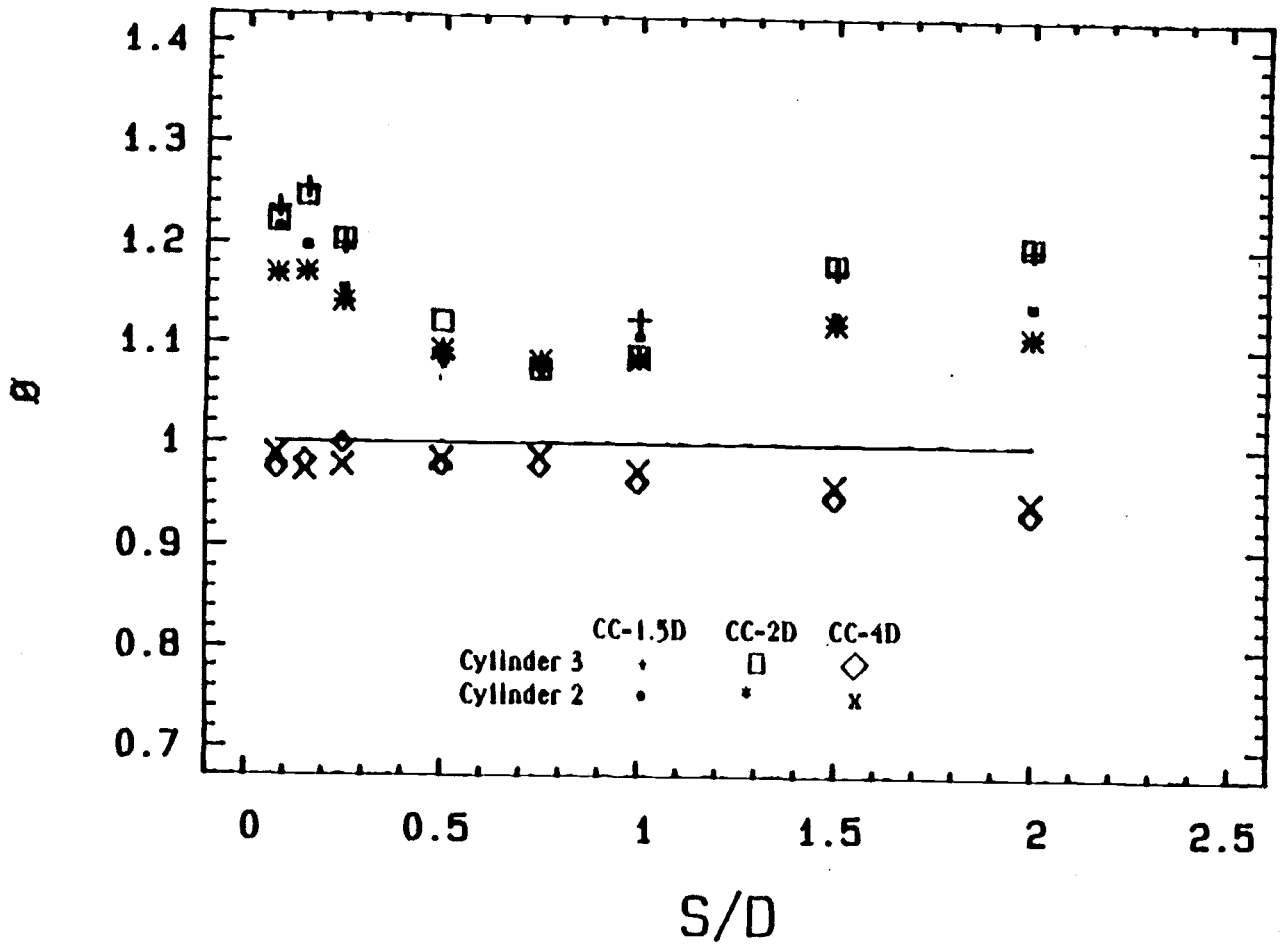

Figure 4.3 The effect of wall spacing on the normalized temperature at q= 149.014 W/m^2.

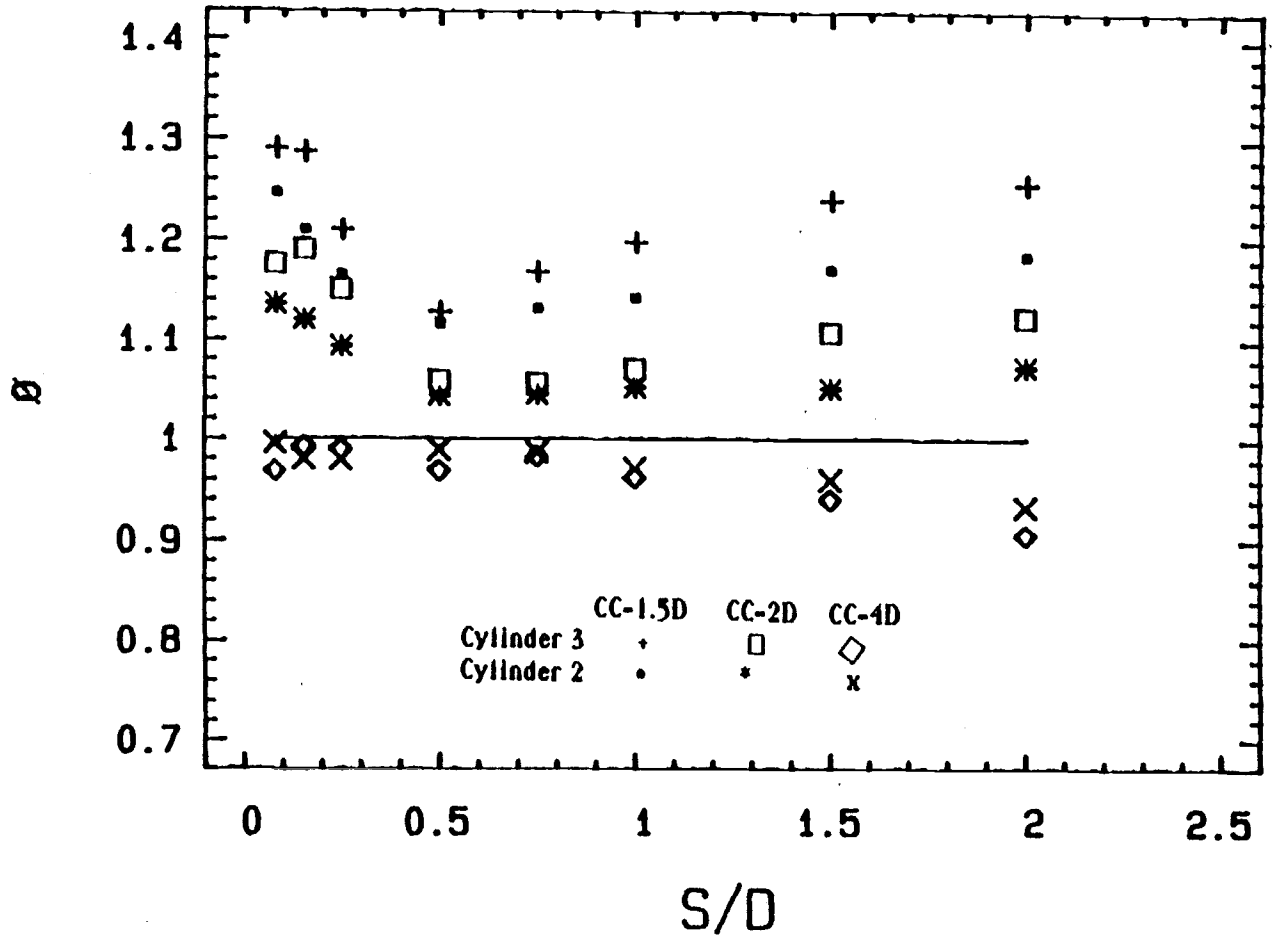

Figure 4.4 The effect of wall spacing on the normalized temperature at q= 493.380 W/m^2.

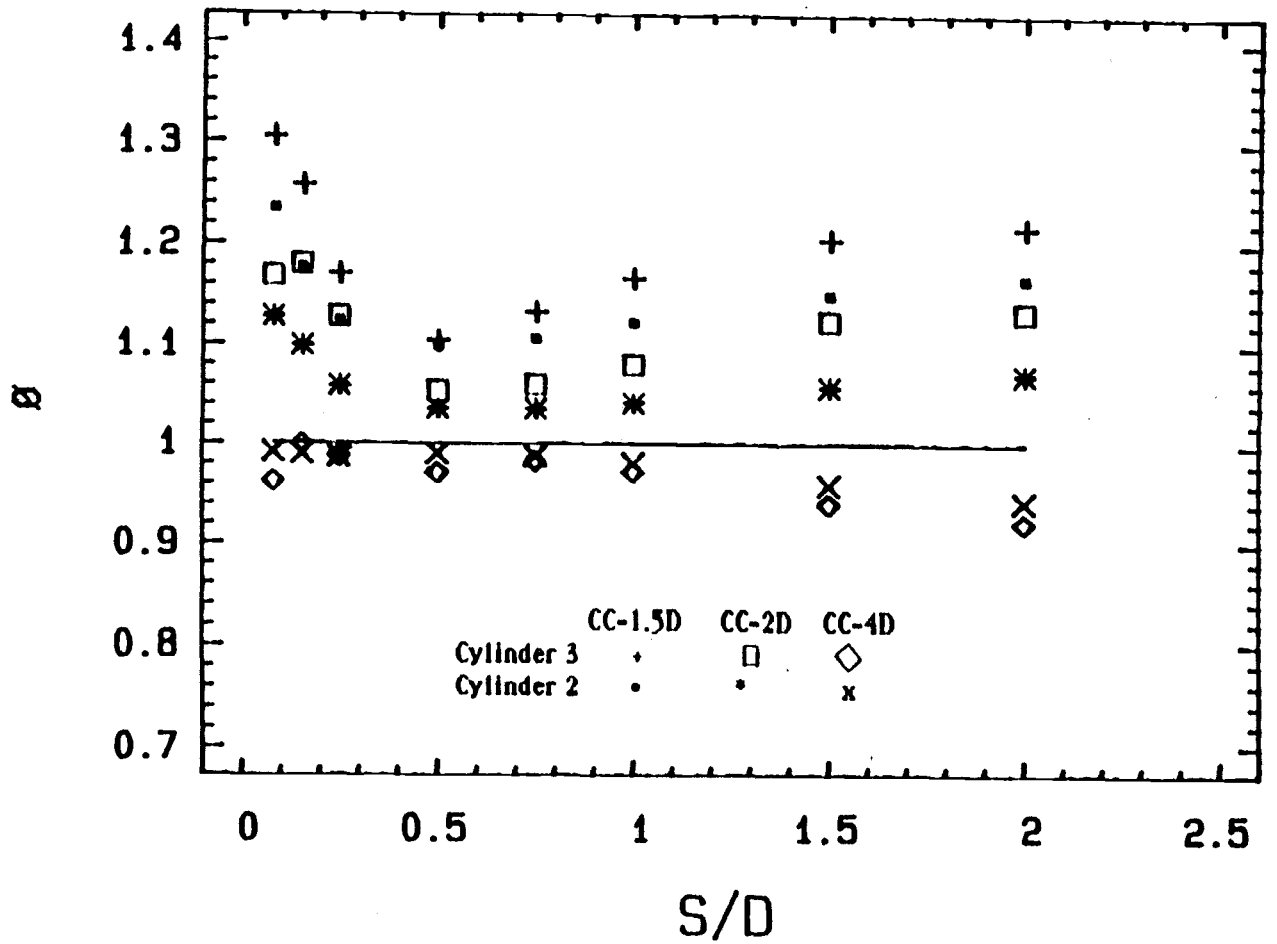

Figure 4.5 The effect of wall spacing on the normalized temperature at q= 986.762 W/m^2.

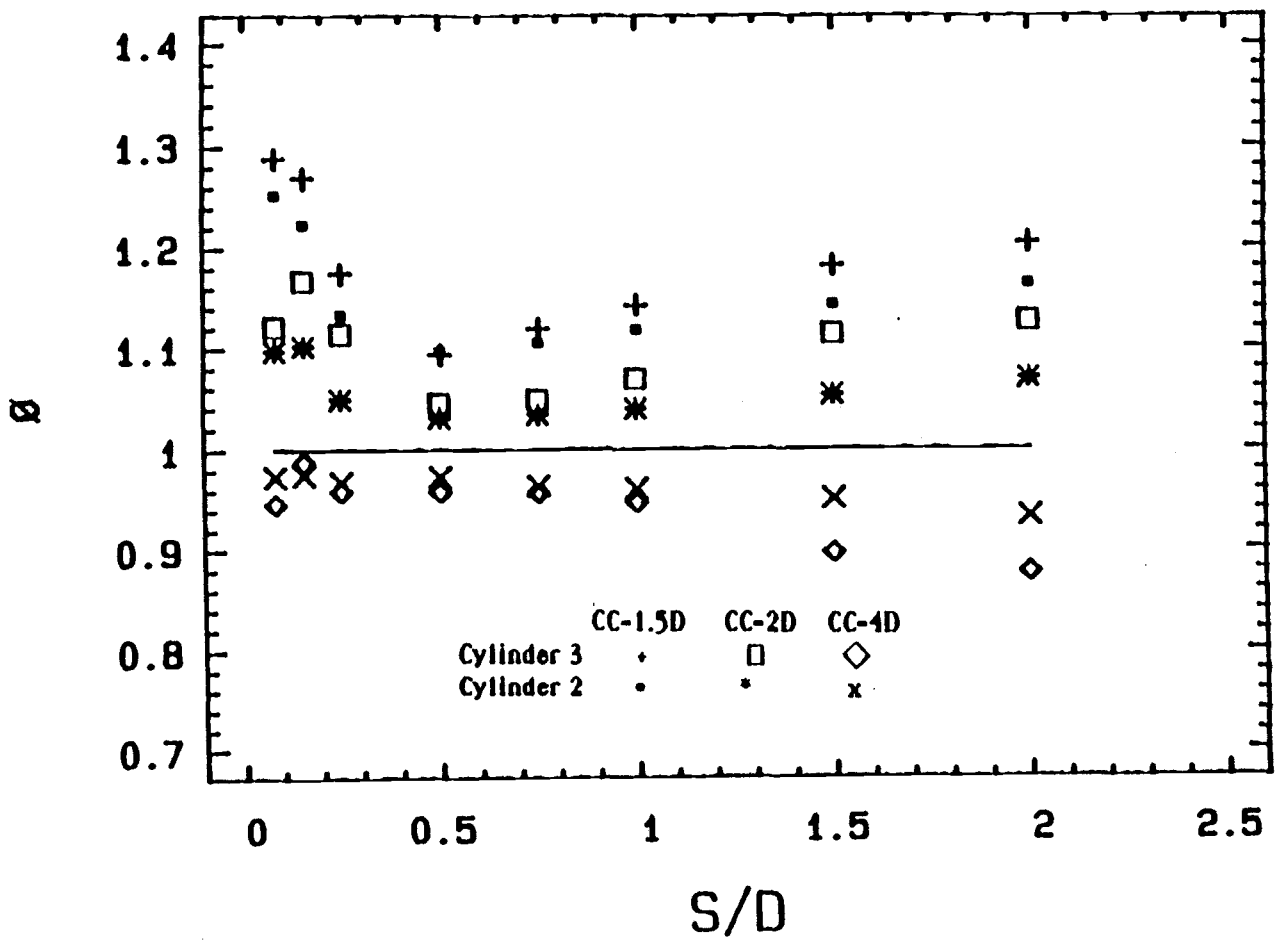

Figure 4.6 The effect of wall spacing on the normalized temperature at q= 1480.143 W/m^2.

plume [13,18 and 19].

The cylinders are more sensitive to the wall spacing ratio, S/D, at a higher input power than at a lower input power. At the higher input power, the normalized temperature data for CC = 1.5 D and CC = 2D decreases sharply as the S/D increases from 0.081 to S/D = 0.5. Then the normalized temperature increases as S/D increases from 0.5 to 2.0, and attempts to reach the value of ϕ when S/D is infinity. This can be observed by comparing Figures 4.2 to 4.6 with Figure 4.7. Also, at S/D = 0.5, the normalized excess temperature difference between cylinders 2 and 3 is very small and sometimes reaches zero. This indicates that the behavior of these cylinders is the same at wall spacing ratio, S/D = 0.5. As the wall spacing ratio diverts from S/D = 0.5, in either direction, the value of $(\phi_3 - \phi_2)$ increases.

For CC = 4D, the normalized excess temperature, ϕ , is less than one for both cylinders (cylinders 2 and 3). The behavior of these cylinders was not consistent. In general, the maximum difference between the normalized excess temperatures for cylinders 2 and 3 is less than 0.03% from that of the lowest cylinder, where q_1= 49.338 w/m^2. This indicates that the upper cylinders attain a lower temperature than the lowest cylinder. This condition was also reported by Marsters [13], Marsters et. al. [18], and by Lieberman et. al. [12]. At higher input power than q_1 and at S/D < 1.0, this difference, $(\phi_3 - \phi_2)$, reaches zero. This indicates that both cylinders 2 and 3 behave in the same manner.

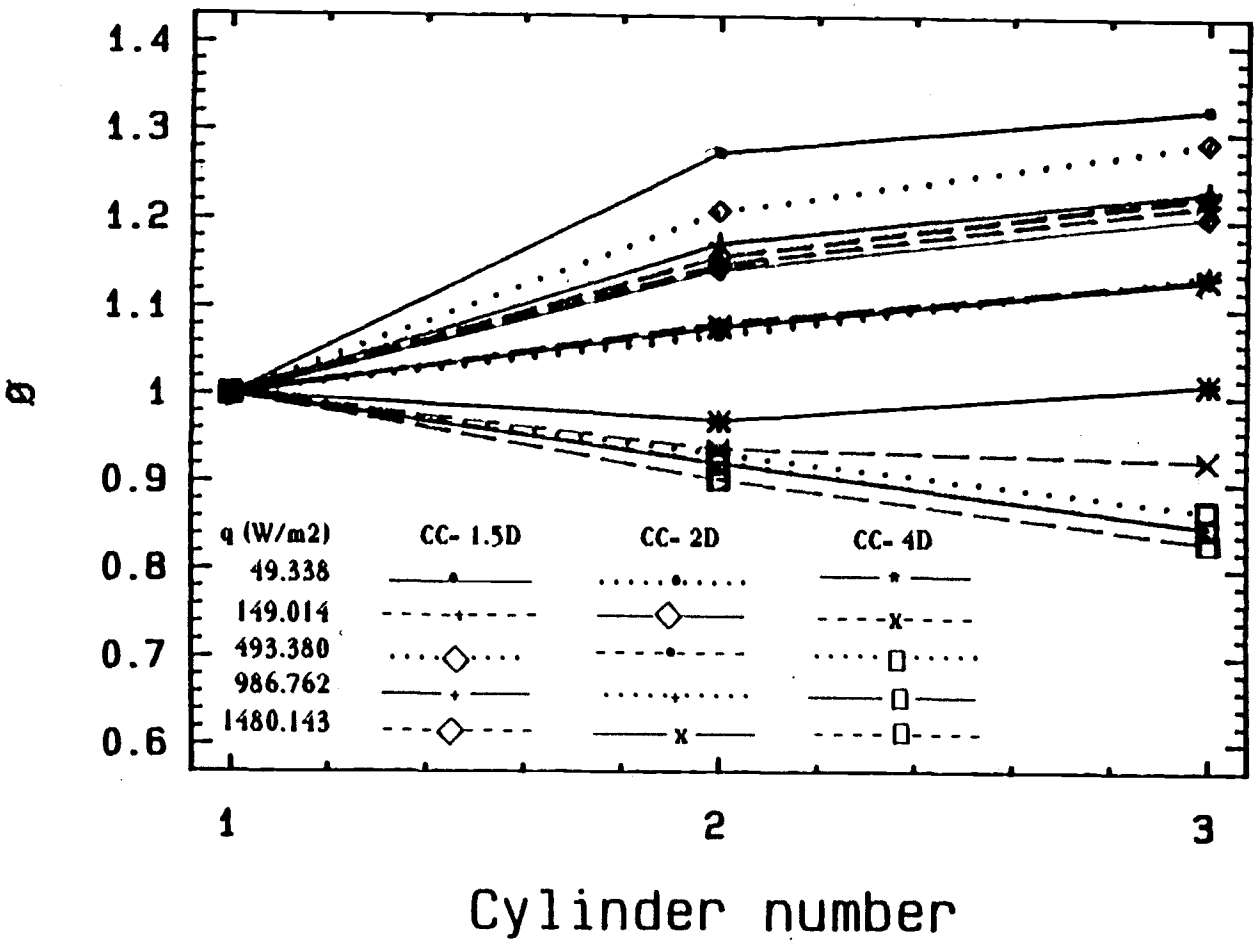

Figure 4.7 The effect of cylinder's position in the array on the normalized temperature , ø, at S/D= infinity (no wall condition) .

The dropoff in the normalized temperature is minimal and almost constant for S/D < 1.0, but the dropoff increases as S/D increases above 1.0. In all the cases (CC = 1.5 D, CC = 2D, and CC = 4D), the upper cylinders behave more like the lowest cylinder at S/D ~ 0.5.

4.3 Heat Transfer Coefficient Results

The heat transfer capability of each cylinder is characterized by its Nusselt number. At the beginning of this section, the effect of the wall spacing on the results of the lowest cylinder, cylinder 1, will be compared to the Nusselt number of a free single cylinder. Then the results of all the cylinders for all the cases (CC = 1.5 D, 2D, and 4D) will be presented and compared to the case where there is no wall, S/D = infinity .

4.3.1 The effect of the wall spacing on the lowest cylinder of the array

The Nusselt number versus the modified Rayleigh number for the lowest cylinder at different wall spacings was plotted on Figures 4.8 to 4.10. Also the Nusselt numbers from equation 4.1 for a free single cylinder were superimposed on these figures. In all the cases, the Nu_1 values at S/D = 0.5 lie higher than the values for the free cylinder. This enhancement in Nu is very

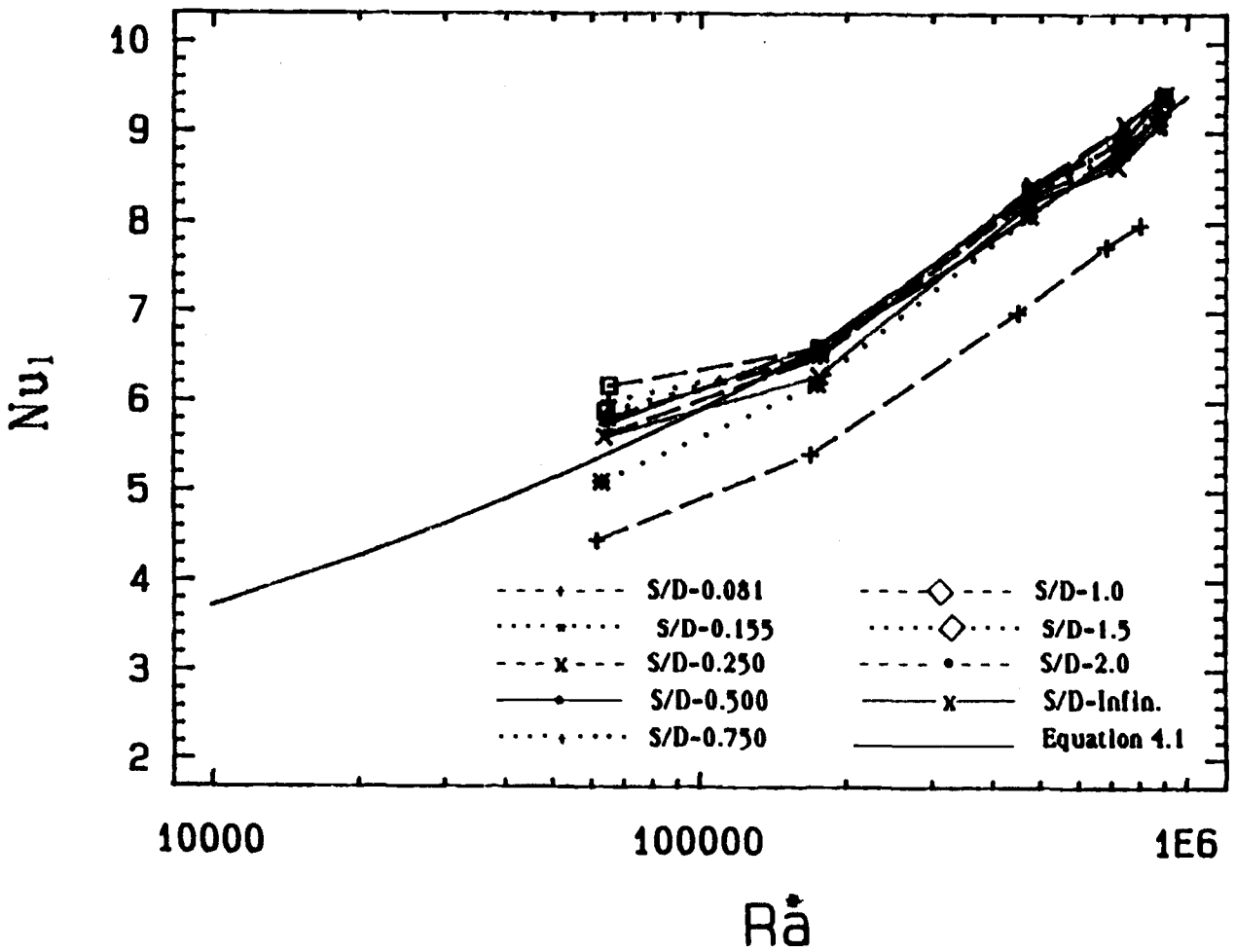

Figure 4.8 The average Nusselt number of the lowest cylinder, Nu_1, versus Ra^*, at CC=1.5D.

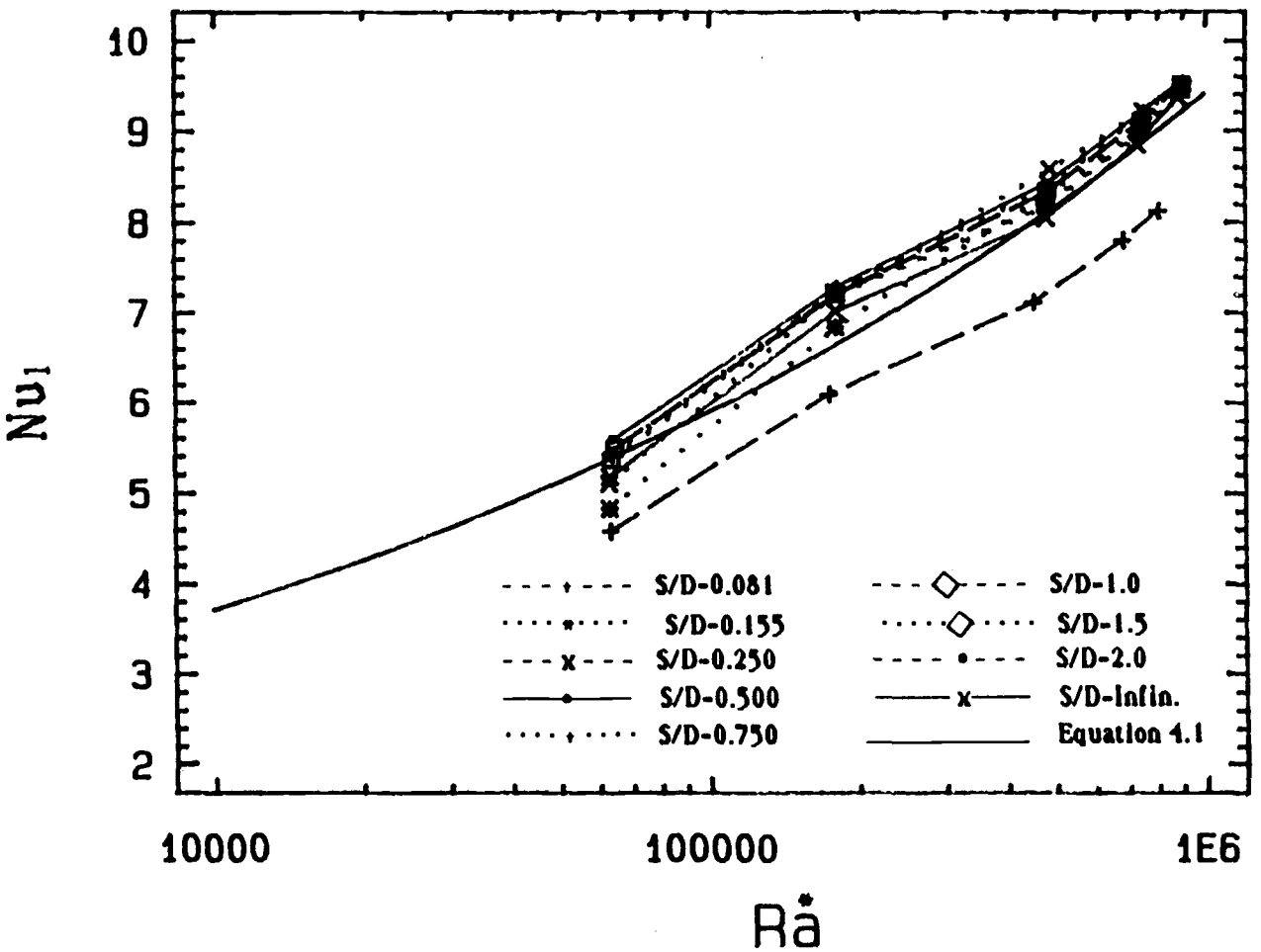

Figure 4.9 The average Nusselt number of the lowest cylinder, Nu_1, versus Ra^*, at CC=2D.

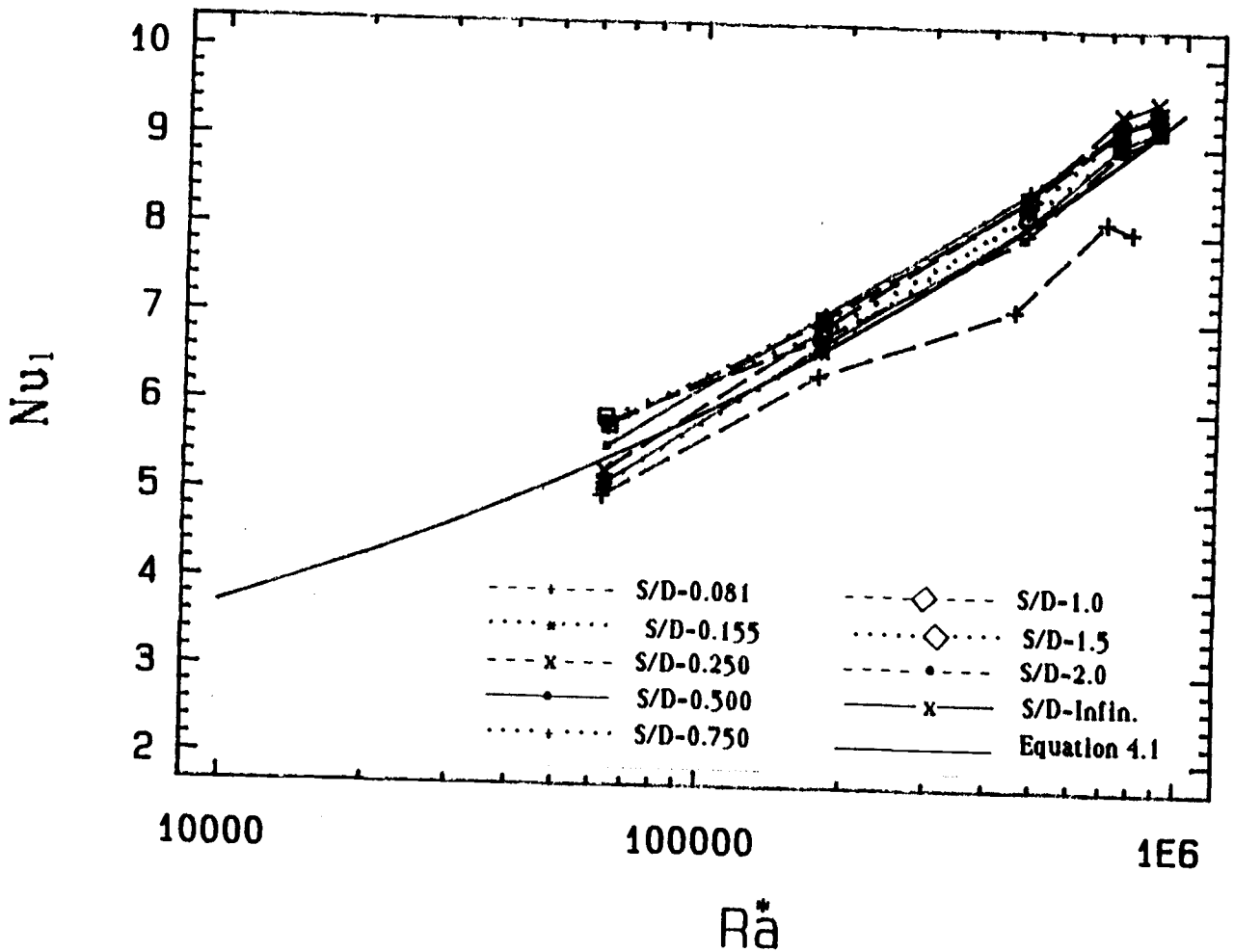

Figure 4.10 The average Nusselt number of the lowest cylinder, Nu_1, versus Ra^*, at CC=4D.

small. It is about 5% maximum. For the rest of the values of the wall spacing, with the exception of S/D = 0.081, the Nu_1 values lie between S/D = 0.5 and the values of the free cylinder. The maximum percentage of the Nu_1 enhancement is less than the uncertainty in the values of Nu. Therefore, the effect of the wall spacing, where S/D > 0.155, on the lowest cylinder is minimal and the lowest cylinder can be regarded as a free single cylinder.

The Nusselt number at S/D = 0.081 is degraded from that of the free cylinder by 10 to 12% for CC = 1.5 D and 2D and by 0.03 to 10% for CC = 4D. From these plots (Figures 4.8 - 4.10), it can be seen that there is a degradation in Nu_1 as S/D increases from 0.5 to infinity where the Nu_1 values reach the free single cylinder values. This is also shown in Figures 4.11, 4.12 and 4.13 where Nu_i versus Ra^* were plotted for all the cylinders at S/D = infinity. When equation 4.1 is superimposed on these figures, it becomes apparent that the lowest cylinder in a free array (i.e., S/D = infinity) behaves the same as a free single cylinder and it is not affected by the presence of the cylinders above it. This fact was also reported by Marsters [13], Marsters et. al. [18], and Tokura et. al. [19]. The presence of the lowest cylinder degrades the Nusselt number for the cylinders above it at the small center-to-center spacings, CC = 1.5 D and CC = 2D. On the other hand, at CC = 4D, the presence of the lowest cylinder enhances the Nusselt number for cylinders 2 and 3. At CC = 4D, the plume has the opportunity to blend with the surrounding air particles and reach

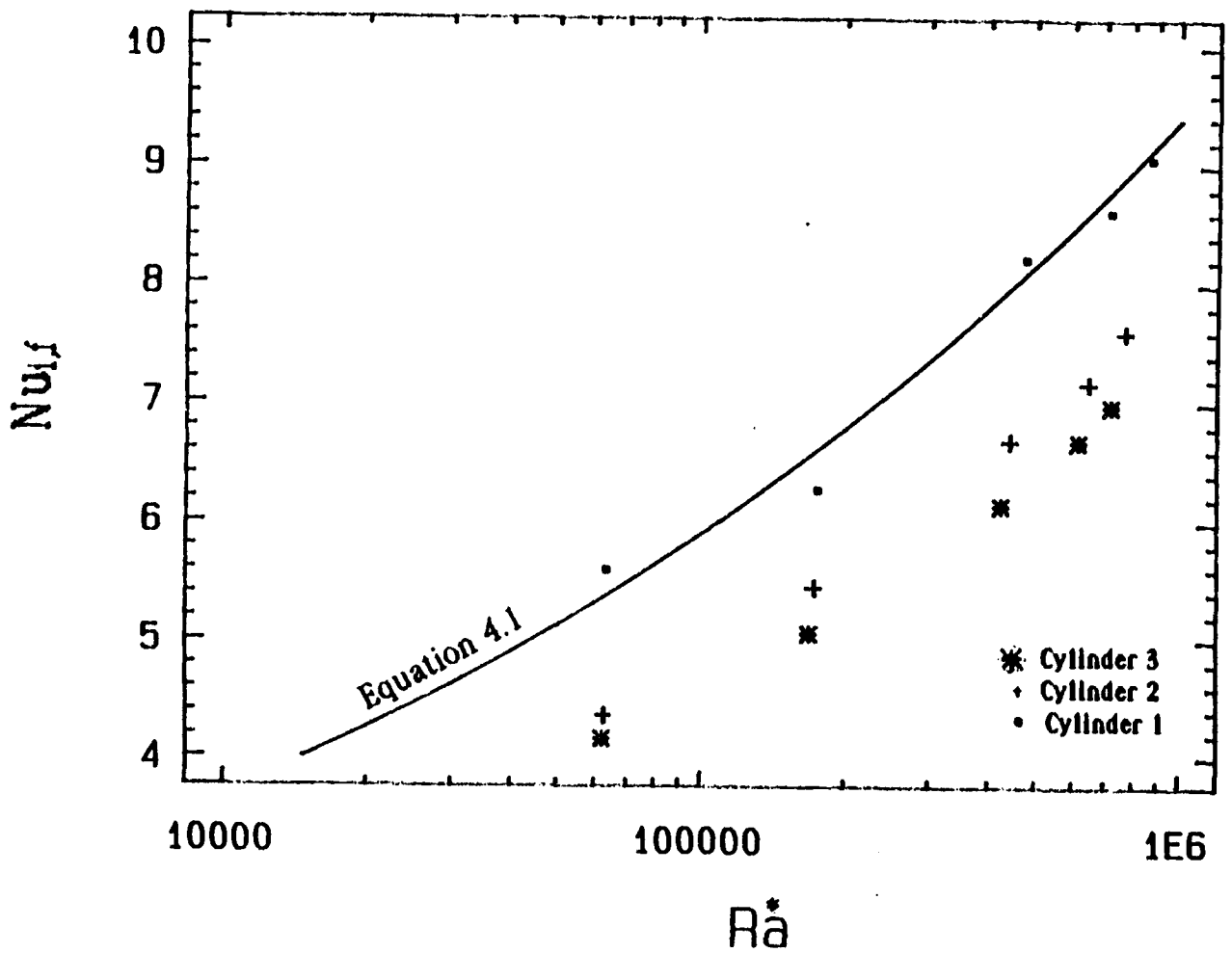

Figure 4.11 The average Nusselt number for the array's cylinders without a wall, $Nu_{i,f}$, Vs. Ra^* at CC=1.5D .

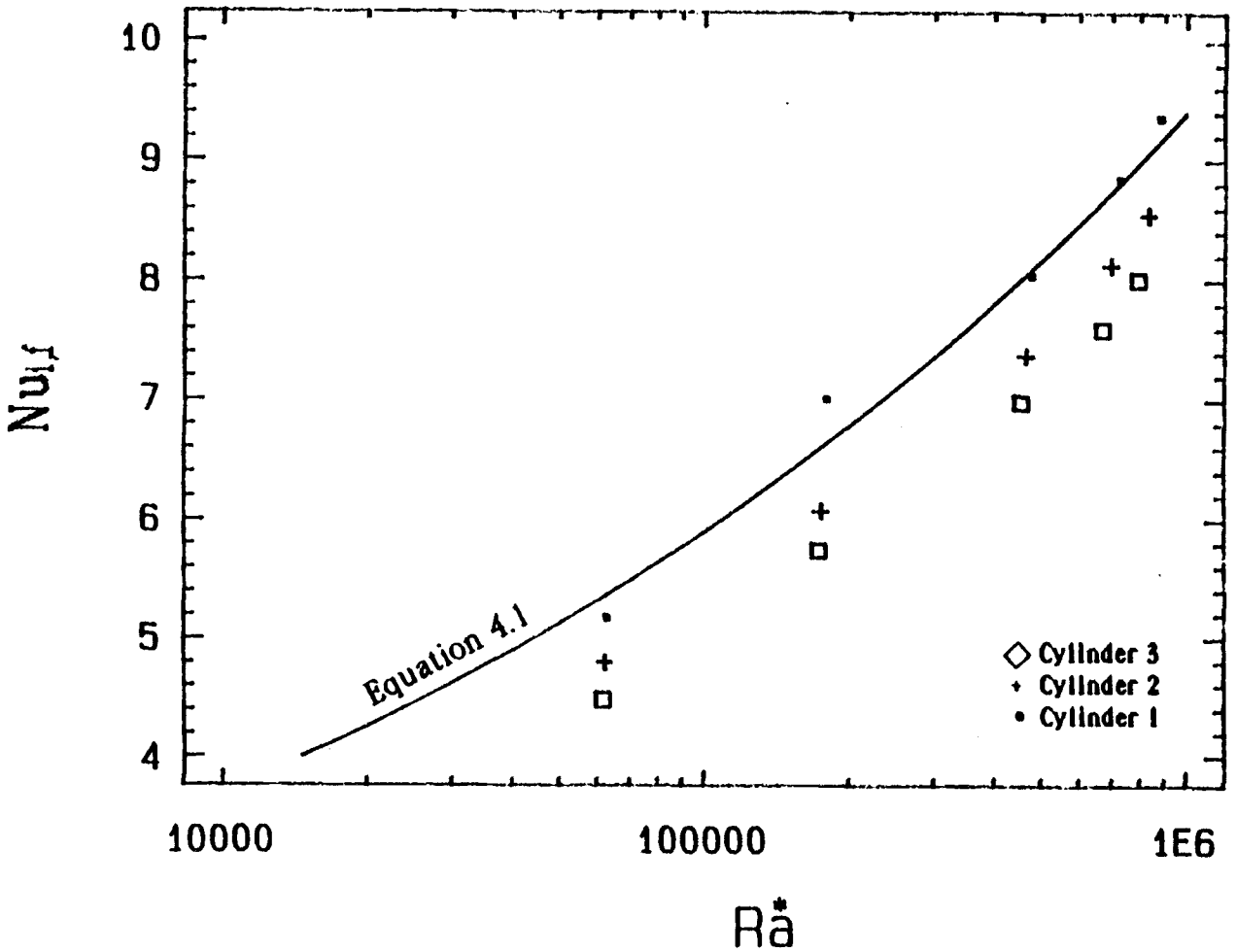

Figure 4.12 The average Nusselt number for the array's cylinders without a wall, $Nu_{i,f}$, Vs. Ra^* at CC=2D .

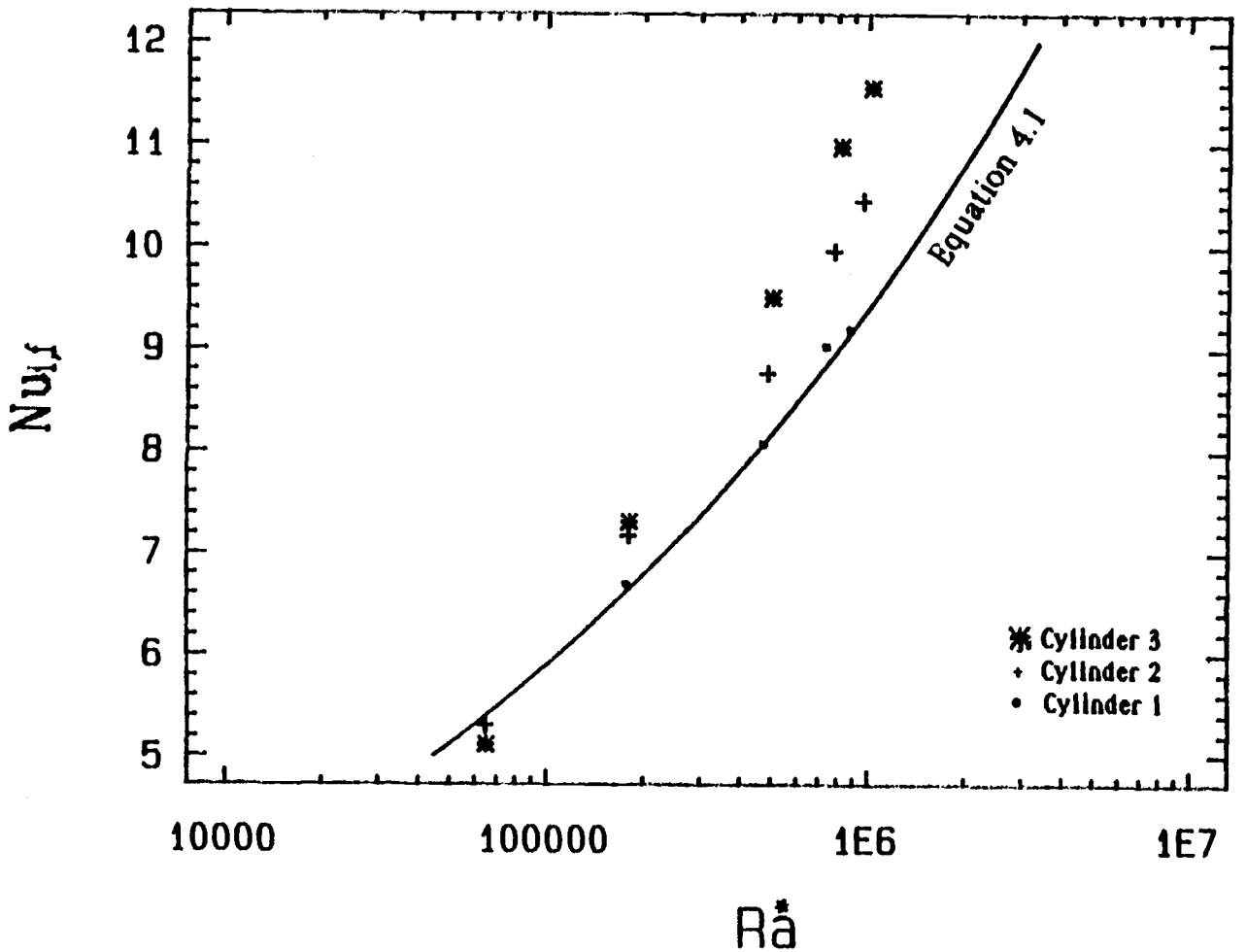

Figure 4.13 The average Nusselt number for the array's cylinders without a wall, $Nu_{j,f}$, Vs. Ra^* at CC=4D .

the upper cylinder(s) at a temperature lower than that when CC = 1.5 D or CC = 2D.

The enhancement of the upper cylinder(s) Nusselt numbers were noticed by Marster [13] and Tokura et. al. [19]. For the three cylinder array without a wall, Marsters showed that the enhancement in Nu starts at CC > 4D, and for CC = 4D, the Nu is almost the same as for the free cylinder. Tokura et. al. showed that Nu for the upper cylinder(s) is higher than that of the lowest cylinder when CC = 3D.

4.3.2 The Effect of the wall spacing on the heat transfer from the cylinders of the array

The Nusselt numbers versus S/D, for all the cases and for every cylinder, at specific heat flux are plotted in Figures 4.14 through 4.19. At CC = 1.5 D and CC=2D, the Nusselt numbers for the upper cylinders, cylinders 2 and 3, increase rapidly as S/D increases from 0.081 to 0.5. Then as the S/D values increase, the Nu values decrease and approach the Nu values for the no wall case. The degradation in the Nu values for the third cylinder is greater than that for the second cylinder. In both cases, CC = 1.5D and CC = 2D, the Nu values degraded as the cylinder position becomes higher in the array. This degradation reaches its minimum at S/D = 0.5, where Nu values for cylinders 2 and 3 are almost the same and are closest to the Nu values for the lowest

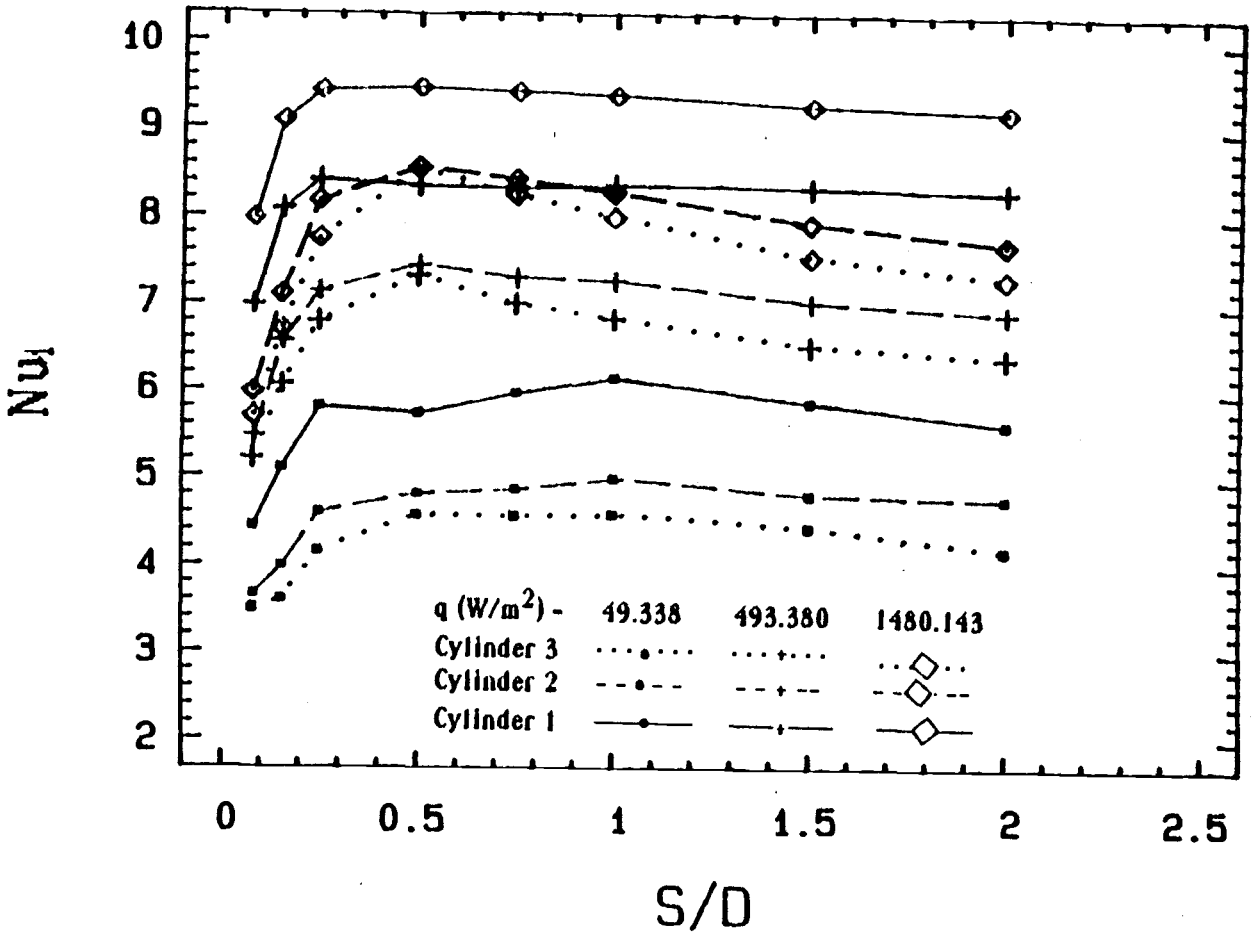

Figure 4.14 The effect of the wall spacing on the average Nusselt number of each cylinder, Nu_j , at CC=1.5D .

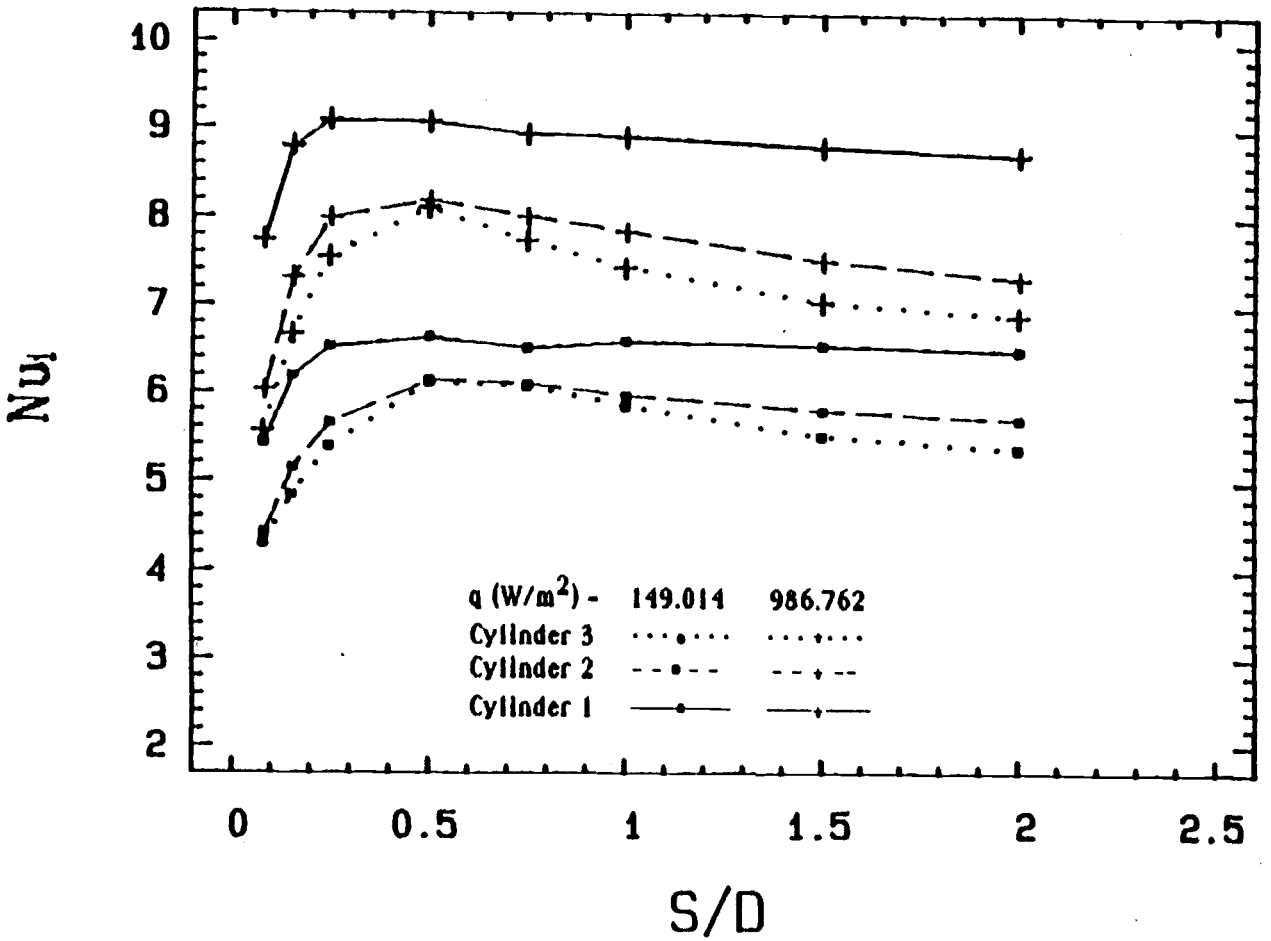

Figure 4.15 The effect of the wall spacing on the average Nusselt number of each cylinder, Nu_i , at CC=1.5D .

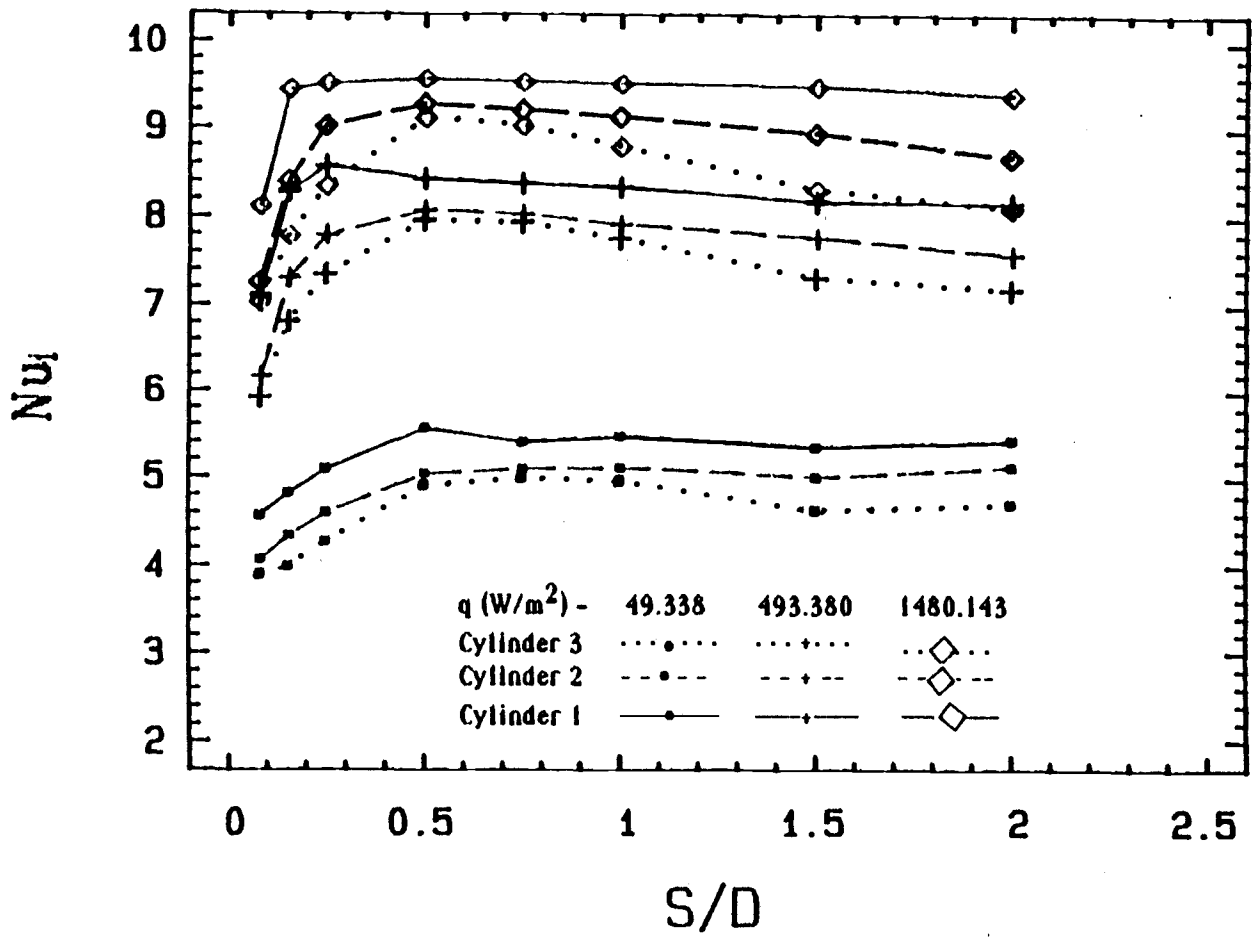

Figure 4.16 The effect of the wall spacing on the average Nusselt number of each cylinder, Nu_i , at CC=2D .

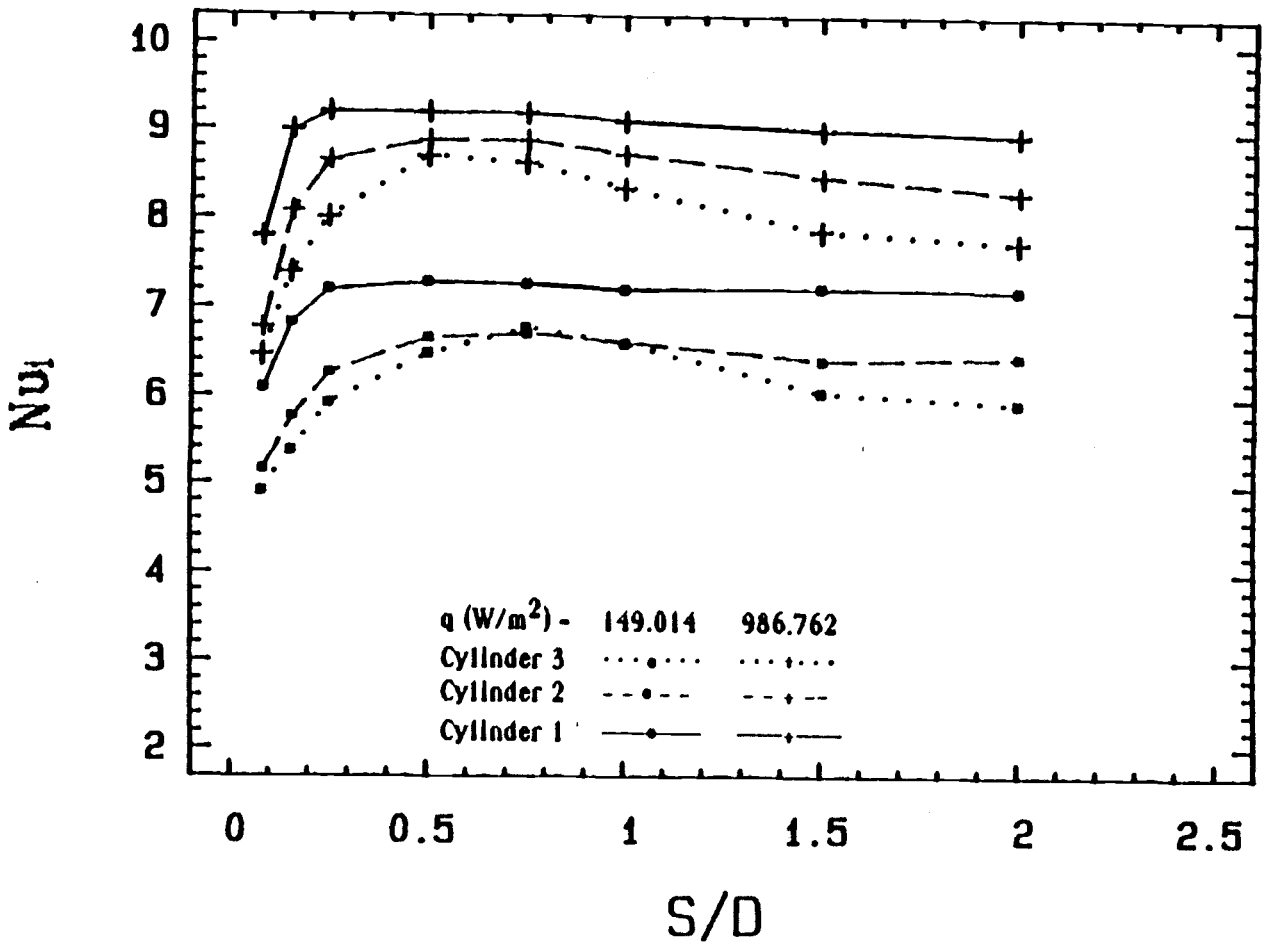

Figure 4.17 The effect of the wall spacing on the average Nusselt number of each cylinder, Nu_i , at CC=2D .

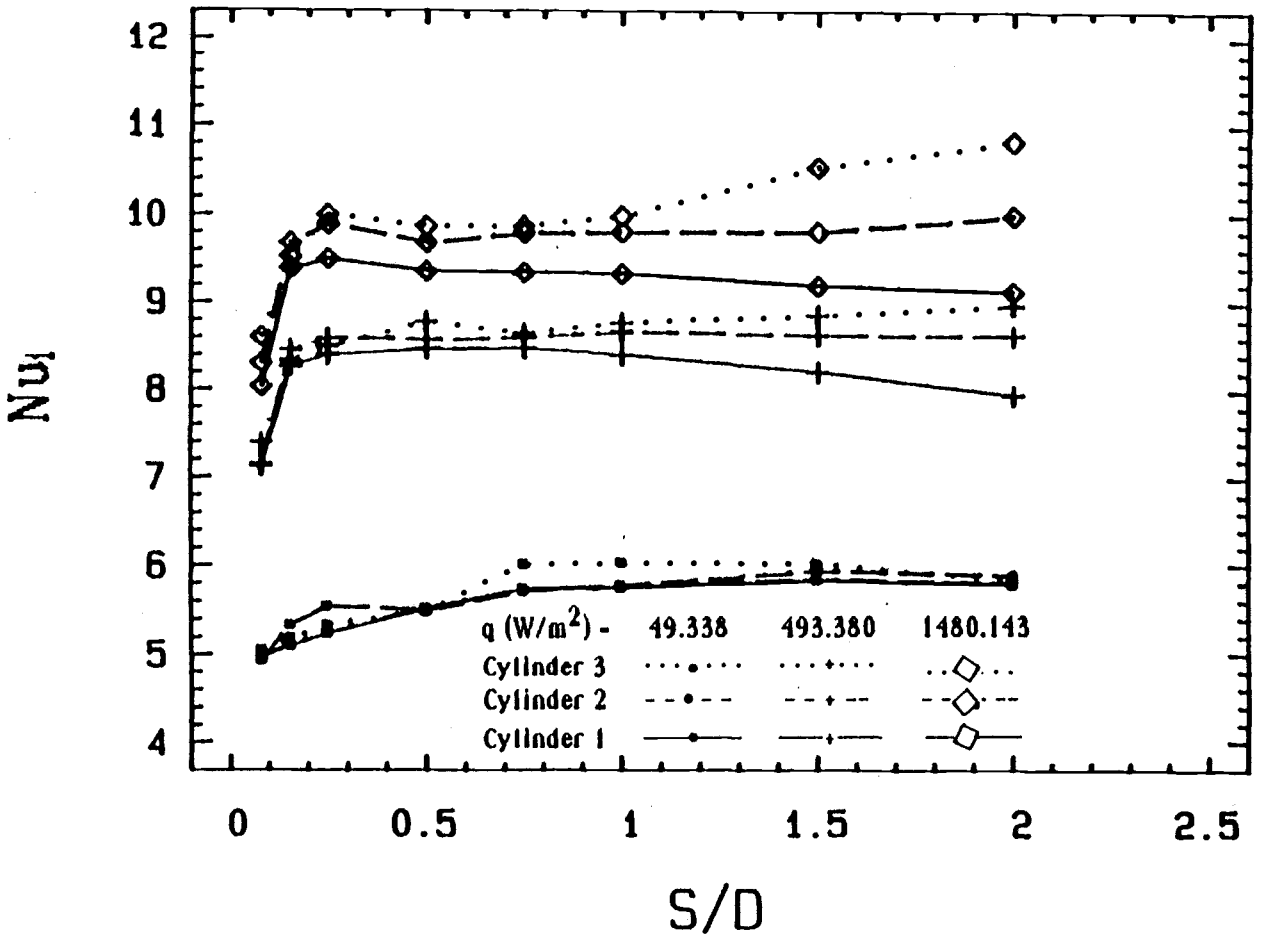

Figure 4.18 The effect of the wall spacing on the average Nusselt number of each cylinder, Nu_i , at CC=4D .

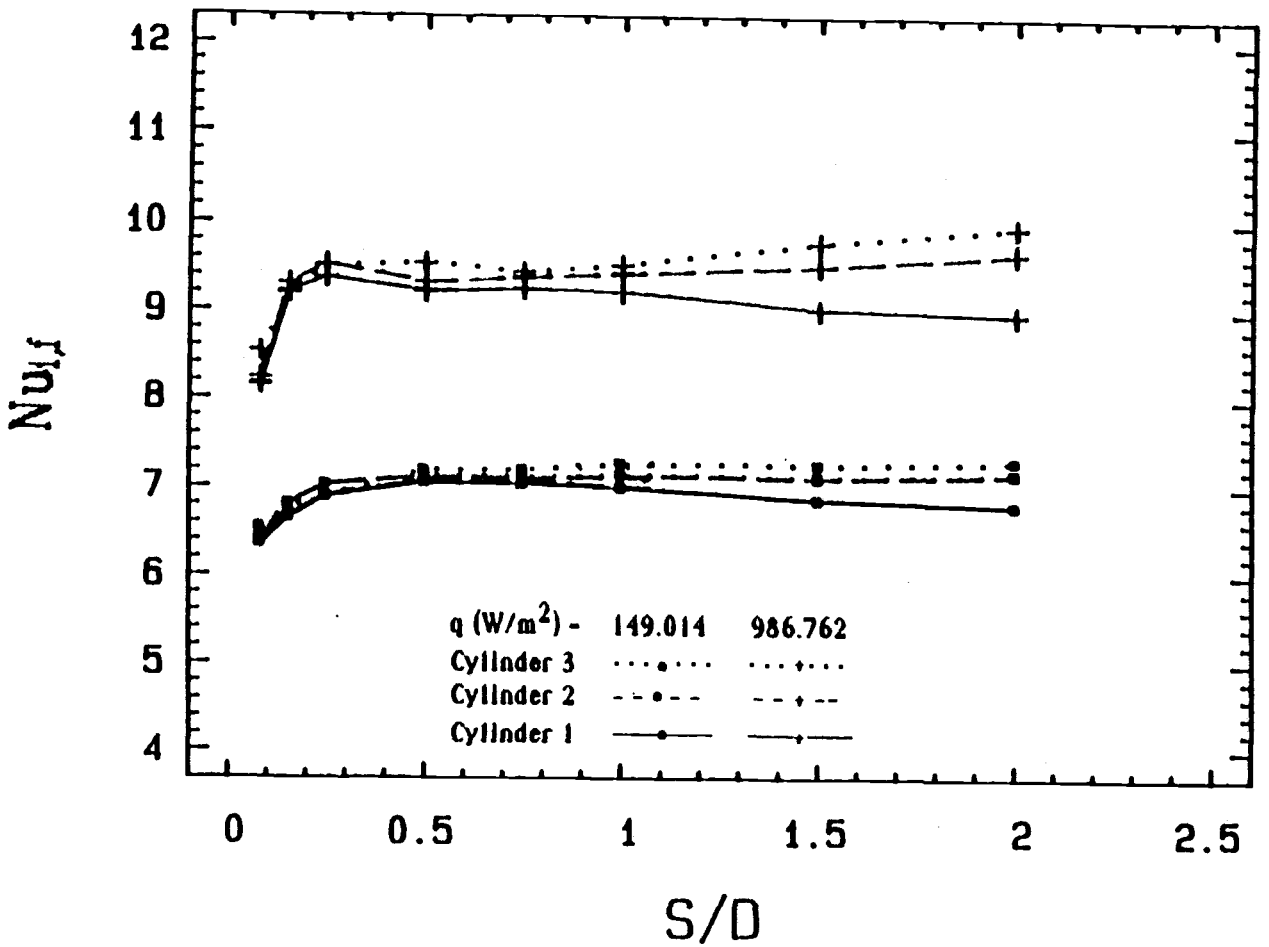

Figure 4.19 The effect of the wall spacing on the average Nusselt number of each cylinder, Nu_i , at CC=4D .

cylinder.

For CC = 4D, Nu values for all the cylinders increase sharply as S/D increases from 0.081 to 0.25. When S/D becomes higher than 0.25, the Nu values of the lowest cylinder stays the same. While for the upper cylinders, the Nu values are the same up to S/D = 1. At S/D > 1, the Nu_i values for cylinders 2 and 3 increase in an attempt to reach the $Nu_{i,f}$ values at S/D= infinity (i.e. no wall cases).

The ratios, $Nu_i/Nu_{i,f}$, of the Nusselt number for each cylinder at various S/D to the Nusselt number for that cylinder (no wall condition) at the same input heat flux are plotted in Figures 4.20 through 4.34. First, the discussion will be focussed on those cases where center-to-center spacings are small, CC = 1.5D and CC = 2D, shown in Figures 4.20 to 4.29. In these figures all the cylinders experience the same percentage of degradation, which is about 20% at S/D = 0.081. This degradation decreases as the S/D increases and the values of $Nu_i/Nu_{i,f}$ reach unity at $0.155 < S/D < 0.25$ for low heat flux cases and at S/D = 0.155 for higher heat flux cases. At S/D > 0.25, the effect of the wall spacing on the heat transfer of the cylinder depends on the position of the cylinder in the array. For all the heat flux values, except the lowest values (q = 49.388 w/m2), the upper cylinders have the highest enhancement at S/D approximately equal to 0.5. At the peak, the highest cylinder in the array has an enhancement between 15% to 22% above the no wall case, while the second

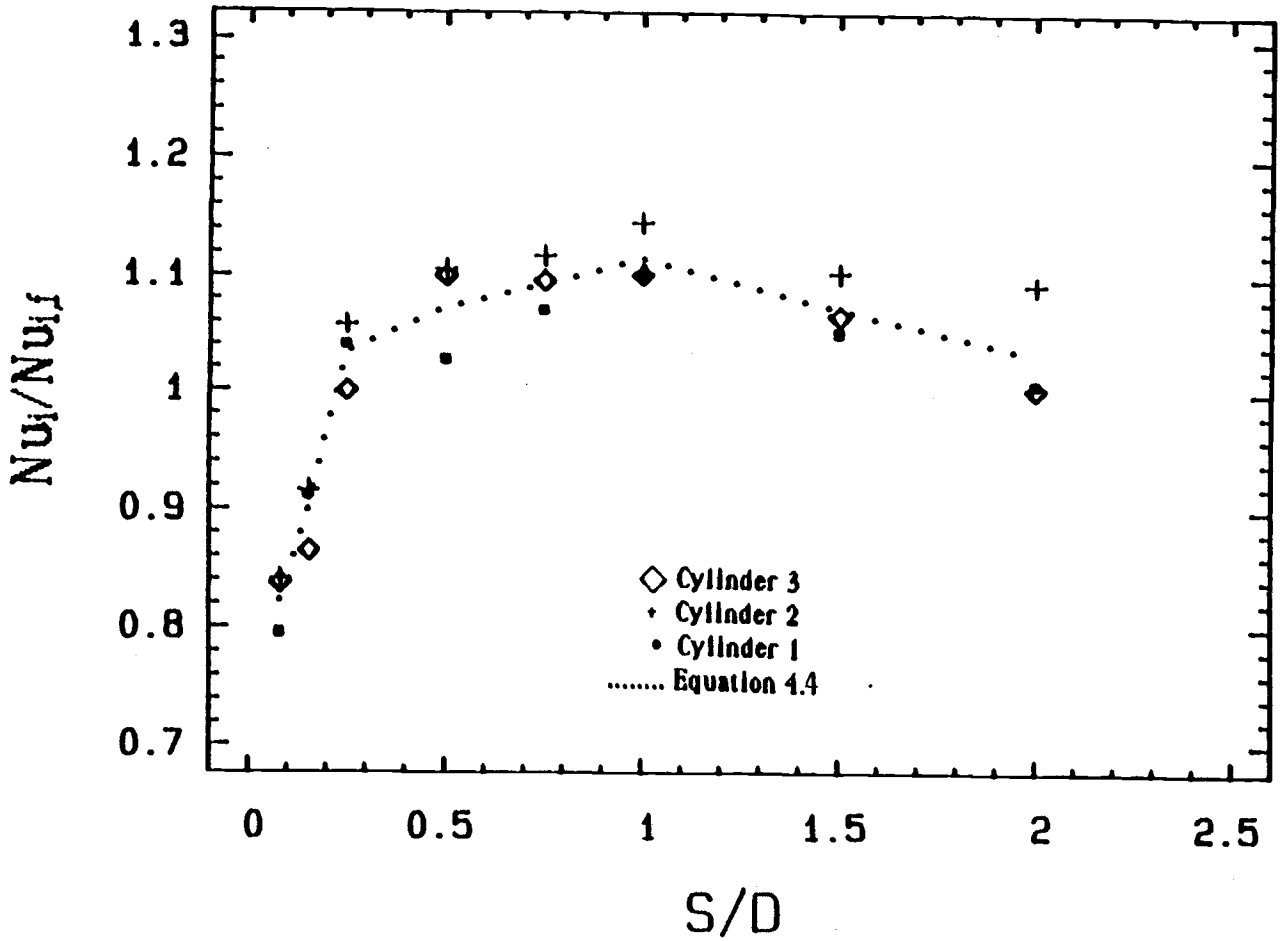

Figure 4.20 The effect of the wall spacing on the Nusselt number ratio, $Nu_i/Nu_{i,f}$, at CC=1.5D and q=49.338 (W/m^2).

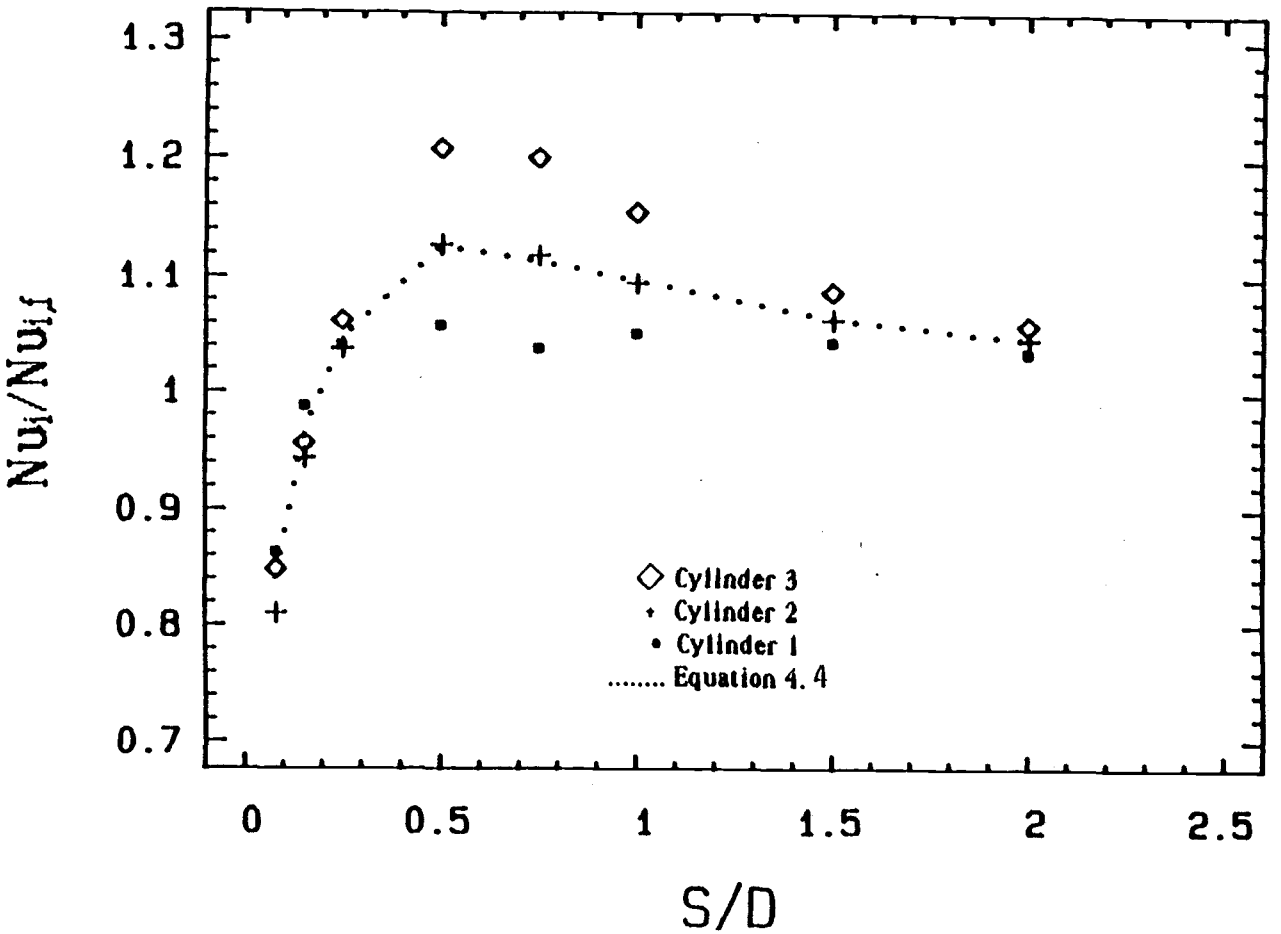

Figure 4.21 The effect of the wall spacing on the Nusselt number ratio, $Nu_i/Nu_{i,f}$, at CC=1.5D and q=149.014 (W/m^2).

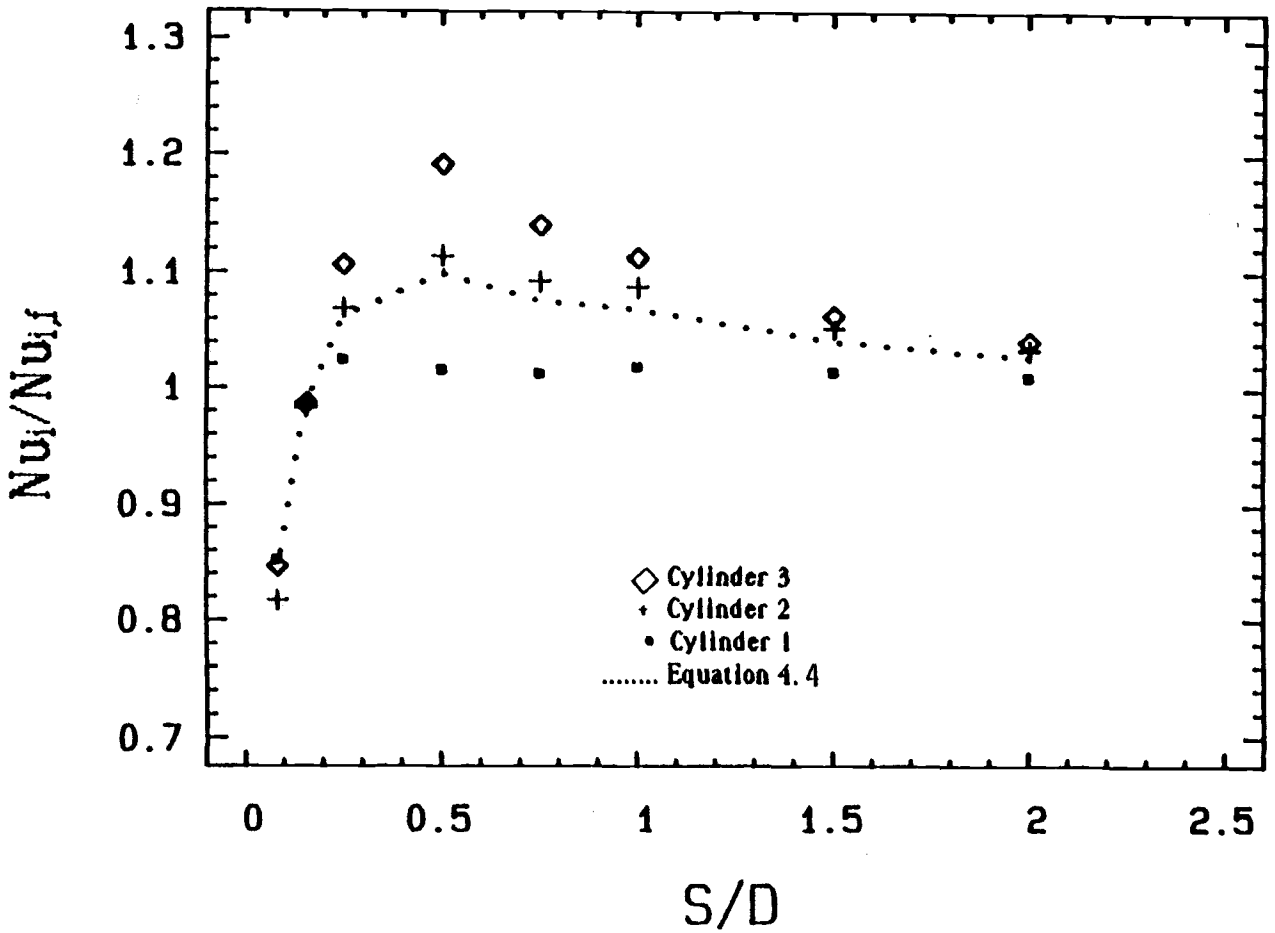

Figure 4.22 The effect of the wall spacing on the Nusselt number ratio, $Nu_i/Nu_{i,f}$, at CC=1.5D and q=493.380 (W/m^2).

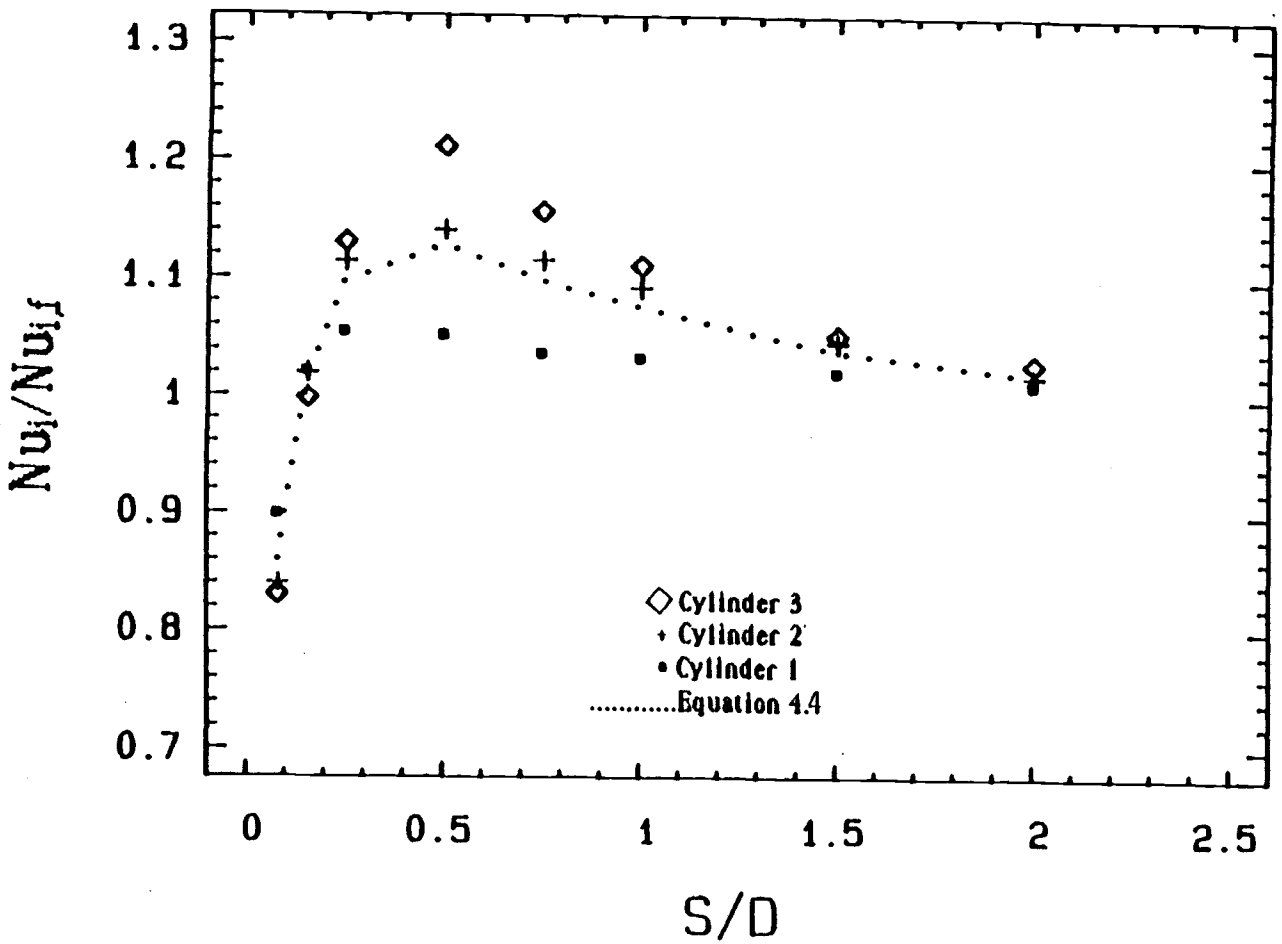

Figure 4.23 The effect of the wall spacing on the Nusselt number ratio, $Nu_i/Nu_{i,f}$, at CC=1.5D and q=986.762 (W/m^2).

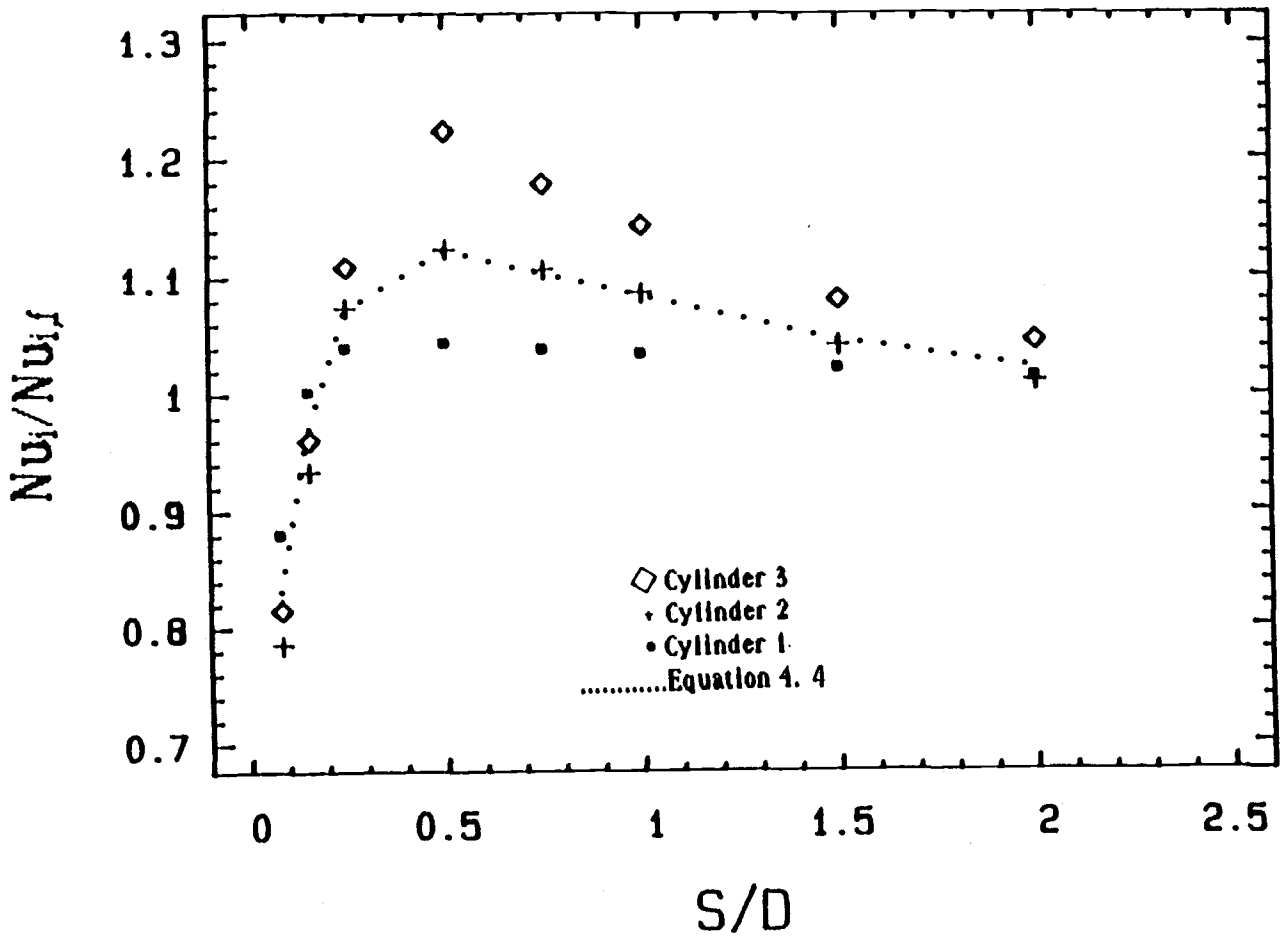

Figure 4.24 The effect of the wall spacing on the Nusselt number ratio, $Nu_i/Nu_{i,f}$, at CC=1.5D and q=1480.143 (W/m^2).

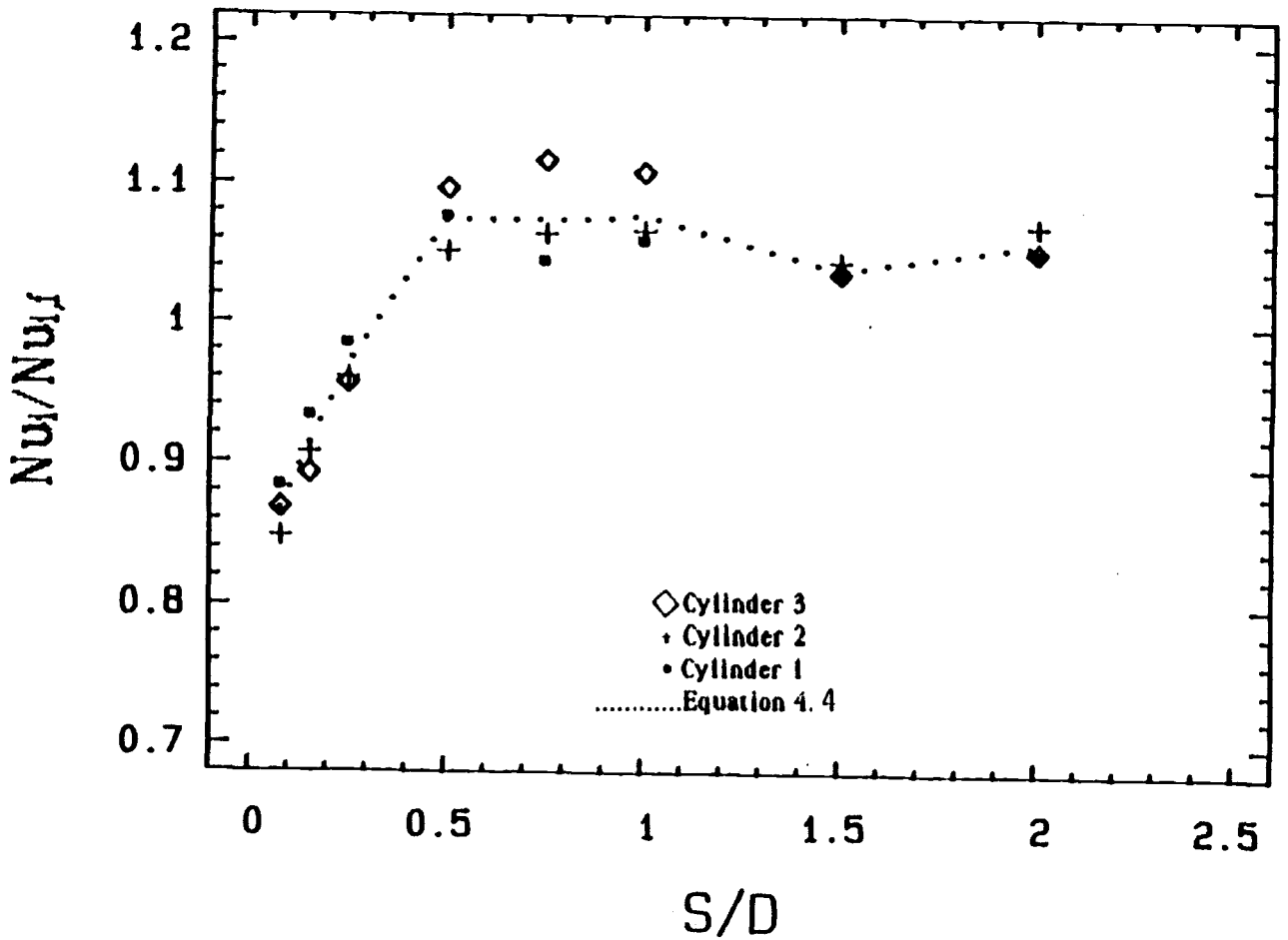

Figure 4.25 The effect of the wall spacing on the Nusselt number ratio, $Nu_j/Nu_{j,f}$, at CC=2D and q=49.338 (W/m^2).

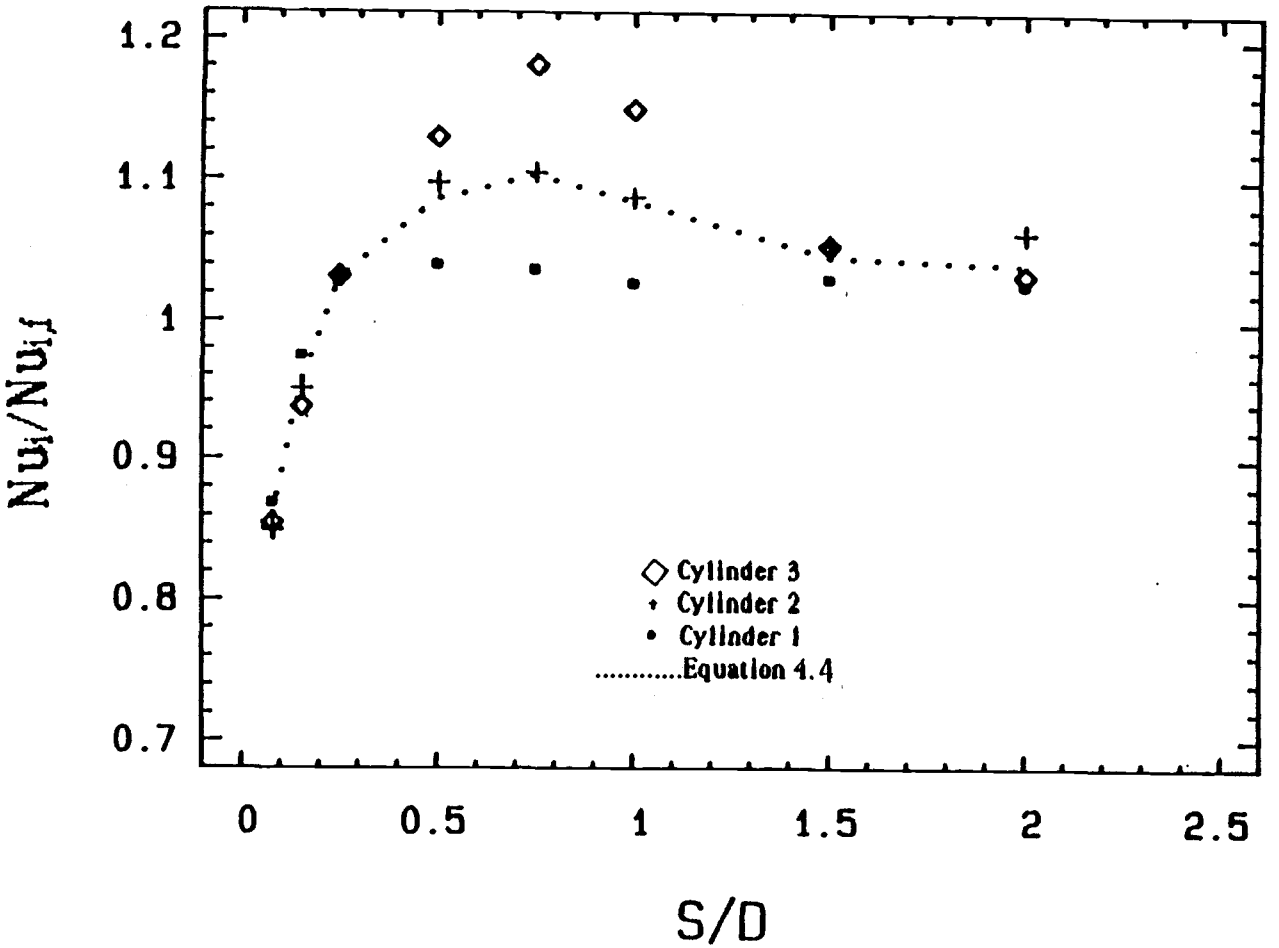

Figure 4.26 The effect of the wall spacing on the Nusselt number ratio, $Nu_i/Nu_{i,f}$, at CC=2D and q=149.014 (W/m^2).

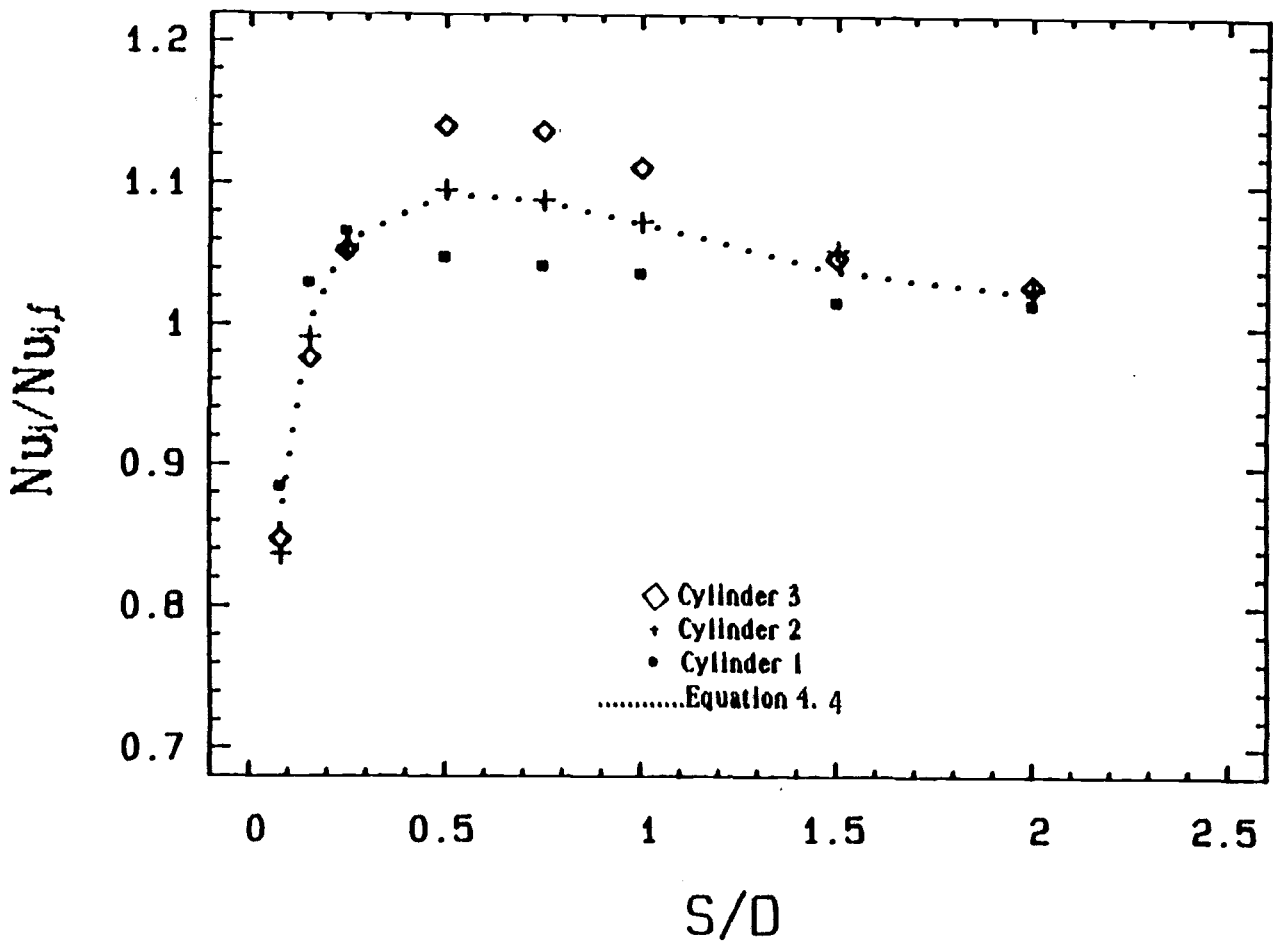

Figure 4.27 The effect of the wall spacing on the Nusselt number ratio, $Nu_i/Nu_{i,f}$, at CC=2D and q=493.380 (W/m^2).

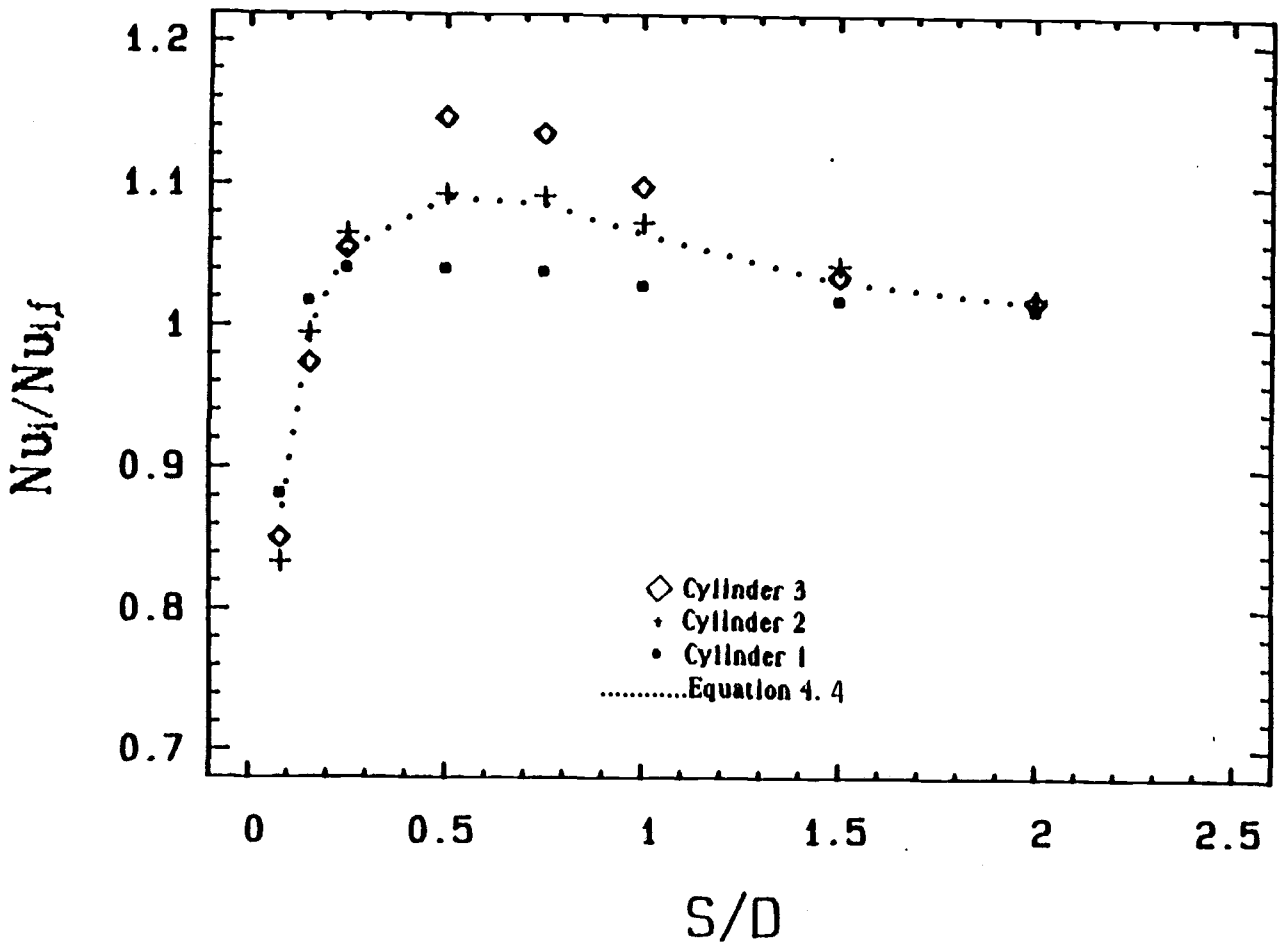

Figure 4.28 The effect of the wall spacing on the Nusselt number ratio, $Nu_i/Nu_{i,f}$, at CC=2D and q=986.762 (W/m^2).

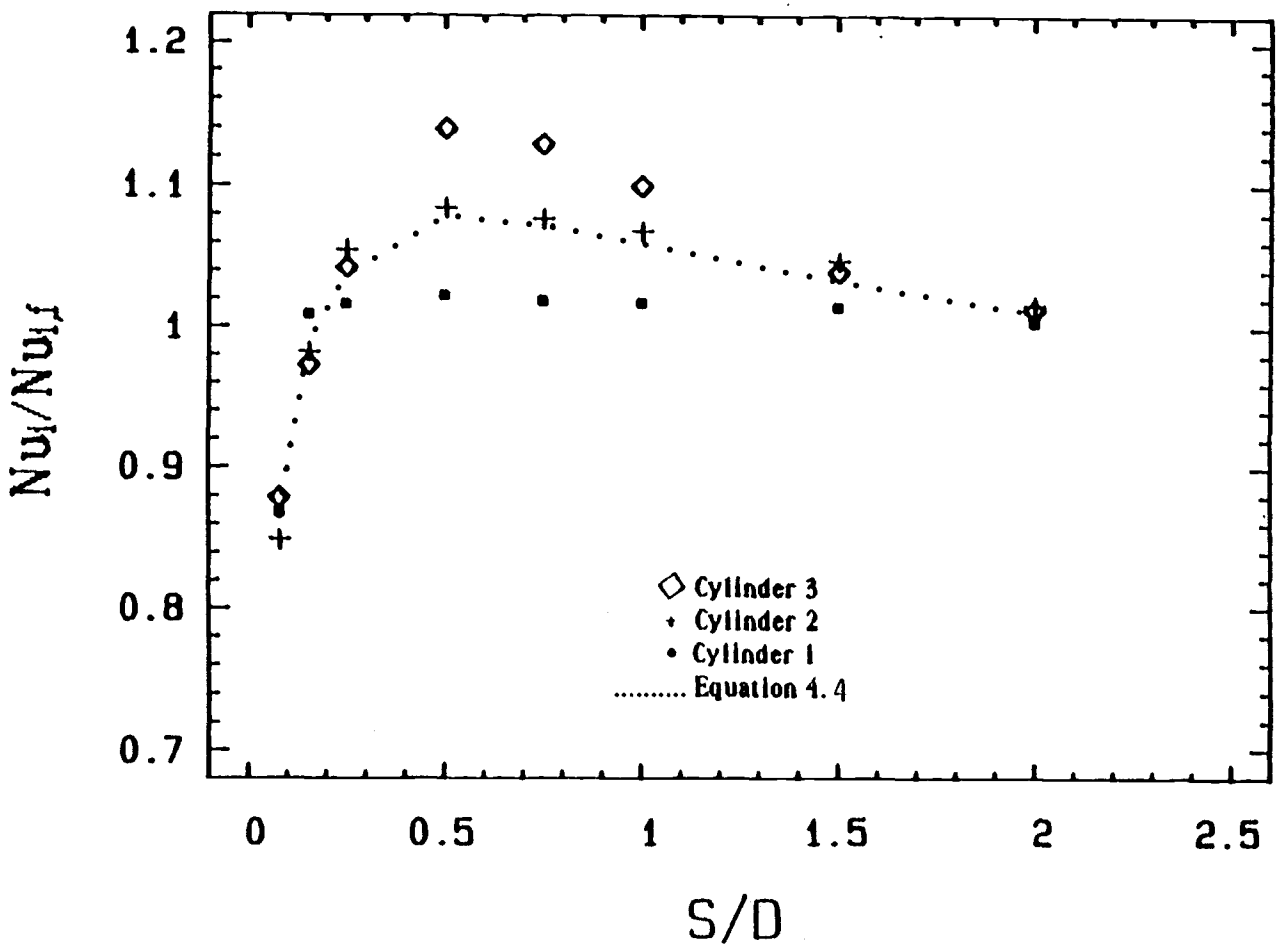

Figure 4.29 The effect of the wall spacing on the Nusselt number ratio, $Nu_i/Nu_{i,f}$, at CC=2D and q=1480.143 (W/m^2).

cylinder has an enhancement between 9% to 15%. The lowest cylinder in the array reaches the peak with an enhancement of about 5% maximum at S/D = 0.25 at all the heat flux values except the lowest value. At the lowest heat flux value (q = 49.338 w/m2), all the cylinders reach the peak at S/D = 1 for both of the cases (CC = 1.5D and CC = 2D). Cylinder 3 at CC = 2D has the highest enhancement (i.e., 10%) of any cylinder. The second cylinder at CC = 1.5D shows the highest enhancement (i.e., 14%) compared to the no wall case at S/D > 0.75. For CC = 1.5D and CC = 2D, all the cylinders' enhancements decrease as the S/D value increases from the S/D values at the peak in an attempt to reach the $Nu_i/Nu_{i,f}$ value of unity.

Next, the discussion will be focussed on the effect of the wall spacing, S/D, on $Nu_i/Nu_{i,f}$ for CC = 4D, as shown in Figures 4.30 to 4.34. The lowest cylinder shows a 10% maximum degradation at S/D = 0.081. As S/D increases higher than 0.155, the $Nu_i/Nu_{i,f}$ of the lowest cylinder increases to its maximum of 10% at S/D = 1.0 at the lowest heat flux, q = 49.338 w/m^2. For the higher heat flux values, the maximum enhancement for the lowest cylinder was 5% at S/D = 0.5.

For the lowest heat flux values, the three cylinders have similar ratios of $Nu_i/Nu_{i,f}$ up to S/D = 0.5 where the middle cylinder shows the lowest enhancement. As S/D increases from 0.5 at lowest heat flux, the highest cylinder shows higher enhancement than the lowest cylinder, while the middle cylinder

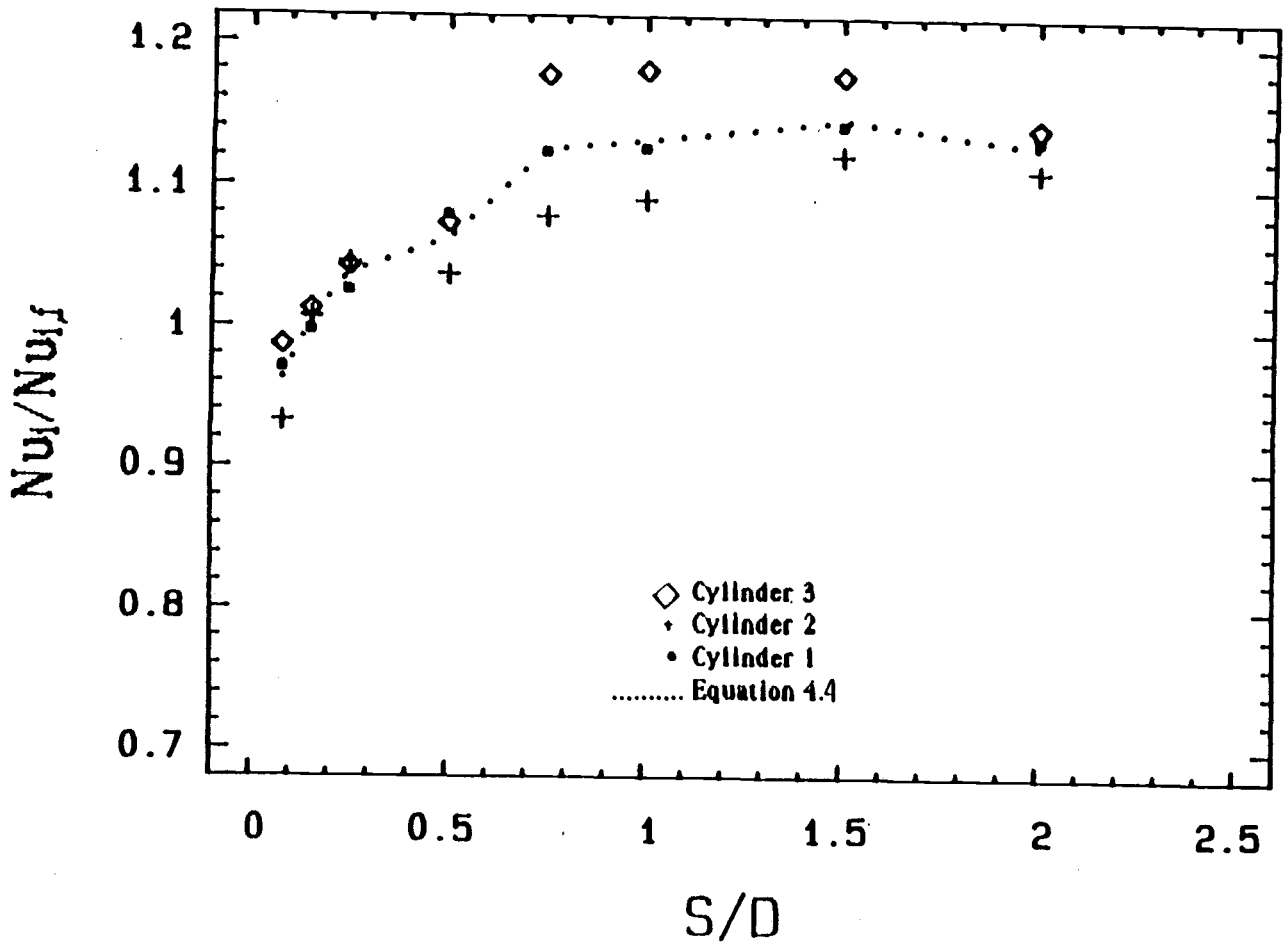

Figure 4.30 The effect of the wall spacing on the Nusselt number ratio, $Nu_i/Nu_{i,f}$, at CC=4D and q=49.338 (W/m^2).

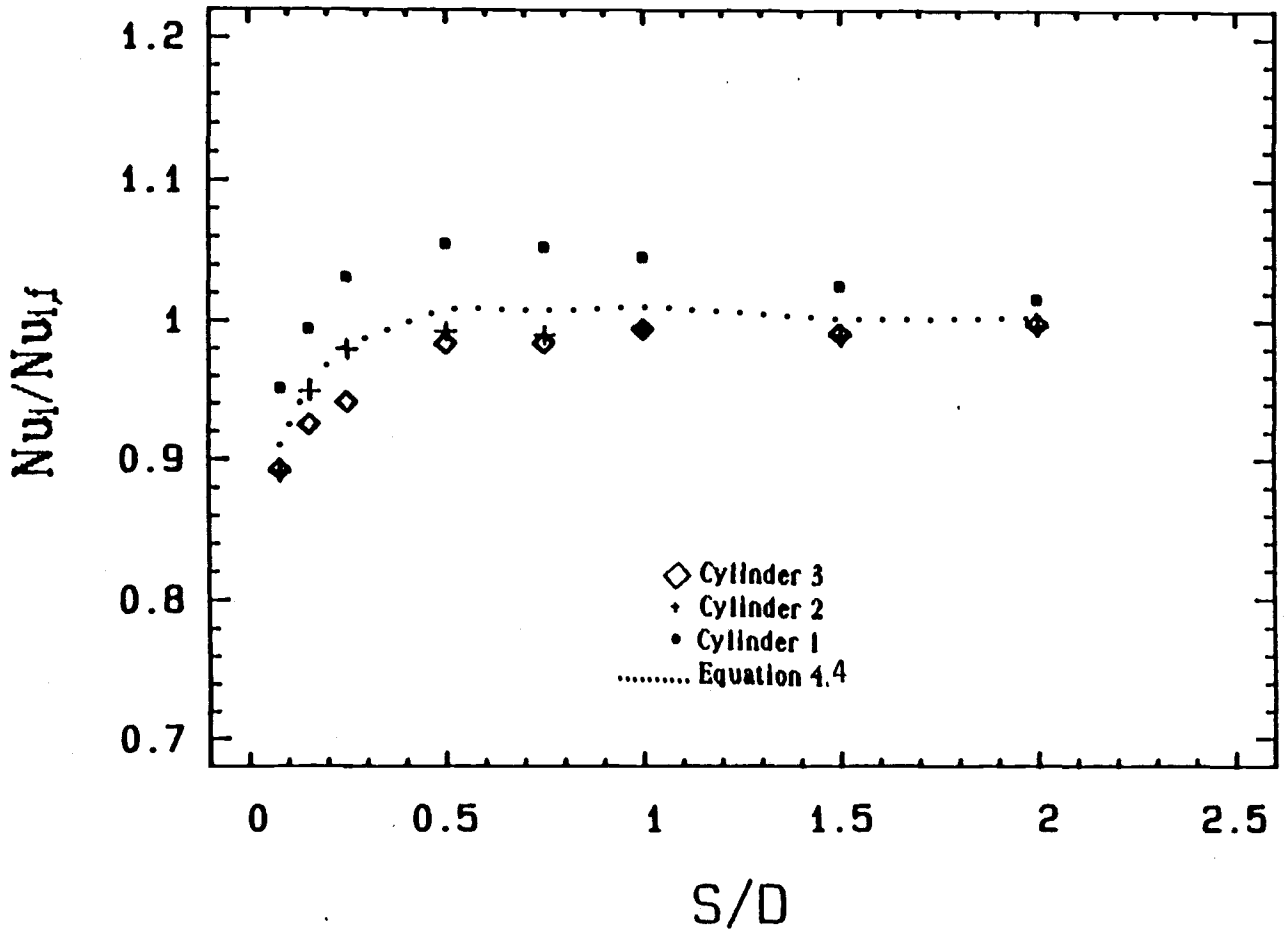

Figure 4.31 The effect of the wall spacing on the Nusselt number ratio, $Nu_i/Nu_{i,f}$, at CC=4D and q=149.014 (W/m^2).

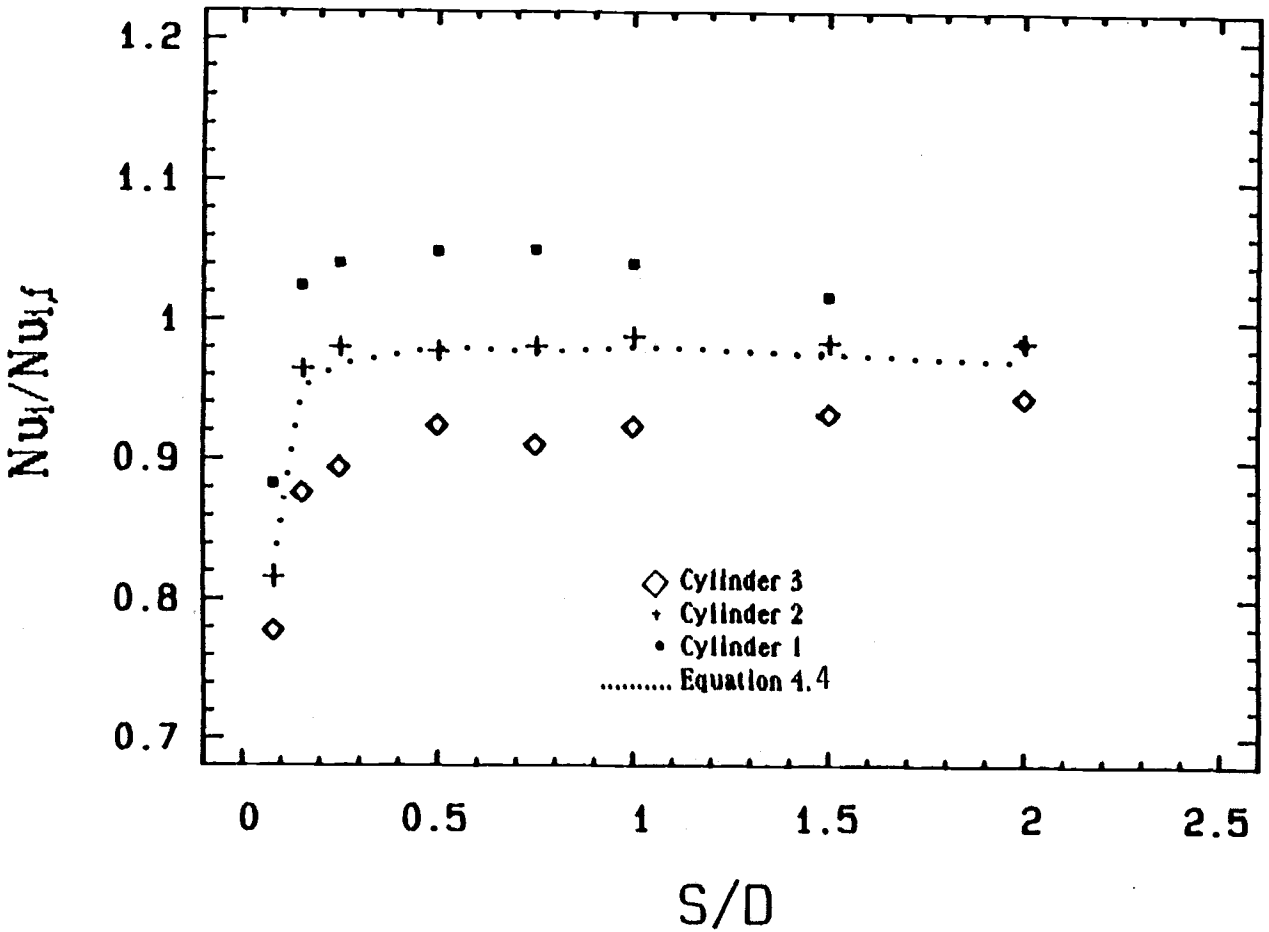

Figure 4.32 The effect of the wall spacing on the Nusselt number ratio, $Nu_i/Nu_{i,f}$, at CC=4D and q=493.380 (W/m^2).

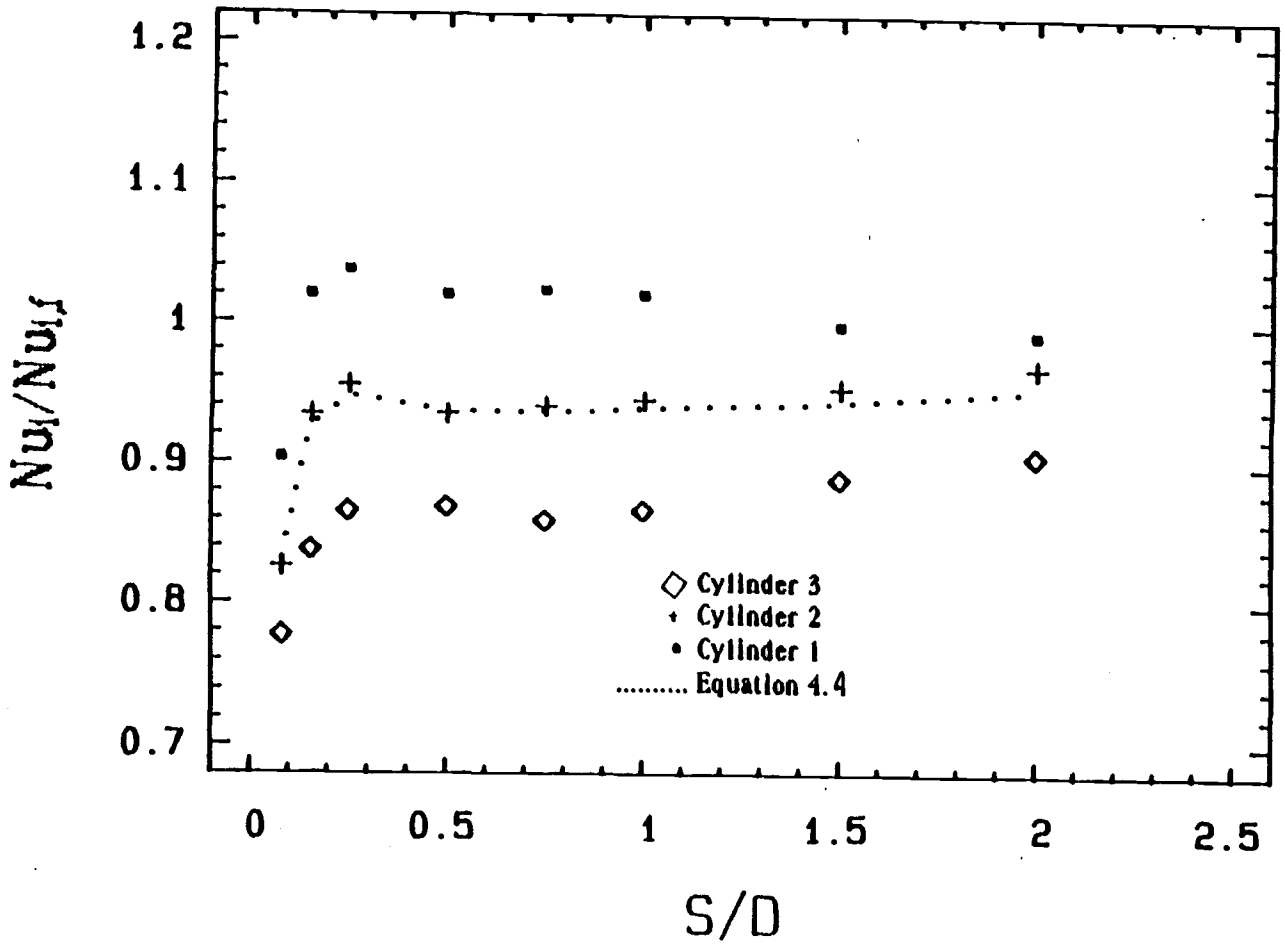

Figure 4.33 The effect of the wall spacing on the Nusselt number ratio, $Nu_i/Nu_{i,f}$, at CC=4D and q=986.762 (W/m^2).

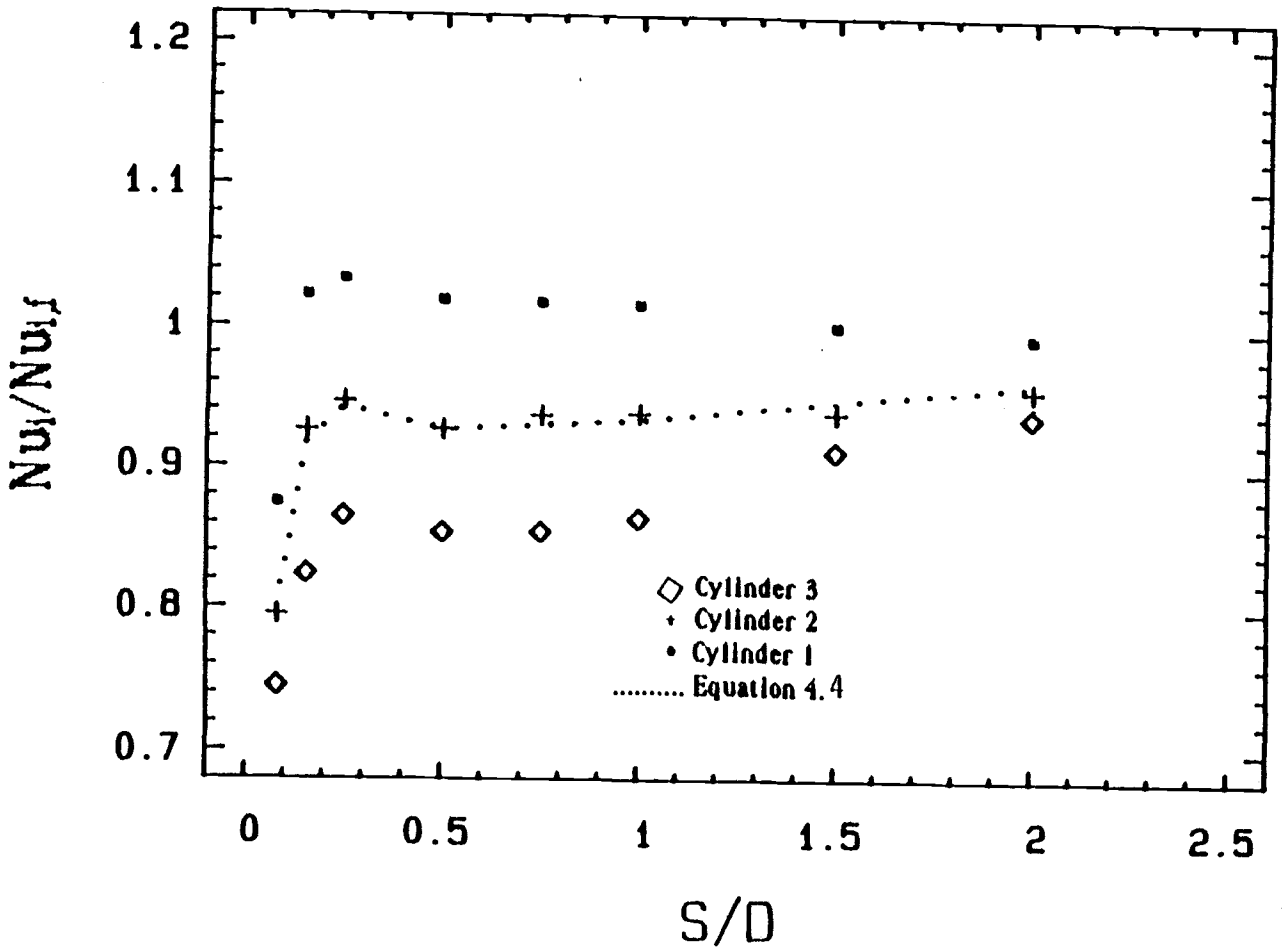

Figure 4.34 The effect of the wall spacing on the Nusselt number ratio, $Nu_i/Nu_{i,f}$, at CC=4D and q=1480.143 (W/m^2).

stays at a lower enhancement than the lowest cylinder. At the lowest heat flux, the maximum enhancement of the highest cylinder is 18% at S/D = 1.0, while for the second cylinder it was 6% at S/D = 1.0.

When the heat flux is higher than 49.338 w/m^2, the maximum enhancement in the lowest cylinder was 5% at S/D values between 0.25 and 0.5. For the upper cylinders, the $Nu_i/Nu_{i,f}$ values were less than one for q > 49.338 w/m2. These degradations are between 12% to 24% at S/D = 0.081 and they decrease as S/D increases. The reduction of $Nu_3/Nu_{3,f}$ from unity is twice the reduction of $Nu_2/Nu_{2,f}$ from unity. These values, $Nu_i/Nu_{i,f}$ (i=2 & 3) , increase as S/D increases.

The average Nusselt number ratio for the whole array, $Nu_{av/f}$, is superimposed on Figures 4.20 to 4.34, where $Nu_{va/f}$ is shown by the dotted line, as calculated from:

$$Nu_{av} = \frac{\sum_{i=1}^{3} Nu_i}{3.0} \tag{4.4}$$

$$Nu_{av/f} = \frac{Nu_{av}}{\frac{\sum_{i=1}^{3} Nu_{i,f}}{3.0}} \tag{4.5}$$

Although $Nu_{av/f}$ is plotted as a line, the plot is a point to point curve. At q = 49.338 w/m^2, $Nu_{av/f}$ shows an 8%

enhancement for CC = 1.5 and CC = 2D at an S/D between 0.75 and 1.0. For CC = 4D, Nu_{av} has about 14% enhancement at an S/D between 1.0 and 1.5. For CC = 1.5D and CC = 2D with q > 49.338 w/m^2, the $Nu_{av/f}$ values have peaks, with 8 - 12% enhancement, at $.5 \leq S/D < 0.75$. The $Nu_{av/f}$ decreases sharply as S/D decreases from 0.5 and reaches its lowest value about 0.82 at CC = 1.5 and about 0.84 at CC = 2D at S/D = 0.081. When S/D increases to more than .75, the $Nu_{av/f}$ values decrease slowly in an attempt to reach unity at S/D = infinity.

The $Nu_{av/f}$ values for CC = 4D are always less than one when q > 49.338 w/m^2. These values increase sharply as S/D increases from 0.081 to 0.5. Then the increments in these values of $Nu_{av/f}$ become smaller as $Nu_{av/f}$ attempts to reach unity.

Figures 4.35 to 4.37 show the Nusselt number ratios, $Nu_{av/s}$, of the Nu_{av} values to the Nusselt numbers of a single cylinder, Nu_s, as calculated from equation 4.1 at Ra^* of the lowest cylinder of the array. The $Nu_{av/s}$ is defined in the following equation:

$$Nu_{av/s} = \frac{Nu_{av}}{Nu_s} = \frac{\dfrac{\sum_{i=1}^{3} Nu_i}{3.0}}{[\,0.571\, Ra_1^{*\,0.2027}\,]} \qquad (4.6)$$

The enhancements of Nu_{av} from Nu_s were insignificant and $Nu_{av/s}$ are mostly equal or less than one at CC = 1.5D and CC = 2D. In both cases, there were peak values at $.5 \leq S/D < .75$, except at

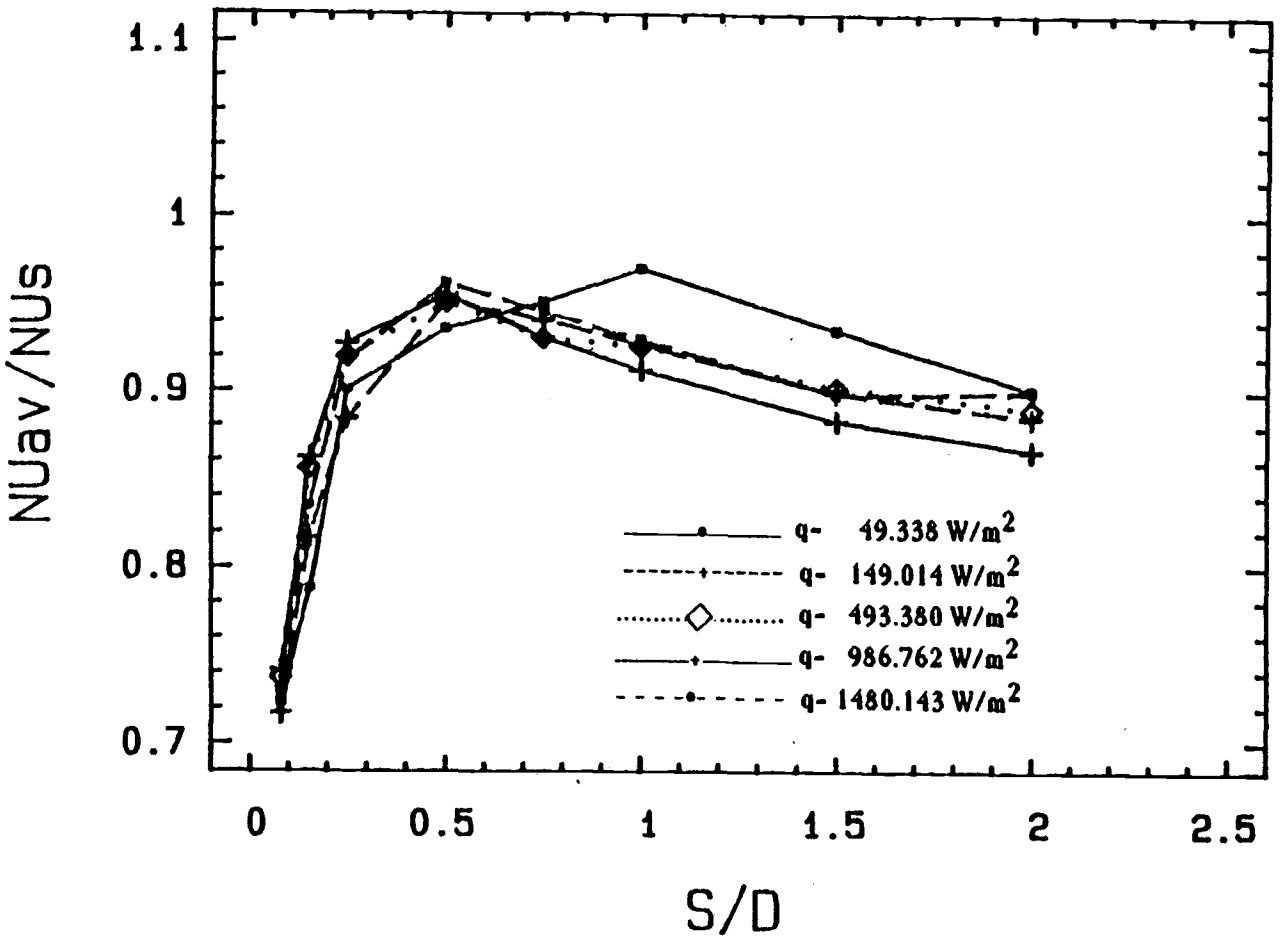

Figure 4.35 The effect of the wall spacing on the average Nusselt number of the whole array at CC=1.5D .

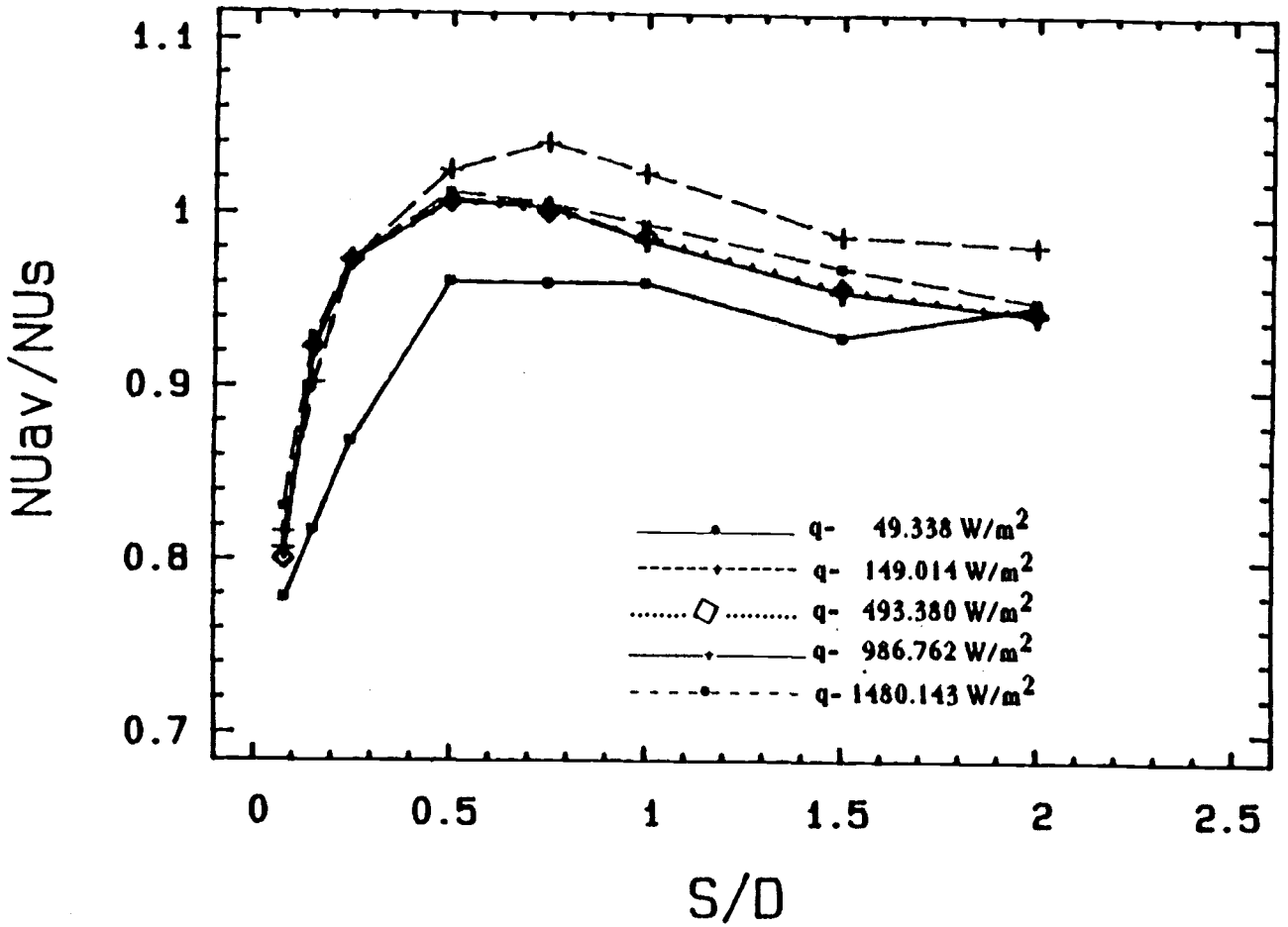

Figure 4.36 The effect of the wall spacing on the average Nusselt number of the whole array at CC=2D .

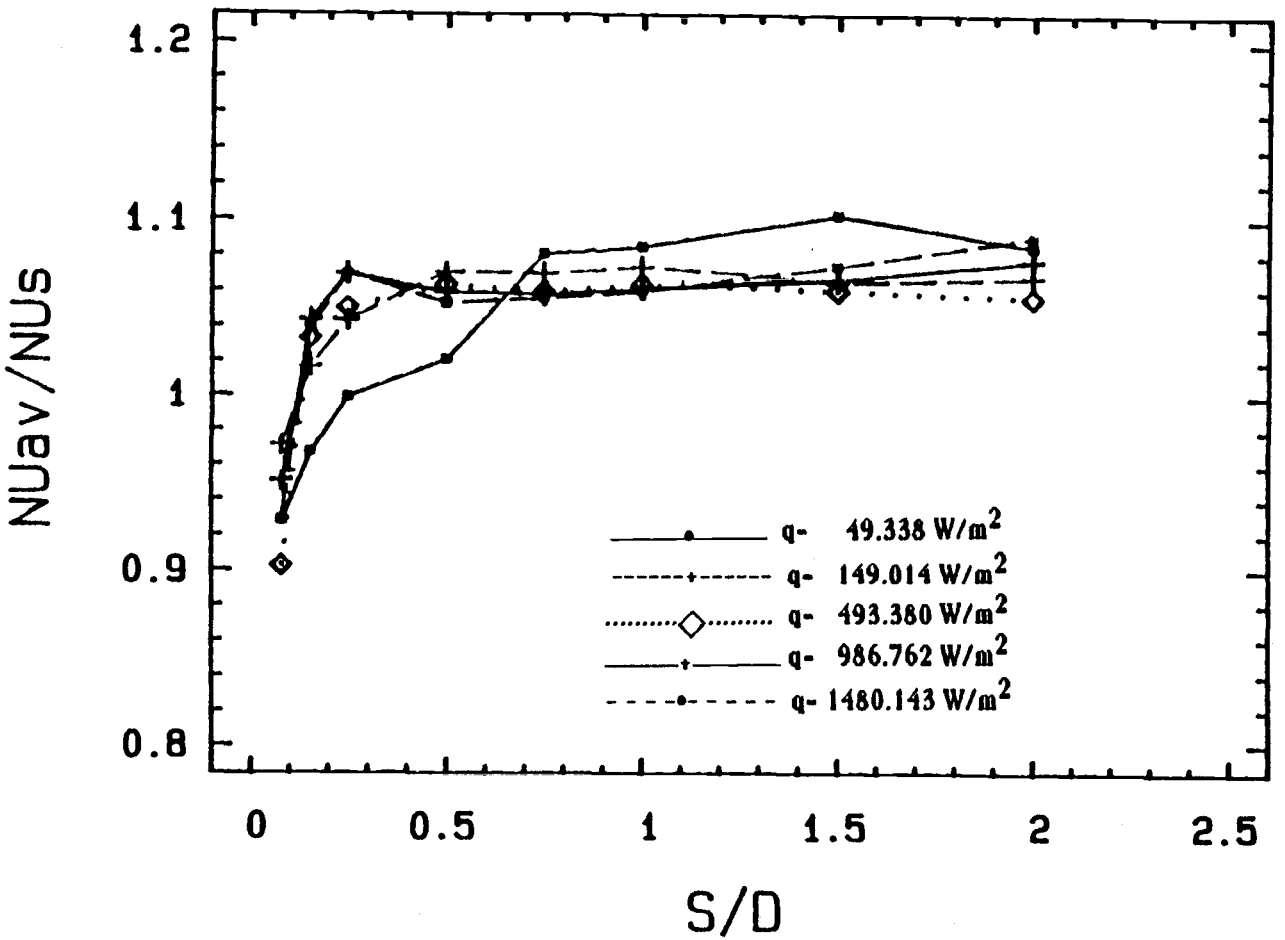

Figure 4.37 The effect of the wall spacing on the average Nusselt number of the whole array at CC=4D .

the lowest heat flux, where the peaks were at .75 $\leq$ S/D < 1.0. For CC = 4D, there was a maximum of an 8% enhancement in Nu_{av} values at .25 < S/D $\leq$ .5 in all the heat values, except the lowest heat flux where the maximum enhancement was 10% at 1.0 $\leq$ S/D < 1.5.

4.4 Data Correlation

The experimental data will be represented in emperical equations in this section. The average Nusselt number for each cylinder of the array was fitted in a single equation at a specified S/D value and a specified CC value. In these equations, the average Nusselt values, Nu_i, were represented as a function of Ra_i^*, cylinder position in the array (Y_i), and center-to-center spacing (CC). Figure 4.38 shows the (Y_i) dimensions. The general form of this relation is:

$$\frac{Nu_i}{Ra_i^{*\,0.2}} = A_1 + A_2 \,\mathrm{Exp}\left[-A_3 \left(\frac{Y_i}{CC} \right) \right] \qquad (4.7)$$

The values of A_1, A_2, and A_3 are shown in Table 4.1. The r^2 for each case was also shown in this table. The Nu_i values, at S/D = 0.5 , as calculated from equation 4.7 were superimposed on the experimental data, as shown in figures 4.39 to 4.41.

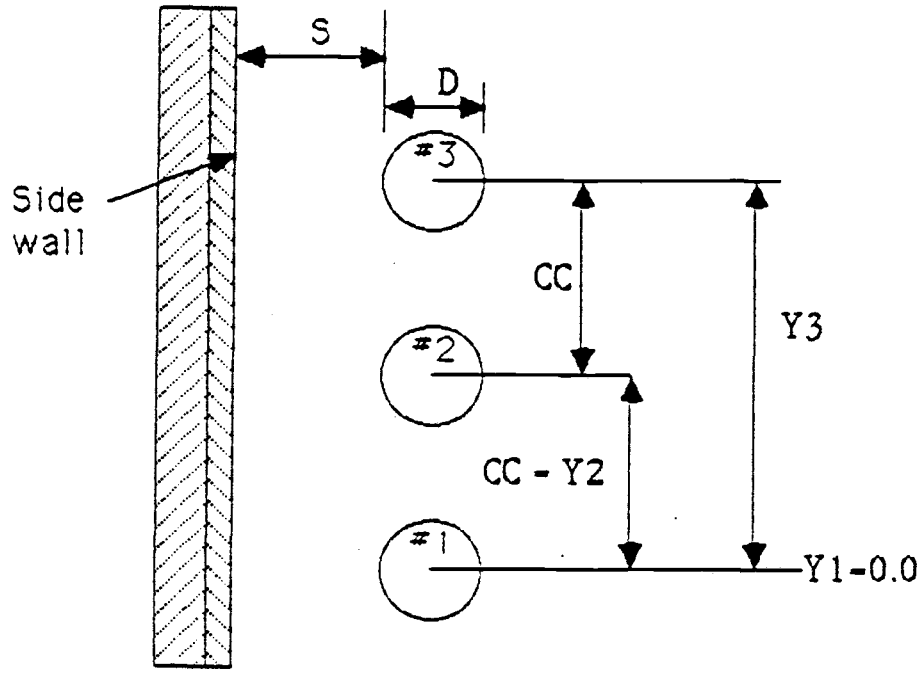

Figure 4.38 The measurement of Yi dimention as used in equation 4.7.

Table 4.1 Coefficients of equation 4.7, $Nu_i/Ra_i^{*0.2} = A_1 + A_2\ Exp[\ -A_3\ (Y_i/CC)]$.

	CC = 1.5D				CC = 2D				CC = 4D			
S/D	A_1	A_2	A_3	r^2%	A_1	A_2	A_3	r^2%	A_1	A_2	A_3	r^2%
0.081	0.38816	0.12099	1.68782	95	0.44023	0.08724	1.23577	86	0.53390	0.00448	-0.86297	40
0.155	0.42637	0.15017	1.15017	89	0.46097	0.14512	0.62651	94	0.49841	0.10969	-0.02341	6.4
0.250	0.47994	0.12880	1.08535	88	0.48866	0.13475	0.46858	93	0.49055	0.12841	-0.05972	44
0.500	0.53707	0.07132	1.97020	83	0.57548	0.04468	0.84132	74	0.52552	0.08878	-0.11651	74
0.750	0.52015	0.08865	1.43274	83	0.86924	-0.25232	-0.06193	61	0.59267	0.02977	-0.15812	71
1.000	0.50866	0.10537	1.28668	83	0.56256	0.05466	0.83912	80	0.49579	0.12126	-0.10031	74
1.500	0.47515	0.12910	1.05709	94	0.36239	0.24567	0.17936	81	0.39546	0.21512	-0.09113	70
2.000	0.45226	0.14330	0.89824	96	0.36551	0.24209	0.19971	90	0.26659	0.33887	-0.07347	70
INFIN.	0.44692	0.14101	1.13765	96	0.46811	0.12704	0.51142	85	0.09139	0.50926	-0.08129	80

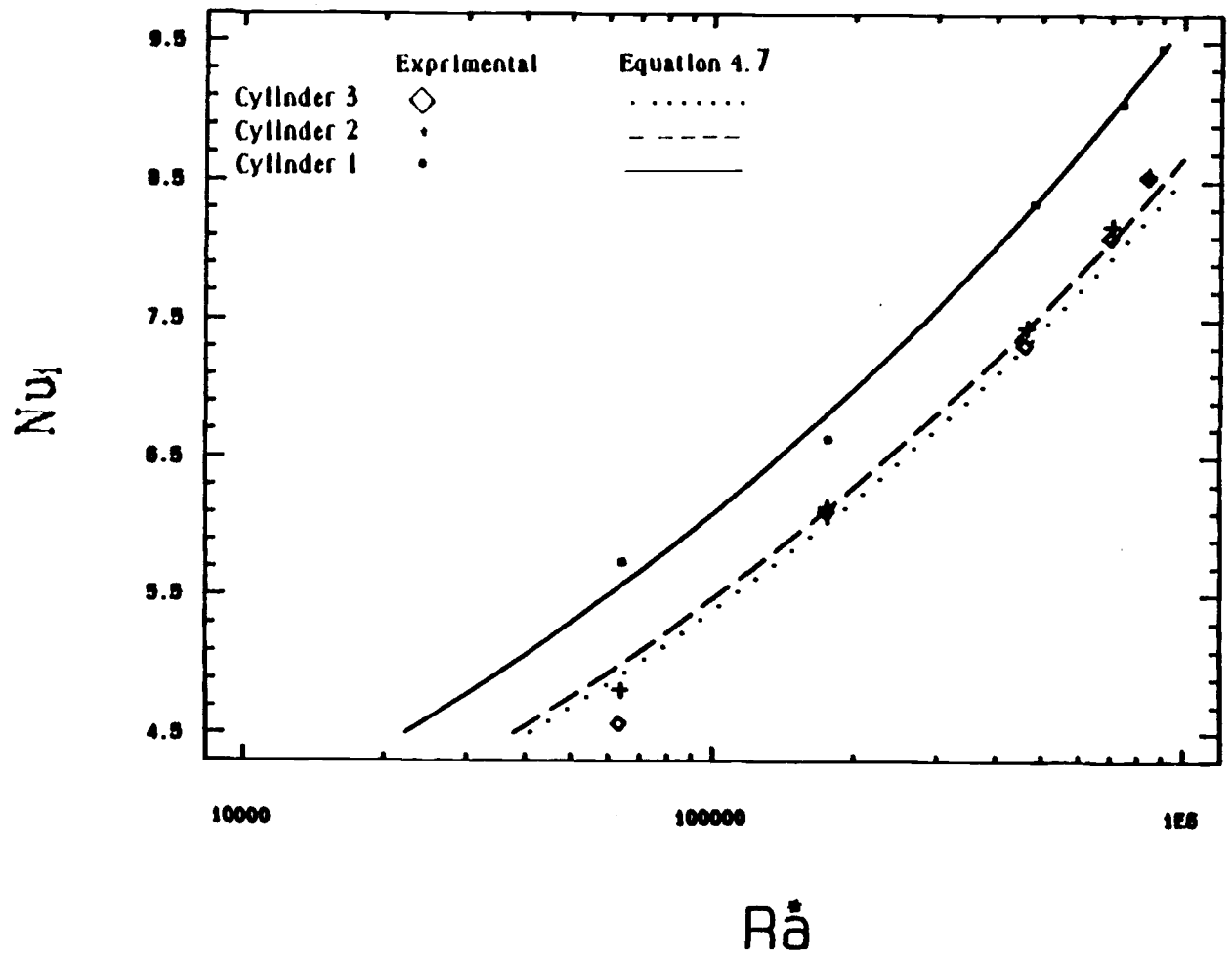

Figure 4.39 The experimental Nu_j values and correlated Nu_j values Vs. Ra^* at S/D=0.5 and CC=1.5D .

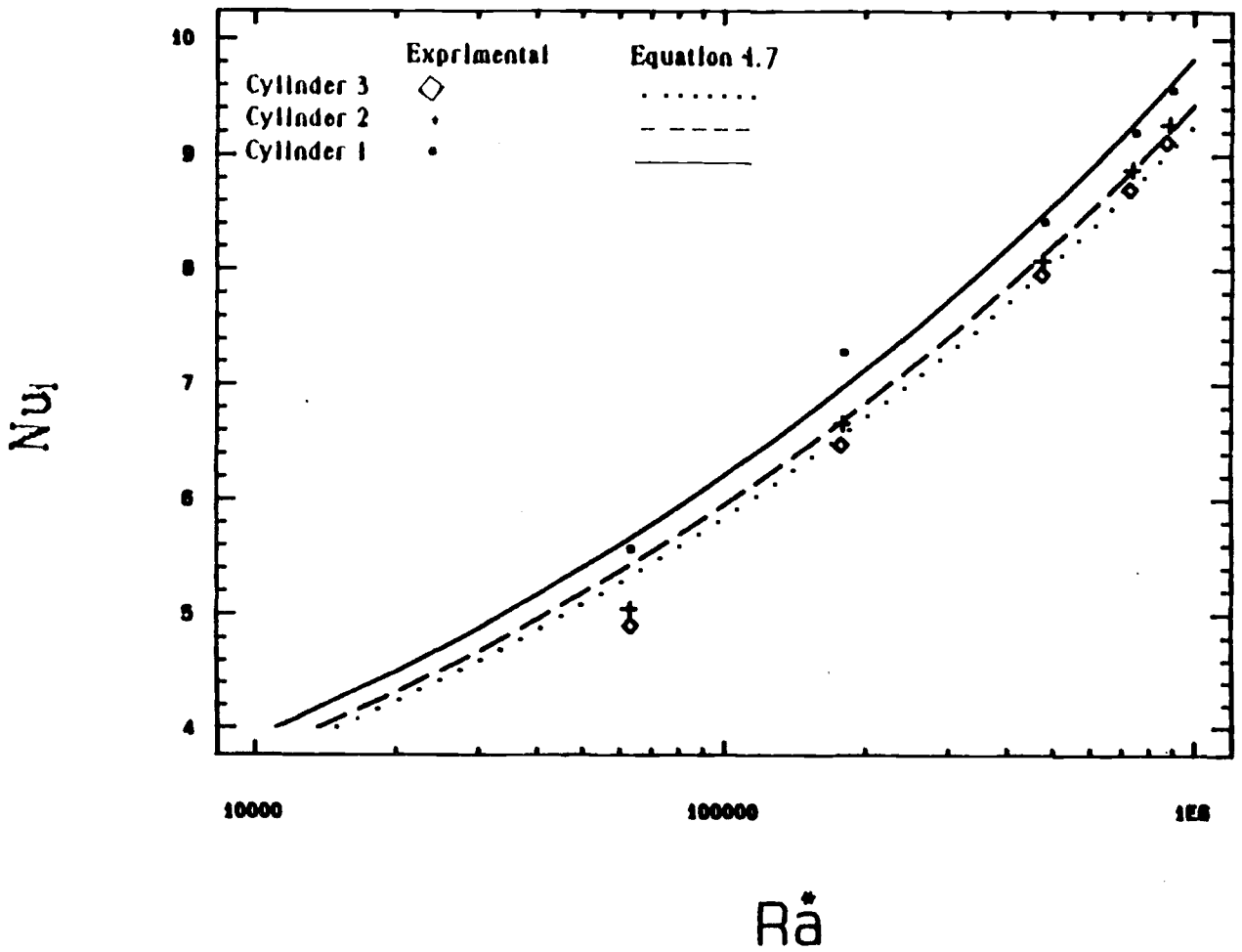

Figure 4.40 The experimental Nu_j values and correlated Nu_j values Vs. Ra^* at S/D=0.5 and CC= 2D .

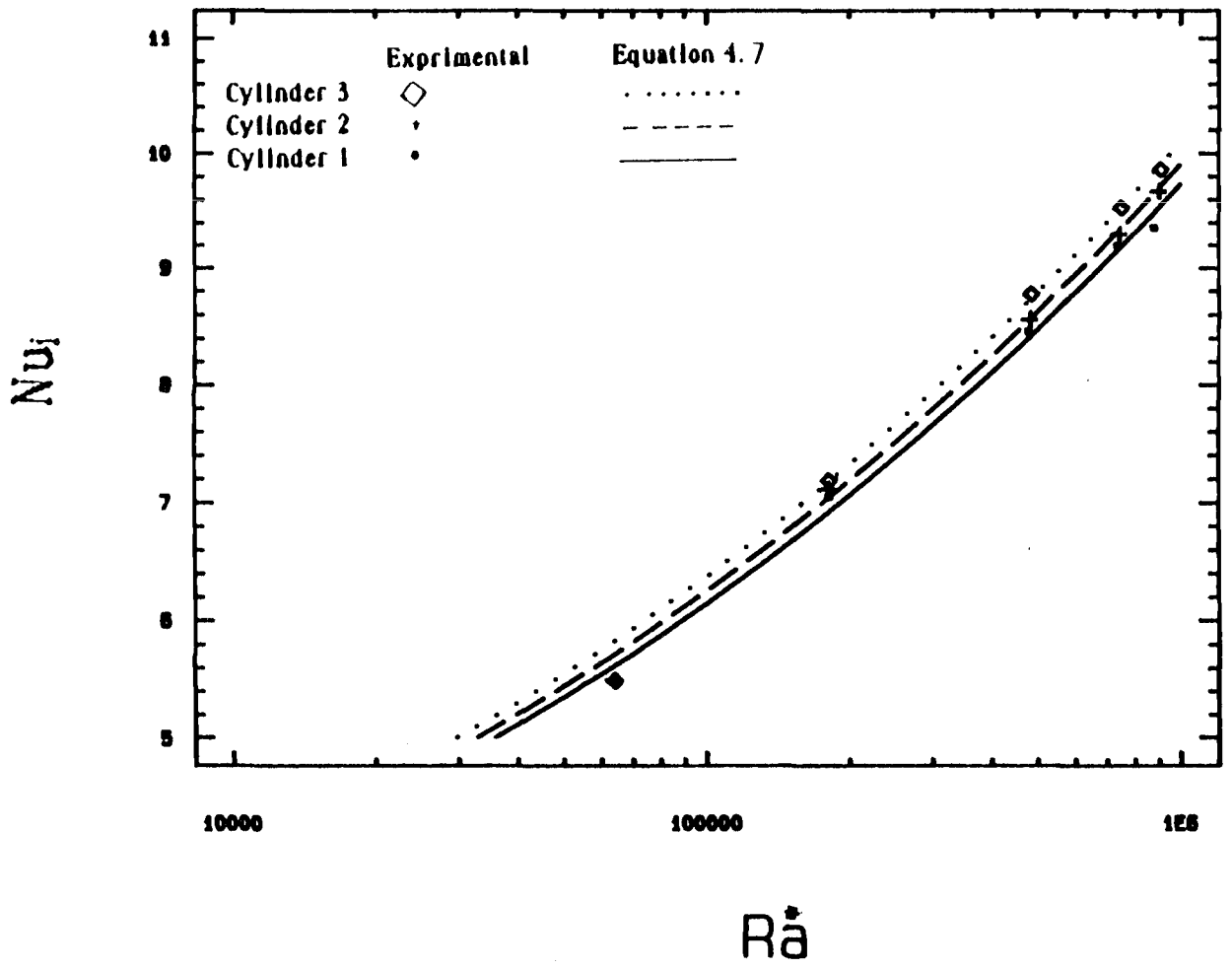

Figure 4.41 The experimental Nu_j values and correlated Nu_j values Vs. Ra^* at S/D=0.5 and CC=4D .

Table 4.2 shows the coefficient of the curve fitting, which is defined in Equation 4.8, for the average Nusselt number for the whole array, Nu_{av}.

$$Nu_{av} = \frac{\sum_{i=1}^{3} Nu_i}{3.0} = B_1 \, Ra^{*0.2} \qquad (4.8)$$

Table 4.2 Correlation coefficient, B_1, for equation 4.8, $Nu_{av} = B_1 \; Ra_1{}^{*0.2}$

	CC = 1.5D		CC = 2D		CC = 4D	
S/D	B_1	r^2%	B_1	r^2%	B_1	r^2%
0.081	0.43243	99.5	0.47916	98.8	0.55287	98.2
0.155	0.49607	98.0	0.53926	97.1	0.60844	98.7
0.250	0.54069	99.2	0.56980	97.5	0.62368	98.8
0.500	0.56403	99.7	0.59535	99.2	0.62452	99.5
0.750	0.55490	99.8	0.59425	98.9	0.62771	99.9
1.000	0.55014	99.1	0.58631	99.2	0.63009	99.9
1.500	0.53139	99.3	0.56906	99.2	0.63291	99.7
2.000	0.52108	99.6	0.56284	99.5	0.63612	99.5
INFIN.	0.50840	99.7	0.55027	99.3	0.64887	95.4

CHAPTER 5

TWO WALLS: RESULTS AND DISCUSSION

This chapter will focus on the effects of the asymmetrically placed cylinders array between two parallel walls. As shown in Chapter 4, the maximum enhancement in a single wall condition occurs at S/D ~ 0.5. To investigate whether or not there is any possibility to enhance the heat transfer coefficient in two wall cases, the following conditions will be discussed in this chapter. For two wall cases, the left wall was kept at S/D = 0.5, while the right wall spacings were varied as follows: $(S/D)_R$ = 0.50, 0.75, 1.00, 1.50, 2.00, 2.50, and 3.50 for the same heat flux values of the single wall (i.e., 49.338 w/m^2, 149.014 w/m^2, 493.38 w/m^2, 986.762 w/m^2, and 1480.143 w/m^2). The same cylinder center-to-center spacings were used in the two wall cases as in the single wall cases (i.e., CC = 1.5D, 2D, and 4D).

5.1 The effects of the right wall spacing, $(S/D)_R$, on the temperature distribution along the array

The normalized access temperature, $\emptyset$, as shown in equation 4.3, was used to show the effects of the wall spacing on the cylinders of the array. $\emptyset$ versus $(S/D)_R$ for all the cases (CC = 1.5D, 2D, 4D) at a specific heat flux value are shown in figures 5.1 through 5.5. From these figures the $\emptyset$ values for the upper

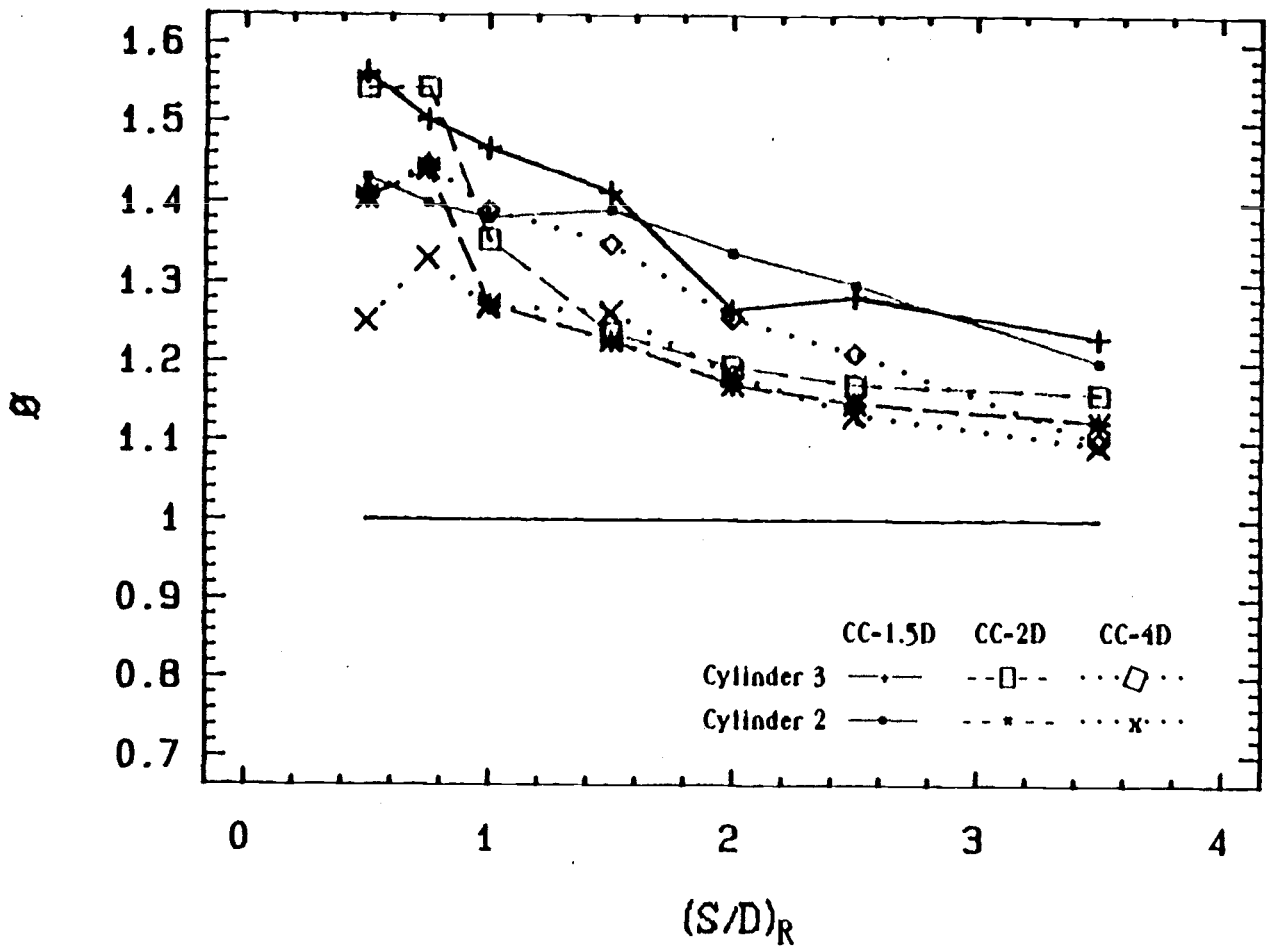

Figure 5.1 The effect of right wall spacing on the normalized temperature at q= 49.338 W/m^2.

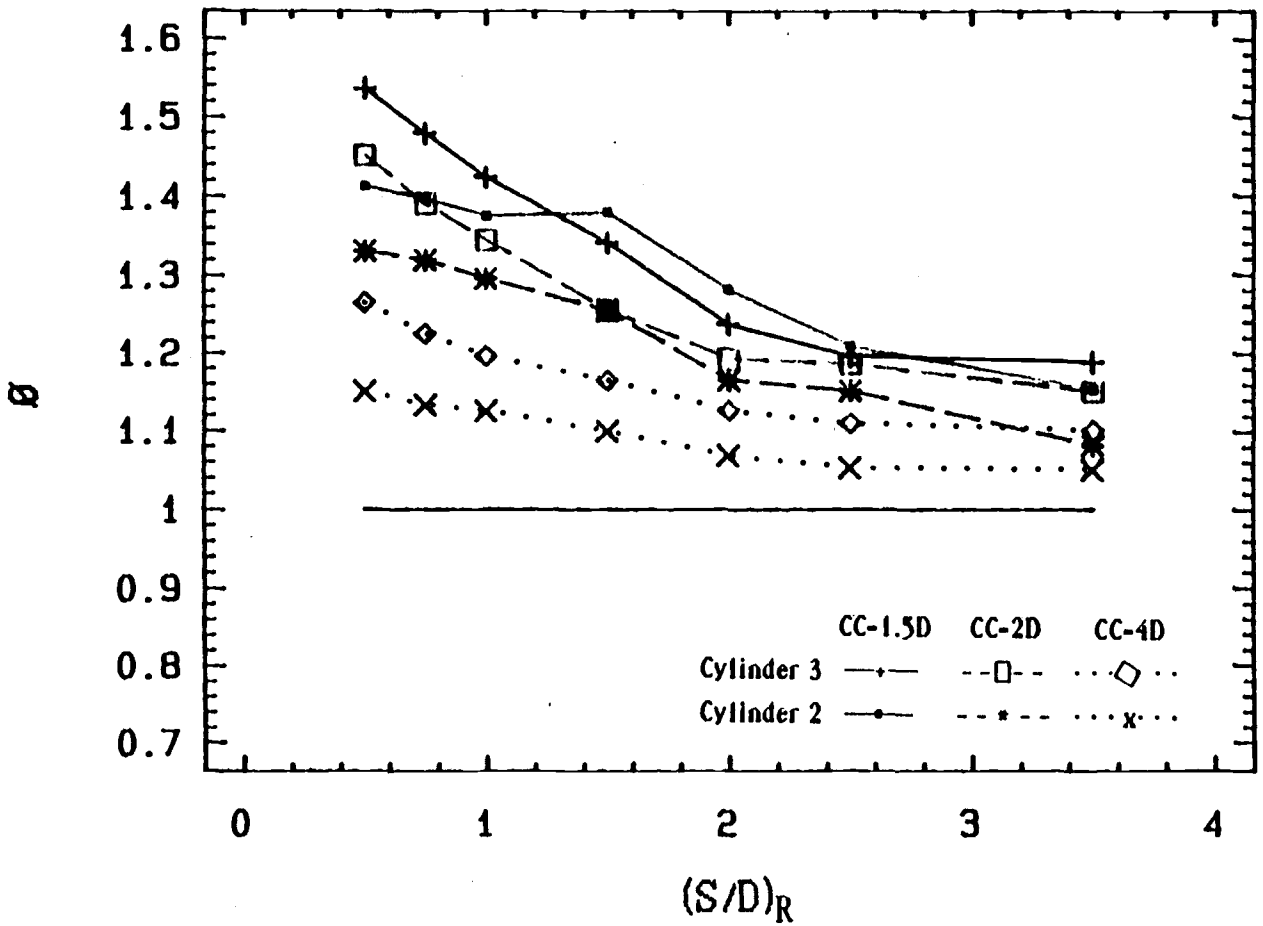

Figure 5.2 The effect of right wall spacing on the normalized temperature at q= 149.014 W/m^2.

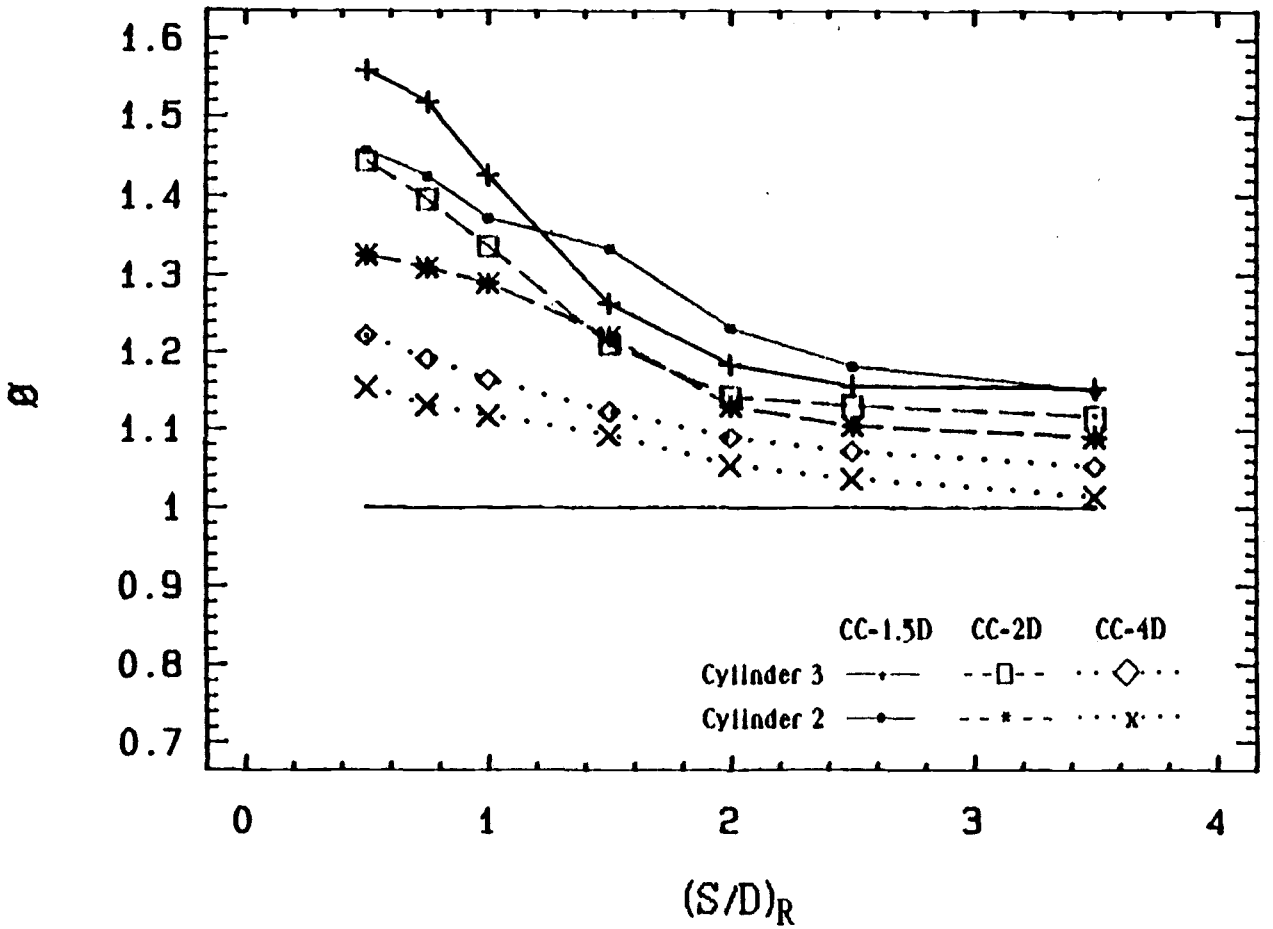

Figure 5.3 The effect of right wall spacing on the normalized temperature at q= 493.380 W/m^2.

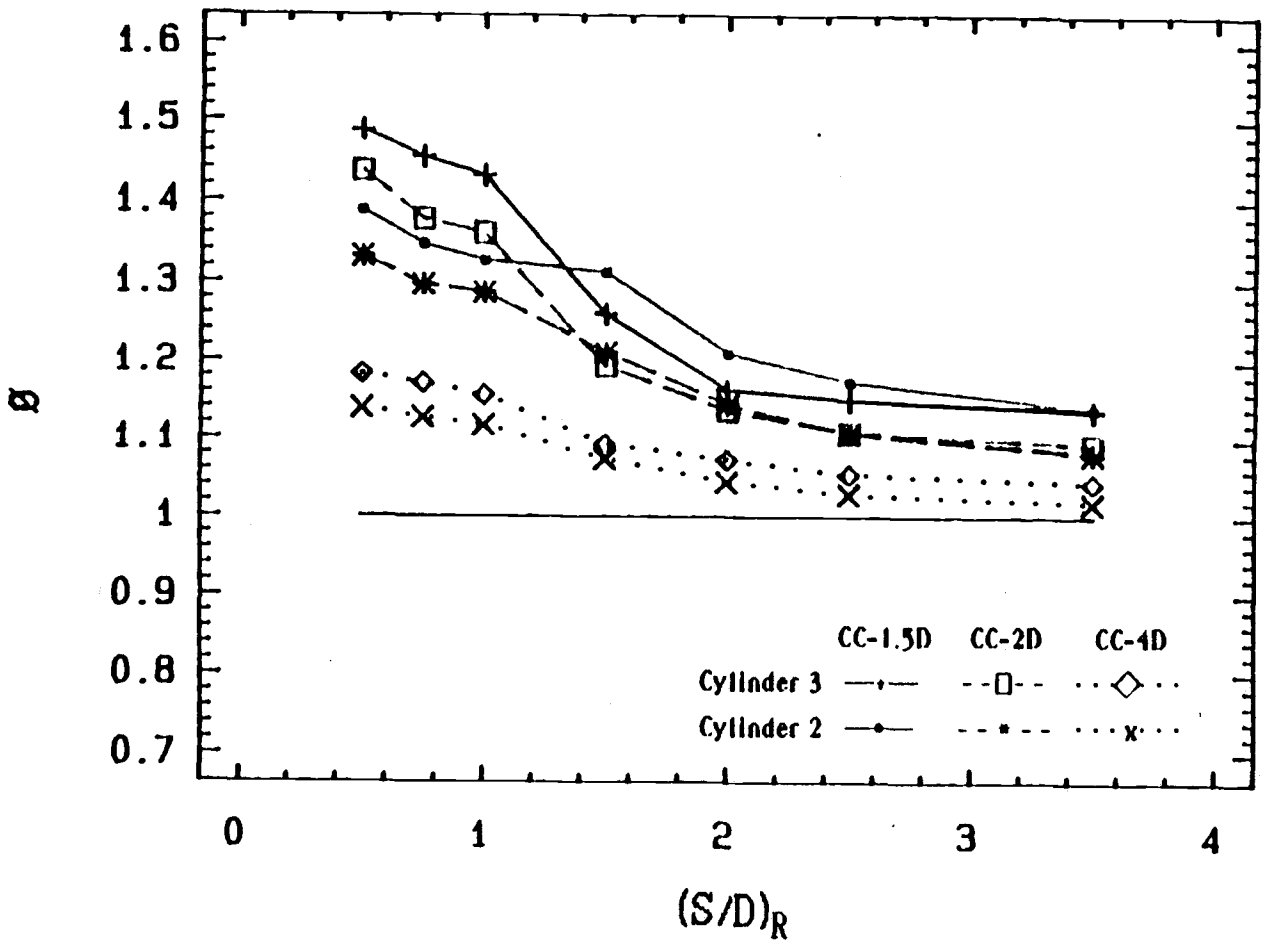

Figure 5.4 The effect of right wall spacing on the normalized temperature at q= 986.762 W/m^2.

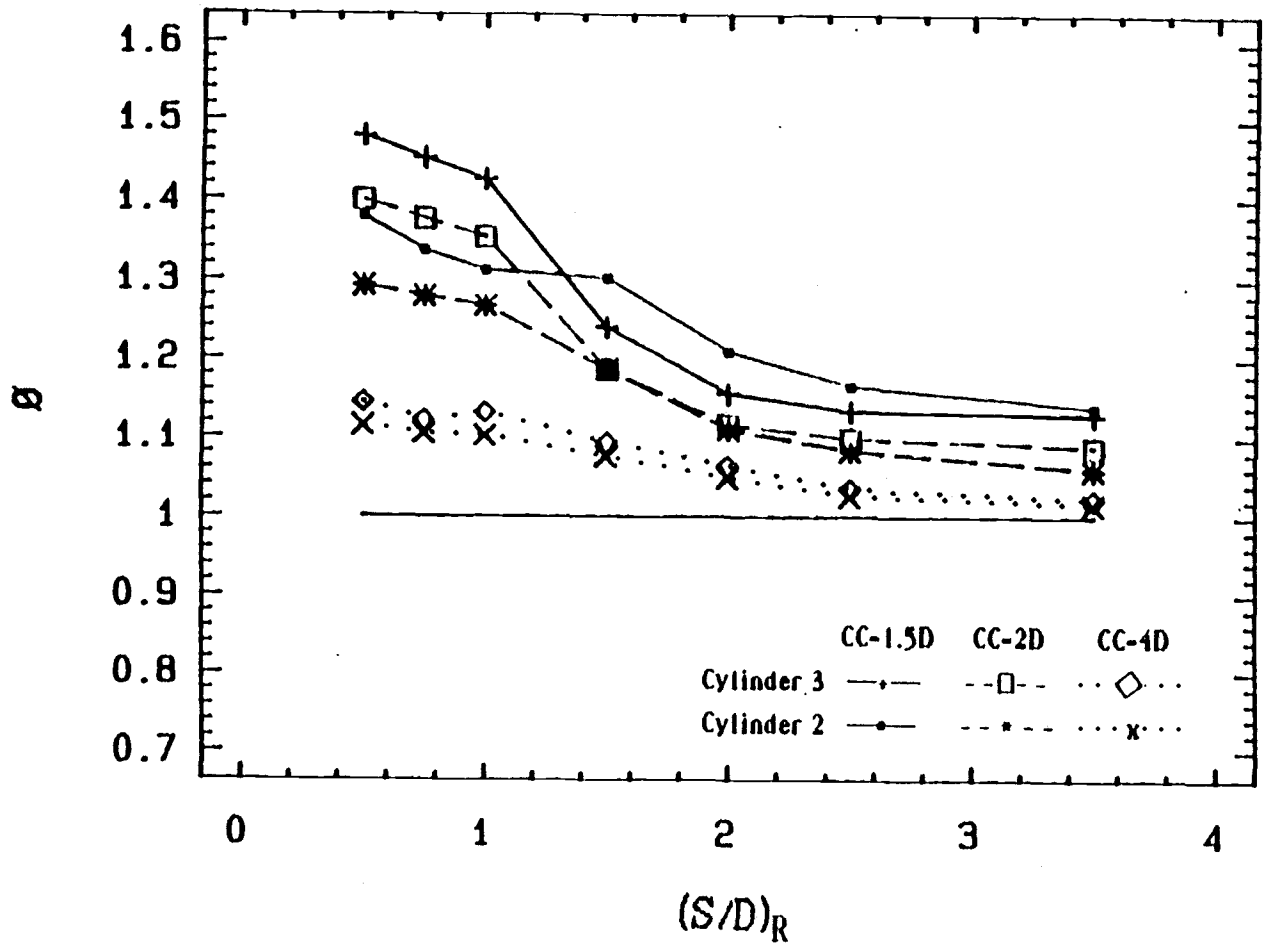

Figure 5.5 The effect of right wall spacing on the normalized temperature at q= 1480.143 W/m^2.

cylinders, cylinders 2 and 3, are shown to be greater than one and the Ø values are shown to decrease as the $(S/D)_R$ increases. Also, the reduction in Ø values, as $(S/D)_R$ increased, was found to decrease as the center-to-center spacing (CC) increased. Therefore, Ø is more sensitive to $(S/D)_R$ as the CC values decrease.

5.2 The effects of the right wall spacing, $(S/D)_R$, on the heat transfer from each cylinder in the array

The average Nusselt number, $Nu_{i,Rw}$, for each cylinder was calculated from equation 3.2 as discussed in chapter 3. Figures 5.6 through 5.11 show the effects of the right wall spacing $(S/D)_R$ on the Nusselt number of each cylinder at a specific input heat flux value. Figures 5.6 and 5.7 were plotted for CC = 1.5D and Figures 5.8 and 5.9 were plotted for CC = 2D. From these figures, the effects of $(S/D)_R$ on $Nu_{i,Rw}$ for CC = 1.5D are similar to the effects of $(S/D)_R$ on $Nu_{i,Rw}$ for CC = 2D. Figures 5.6 to 5.9 also show that the Nusselt numbers of the lowest cylinder decrease as $(S/D)_R$ increases. For the upper cylinders, the Nusselt numbers increase as $(S/D)_R$ increases. It can be noticed that the lowest cylinder is more sensitive to the wall spacing $(S/D)_R$ than the upper cylinders (cylinders 2 and 3) and has the highest Nu values at a specific heat flux.

The highest cylinder has the lowest Nu value at a specific heat flux and $(S/D)_R < 1.5$. At $(S/D)_R > 1.5$, $Nu_{2,Rw}$ and $Nu_{3,Rw}$ were found to have almost the same values, and at times $Nu_{3,Rw}$

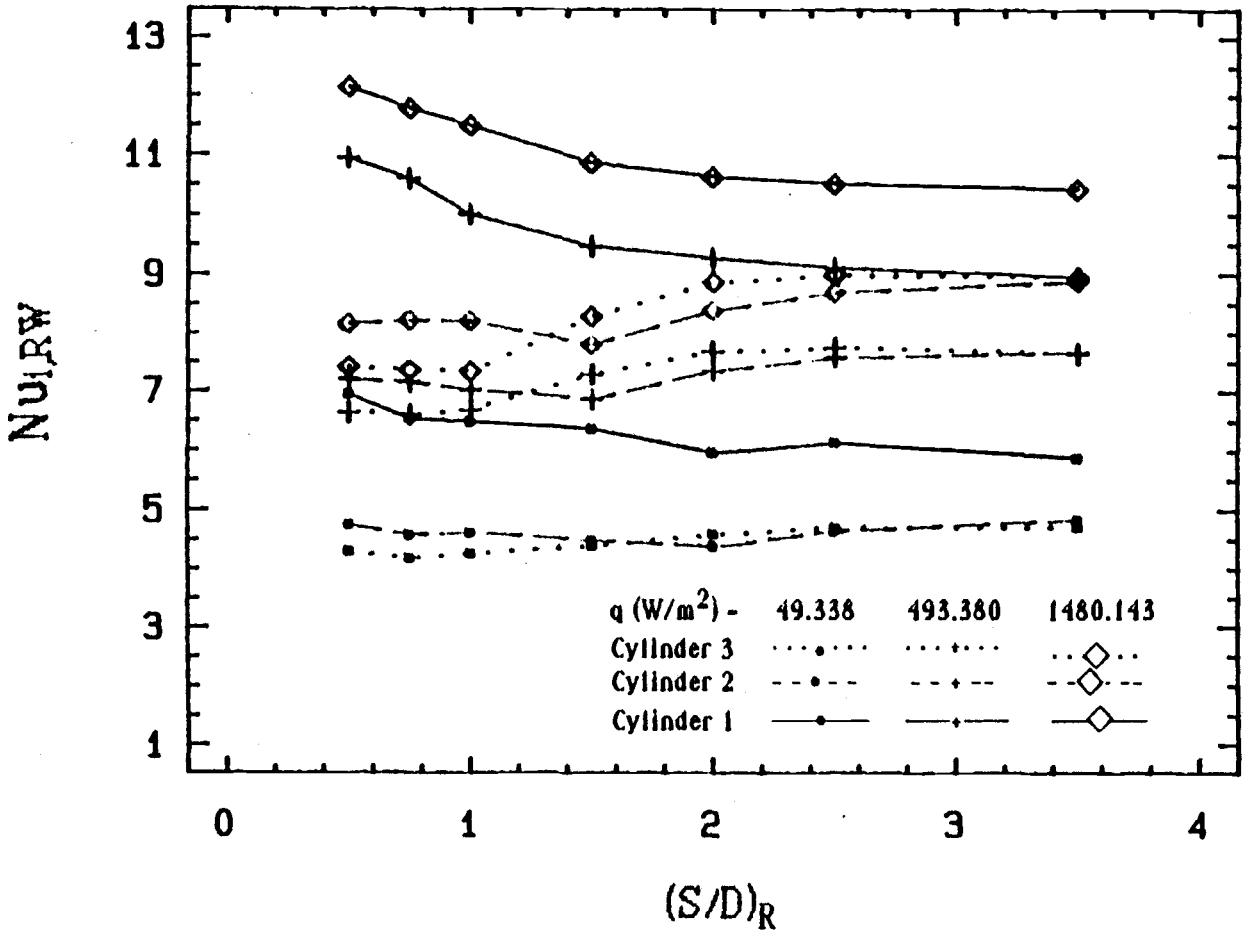

Figure 5.6 The effect of the right wall spacing on the average Nusselt number of each cylinder, $Nu_{i,RW}$, at CC=1.5D .

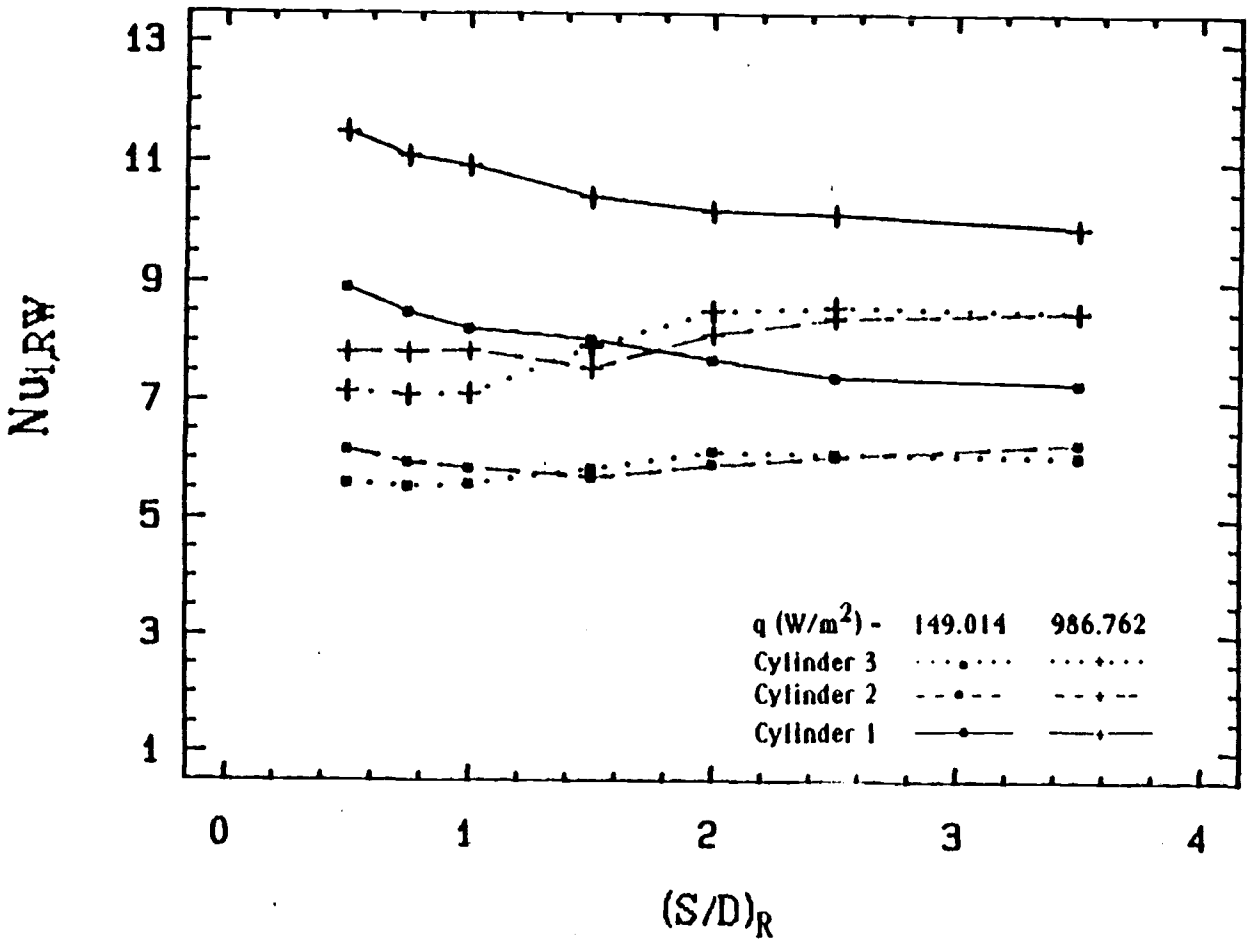

Figure 5.7 The effect of the right wall spacing on the average Nusselt number of each cylinder, $Nu_{i,RW}$, at CC=1.5D .

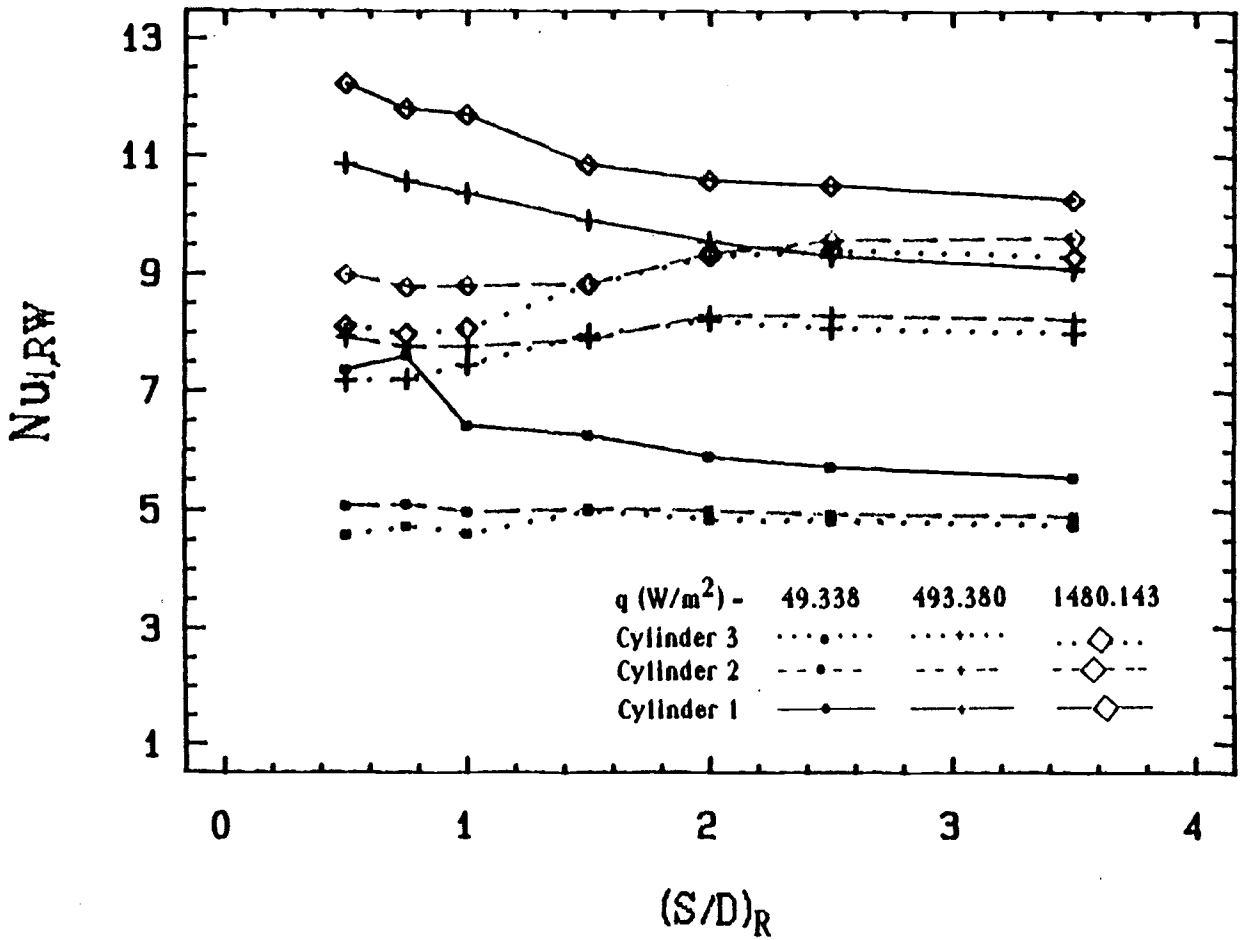

Figure 5.8 The effect of the right wall spacing on the average Nusselt number of each cylinder, $Nu_{i,RW}$, at CC=2D

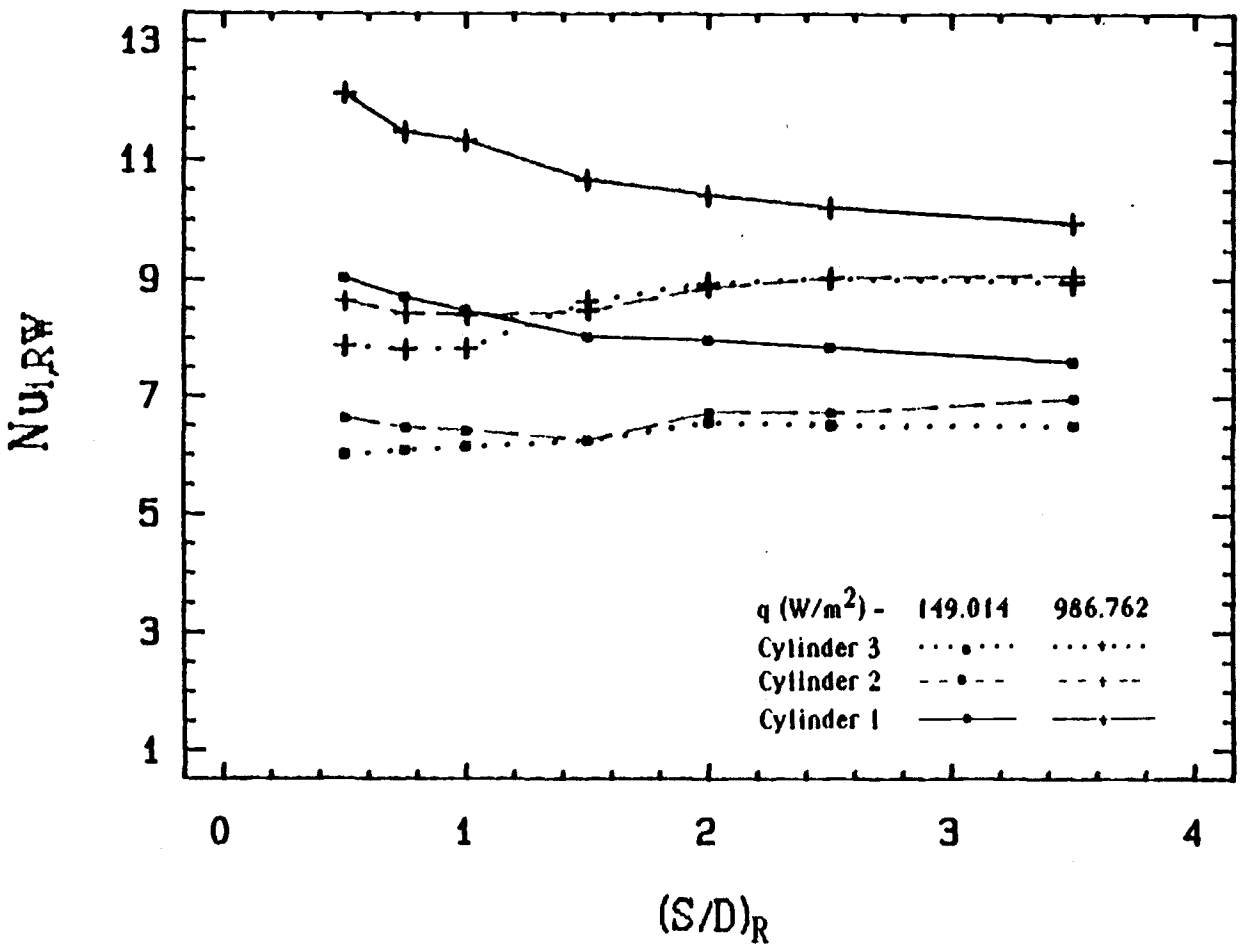

Figure 5.9 The effect of the right wall spacing on the average Nusselt number of each cylinder, $Nu_{i,RW}$, at CC=2D

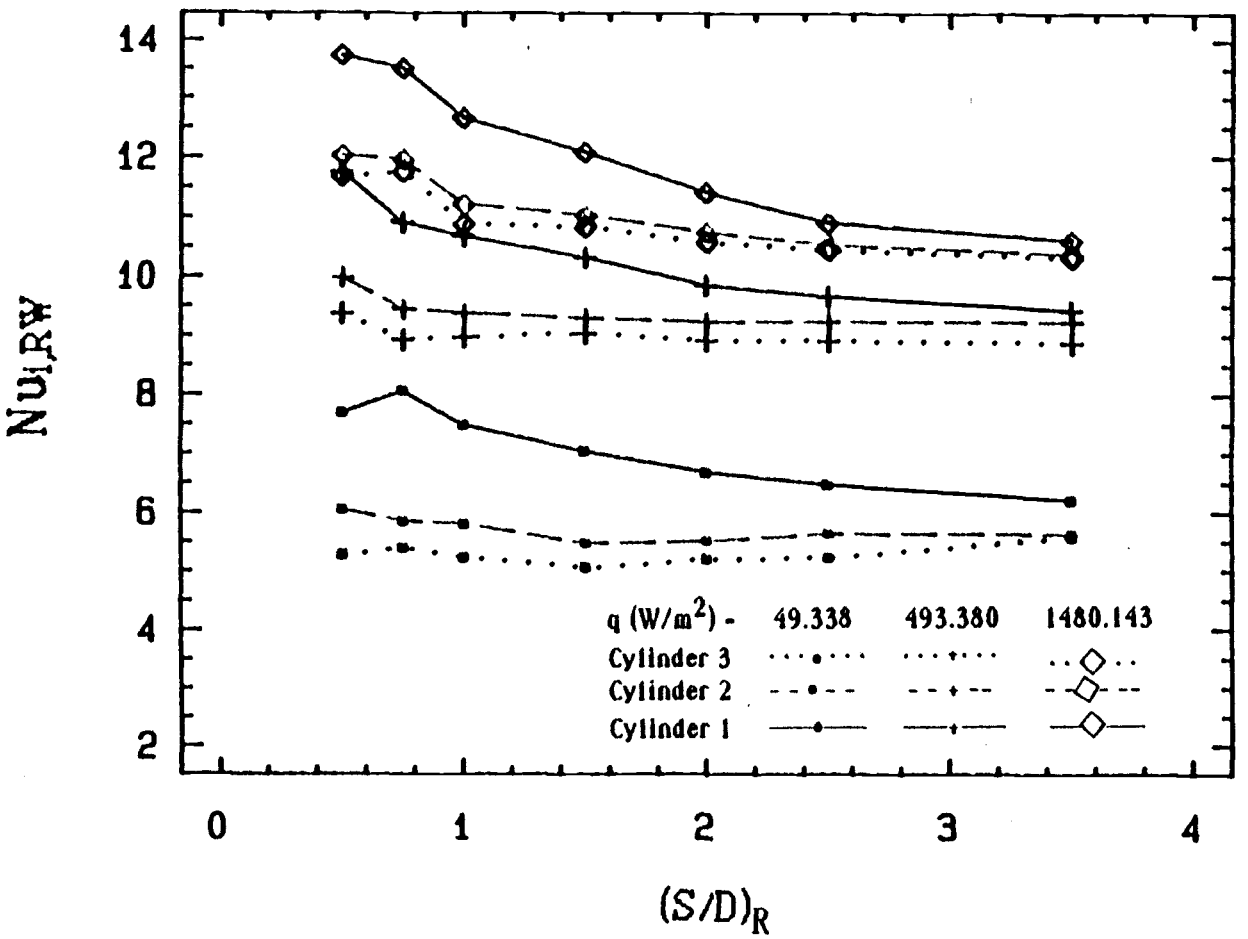

Figure 5.10 The effect of the right wall spacing on the average Nusselt number of each cylinder, $Nu_{i,RW}$, at CC=4D .

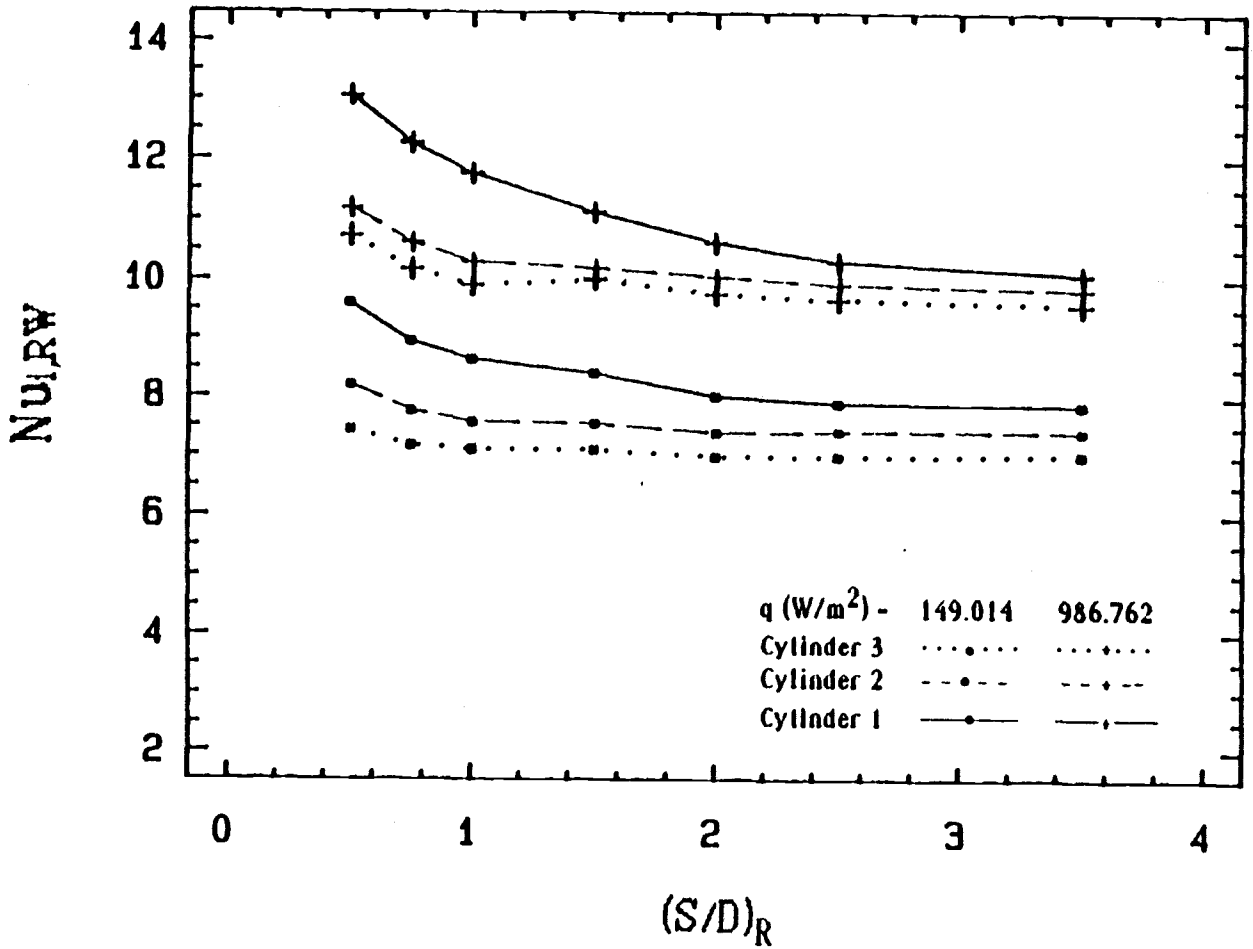

Figure 5.11 The effect of the right wall spacing on the average Nusselt number of each cylinder, $Nu_{i,RW}$, at CC=4D .

became higher than $Nu_{2,Rw}$. This can be explained as follows. At $(S/D)_R < 1.5$, the plume was restricted to upward movement, and the upper cylinders were surrounded by a high temperature plume. As the right wall spacing $(S/D)_R$ increased, the plume at the right side of the array had a lower velocity than the plume at the left side of the array. The high velocity of the plume at the left side of the array created an unbalanced pressure at the top of the array and caused a reversed current from the ambient to the spacing between the two walls above the array. This current removed more heat from the top cylinder, which resulted in an increase of the $Nu_{3,Rw}$ value.

At CC = 4D, the Nusselt numbers for the three cylinders decrease as $(S/D)_R$ increases, as shown in figures 5.10 and 5.11. At a specific heat flux value, the lowest cylinder has the highest Nusselt number in the array, the second cylinder has the next highest Nusselt number, and the highest cylinder (cylinder 3) has the lowest Nusselt number. These findings are unlike the single wall case, where Nu_3 is the highest and Nu_1 is the lowest.

This is because the right wall restricted all the air particles to move in the direction of the high temperature raised plume, which surrounded the upper cylinders. This will be discussed in detail in Chapter 6.

Three different Nusselt number ratios were used in this chapter to study the effects of the right wall spacing on the cylinders of the array. These ratios are:

1) $(Nu_{i,Rw}/Nu_{i,E})$, the Nusselt number of each cylinder to the Nusselt number as calculated from equation 4.1, $Nu_{1,E} = 0.571\ Ra_{1,f}^{*0.2027}$, where $Ra_{1,f}^{*}$ is the modified Rayleigh number value of the lowest cylinder when there is no wall (i.e., free array) at the same q. This ratio is shown in the following equation:

$$\frac{Nu_{i,RW}}{Nu_{i,E}} = \frac{Nu_{i,RW}}{[\,0.571\ Ra_{1,f}^{*\,0.2027}\,]} \qquad (5.1)$$

2) $(Nu_{i,Rw}/Nu_{i,0.5})$, the Nusselt number of each cylinder to the Nusselt number of the same cylinder with the presence of a single wall at S/D = 0.5.
3) $(Nu_{i,Rw}/Nu_{i,f})$, the ratio of the Nusselt number of each cylinder to the Nusselt number of the same cylinder when there is no wall (i.e., free array).

The deviation of $Nu_{i,Rw}$ from the Nusselt number value of a free cylinder, $Nu_{i,s}$, can be noted by the $Nu_{i,Rw}/Nu_{i,E}$ ratio. This is attributable to the fact that the lowest cylinder in a free array behaves the same as a free single cylinder, as shown in Chapter 4. Figures 5.12 to 5.17 show the $Nu_{i,Rw}/Nu_{i,E}$ versus $(S/D)_R$. At CC= 1.5D and CC = 2D, there was a 30% to 40% enhancement in the lowest cylinder (cylinder 1) when the right wall spacing was $(S/D)_R$ = 0.5 (i.e., the array was placed midway between the two walls). For CC = 4D, this enhancement was between 40% and 50%.

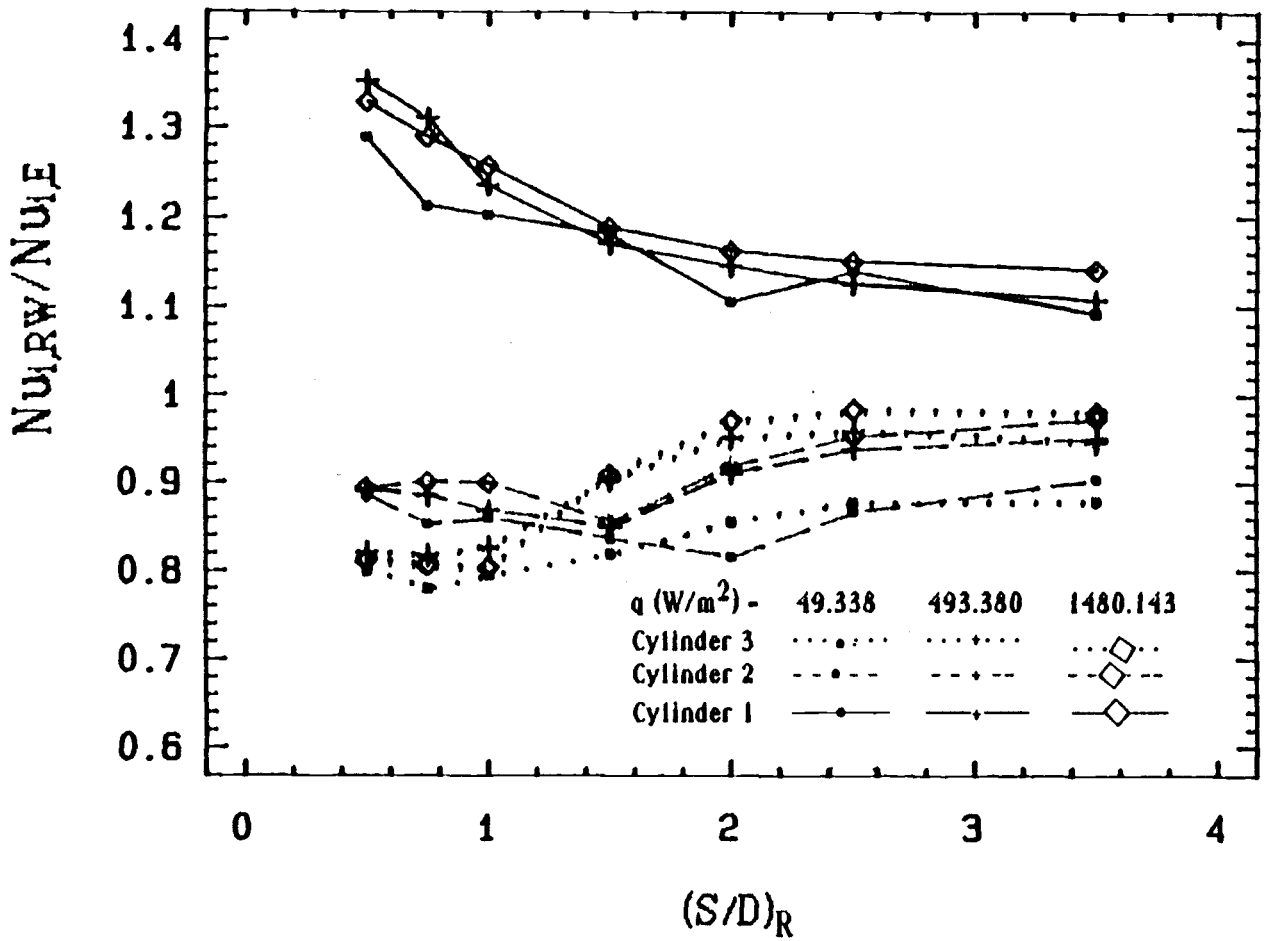

Figure 5.12 The effect of the wall spacing on the Nusselt number ratio, $Nu_{i,RW}/Nu_{i,E}$, at CC=1.5D .

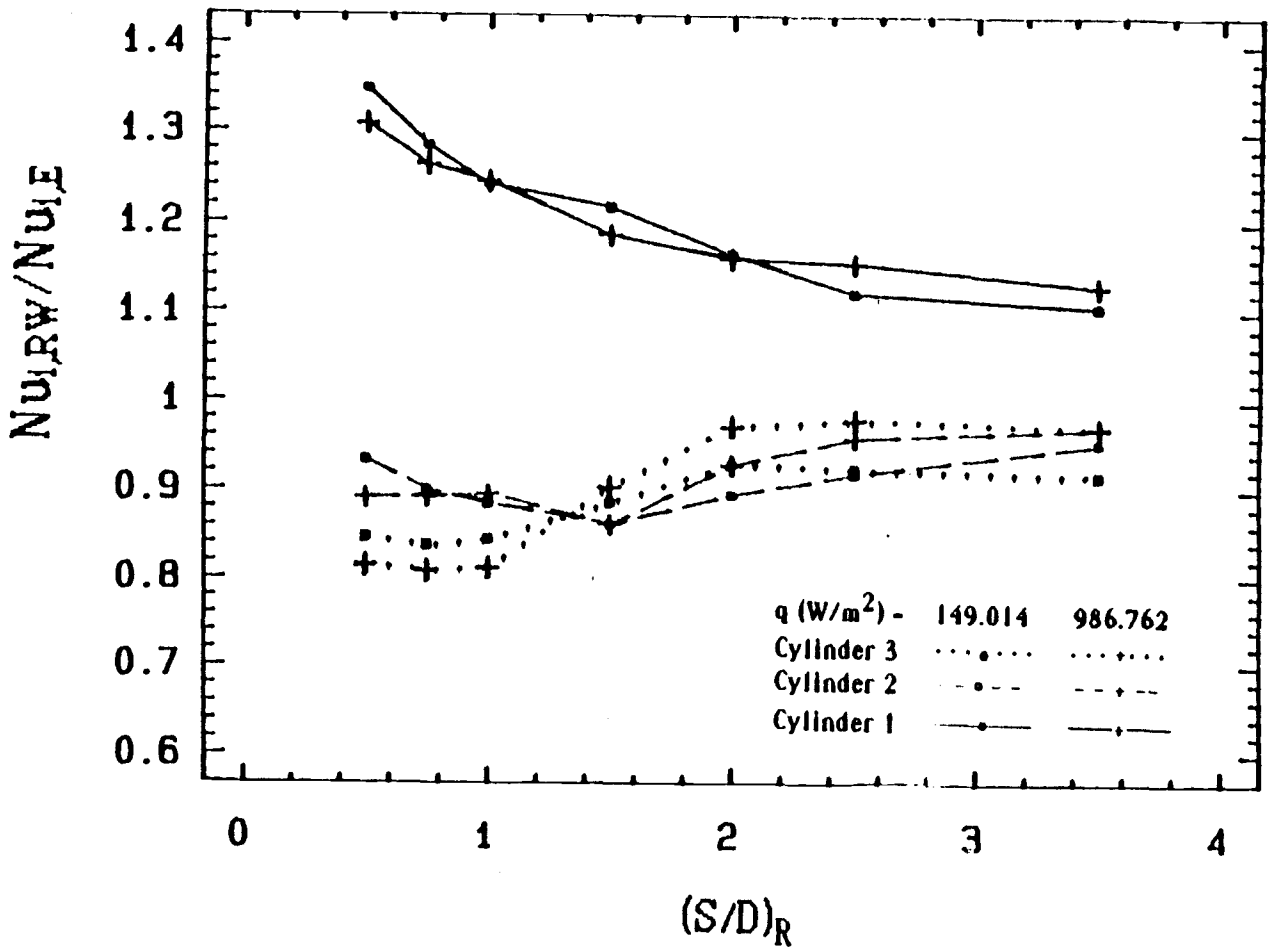

Figure 5.13 The effect of the wall spacing on the Nusselt number ratio, $Nu_{i.RW}/Nu_{i,E}$, at CC=1.5D .

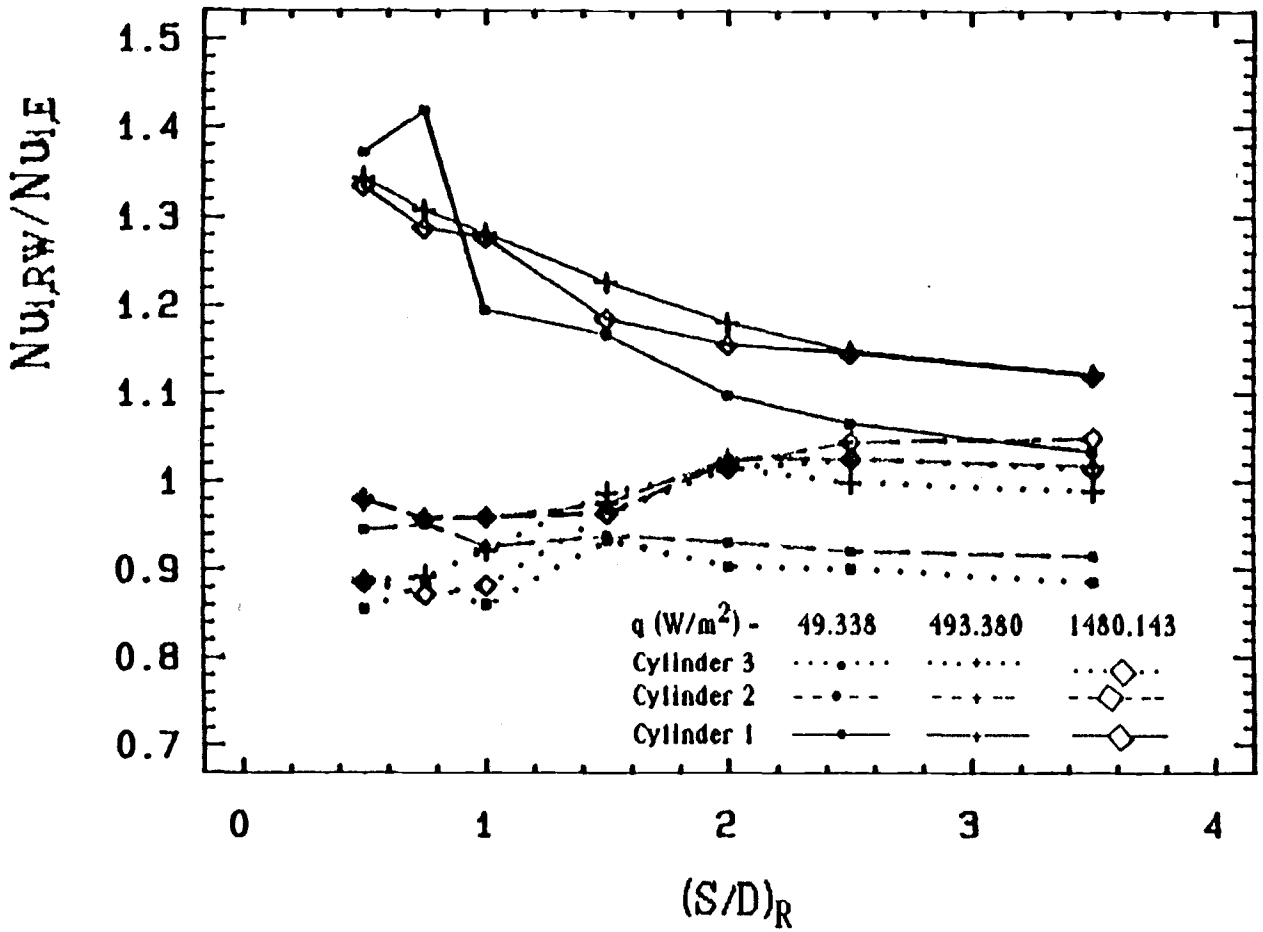

Figure 5.14 The effect of the wall spacing on the Nusselt number ratio, $Nu_{i,RW}/Nu_{i,E}$, at CC=2D.

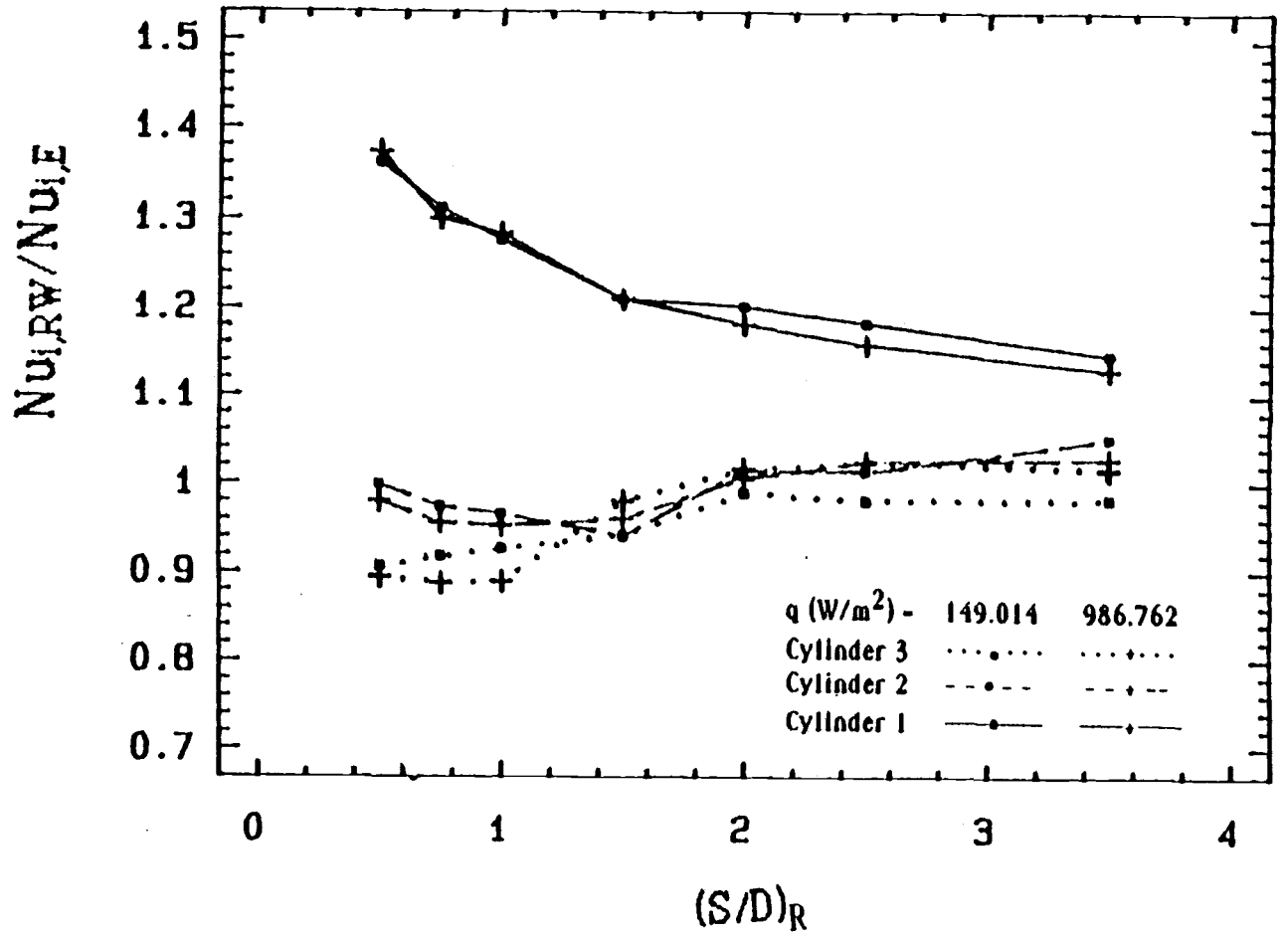

Figure 5.15 The effect of the wall spacing on the Nusselt number ratio, $Nu_{i,RW}/Nu_{i,E}$, at CC=2D.

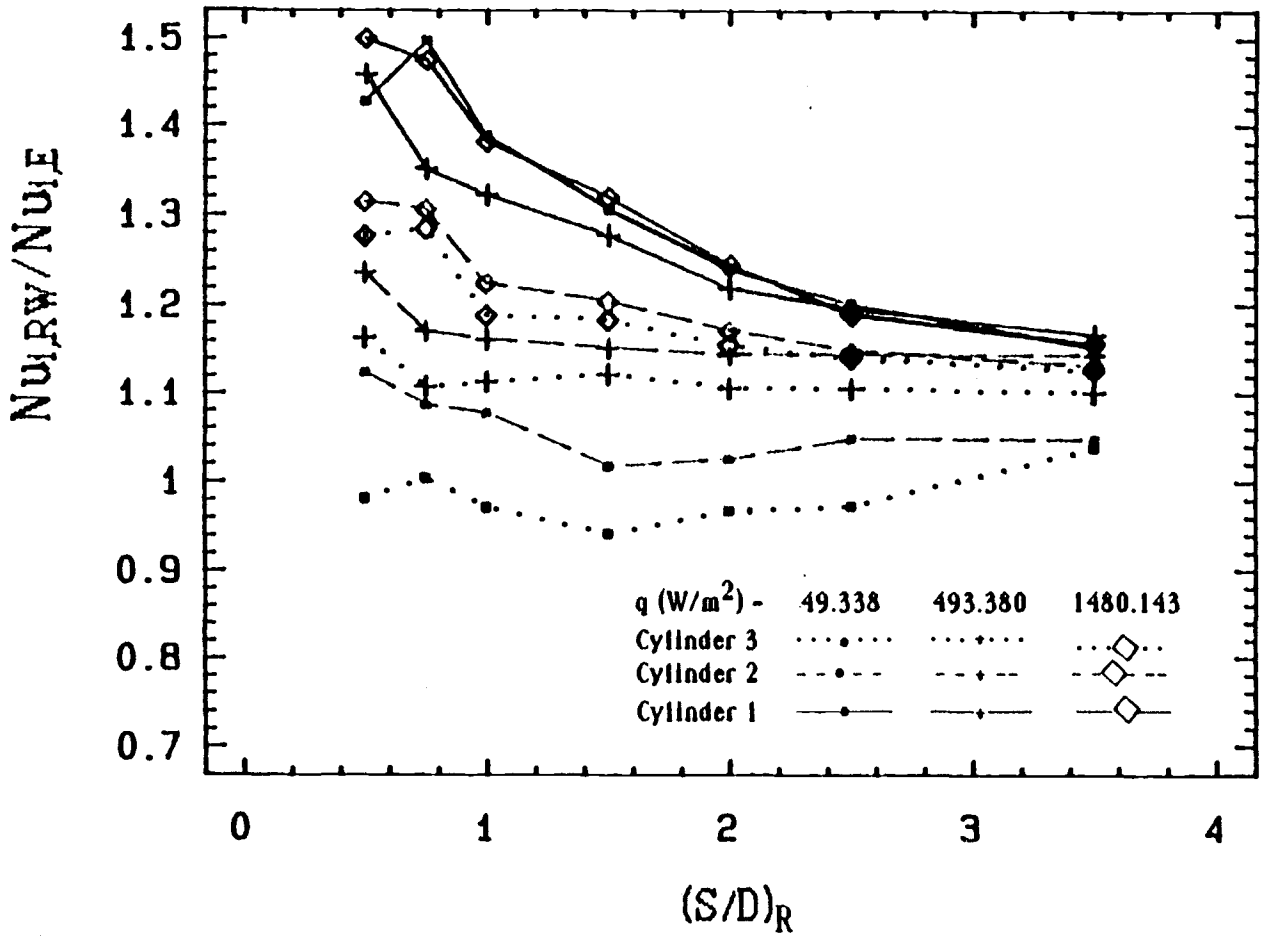

Figure 5.16 The effect of the wall spacing on the Nusselt number ratio, $Nu_{i,RW}/Nu_{i,E}$, at CC=4D.

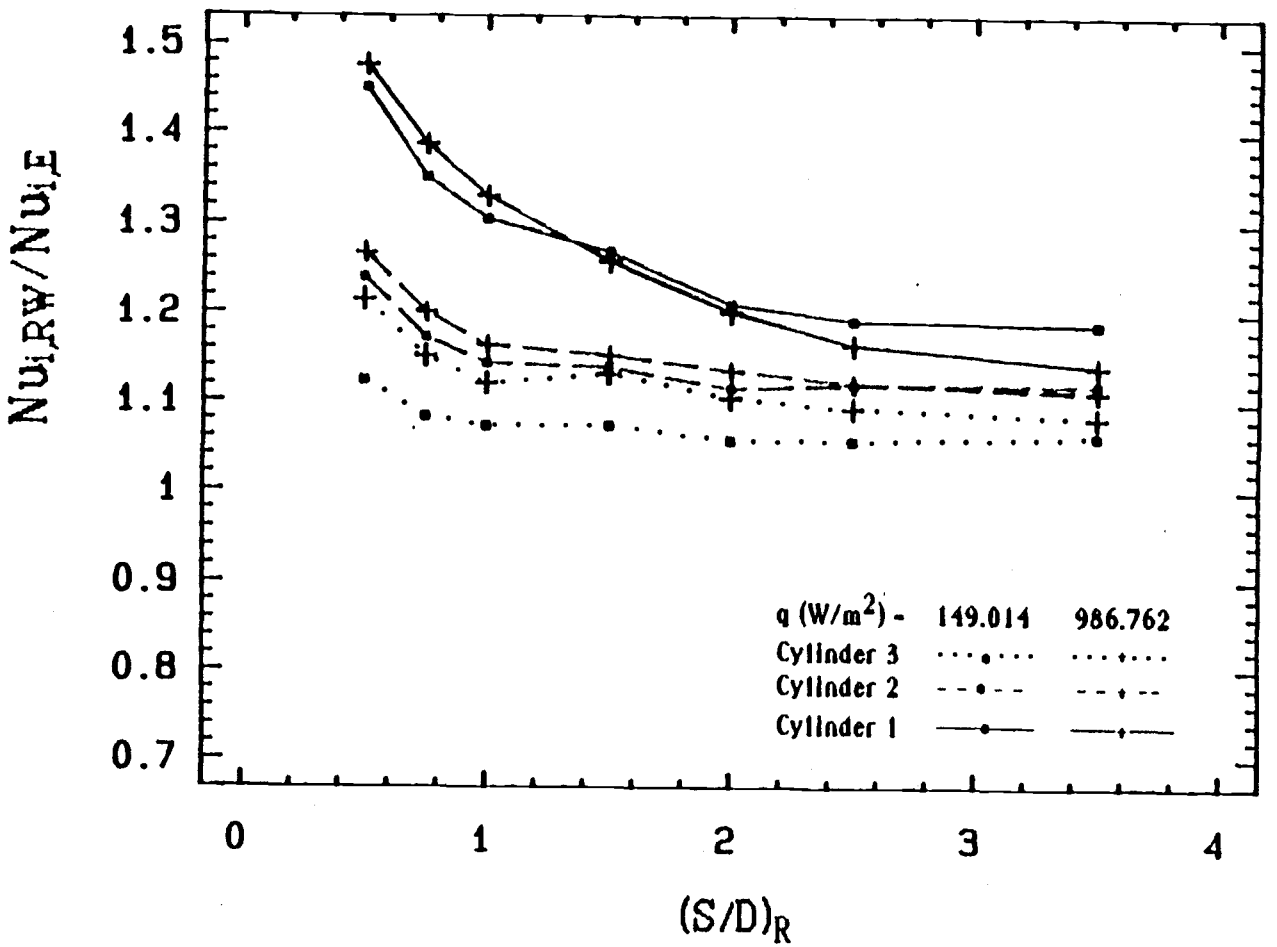

Figure 5.17 The effect of the wall spacing on the Nusselt number ratio, $Nu_{i,RW}/Nu_{i,E}$, at CC=4D.

For all the CC values, the ratio, $Nu_{1,Rw}/Nu_{1,E}$, decreased as the $(S/D)_R$ increased.

The behavior of the lowest cylinder ratios, $Nu_{1,Rw}/Nu_{1,0.5}$ (as shown in figures 5.18 to 5.23) and $Nu_{1,Rw}/Nu_{1,f}$ (as shown in figures 5.24 to 5.29) is the same as the behavior of $Nu_{1,Rw}/Nu_{1,E}$. This is because $Nu_{1,E}$ represents the correlated function of $Nu_{1,f}$ (which is the exact value), and $Nu_{1,0.5}$ is about 5% higher than $Nu_{1,E}$ as shown in chapter 4.

In figures 5.12 to 5.29, the upper cylinders (cylinders 2 and 3) have the same pattern at CC = 1.5D and CC = 2D. While at CC = 4D, the upper cylinders behave differently. The Nusselt number ratios show three stages for the upper cylinders at CC = 1.5D and CC = 2D. The first stage is between $(S/D)_R$ = 0.5 to 1.0, where the Nusselt number ratios were almost the same at a specific q. The second stage range is from $(S/D)_R$ = 1.0 to 2.0. In this stage the ratios ($Nu_{i,Rw}/Nu_{i,E}$, $Nu_{i,Rw}/Nu_{i,0.5}$, and $Nu_{i,Rw}/Nu_{i,f}$) increase sharply as $(S/D)_R$ increases. The third stage starts at $(S/D)_R$ = 2.0 and the ratios are less sensitive to $(S/D)_R$ changes.

The second cylinder shows a 2% to 10% degradation in the first stage of ($Nu_{i,Rw}/Nu_{i,E}$) and ($Nu_{i,Rw}/Nu_{i,0.5}$), while the third cylinder shows an 8% to 20% degradation in this stage. This means that the ($Nu_{i,Rw}/Nu_{i,E}$) and ($Nu_{i,Rw}/Nu_{i,0.5}$) for the third cylinders are lower than that of the second cylinder at CC = 1.5D and CC = 2D. The second stage is the transition stage where the Nu ratios for the third cylinder cross the Nu ratios of the second

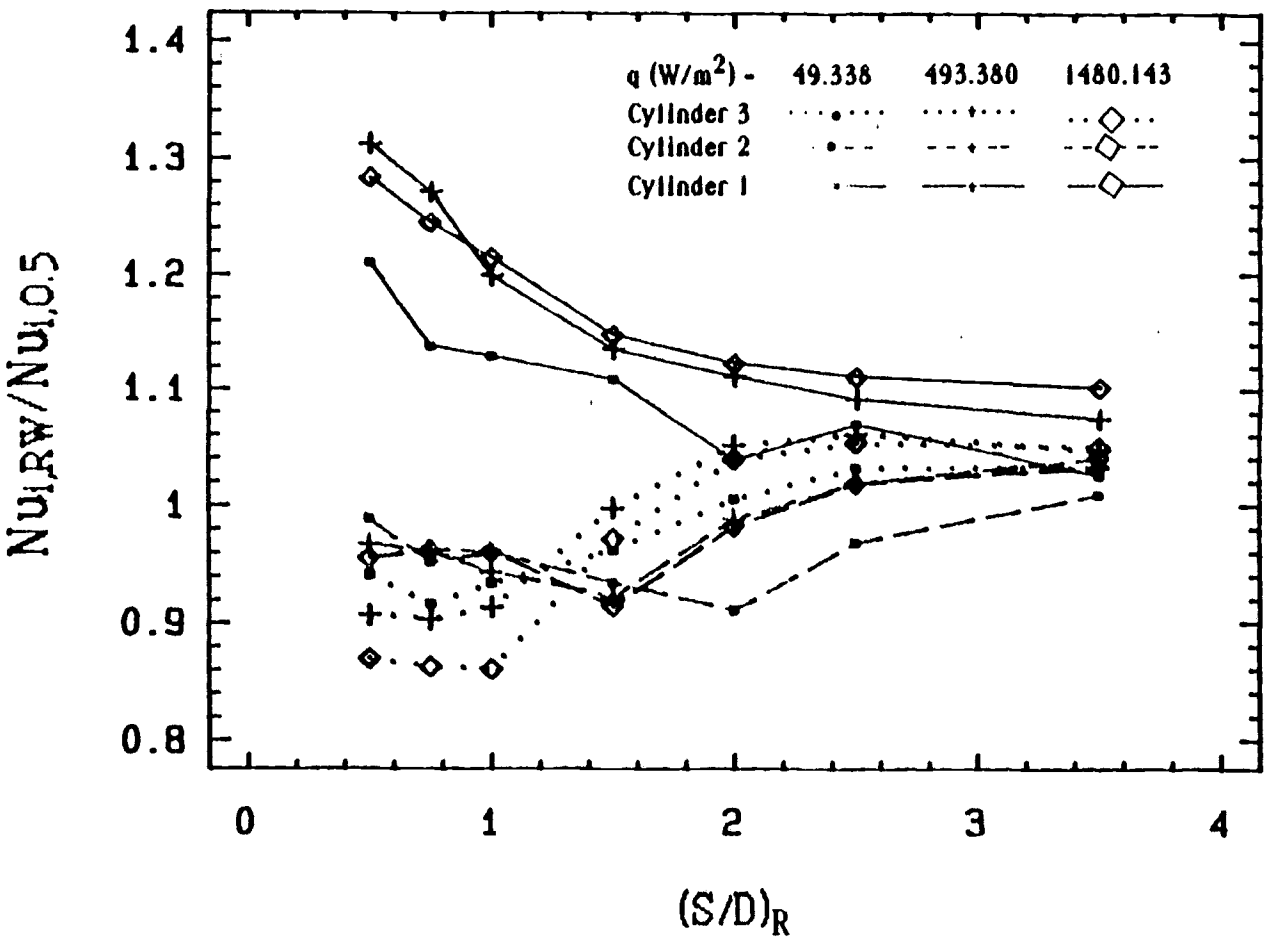

Figure 5.18 The effect of the wall spacing on the Nusselt number ratio, $Nu_{i,RW}/Nu_{i,0.5}$, at CC=1.5D.

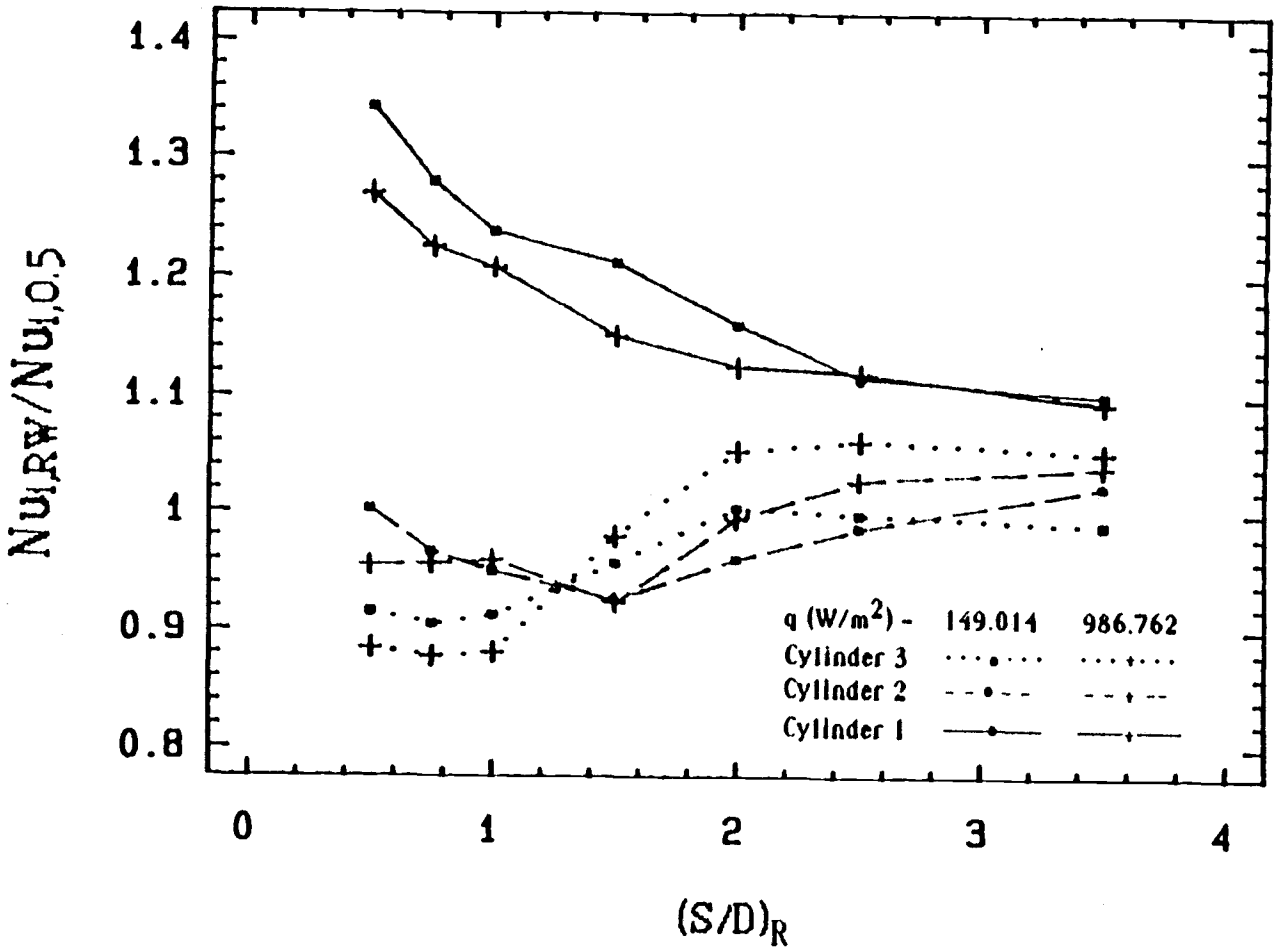

Figure 5.19 The effect of the wall spacing on the Nusselt number ratio, $Nu_{i,RW}/Nu_{i,0.5}$, at CC=1.5D.

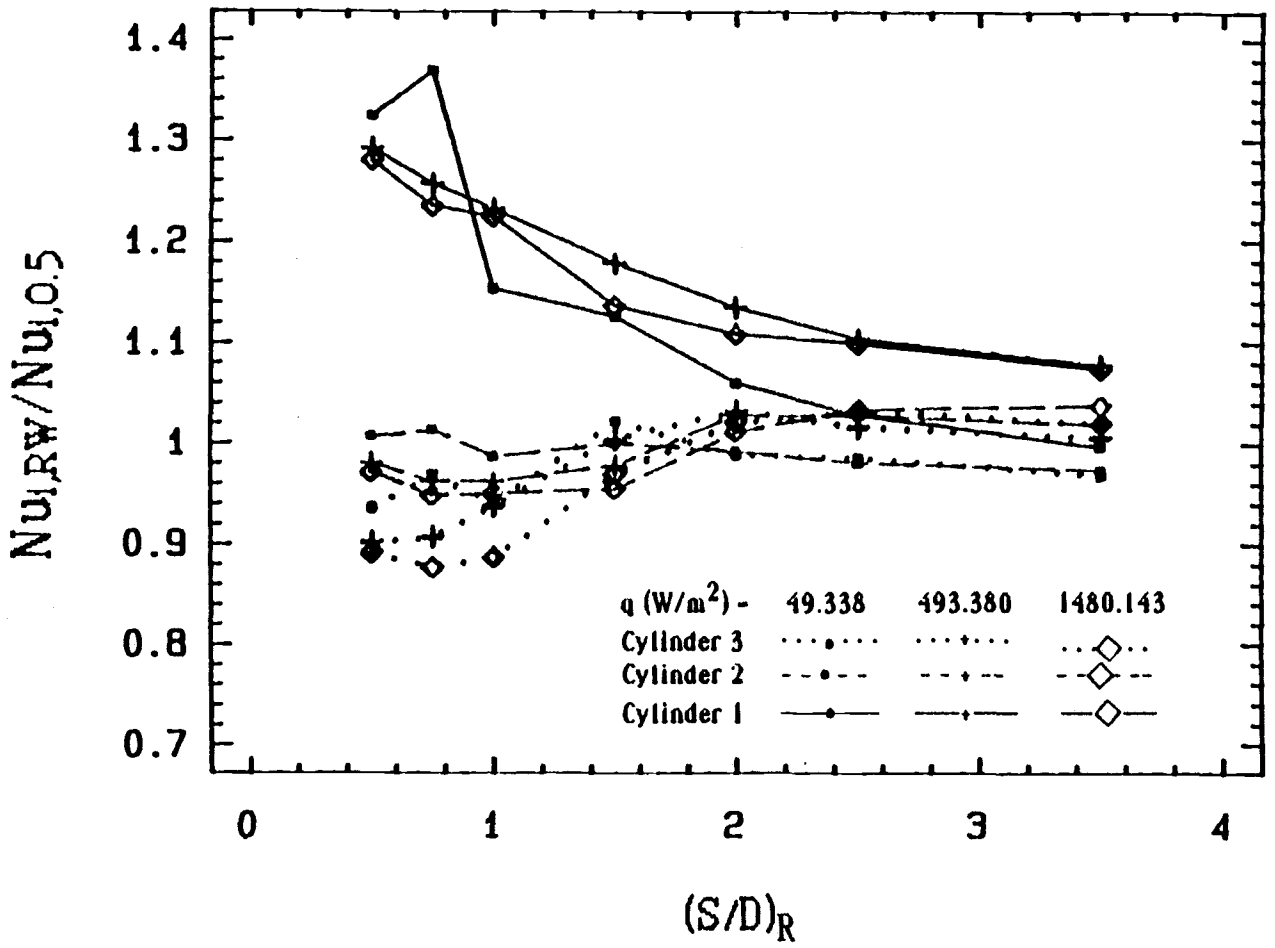

Figure 5.20 The effect of the wall spacing on the Nusselt number ratio, $Nu_{i,RW}/Nu_{i,0.5}$, at CC=2D.

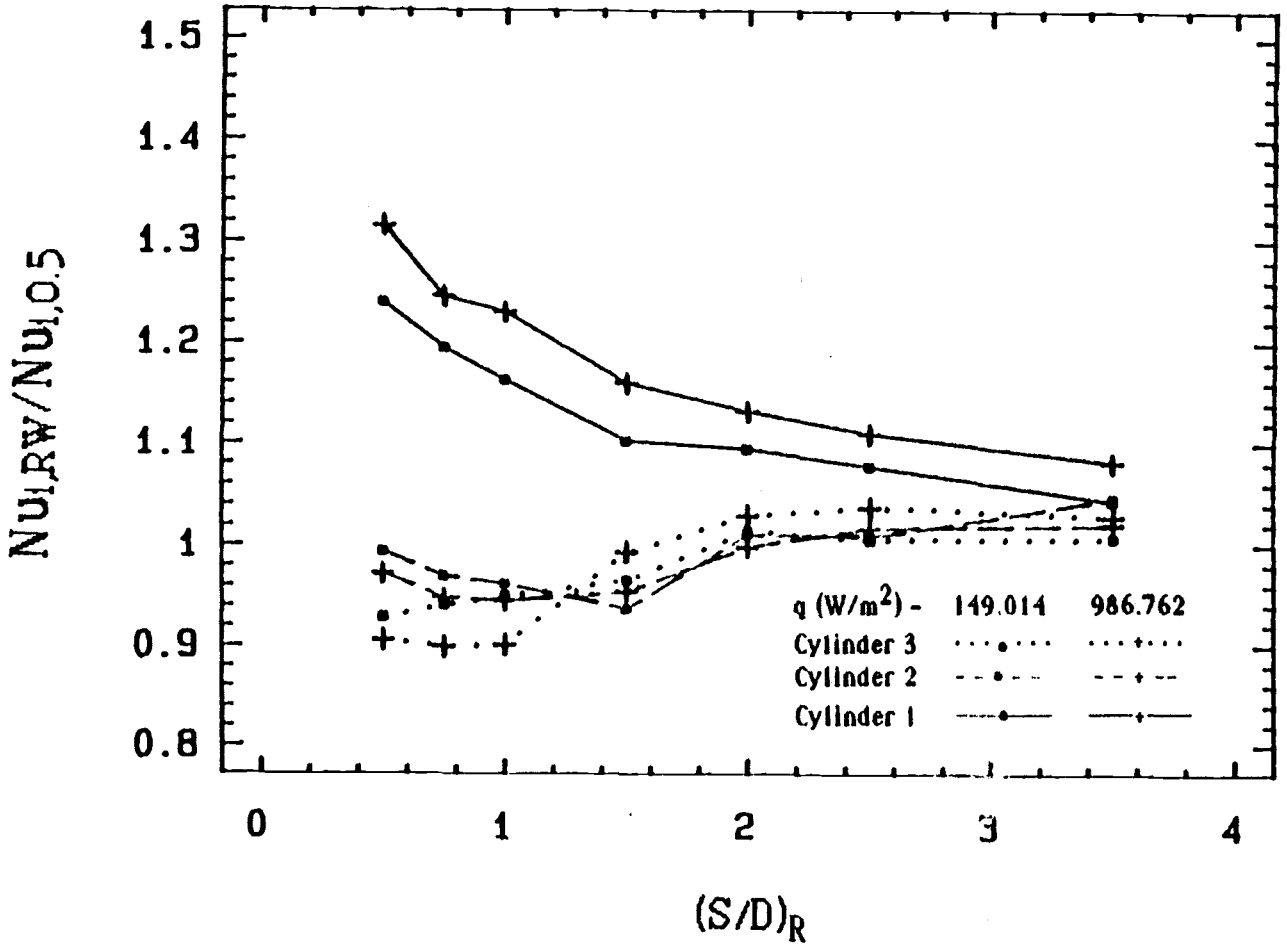

Figure 5.21 The effect of the wall spacing on the Nusselt number ratio, $Nu_{i,RW}/Nu_{i,0.5}$, at CC=2D.

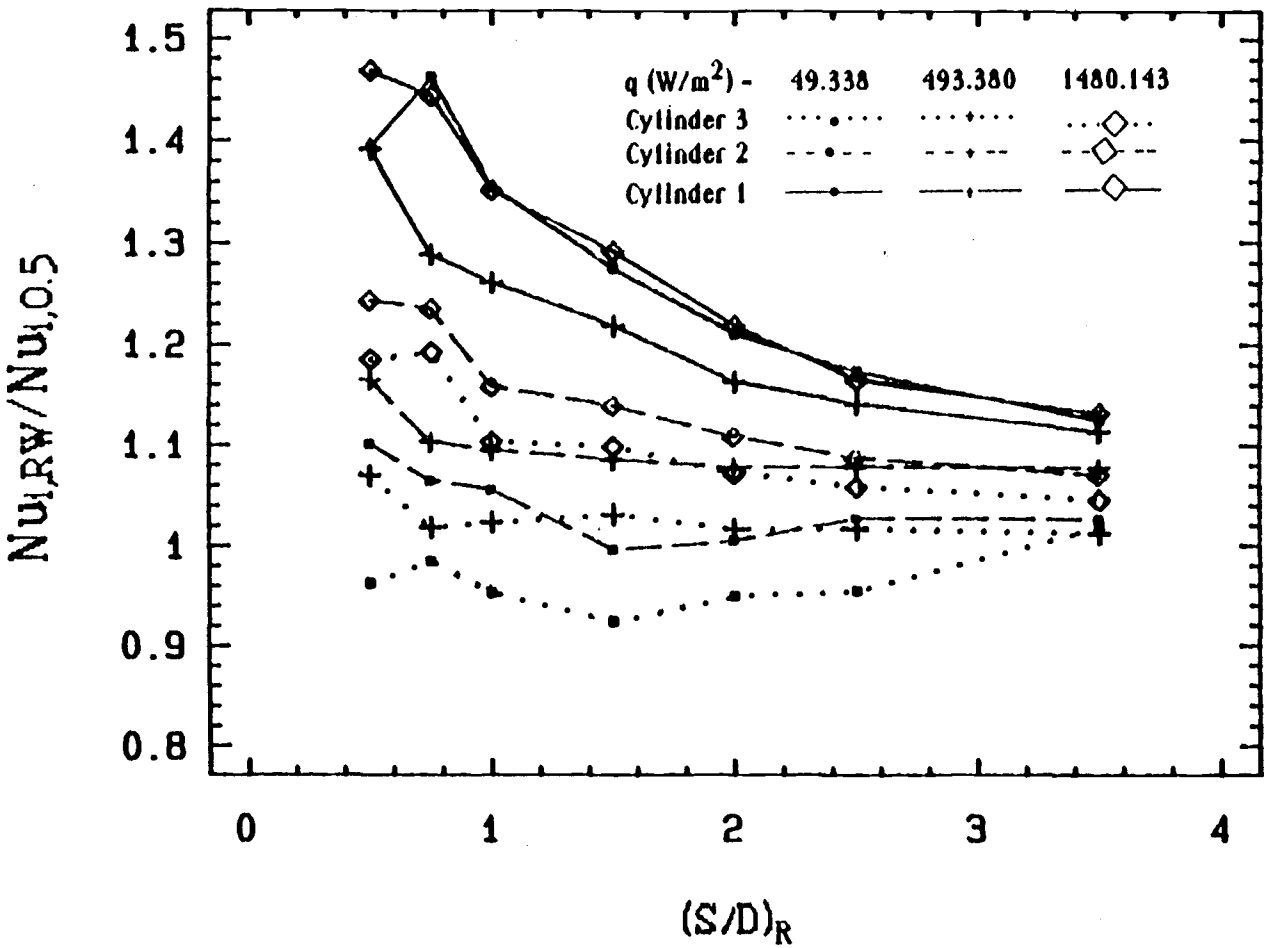

Figure 5.22 The effect of the wall spacing on the Nusselt number ratio, $Nu_{i,RW}/Nu_{i,0.5}$, at CC=4D.

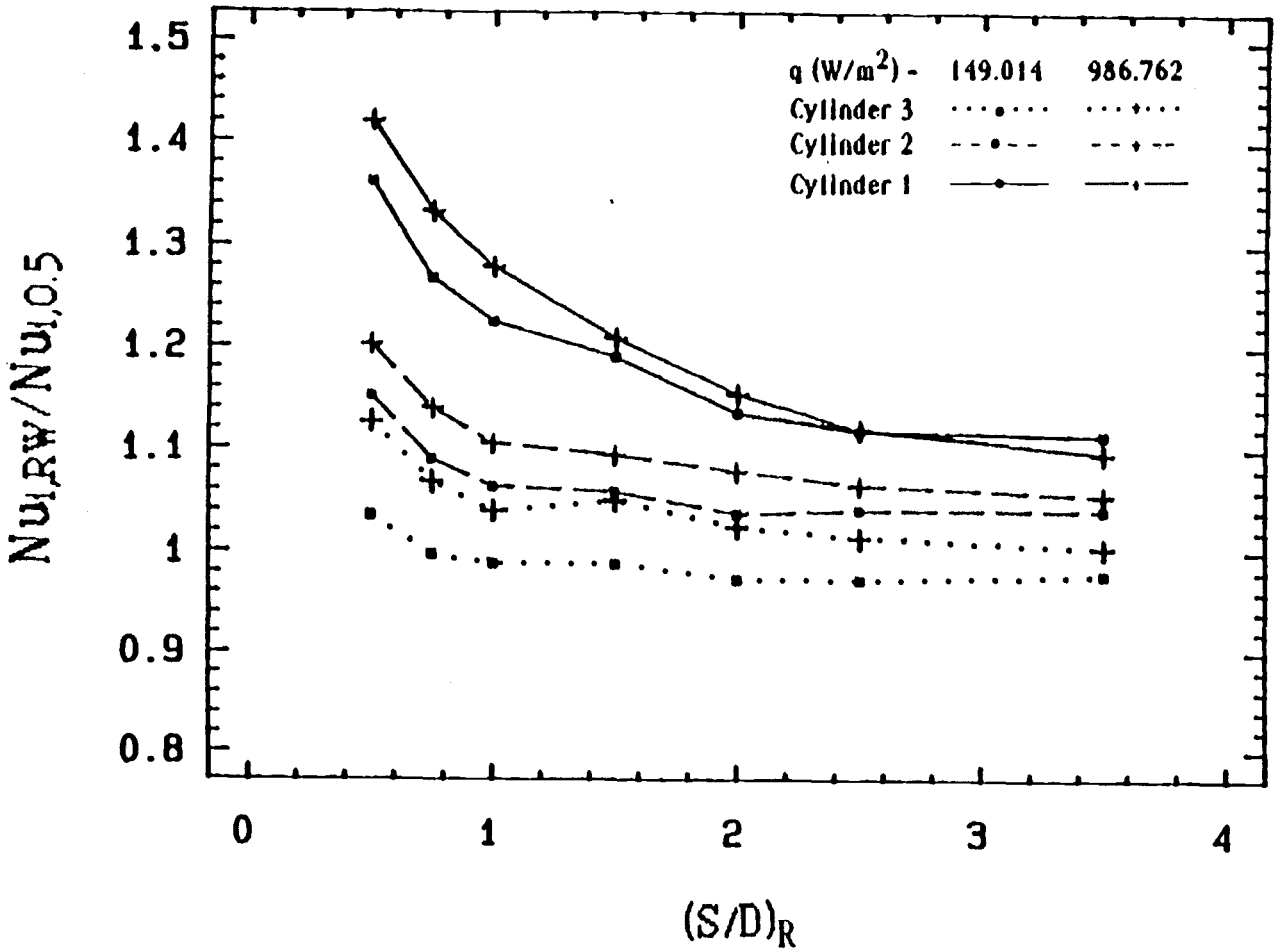

Figure 5.23 The effect of the wall spacing on the Nusselt number ratio, $Nu_{i,RW}/Nu_{i,0.5}$, at CC=4D.

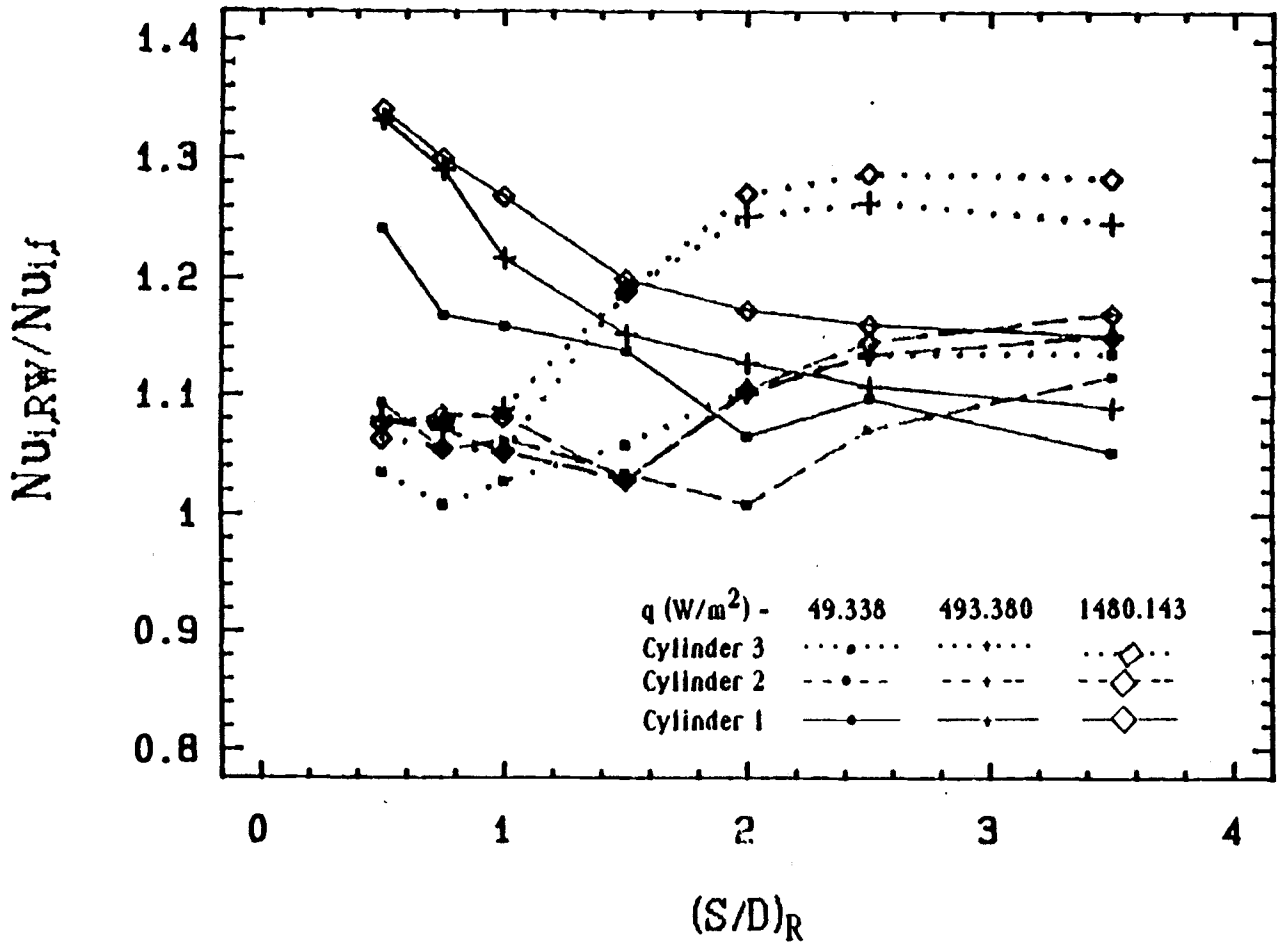

Figure 5.24 The effect of the wall spacing on the Nusselt number ratio, $Nu_{i,RW}/Nu_{i,f}$, at CC=1.5D..

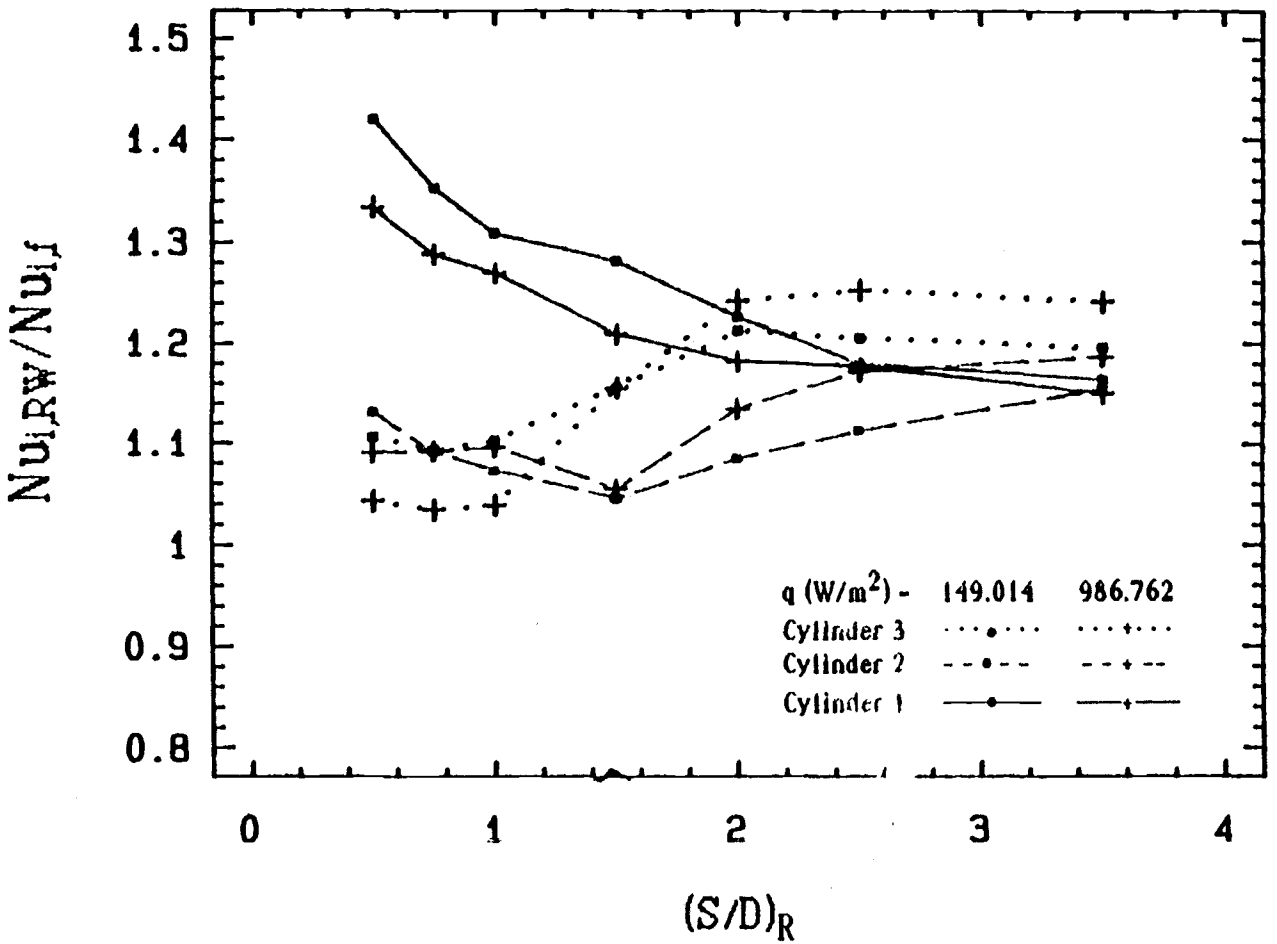

Figure 5.25 The effect of the wall spacing on the Nusselt number ratio, $Nu_{i,RW}/Nu_{i,f}$, at CC=1.5D.

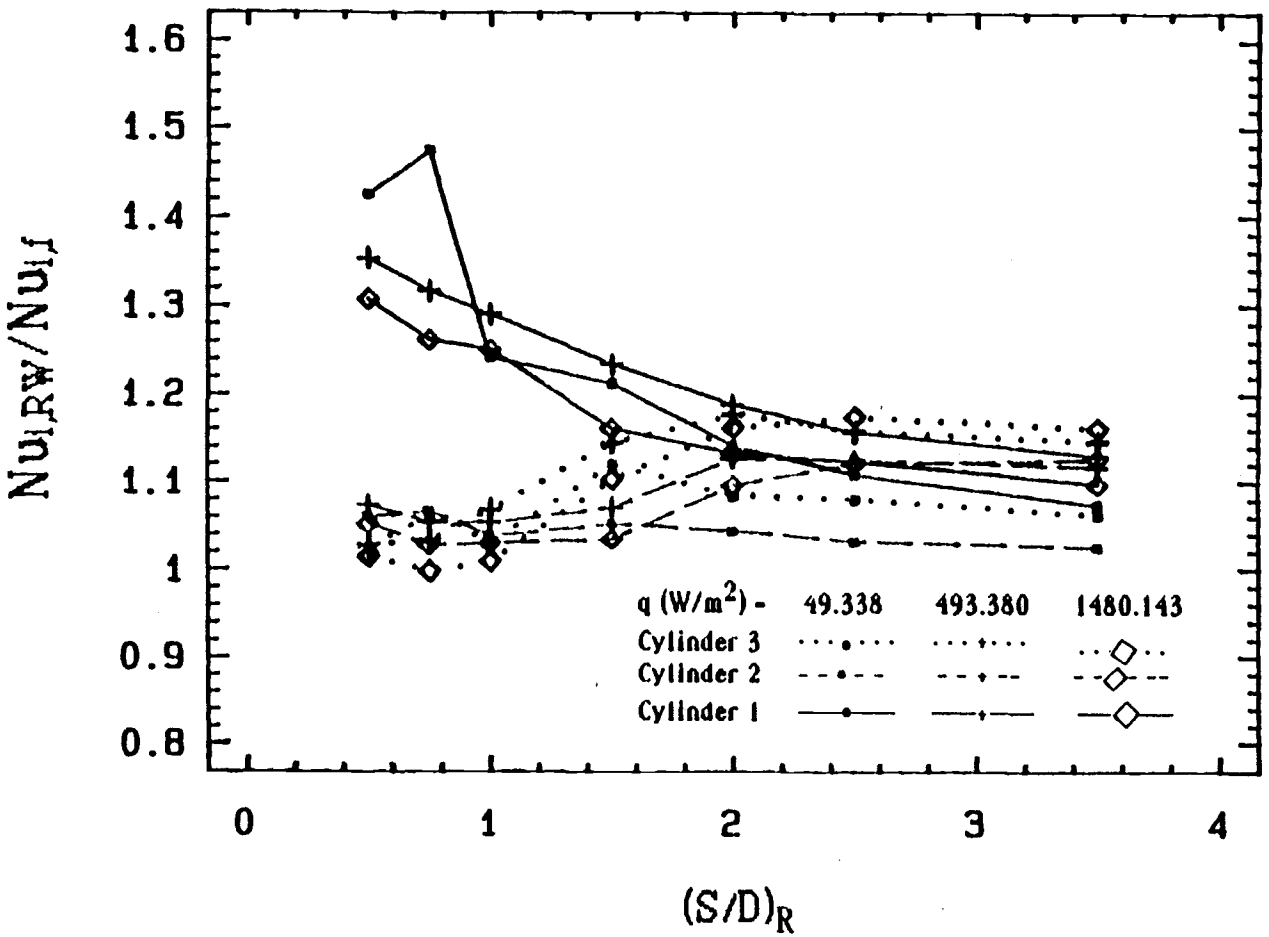

Figure 5.26 The effect of the wall spacing on the Nusselt number ratio, $Nu_{i,RW}/Nu_{i,f}$, at CC=2D.

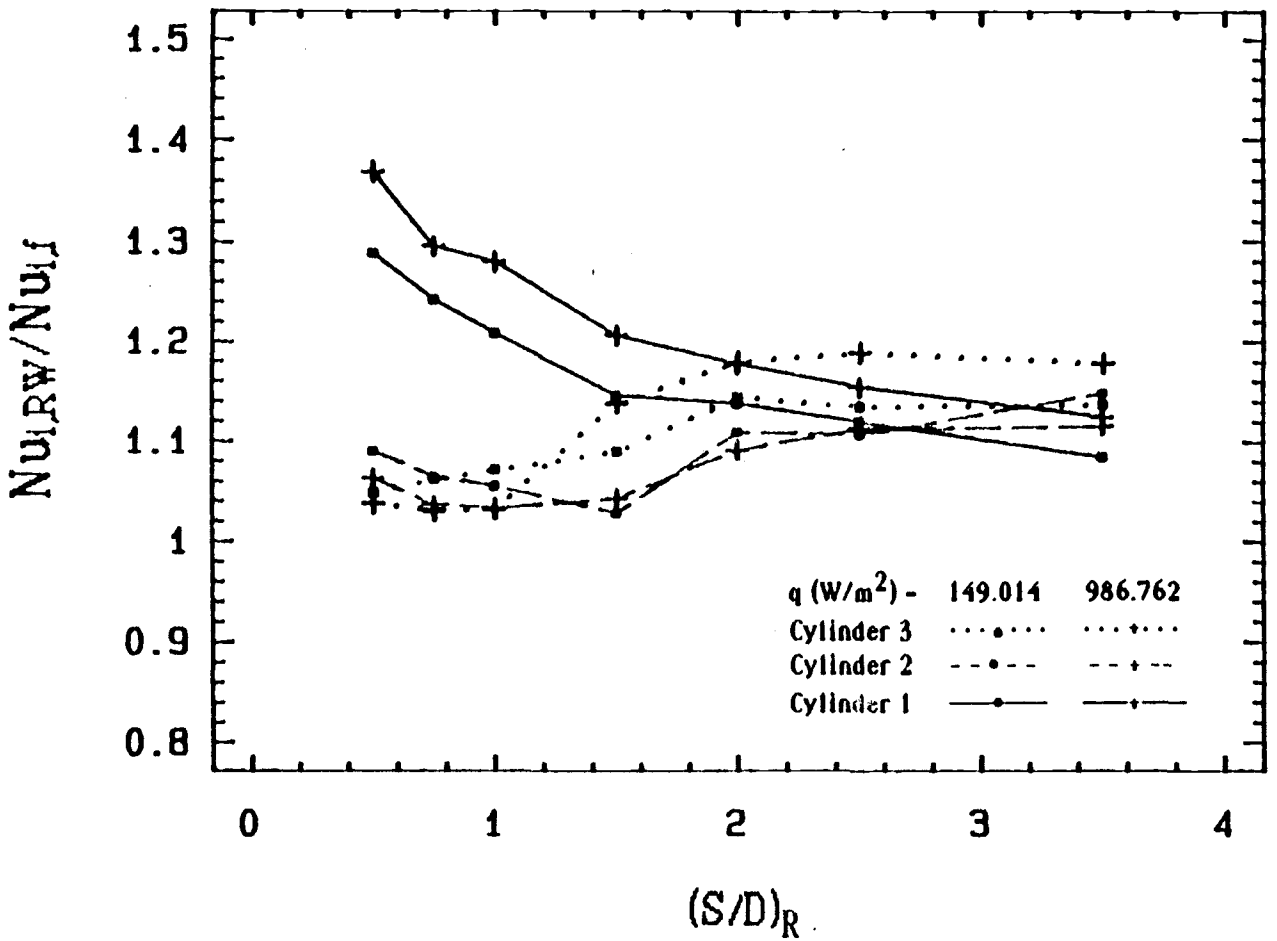

Figure 5.27 The effect of the wall spacing on the Nusselt number ratio, $Nu_{i,RW}/Nu_{i,f}$, at CC=2D.

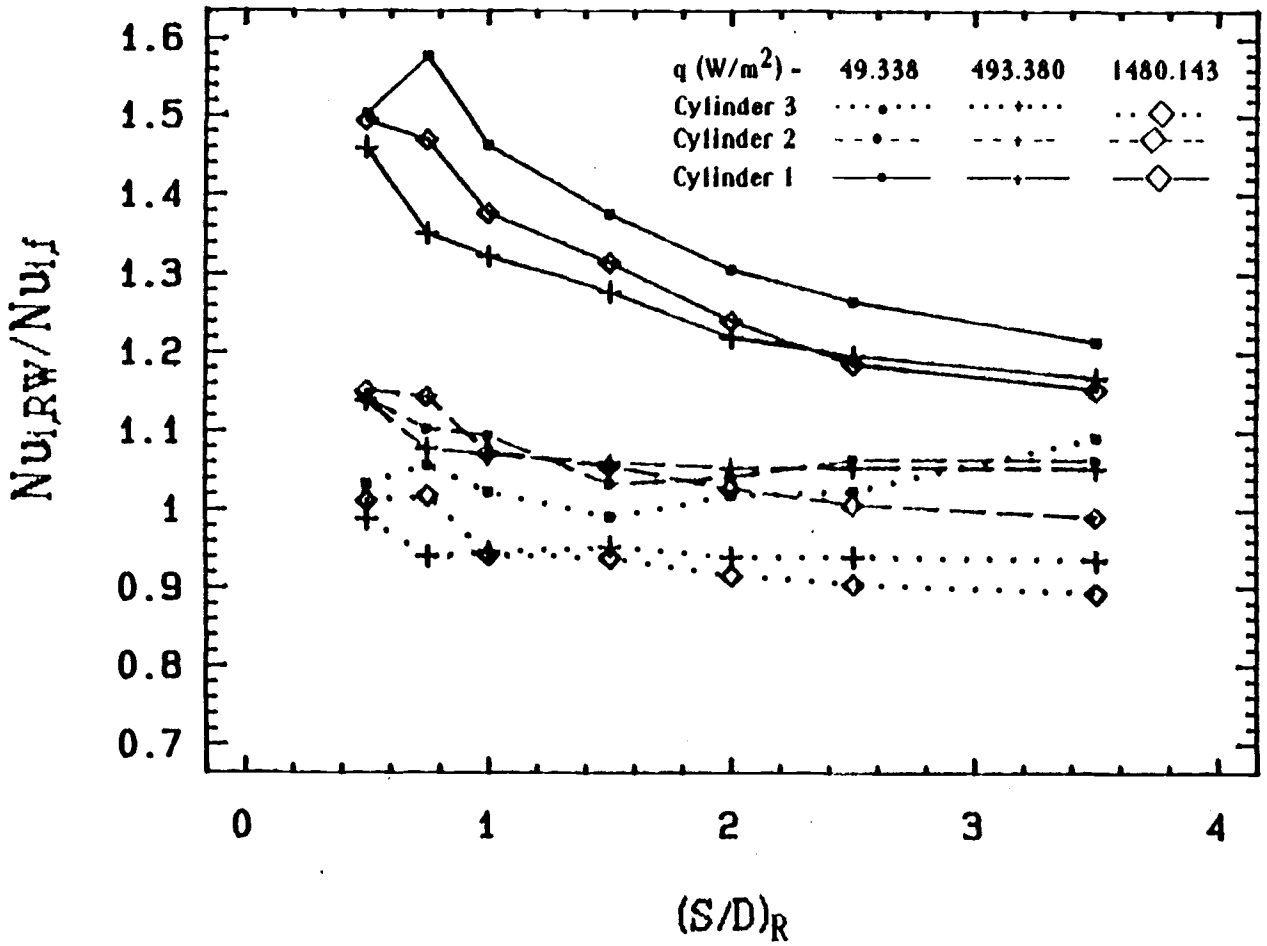

Figure 5.28 The effect of the wall spacing on the Nusselt number ratio, $Nu_{i,RW}/Nu_{i,f}$, at CC=4D.

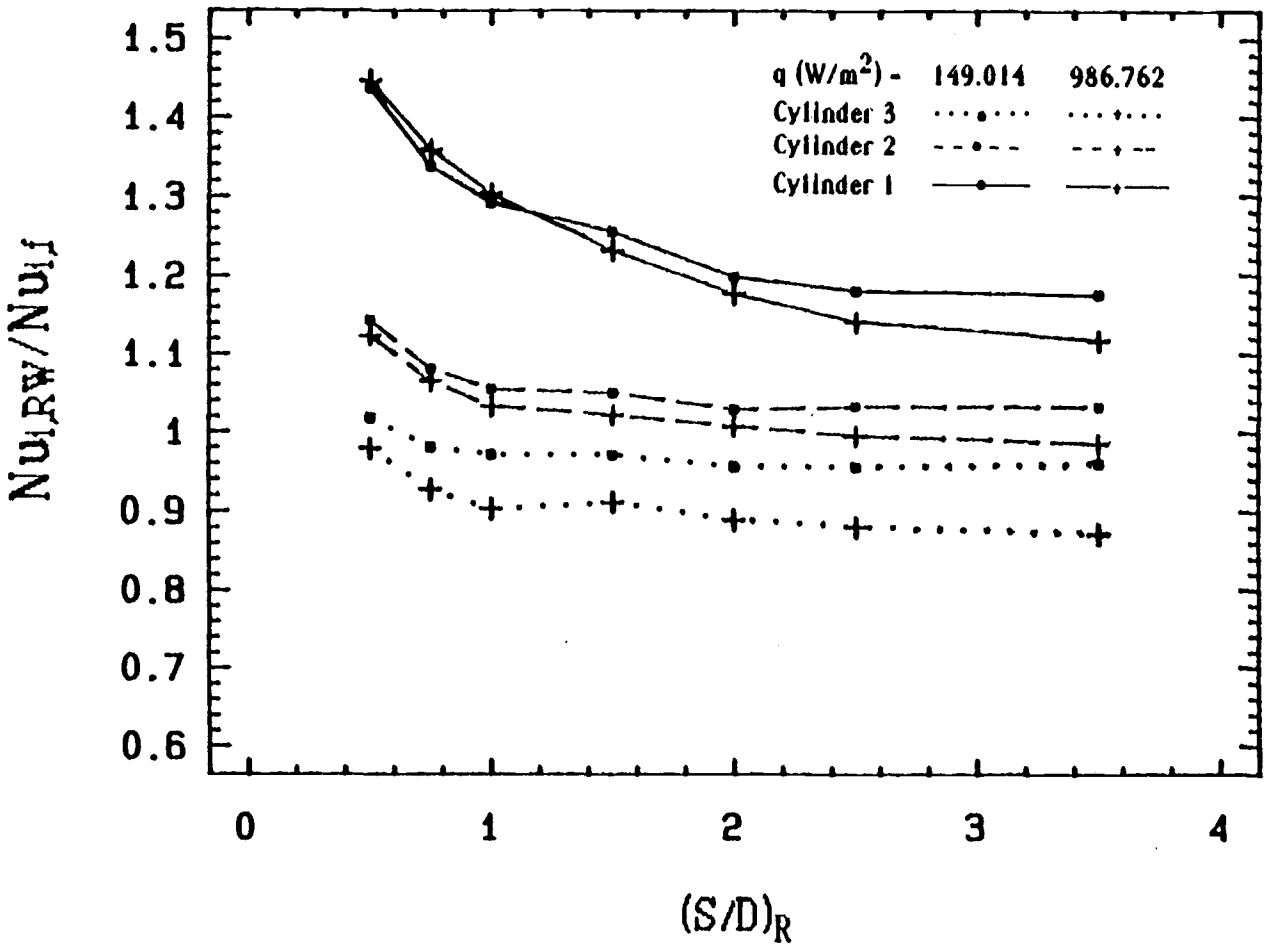

Figure 5.29 The effect of the wall spacing on the Nusselt number ratio, $Nu_{i,RW}/Nu_{i,f}$, at CC=4D.

cylinder at $(S/D)_R \sim 1.25$. The ratio values of the third cylinder become higher than that of the second cylinder in the second stage, as shown in figures 5.12 to 5.15 and 5.18 to 5.21. In the third stage, the degradation in the ratios ($(Nu_{i,Rw}/Nu_{i,E})$ and $(Nu_{i,Rw}/Nu_{i,0.5})$) values were less than those in the first two stages. In general, the upper cylinders at CC = 1.5D show a higher degradation than at CC = 2D. There were no significant enhancements in the upper cylinders' Nusselt numbers from $Nu_{i,E}$ and $Nu_{i,0.5}$.

The upper cylinders' Nusselt numbers were enhanced, relative to $Nu_{i,f}$, with the presence of the second wall at CC = 1.5D and CC = 2D. This is shown in figures 5.24 to 5.27. In these figures, the three stages relative to $(S/D)_R$ are also shown. In the first stage, the second cylinder has an enhancement higher than the third cylinder. The enhancement of the second cylinder in the second stage increases as $(S/D)_R$ increases from 1.0 to 2.0. In the third stage, the increment of $(Nu_{i,Rw}/Nu_{i,f})$ in the second cylinder is slower than in the second stage and it reaches the same enhancement as the first cylinder by the end of this stage. For the highest cylinder (cylinder 3), $(Nu_{3,Rw}/Nu_{3,f})$ increases sharply after the first stage and crosses the lines of the first cylinder by the end of the second stage. In the third stage the third cylinder has a higher enhancement than the lowest cylinder. The enhancement in $(Nu_{3,Rw}/Nu_{3,f})$ at CC = 1.5D in the second and third stages (i.e., $(S/D)_R$ = 1.0 to 3.5) is higher than

the enhancement at CC = 2D in the same stages.

For CC = 4D, the Nusselt number ratios ($Nu_{i,Rw}/Nu_{i,E}$) , ($Nu_{i,Rw}/Nu_{i,0.5}$), and ($Nu_{i,Rw}/Nu_{i,f}$) were shown in figures 5.16, 5.17, 5.21, 5.22, 5.28 and 5.29. In these figures, the cylinders' enhancements have the same pattern in which the first cylinder has the highest enhancement (between 40% to 55% at $(S/D)_R$ = 0.5). The second cylinder enhancement is always higher than the third cylinder enhancement. The enhancement of the first cylinder is more sensitive to the wall spacing $(S/D)_R$ than the upper cylinders (cylinders 2 and 3) and decreases as $(S/D)_R$ increases.

5.3 The effects of right wall spacing on the average Nusselt number of the whole array, $Nu_{av,RW}$

The arithmetic mean of the Nusselt numbers of all the cylinders of the array was calculated, as shown in equation 5.2, at specific $(S/D)_R$ and specific heat flux.

$$Nu_{av,RW} = \frac{\sum_{i=1}^{3} Nu_{i,RW}}{3.0} \qquad (5.2)$$

Figures 5.30 through 5.32 show the $Nu_{av,RW}$ versus $(S/D)_R$ for CC = 1.5D, 2D, and 4D, respectively. At CC= 1.5D and CC = 2D, the $Nu_{av,RW}$ values are insensitive to the right wall spacing, $(S/D)_R$. This indicates that the total enhancement of $Nu_{i,RW}$ - total degradation of $Nu_{i,RW}$ is a constant value at a specific heat flux

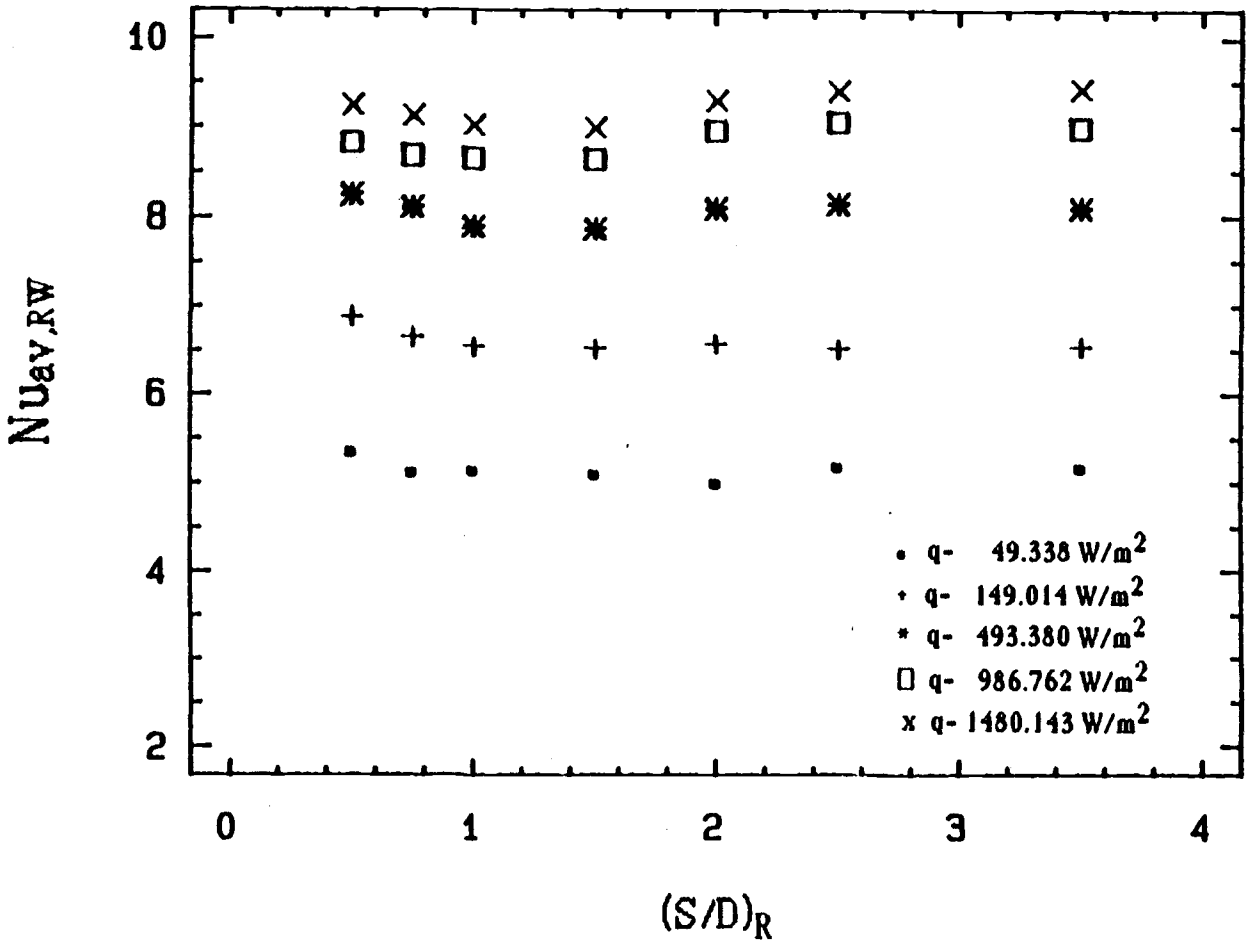

Figure 5.30 The effect of the wall spacing on the average Nusselt number of the whole array at CC=1.5D.

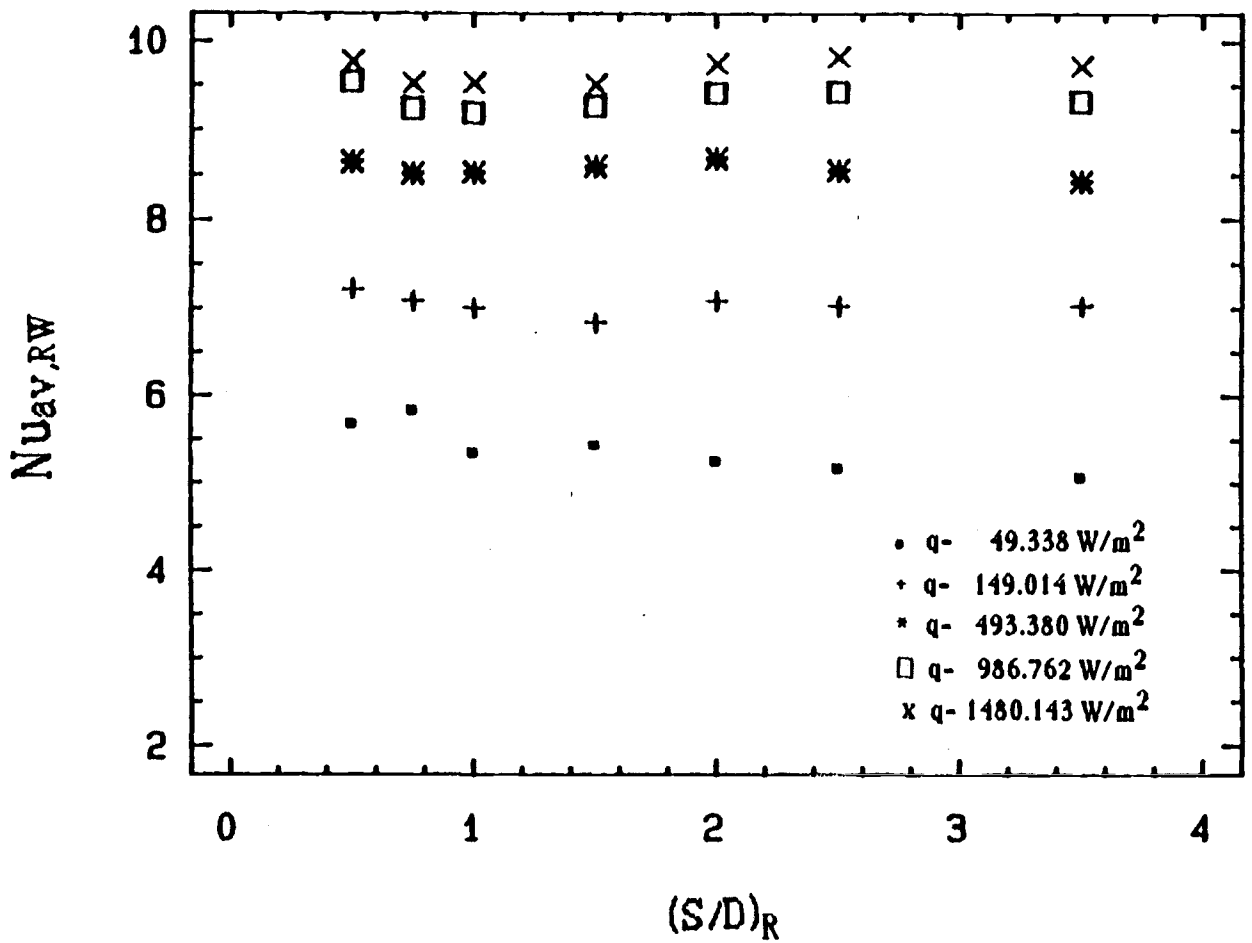

Figure 5.31 The effect of the wall spacing on the average Nusselt number of the whole array at CC=2D .

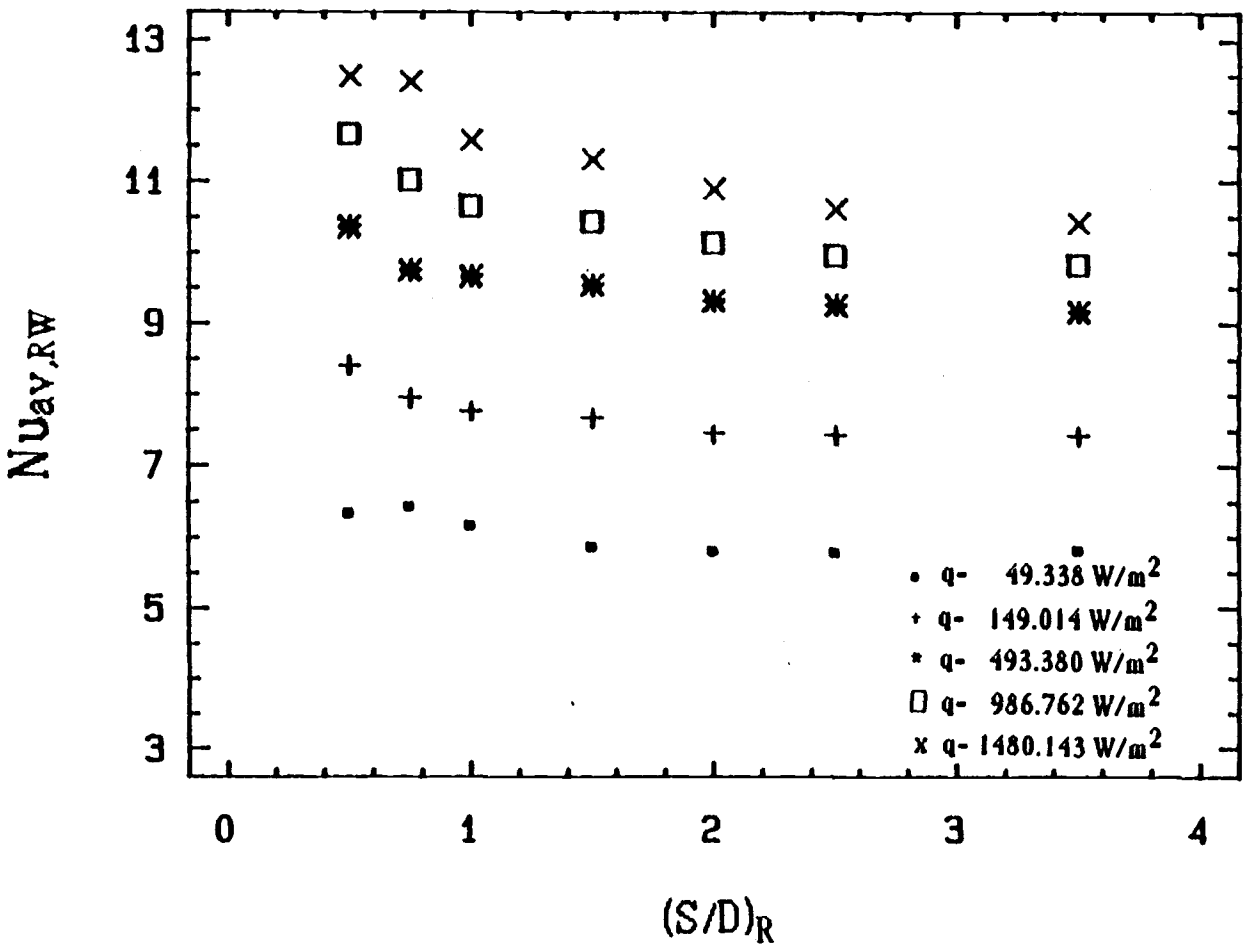

Figure 5.32 The effect of the wall spacing on the average Nusselt number of the whole array at CC=4D .

value. There is an insigificant drop (approximately 5% maximum) in the average Nusselt number at $(S/D)_R$ between 0.75 and 2.0, as shown in figures 5.30 and 5.31.

The $Nu_{av,RW}$ for CC = 4D is shown to be decreasing as the $(S/D)_R$ increases, figure 5.32. This is an expected result for CC = 4D since the $Nu_{i,RW}$ values for all cylinders decreases with the increasing of $(S/D)_R$ values, as shown in the previous section. In all the cases of CC, the $Nu_{av,RW}$ increases as the heat flux values increase.

The average Nusselt number for the whole array, $Nu_{av,RW}$, was compared to the correlated Nusselt number of a free cylinder through the following ratio:

$$Nu_{av,RW/f} = \frac{Nu_{av,RW}}{[\,0.571\, Ra_{1,f}^{*\,0.2027}\,]} \qquad (5.3)$$

Where $Ra_{1,f}^{*}$ is the modified Rayleigh number of the lowest cylinder for a free array (i.e., no wall) at the same heat flux value at which the $Nu_{av,RW}$ was calculated from equation 5.2. This ratio, $Nu_{av,RW/f}$, versus $(S/D)_R$ was plotted in figures 5.33 to 5.35 for CC = 1.5D, 2D, and 4D, respectively. These figures show that the $Nu_{av,RW}$ values are enhanced by the presence of the right wall for all the heat flux values except the lowest value, q = 49.338 w/m2, for CC= 1.5D and 2D. In general, the figures of the

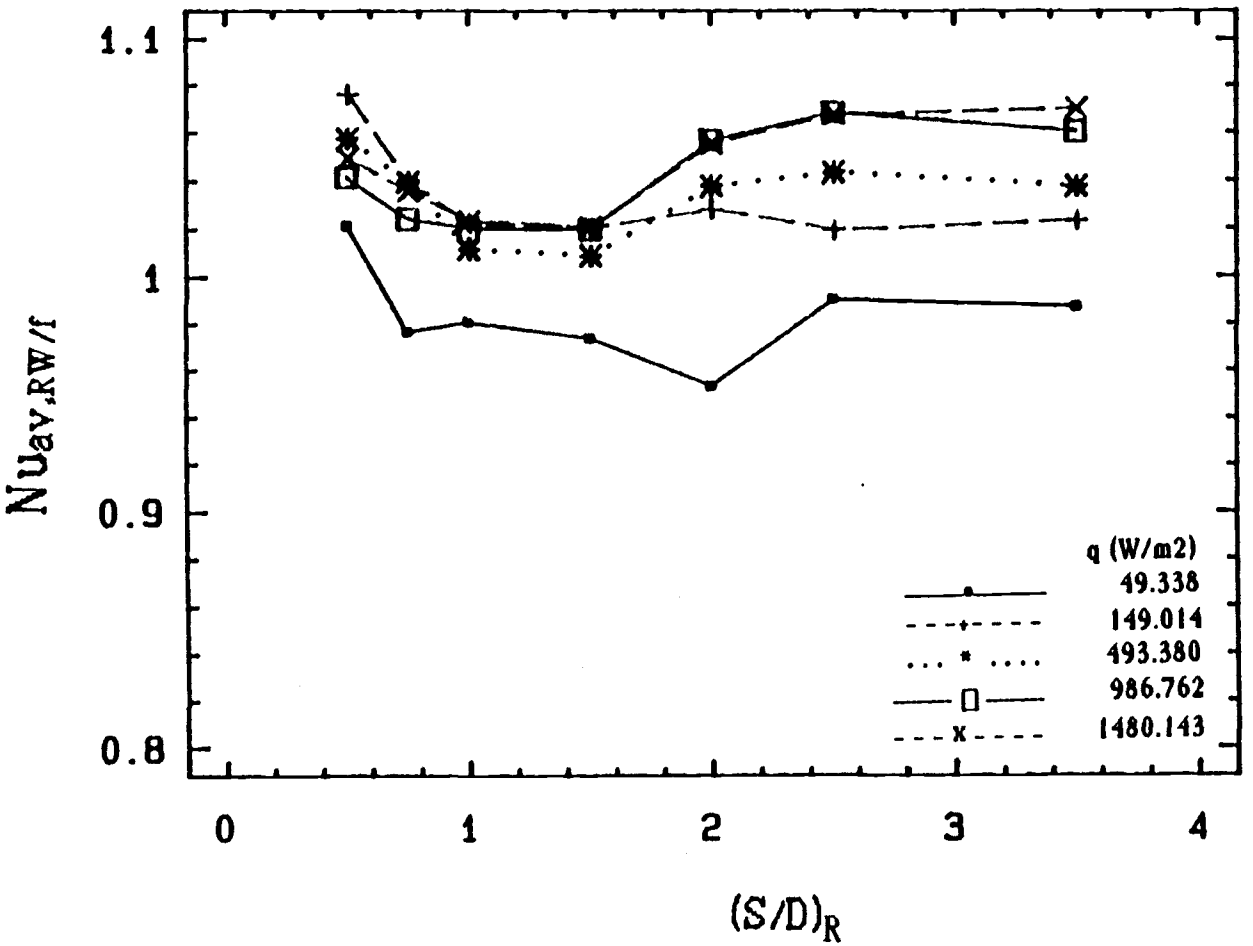

Figure 5.33 The effect of the wall spacing on the Nusselt number ratio, $Nu_{i,RW}/Nu_{i,f}$, at CC=1.5D.

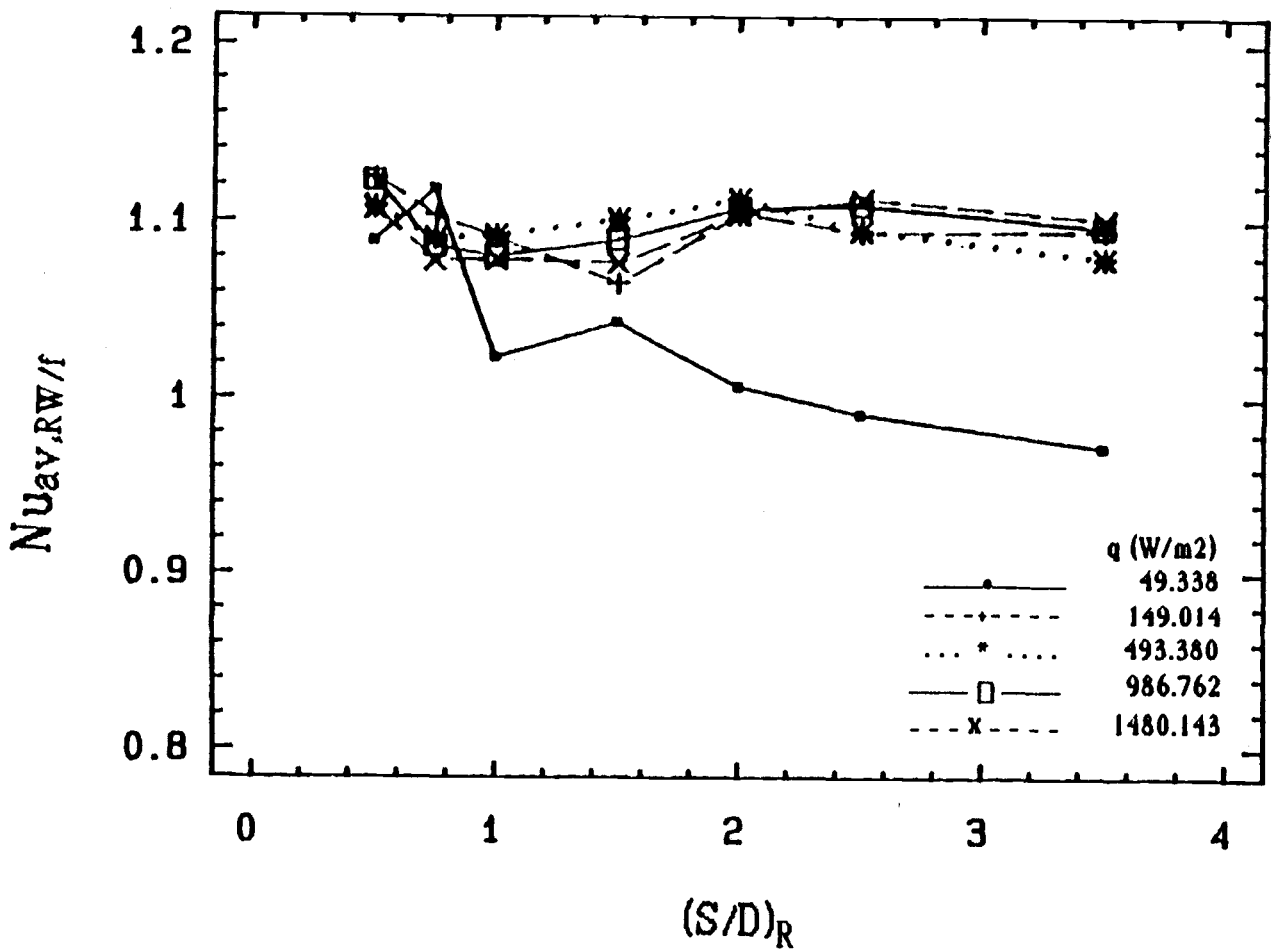

Figure 5.34 The effect of the wall spacing on the Nusselt number ratio, $Nu_{i,RW}/Nu_{i,f}$, at CC=2D.

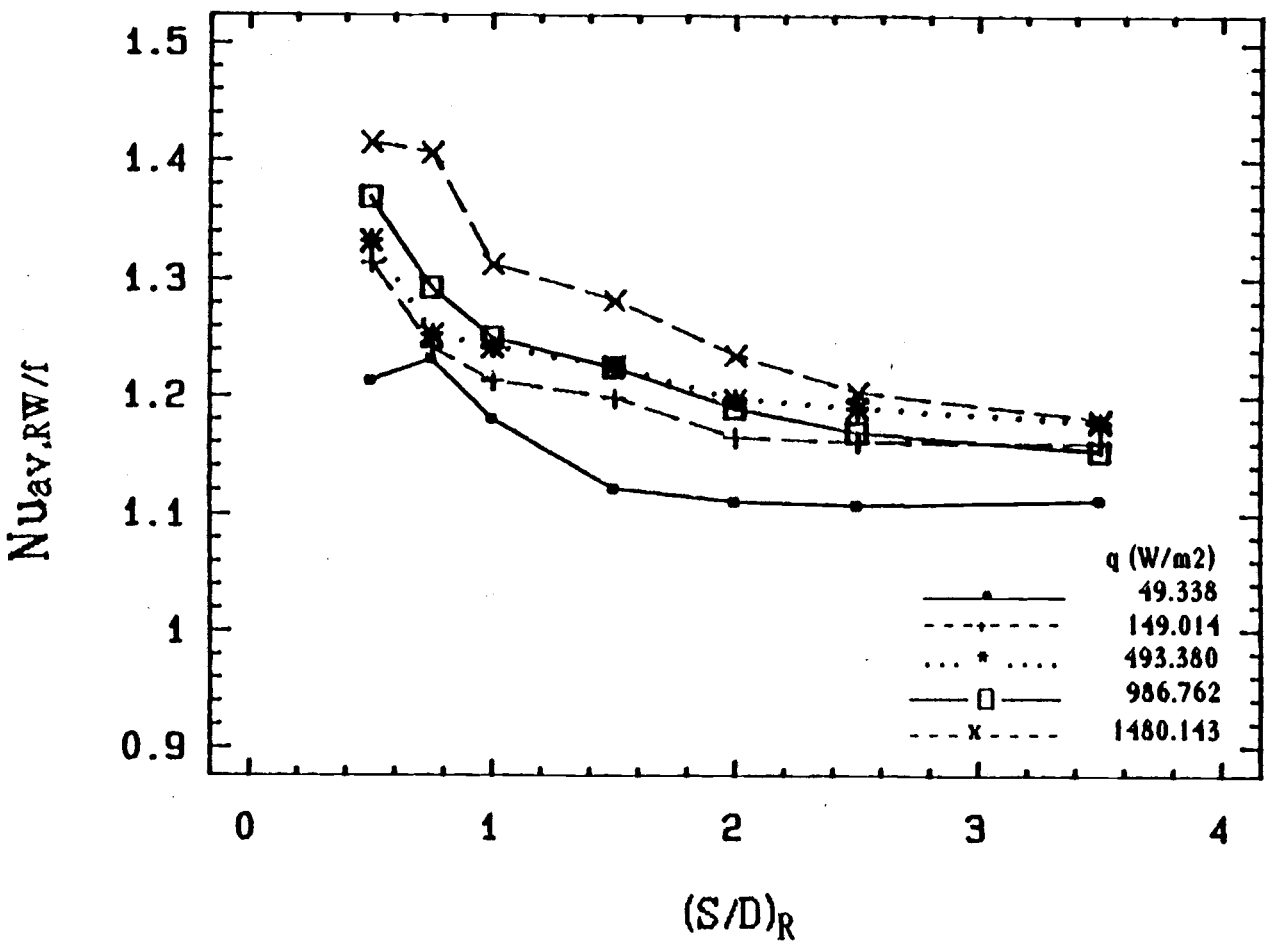

Figure 5.35 The effect of the wall spacing on the Nusselt number ratio, $Nu_{i,RW}/Nu_{i,f}$, at CC=4D.

enhancement of $Nu_{av,RW}$ increase as the center-to-center spacing, CC, increases. The maximum enhancement occurs when the walls are placed symmetrically to the array (i.e., $(S/D)_R = 0.5$). These enhancements were between 2% to 8% for CC = 1.5D, 9% to 13% for CC = 2D, and 20% to 44% for CC = 4D. The exact value of these enhancements depends on the heat flux value, q. Figure 5.33 shows that there is a degradation of about 4% maximum in $Nu_{av,RW/f}$ at the lowest heat flux value for $(S/D)_R > 0.5$.

There was a heat transfer degradation in the lowest heat flux case at CC = 2D and $(S/D)_R > 2.0$. Maximum degradation in this case was 3% at $(S/D)_R = 3.5$, as shown in figure 5.34. In general, the enhancement in $Nu_{av,RW/f}$ at CC = 1.5D and 2D decrease as $(S/D)_R$ increase from 0.5 to 1.50. At $(S/D)_R>1.50$, the enhancement in $Nu_{av,RW/f}$ values increase due to the enhancement in the Nusselt number of the highest cylinder, $Nu_{3,RW}$, in the second and third stages due to the feed back current. The enhancement in $Nu_{av,RW/f}$ at CC = 1.5D and 2D are insensitive to the right wall spacing at $(S/D)_R$ greater than 2.0 . This is contradictory to the enhancement of $Nu_{av,RW}$ for CC = 4D, where the ratio, $Nu_{av,RW/f}$, decreases continuously as $(S/D)_R$ increases, as shown in figure 5.35. Also, it can be noticed from figure 5.35 that the enhancement decreased by 10% at the lowest q and by 24% at the highest q between $(S/D)_R = 0.5$ and $(S/D)_R=3.5$.

The effects of the right wall spacing on $Nu_{av,RW}$ compared to

the average Nusselt number of the whole array for a single wall at S/D = 0.5, $Nu_{av,0.5}$, were investigated through the $Nu_{av,RW}$ to $Nu_{av,0.5}$, ratio. The ratio ($Nu_{av,RW}/Nu_{av,0.5}$) versus $(S/D)_R$ is presented in figures 5.36 to 5.38. In general, there was no degradation in $Nu_{av,RW}$ relative to $Nu_{av,0.5}$. The enhancements in ($Nu_{av,RW}/Nu_{av,0.5}$) at CC = 1.5D were between 4% and 9% at $(S/D)_R$ = 0.5 and between 2% and 7% at $(S/D)_R$ = 3.5. For CC = 2D, the enhancements were approximately 8% at $(S/D)_R$ = 0.5 and approximately 3% at $(S/D)_R$ = 3.5 at all q values, except q = 49.338 w/m2, as shown in figure 5.37. Also, figures 5.36 and 5.37 show that the enhancements in $Nu_{av,RW}$ values are insensitive to the right wall spacings at $(S/D)_R > 2.0$.

Figure 5.38 shows the enhancements of $Nu_{av,RW}$ at CC = 4D, relative to $Nu_{av,0.5}$. The pattern of the values is the same as that in figure 5.35, except that the values in figure 5.38 are shifted 10% lower than those in figure 5.35. Unlike the ($Nu_{av,RW}/Nu_{av,0.5}$) at CC = 1.5D and 2D, the ($Nu_{av,RW}/Nu_{av,0.5}$) at CC=4D is more sensitive to $(S/D)_R$ and it decreases as $(S/D)_R$ increases.

5.4 Data Correlation

The curve fitting of the data was presented to fit the Nusselt number as a function of the modified Rayleigh number to the 0.2 power. This relation is shown in equation 5.4:

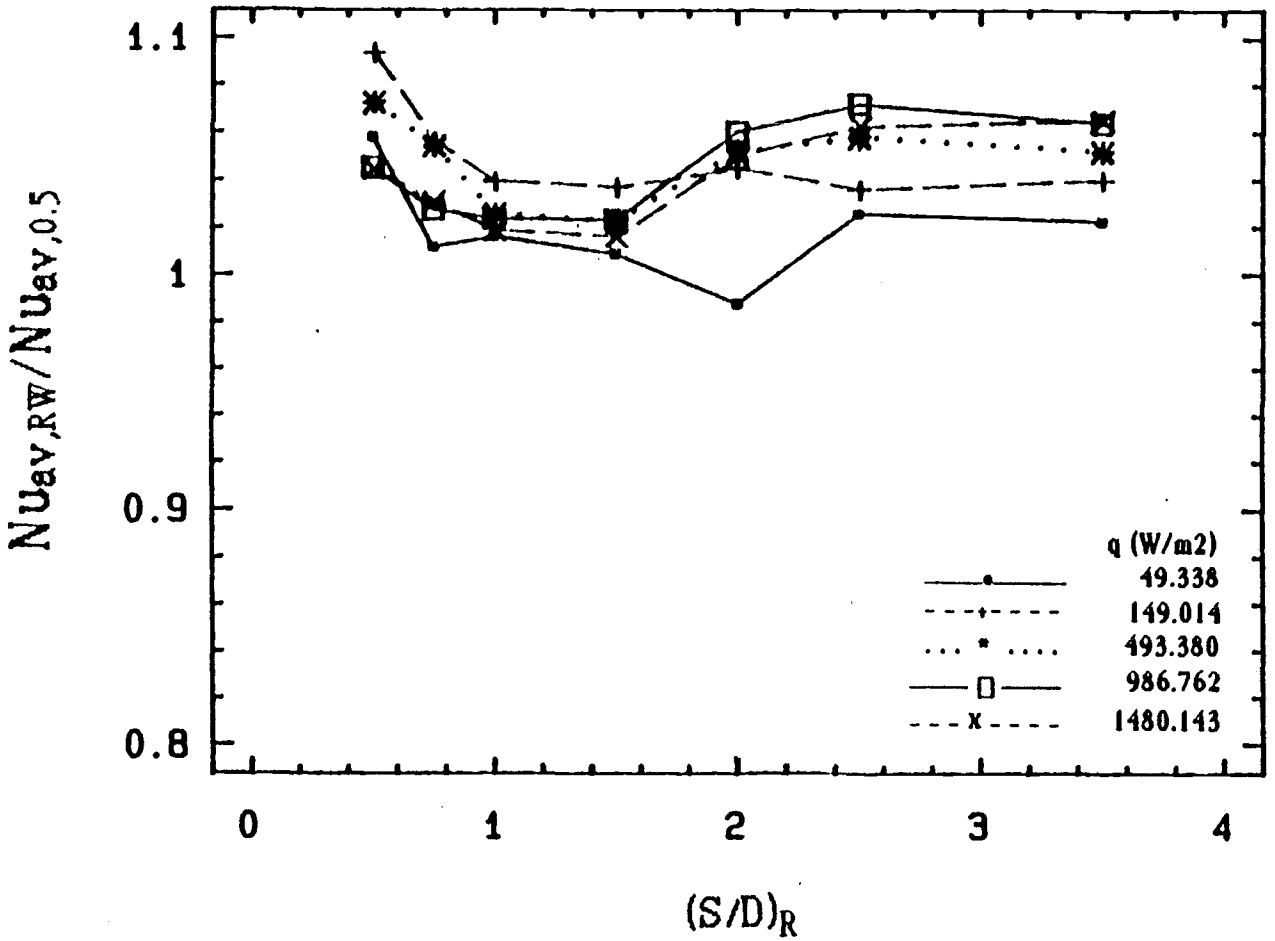

Figure 5.36 The effect of the wall spacing on the Nusselt number ratio, $Nu_{i,RW}/Nu_{i,0.5}$, at CC=1.5D.

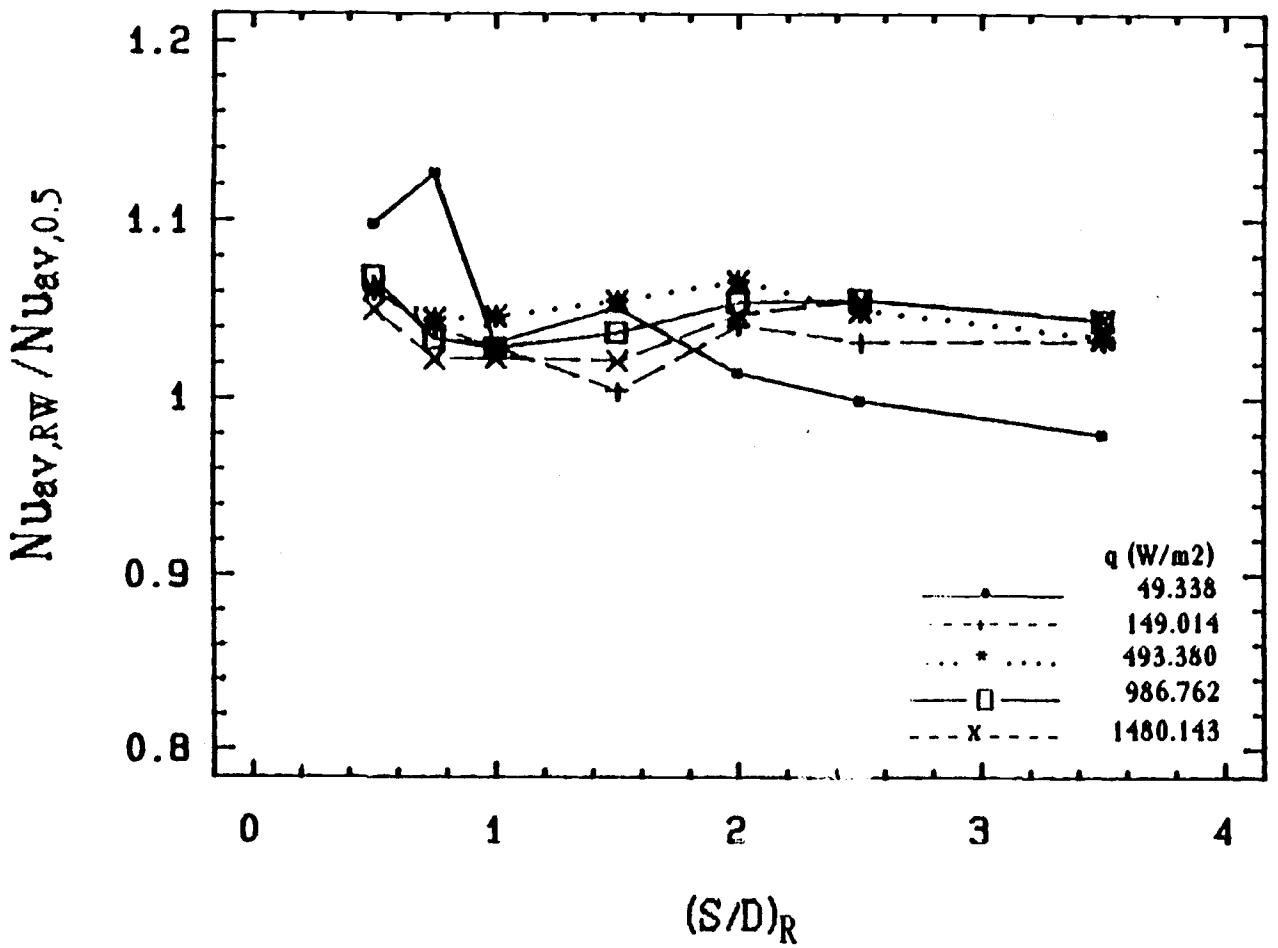

Figure 5.37 The effect of the wall spacing on the Nusselt number ratio, $Nu_{i,RW}/Nu_{i,0.5}$, at CC=2D.

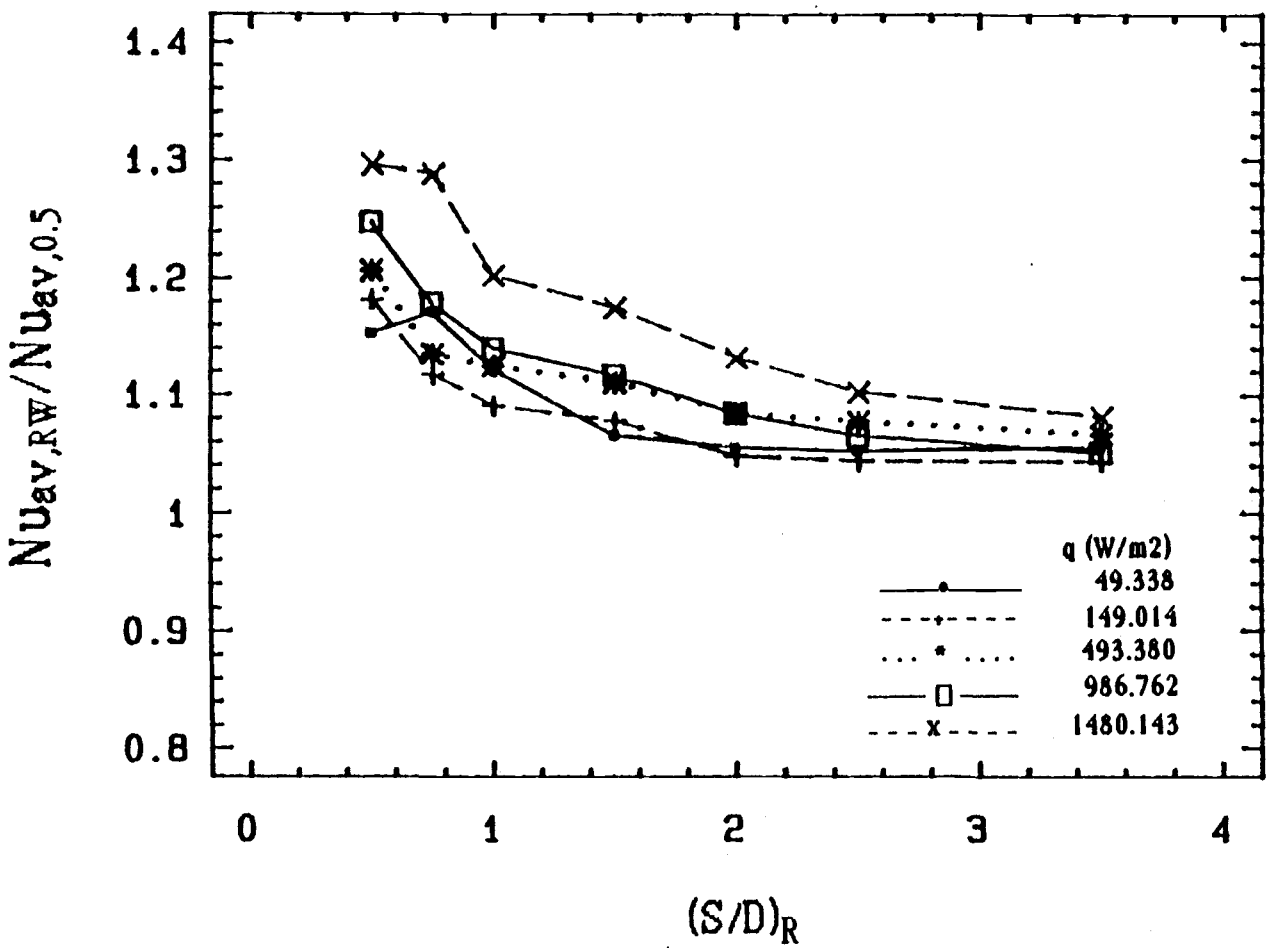

Figure 5.38 The effect of the wall spacing on the Nusselt number ratio, $Nu_{i,RW}/Nu_{i,0.5}$, at CC=4D.

$$Nu_{i,RW} = B_1 \ Ra_{i,RW}^{*0.2} \qquad (5.4)$$

The correlation coefficient, B_1, for each cylinder at specific $(S/D)_R$ is shown in table 5.1 with r^2 values for each case.

Table 5.1 The correlation coefficient, B_1 , in equation 5.4 .

		Cylinder 1		Cylinder 2		Cylinder 3	
CC	S/D	B_1	r^2%	B_1	r^2%	B_1	r^2%
1.5D	0.50	0.7647	98.9	0.5342	99.4	0.4922	99.3
1.5D	0.75	0.7385	98.8	0.5301	98.9	0.4882	98.9
1.5D	1.00	0.7190	99.8	0.5276	98.9	0.4911	99.2
1.5D	1.50	0.6906	99.6	0.5117	99.4	0.5326	97.4
1.5D	2.00	0.6717	99.6	0.5386	96.7	0.5622	96.8
1.5D	2.50	0.6648	99.8	0.5556	97.7	0.5667	97.1
1.5D	3.50	0.6542	99.7	0.5667	98.7	0.5631	97.2
2.0D	0.50	0.7797	99.2	0.5793	99.4	0.5302	99.2
2.0D	0.75	0.7572	95.9	0.5691	99.9	0.5310	99.5
2.0D	1.00	0.7394	99.1	0.5664	99.5	0.5353	98.3
2.0D	1.50	0.6990	99.2	0.5693	99.3	0.5728	98.8
2.0D	2.00	0.6809	98.4	0.5953	98.0	0.5907	97.4
2.0D	2.50	0.6696	98.3	0.6007	97.4	0.5907	97.0
2.0D	3.50	0.6537	98.4	0.6034	96.8	0.5857	96.8
4.0D	0.50	0.8430	99.9	0.7281	97.5	0.6897	93.5
4.0D	0.75	0.8094	96.5	0.6976	93.4	0.6729	92.3
4.0D	1.00	0.7758	98.9	0.6818	97.9	0.6532	95.3
4.0D	1.50	0.7436	99.3	0.6723	96.8	0.6536	94.6
4.0D	2.00	0.7104	99.5	0.6632	97.8	0.6434	96.2
4.0D	2.50	0.6914	99.6	0.6597	98.7	0.6402	96.7
4.0D	3.50	0.6769	99.4	0.6655	98.8	0.6402	98.7

Figures 5.39 through 5.41 show the calculated Nusselt

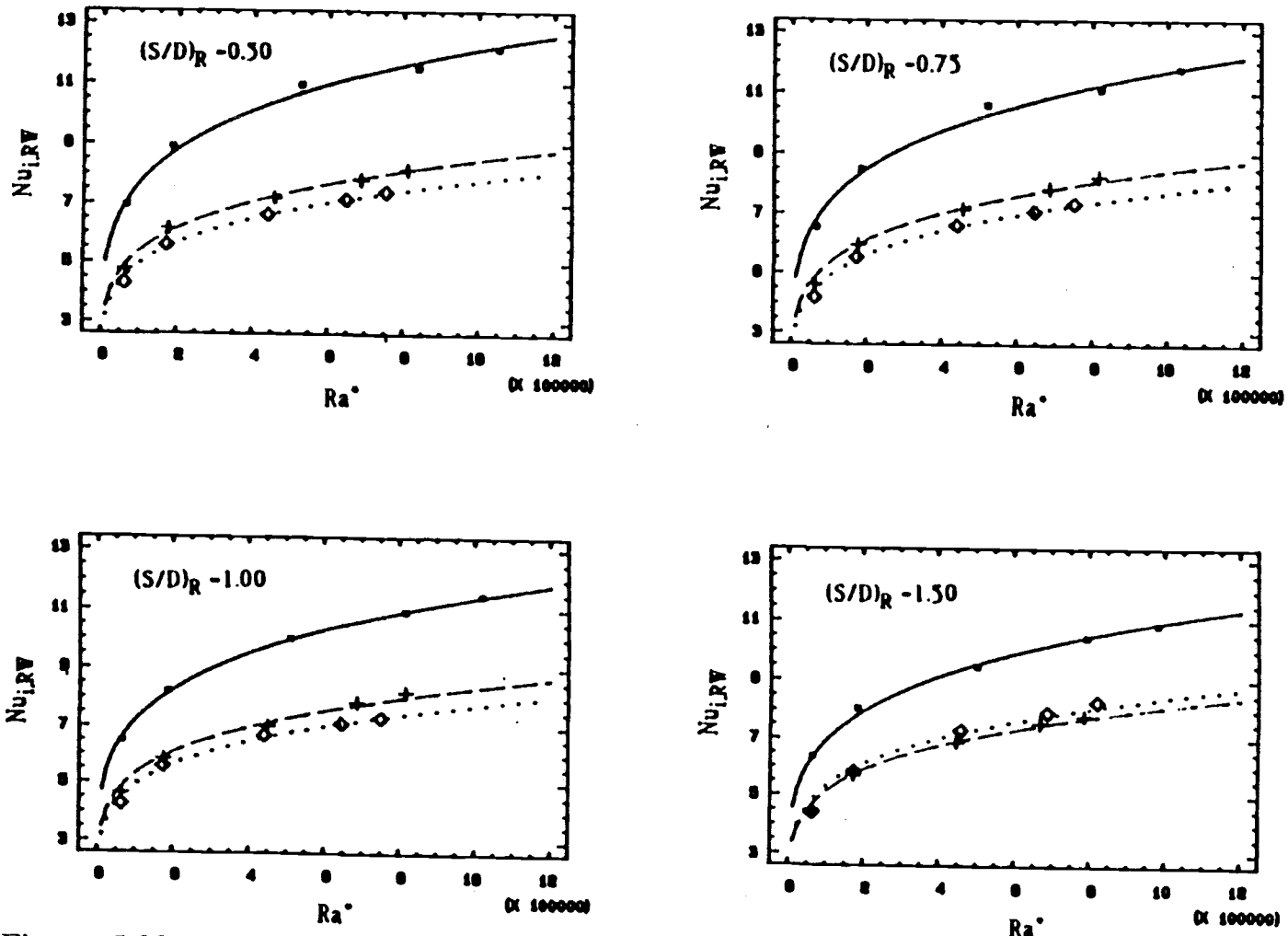

Figure 5.39-a The experimental $Nu_{i,RW}$ values and the correlated $Nu_{i,RW}$ values Vs. Ra^* at CC=1.5D .

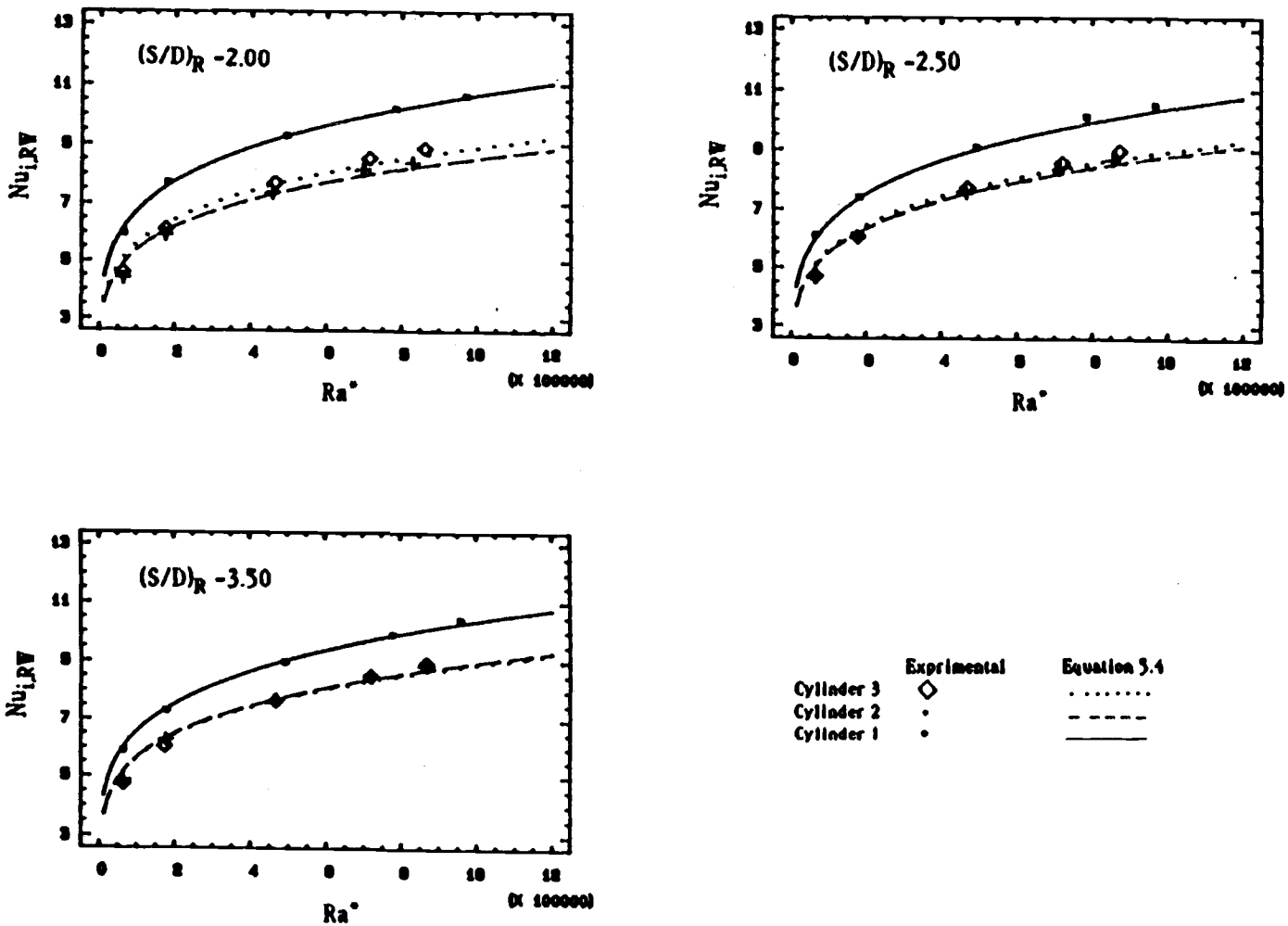

Figure 5.39-b The experimental $Nu_{i,RW}$ values and the correlated $Nu_{i,RW}$ values Vs. Ra^* at CC=1.5D .

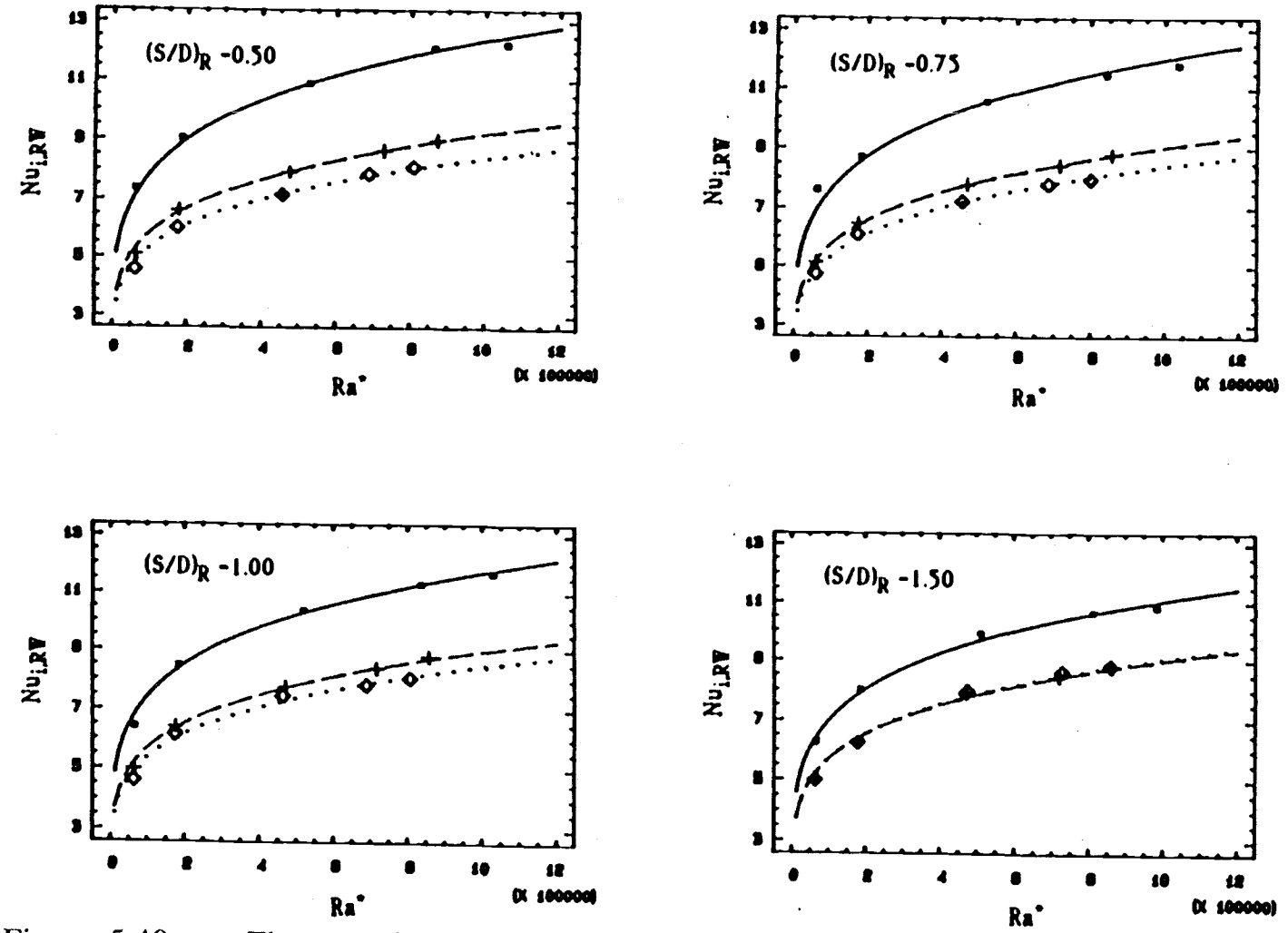

Figure 5.40-a The experimental $Nu_{i,RW}$ values and the correlated $Nu_{i,RW}$ values Vs. Ra^* at CC= 2D .

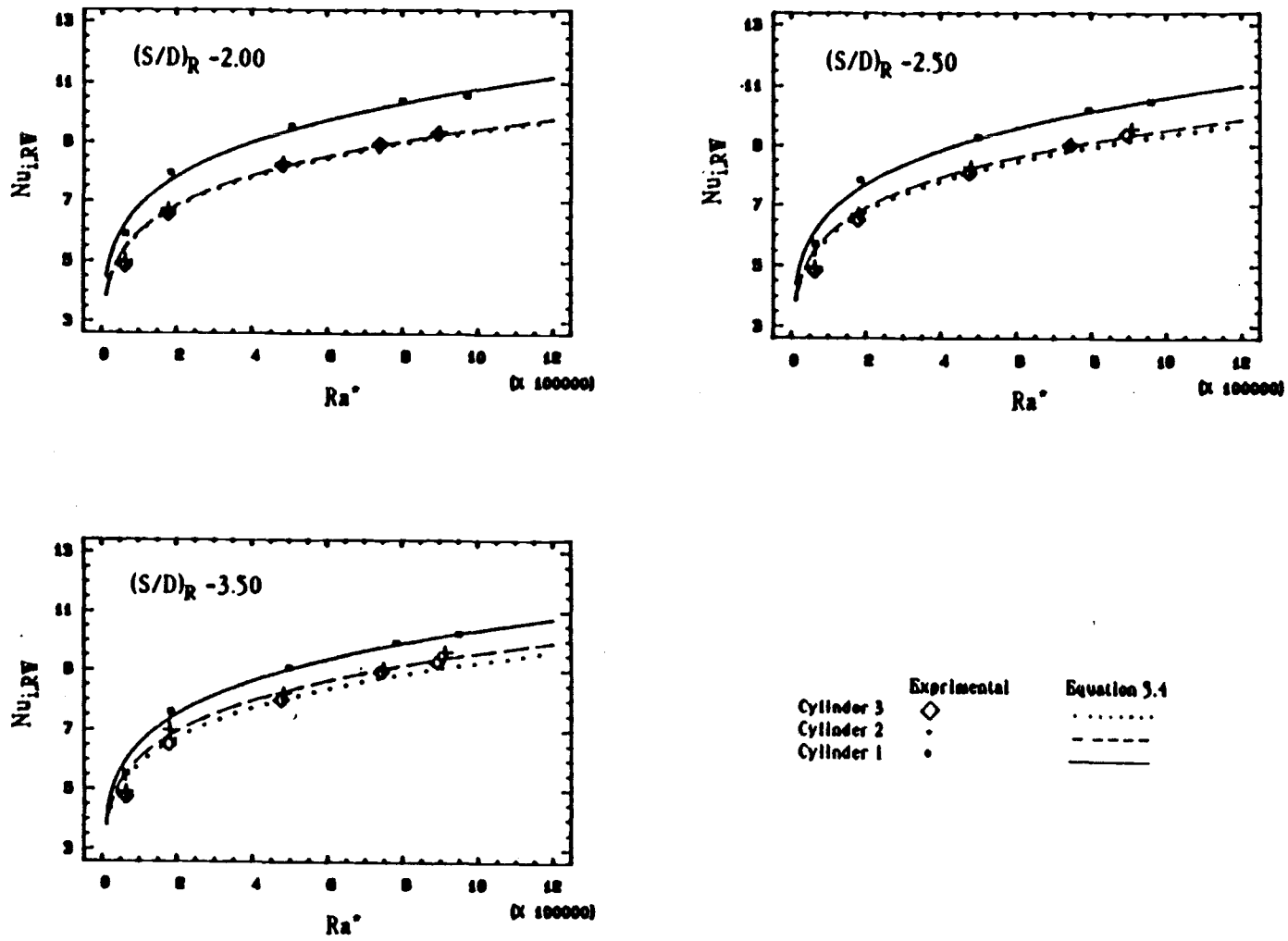

Figure 5.40-b The experimental $Nu_{i,RW}$ values and the correlated $Nu_{i,RW}$ values Vs. Ra^* at CC= 2D .

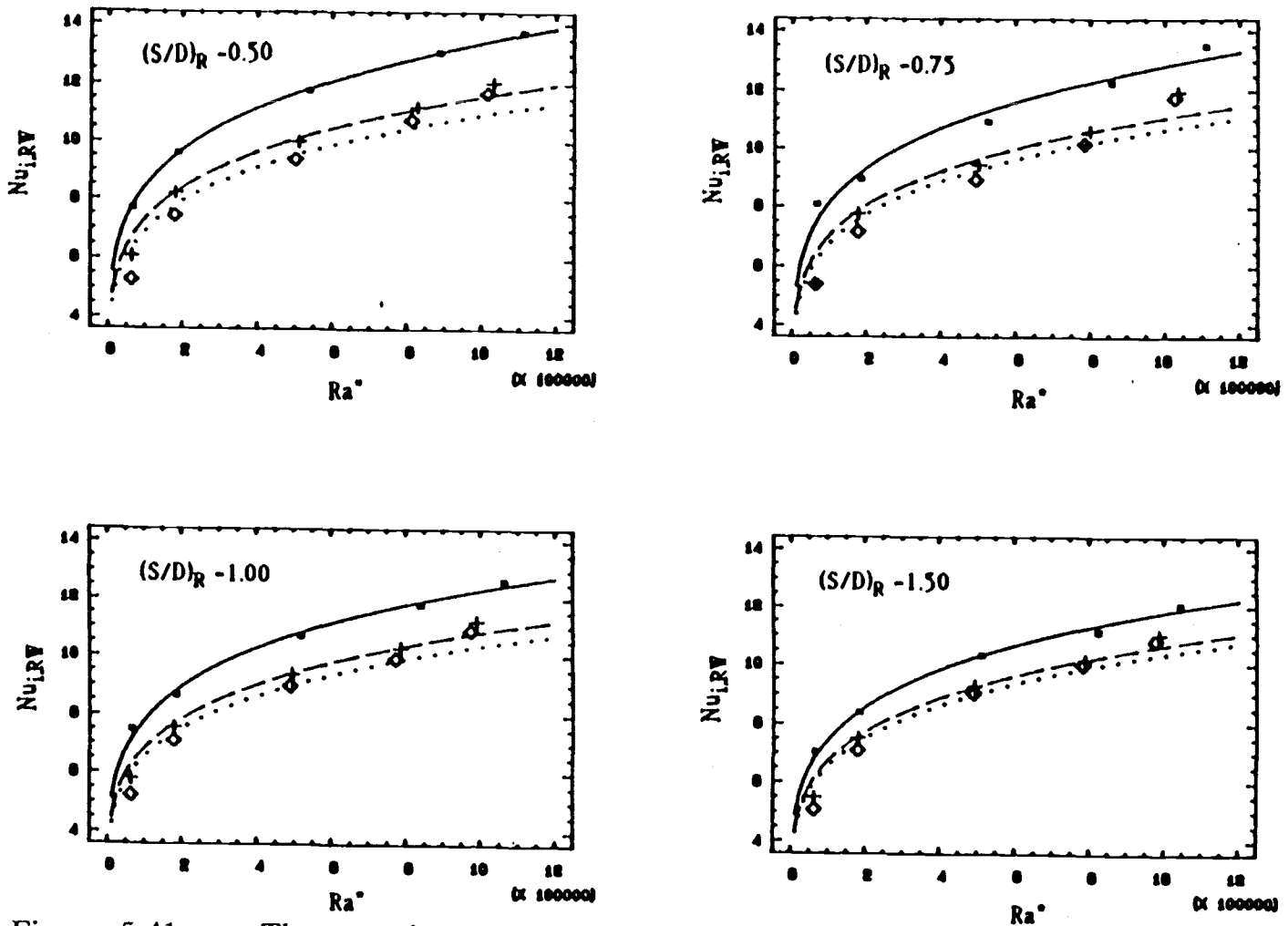

Figure 5.41-a The experimental $Nu_{i,RW}$ values and the correlated $Nu_{i,RW}$ values Vs. Ra^* at CC=4D .

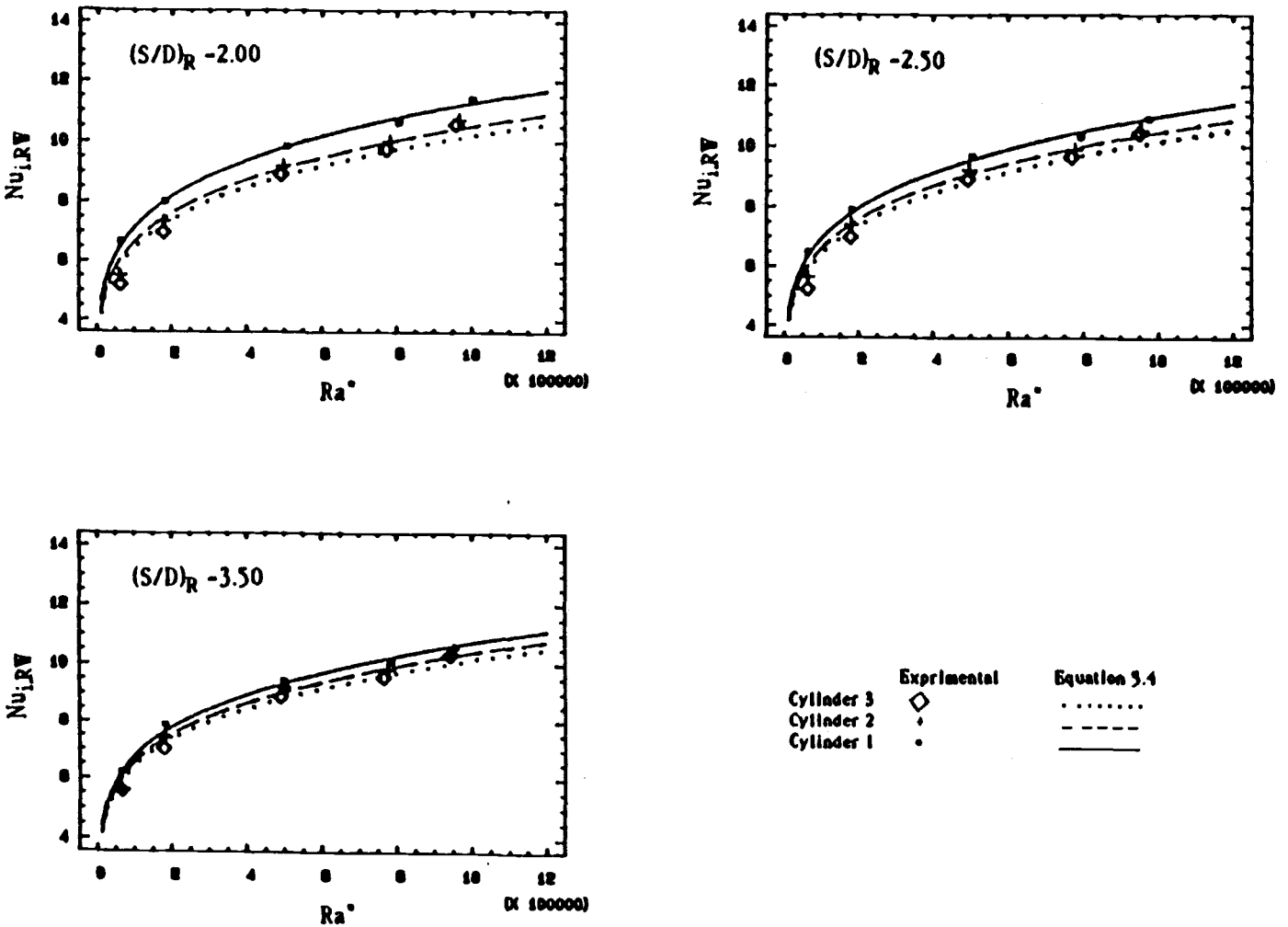

Figure 5.41-b The experimental $Nu_{i,RW}$ values and the correlated $Nu_{i,RW}$ values Vs. Ra^* at CC=4D .

number from equation 5.4 superimposed on the experimental data, for all the CC values.

In these figures, the Nusselt number for the lowest cylinder, $Nu_{1,RW}$, was higher than the $Nu_{2,RW}$ and $Nu_{3,RW}$. The Nusselt numbers for cylinders 2 and 3 are very close when compared to the Nusselt number for cylinder 1. Also, from figures 5.39 to 5.41, the difference between $Nu_{2,RW}$ and $Nu_{3,RW}$ decreases as $(S/D)_R$ increases, with $Nu_{3,RW}$ taking the lowest value. At high $(S/D)_R$ values, the $Nu_{3,RW}$ becomes greater or equal to the $Nu_{2,RW}$. This is due to the enhancement of the Nusselt number of the highest cylinder, $Nu_{3,RW}$. This enhancement occurs as a result of the feedback current. The maximum error in this correlation, as calculated from equation 5.5 , is less than 5% for $18x10^4 < Ra_{1,RW} < 1.6x10^6$ when the lowest heat flux value is not included and about 12% for $6.4x10^4 < Ra_{1,RW} < 1.6x10^6$ when all the heat flux values are considered.

$$\text{Error } \% = \left(\frac{Nu_{experimental} - Nu_{correlation}}{Nu_{experimental}} \right) \times 100 \qquad (5.5)$$

Table 5.2 illustrates the B_1 values and r^2 for the average Nusselt number correlation for the whole array, $Nu_{av,RW}$. This relationship is the same as the one shown in equation 5.4, except that the modified Rayleigh number that is used in this relationship is the modified Rayleigh number of the lowest cylinder in the array, $Ra_{1,RW}$. From equation 5.5 , it is found that

the maximum error in this correlation is less than 3% for $18x10^4 < Ra_{1,RW} < 1.6x10^6$ when the lowest heat flux value is not included and about 10% for $6.4x10^4 < Ra_{1,RW} < 1.6x10^6$ when all the heat flux values are considered.

Table 5.2 The Correlation coefficient, B_1, for $Nu_{av,RW} = B_1 Ra_{1,RW}^{*0.2}$

	CC = 1.5D		CC = 2D		CC = 4D	
S/D	B_1	r^2%	B_1	r^2%	B_1	r^2%
0.50	0.5843	98.9	0.6184	99.5	0.7474	98.1
0.75	0.5737	99.2	0.6084	98.6	0.7214	96.5
1.00	0.5680	99.7	0.6025	99.1	0.6987	98.8
1.50	0.5694	98.6	0.6067	99.5	0.6859	98.2
2.00	0.5844	98.6	0.6176	98.4	0.6694	98.7
2.50	0.5902	99.1	0.6164	98.1	0.6617	99.1
3.50	0.5898	99.1	0.6111	97.8	0.6561	99.4

CHAPTER 6

NUMERICAL ANALYSIS AND FLOW VISUALIZATION

The temperature and velocity distributions and flow visualizations for selected cases will be presented in this chapter. Also, the results of Chapters 4 and 5 will be discussed. In order to prevent repetitious discussion, only a limited number of experimental conditions were chosen to represent the three cases (i.e., CC = 1.5D, 2D and 4D). Further, selection of a limited number of cases allowed for more efficient use of the available executable time for the numerical analysis. This discussion will present the numerical analysis and flow visualization results concurrently.

The numerical analysis was used to present the temperature fields and velocity vectors around the cylinders. A finite difference computer program for three dimensional hydrothermal analysis, Tempest [32], was used to conduct the numerical analysis. Some computer language modifications of this program were necessary in order to use Tempest on the available computing system.

The Floating Point (FPS) super computer was used as the scientific computer and the IBM 4381 was used as the front end computer. Both systems are available at the O.S.U. computer center. Due to the extensive executable time needed for Tempest to reach a steady state condition for the cases of the present

study, those conditions with q = (149.014) w/m2 for a single wall with CC = 1.5D, 2D and 4D and for double walls with CC = 1.5D and 2D will be presented.

Because Tempest accepts either cartesian or polar coordinates but not both, the cylinders were represented by a series of square cells. Also, multi-grid sizes were used to satisfy the code requirements and the physical geometry of the set-up. A sample of the grid system is shown in figure 6.1 for CC = 2D.

The flow visualization was recorded on video tape and slides. The slides were taken by a 135 mm Pentax with a slide film of 1600 ASA. The medium was illuminated by laser sheets as described in Chapter 3.

6.1 Single Wall Cases

The temperature distribution, velocity distribution and flow visualization for CC = 1.5D, 2D and 4D are shown in figures 6.2 through 6.4. All these cases are at q = 149.014 w/m2 and the left wall spacing, (S/D), is equal to 0.5. From the output of the numerical analysis of these cases, the maximum temperature deviation from the experimental data was less than 5% as calculated from equation 6.1:

$$T_{deviation} = \left(\frac{T_{experimental} - T_{numerical}}{T_{experimental}} \right) \times 100 \qquad (6.1)$$

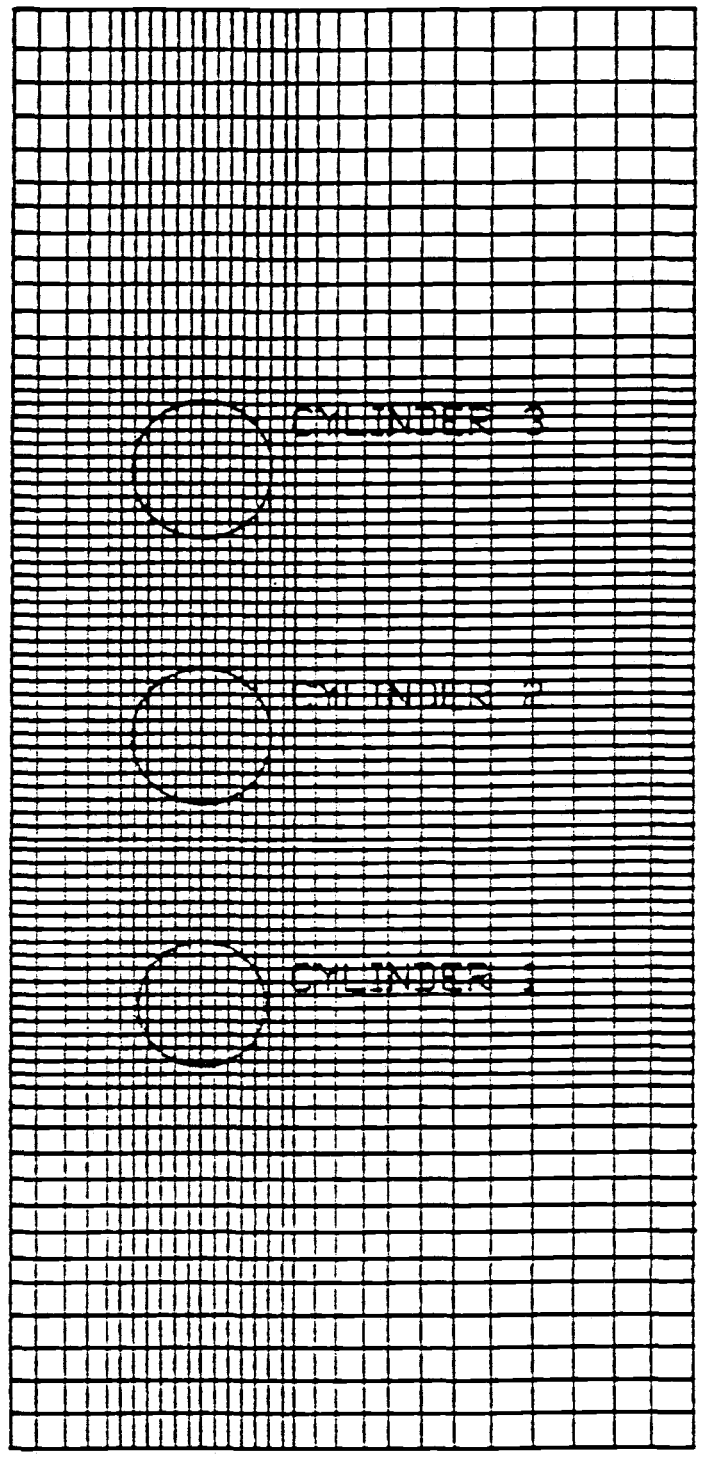

Figure 6.1 The mesh model for TEMPEST for CC=2D array .

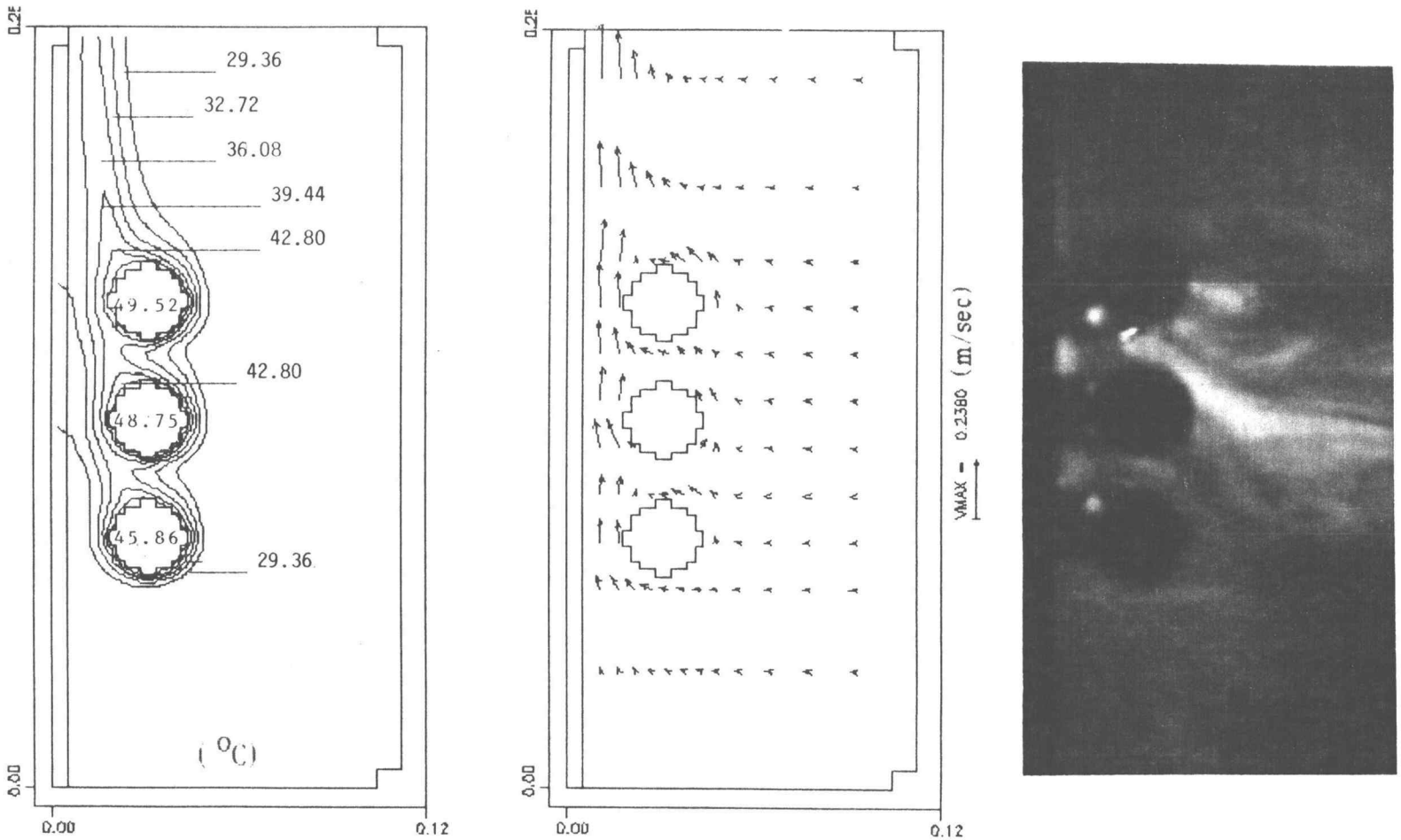

a) Temperature distribution. b) Velocity distribution. c) Flow visualization .

Figure 6.2 Temperature, Velocity, and Flow fields for CC=1.5D array with a single wall at S/D=0.5 .

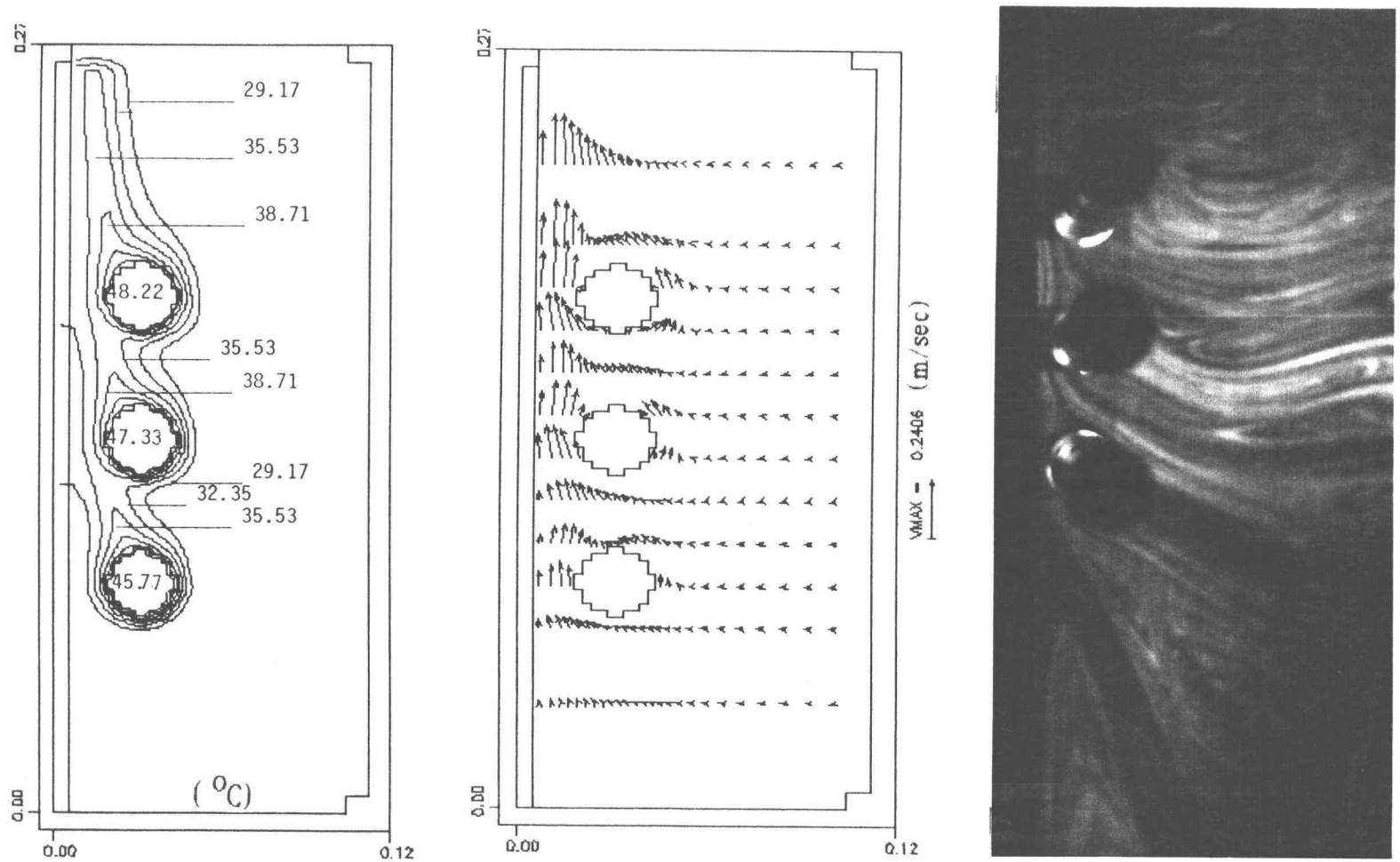

a) Temperature distribution. b) Velocity distribution. c) Flow visualization .

Figure 6.3 Temperature, Velocity, and Flow fields for CC=2D with a single wall at S/D=0.5 .

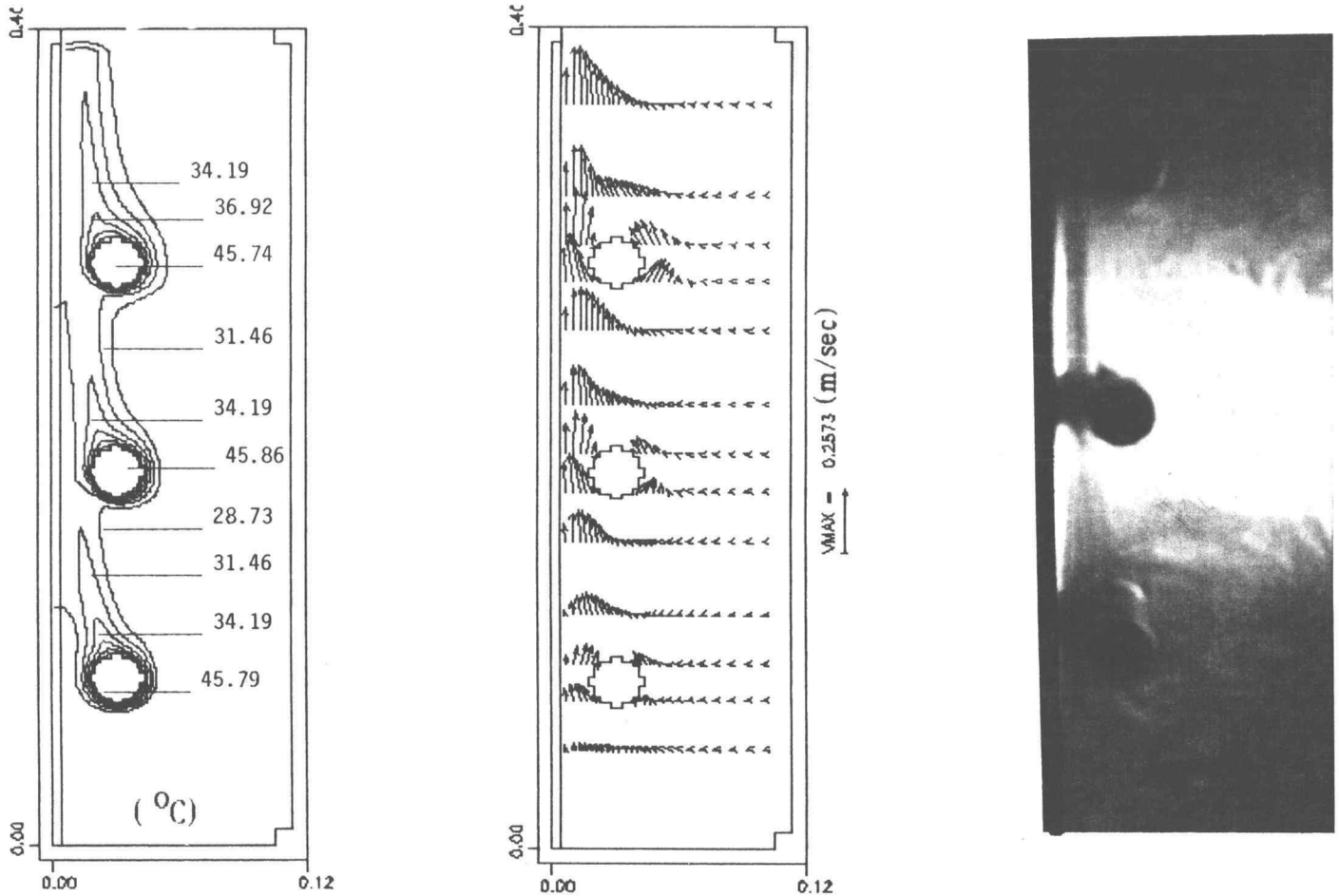

a) Temperature distribution. b) Velocity distribution. c) Flow visualization

Figure 6.4 Temperature, Velocity, and Flow fields for CC=4D with a single wall at S/D=0.5 .

From figures 6.2 through 6.4, it can be seen that the space between the cylinders and the wall act as a chimney where the air particles are at a higher temperature than the ambient. The high temperature zone creates a low density region between the wall and the cylinders of the array. This leads to a low pressure in this region. Due to buoyancy forces, this low pressure drives the air particles horizontally toward the wall through the cylinder-to-cylinder spacing and vertically through the lower cylinder-wall space. As the center-to-center spacing, CC, increases, the raised plume from one cylinder to the next higher cylinder has more time to be mixed with the ambient air particles which were directed toward the wall. Also, as the CC spacing increases, the raised plume from the lower cylinder(s) has fewer flow restrictions given the geometry of the set-up and has more time to be accelerated by the buoyancy forces while it rises. This can be noticed by comparing the velocity vectors of figures 6.2 through 6.4.

From the numerical results at CC = 4D, as shown in figure 6.4(a), the maximum temperature difference between the three cylinders is 0.18 degrees Centigrade, whereas a maximum difference of 0.4 degrees Centigrade is obtained from the experimental results. This indicates that each of the three cylinders acts like a single cylinder due to the balance between the increased temperature of the rising plume (which reduces the heat transfer) and the increased velocity of the plume (which

enhances the heat transfer) as it ascends the array. Furthermore, the flow visualization of figures 6.2 through 6.4 shows that the weak regions above the cylinders were shifted towards the wall. The streamlines of the flow show that the air particles approach the upper cylinders horizontally. For the lowest cylinder, the air particles approach the cylinders in a plane rotating toward the vertical wall. In other words, if there is a single wall at the left side of the array, the upper and lower stagnation points of each cylinder were rotated counter clockwise from the vertical plane (the plane which passes through the axis of each cylinder). This rotation of the stagnation points was at its maximum at S/D = 0.5 and the rotation decreases as the wall-array spacing decreases or increases from S/D = 0.5.

The flow visualization showed that the presence of a single wall induces more air circulation from the ambient around the highest cylinder in the array. This enhances the heat transfer from the highest cylinder and thus explains why the highest cylinder behaves closely to the middle cylinder (cylinder 2). For a free array (no wall case), the flow visualization showed that the streamlines were symmetrically arranged about the plane of the array. Also, the stagnation points of the cylinders lay on the vertical plane which passes along the axis of each cylinder. The flow was laminar around the cylinders in the arrays with small cylinder center-to-center spacings (i.e., CC = 1.5D and 2D). For the highest center-to-center spacing (i.e., CC = 4D), the flow was

laminar around the first and second cylinders and unstable (or in a transition condition) above the second cylinder. In this condition, the streamlines of the flow swung from one side of the array to the other. This instability of the flow began above the second cylinder and its frequency increased as it rose in the array. This explains why the upper cylinders were at a lower temperature than the lowest cylinder. Furthermore, when the power was increased, this instability of the flow began even closer to the second cylinder.

6.2 Two Wall Cases

The flow visualization showed that the flow was laminar and symmetrical about the vertical plane which passes through the centers of the cylinders. This is true only when the arrays were placed symmetrically between the walls (i.e., at $S/D = (S/D)_R = 0.5$ conditions). In this condition, the stagnation points of all the cylinders lay in the same vertical plane and the weak regions lay vertically above the cylinders. The weak regions between the cylinders for CC = 1.5D and 2D were extended to include the whole spaces between the cylinders, as shown in figure 6.5 (a). In these spaces, the flow visualization showed that there were double vortices. The left vortex rotates clockwise, while the right vortex rotates counter clockwise. For CC = 4D, the weak regions were present to a limited distance (i.e.,a distance less than the

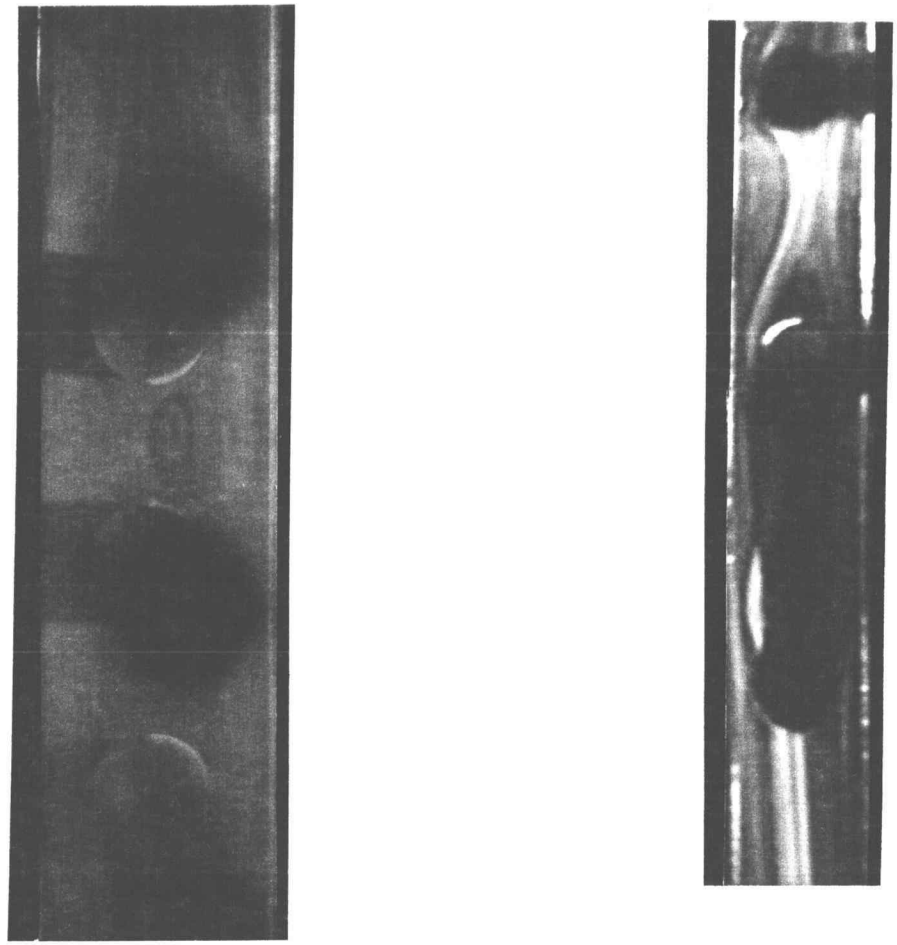

a) Flow visualization, for CC=2D.

b) Flow visualization, for CC=4D.

Figure 6.5 Flow visualization for arrays symmetrically placed between two walls at $S/D=(S/D)_R=0.5$.

cylinder-to-cylinder spacing) above each cylinder, as shown in figure 6.5 (b).

As the array to the right wall spacing, $(S/D)_R$, increased (i.e., the array was placed asymmetrically between the walls), the streamlines of the flow were no longer symmetrical on both sides of the array. This result occurred due to the left wall jet. This jet was established as a result of the higher temperature zone between the array and the left wall to it as compared to the rest of the region.

As the right wall spacing, $(S/D)_R$, increased, the velocity vectors shifted from the vertical direction (for symmetrical walls placements) toward the closest wall to the array. For the region above the array, the left wall jet induced a feedback current (or a reverse current). This current penetrated downward close to the farthest wall (right wall) from the array and introduced cooler air particles between the walls. Then, the reverse current circulated upward along the left wall jet, as shown in figure 6.6 and figure 6.7 .

The penetration of the reversed current became deeper as the farthest wall spacing increased. At large $(S/D)_R$, the reverse current region extended to include the highest cylinder in the array. This flow around the highest cylinder enhanced its heat transfer capability. This explains why the Nusselt number of the highest cylinder became closer to or higher than the Nusselt number of the second cylinder of the array for CC = 1.5D and 2D.

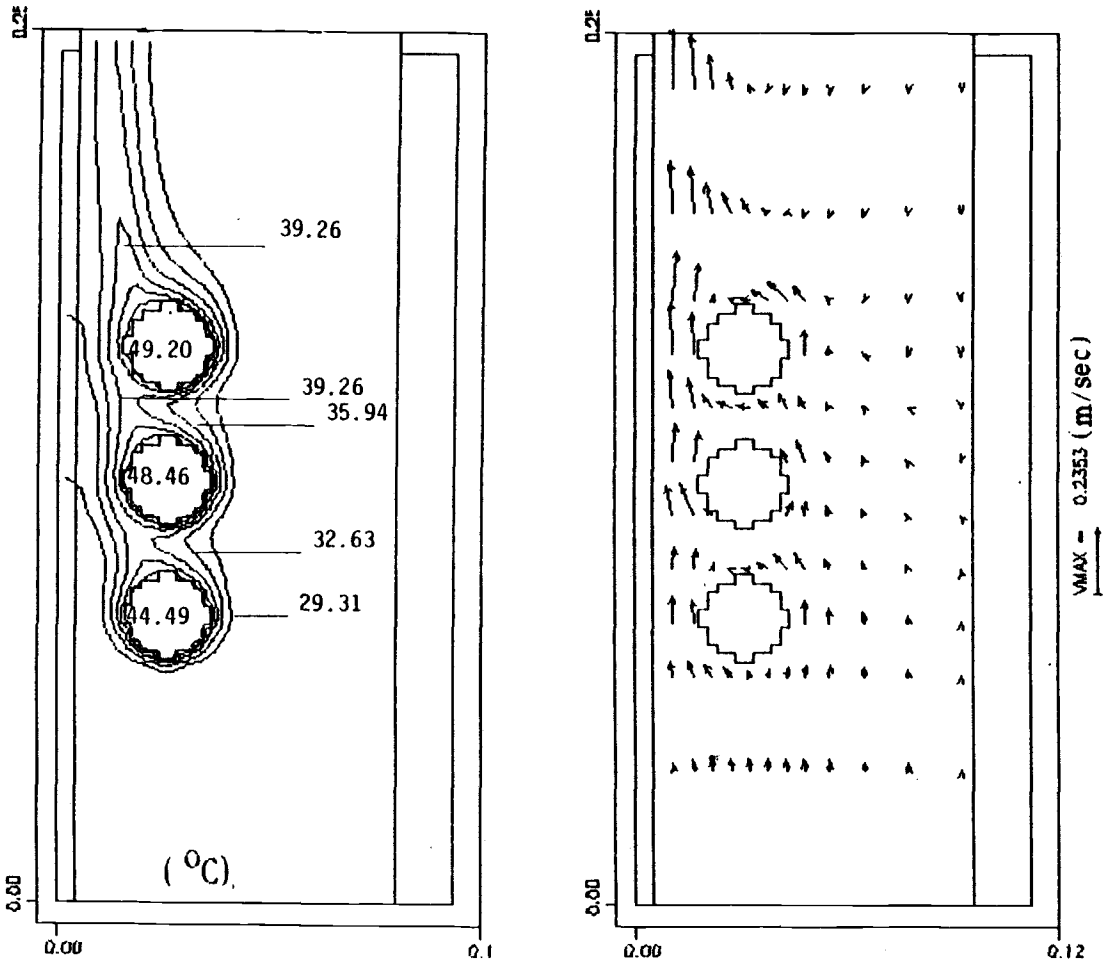

a) Temperature distribution.

b) Velocity distribution.

Figure 6.6 Temperature, and Velocity fields for CC=1.5D array with two walls at S/D=0.5 and $(S/D)_R$=2.0 .

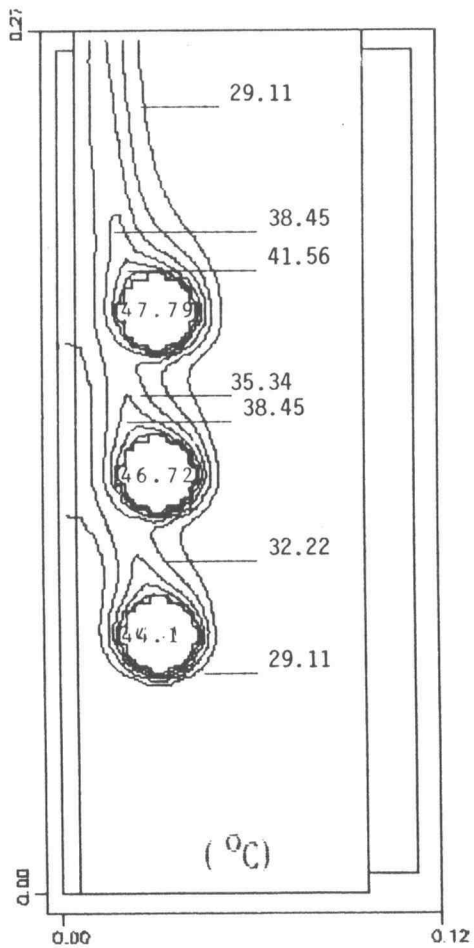

a) Temperature distribution.

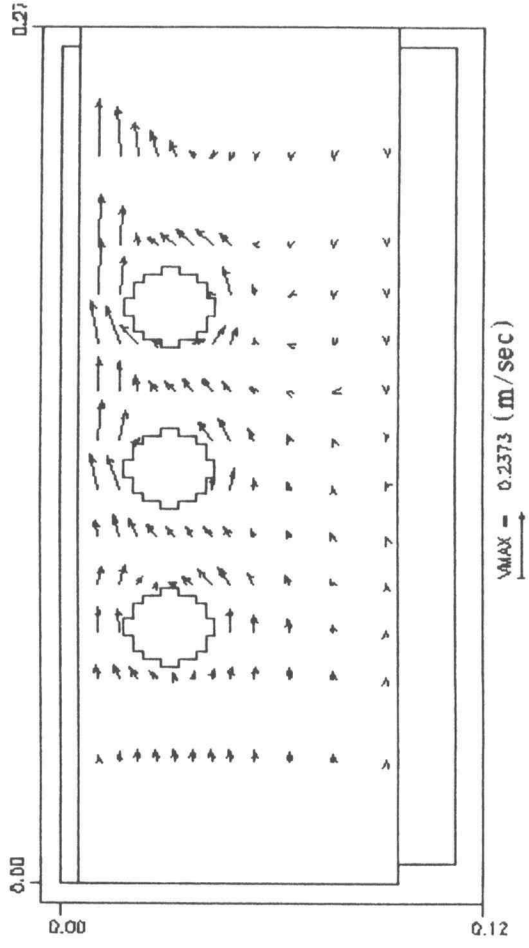

b) Velocity distribution.

c) Flow visualization .

Figure 6.7 Temperature, Velocity, and Flow fields for CC=2D array with two walls at S/D=0.5 and $(S/D)_R$=2.0 .

Figures 6.6 and 6.7 show that the high temperature plume that was rising from the cylinders shifted toward the closest wall to the array as the other wall spacing increased.

CHAPTER 7

CONCLUSIONS AND RECOMMENDATIONS

7.1 Conclusions

This study presented the results of the experimental investigation of heat transfer from an array of three horizontal cylinders aligned vertically parallel to a single wall or parallel to two walls. Three different cylinder center-to-center spacings for the array cylinders were examined, CC = 1.5D, 2D and 4D. The wall-array spacings were varied from 0.081D to infinity for single wall cases. For two wall cases, the left wall spacing was kept at S/D = 0.5, while the right wall spacing varied from $(S/D)_R$ = 0.5 to 3.5. All the cylinders were maintained at constant heat flux. Modified Rayleigh number, based on the diameter of the cylinders, ranged from 6.2×10^4 to 1.2×10^6. Empirical equations were proposed to predict the effects of the experimental parameters on the heat transfer as expressed by the average Nusselt number of each cylinder or the average Nusselt number of the whole array.

This experimental investigation has provided new information concerning natural convection heat transfer from an array of cylinders confined by a single vertical wall or two vertical walls. The new information obtained about the variables

in this experiment can be useful in optimizing the design of heat exchangers and in the packaging design of electrical components. Also, the quantitative results can be employed in applied research concerning heat transfer.

7.1.1 Single wall cases

The experiments have shown that the lowest cylinder in the array behaves as a free single cylinder for all cases in which $S/D \geq 0.155$. The heat transfer from the upper cylinders of the array was affected by the wall-array spacing (S/D values) and the cylinder center-to-center spacing (CC values). The presence of the wall enhanced the heat transfer from the upper cylinders of the array with CC = 1.5D and 2D relative to the no wall cases, while there was degradation in the cylinders' heat transfer capability with CC = 4D. At the two small CC values the maximum enhancement for the free array occurred at $S/D \sim 0.5$. The third cylinder had the maximum enhancement, the second cylinder had the next highest enhancement, and the first cylinder had the lowest enhancement. The Nusselt number for each cylinder can be predicted from equation 4.7 with less than 5% error for $q > 49.338$ w/m^2 and with 10% or less error for $q = 49.338$ w/m^2.

The temperature and velocity distribution from the numerical analysis and the flow visualization showed that the space between the array and the wall acts like a chimney and

creates a left wall jet flow. Further, the closest spacings between each cylinder and the wall acts like a flow reinforcing station.

The second cylinder behaved more like the third cylinder than the first cylinder (i.e., [Nu1 - Nu2] > [Nu2 - nu3]). This was the result of additional cooling of the third cylinder due to increased ambient air circulation above this cylinder. This circulation was induced by the left wall jet. The bottom and top stagnation points on each cylinder were shifted from the vertical plane due to the presence of the wall. In the presence of a single left wall, the stagnation points were shifted counter clockwise. This shifting was at its maximum when S/D ~ 0.5 and decreased as S/D either increased or decreased.

7.1.2 Two wall cases

The lowest cylinder had the highest heat transfer coefficient. This heat transfer coefficient was at its maximum when the walls were symmetrically placed to the array. As the right wall spacing, $(S/D)_R$, increased the Nusselt number of the lowest cylinder decreased. At the largest center-to-center spacing, CC = 4D, the lowest cylinder had the highest enhancement compared to a free single cylinder.

For the upper cylinders at small center-to-center spacings (CC = 1.5D and 2D), the heat transfer coefficient showed an enhancement at $(S/D)_R \geq 1.5$ compared to a free single cylinder or

the single wall cases. At the largest center-to-center spacings (CC = 4D), the upper cylinders showed enhancement in the heat tranfer coefficient with the presence of the right wall for all $(S/D)_R$ values. These enhancements were the highest at the small $(S/D)_R$ and decreased as $(S/D)_R$ increased. When compared to free array cases (i.e., no wall), all the cylinders in all the cases showed an enhancement in the heat transfer coefficient.

The average Nusselt numbers for the whole array were more sensitive to the right wall spacing as the center-to-center values increased. The experimental results showed that the average Nusselt numbers for the whole array were enhanced relative to the average Nusselt number of the free single cylinder and relative to the average Nusselt number of the whole array for single wall cases. These enhancements increased and were more sensitive to $(S/D)_R$ as the cylinders' center-to-center spacings increased. At low center-to-center spacing values (CC = 1.5D and 2D), the enhancement of the whole array was at a minimum at $1 < (S/D)_R < 1.5$. This can be explained by the fact that the degradation in the upper cylinders was higher than the enhancement in the lowest cylinder in this $(S/D)_R$ range. Table 5.2 shows the empirical equation to calculate the average Nusselt number for the whole array.

The flow visualization and the numerical results indicate that the flow was in transition above the array and a reversed current was established between the two walls. This current

region extended from the top of the walls down to enclose the highest cylinder in the array.

7.2 Recommendations

The present work could be extended by considering the following recommendations:

1) An investigation to explore the effects of misalligning one or more of the cylinders of the array. This misallignment might conceivably change the flow pattern around the cylinders, which in turn might affect the heat transfer characteristics.
2) Using different fluids as the test medium, such as water or oil, would provide greater understanding concerning the effects of the Prandtl number on the heat transfer behavior of the array.
3) Changing the diameter of the cylinders and/or the number of the cylinders would add to the understanding of the effects of the array-wall spacings on heat transfer.
4) Developing the flow visualization system to use laser sheets for three dimentional heat transfer flow. This could be accomplished by using two laser sheets perpendicular to each other instead of superimposing one laser sheet on the other.

BIBLIOGRAPHY

1. Kreith, F.; Principles of Heat Transfer, International Textbook, Scranton, 1958.

2. Parsons, J.R.,Jr. and Arey, M.L., Jr.; "Development of Convection Heat Transfer near a Suddenly Heated Horizontal Wire in a Still Fluid", ASME paper no. 84, WA/HT-50, 1984.

3. Parsons, J.R., Jr. and Arey, M.L., Jr.; "Development of Convective Heat Transfer near Suddenly Heated Vertically Aligned Horizontal Wires",Transactions of the ASME, Vol. 109, pp. 912-918, Nov. 1987.

4. Sloan, J.L.; Design and Packaging of Electronic Equipment, Van Nostrand Reinhold Company, Inc., New York, 1985.

5. Sparrow, E.M. and Niethammer, J.E.; "Effect of Vertical Separation Distance and Cylinder-to-Cylinder Temperature Imbalance on Natural Convection for a Pair of Horizontal Cylinders", Transactions of the ASME, Vol. 103, pp. 638-644, Nov. 1981.

6. Bejan, A.; Convection Heat Transfer, John Wiley & Sons, Inc., New York, 1984.

7. Levy, S.; "Integral Methods in Natural Convection Flow", Journal of Applied Mechanics, pp. 515-522, Dec.1955.

8. Holman, J.P.; Heat Transfer, 6th edition, McGraw-Hill Book Co., New York, 1986.

9. Morgan, V.T.; "The Overall Convective Heat Transfer from Smooth Circular Cylinders", in Advances in Heat Transfer, Vol. 11, Academic Press, New York, pp. 199-264, 1975.

10. Dyer, J.R.; "Laminar Natural Convection from a Horizontal Cylinder with a Uniform Convective Heat Flux", Mechanical and Chemical Engineering Transactions, Institution of Engineers, Australia, Vol. MC1, pp. 125-128, May 1965.

11. Kim, C.B., Pontikes, T.J., and Wollersheim, D.E.; "Free Convection from a Horizontal Cylinder with Isothermal and Constant Heat Flux Surface Conditions", Transactions of the ASME, Journal of Heat Transfer, pp. 129- 130, Feb. 1975.

12. Lieberman, J. and Gebhart, B.; "Interactions in Natural Convection from an Array of Heated Elements, Experimental", Int. J. of Heat Transfer, Vol. 12, pp. 1385-1396, 1969.

13. Marsters, G.F.; "Array of Heated Horizontal Cylinders in Natural Convection", Int. J. of Heat Mass Transfer, Vol. 15, pp. 921-933, 1972.

14. Sparrow, E.M. and Boessneck, D.S.; "Effect of Transverse Misalignment on Natural Convection from a pair of Parallel, Vertically Stacked, Horizontal Cylinders", Journal of Heat Transfer, Vol. 105, pp. 241-247, May 1983.

15. Marsters, G.F.; "Natural Convective Heat Transfer from a Horizontal Cylinder in the presence of nearby Walls", The Canadian Journal of Chemical Engineering, Vol. 53, pp. 144-149, April 1975.

16. Sparrow, E.M. and Pfeil, D.R.; "Enhancement of Natural Convection Heat Transfer from a Horizontal Cylinder due to Vertical Shrouding Surfaces", Transactions of the ASME, Vol. 106, pp. 124-130, Feb. 1984.

17. Karim, F., Farouk, B., and Namer, I.; "Natural Convection Heat Transfer from a Horizontal Cylinder between Vertical Confining Adiabatic Walls", Journal of Heat Tranfer, Vol. 108, pp. 291-298, May 1986.

18. Marsters, G.F. and Paulus, G.; "Effects of Confining Walls on Heat Tranfser from a Vertical Array of Heated Horizontal

APPENDICES

Cylinders", Transactions of CSME, Vol. 1, No. 4, pp. 219-222, 1972.

19. Tokura, I., Saito, H., Kishinami, K., and Muramoto, K.; "An Experimental Study of Free Convection Heat Transfer from a Horizontal Cylinder in a Vertical Array set in Free Space between Parallel Walls", Transactions of the ASME, Vol. 105, pp. 102-107, Feb. 1983.

20. Sparrow, E.M. and Chrysler, G.M.; "Natural Convection Heat Transfer Coefficients for a short Horizontal Cylinder attached to a Vertical Plate", Transactions of the ASME, vol. 103, pp. 630-637, Nov. 1981.

21. Sparrow, E.M., Cook, D.S., and Chrysler, G.M.; "Heat Transfer by Natural Convection from an Array of Short, Wall-Attached Horizontal Cylinders", Journal of Heat Transfer, Vol. 104, pp. 125-131, Feb. 1982.

22. Sparrow, E.M., Mendes, P.S., Ansari, M.A., and Parta, A.T.; "Duct-Flow versus External-Flow Natural Convection at a Short, wall-attached Horizontal Cylinder", Int. J. of Heat Mass Transfer, Vol. 26, No. 6, pp. 881-888, 1983.

23. Sparrow, E.M. and Ansari, M.A.; "All-Modes Heat Tranfser from a Horizontal Cylinder Situated Adjacent to Adiabatic, partially enclosing Walls", Int. J. of Heat Mass Transfer, Vol. 27, No. 10, pp. 1855-1864, 1984.

24. McCoy, T.J.; "Natural Convection from a Horizontal Cylinder Parallel to a Heated Vertical Wall", Master's thesis, Mechanical Engineering Dept., Oregon State University, 1988.

25. Temperature Handbook, OMEGA Engineering, Inc., Stamford, CT, 1987.

26. Hot Spot Application Manual, DCC Corporation, Pennsauken, NJ, January 1986.

27. User Manual for DT2801 Series, Document UM-0066-D-1855, Data Translation, Inc, January 1981.

28. User Manual for PC LAB, Document UM-02899-A, Data Translation, Inc, January 1982.

29. Vines, R.G.; "Measurement of Thermal Conductivities of Gases at High Temperatures", Transactions of the ASME, Feb. 1960.

30. Touloukian, Y.S.; "Thermophysical Properties of Matter", The TPRC Data Series: Specific Heat Nonmetallic Liquid and Gases, Vol. 6, 1970.

31. Hilsenrath, J. and Touloukian, Y.S.; "Viscosity, Thermal Conductivity and Prandtl Number for Air, O_2, N_2, No, H_2, Co, H_2, He and A", Transactions of the ASME, pp. 967-985, August 1954.

32. Trent, D.S. and Eyler, L.L.; Tempest: A Three-Dimensional Time-Dependent Computer Program for Hydrothermal Analysis, Vol. 1., Pacific Northwest Laboratory, Richland, Washington, January 1989.

Appendix A

DATA AQUISITION PROGRAM

```
10 '
20 ' This data aquisition program is developed to read four interface cards
30 ' by using four DT2805 boards and four DT707-T screw terminal panels.
40 PRINT "Totale input power, Q = ";
50 INPUT Q   :' Q=()WATT
60 PRINT "CYLINDER-TO-CYLINDER SPACING =";: INPUT CTCS
70 PRINT "Cylinder-Right wall spacing, WS/D = "; :INPUT WSDR
80 PRINT "Cylinder-Left wall spacing, WS/D  = "; :INPUT WSDL
90 ' This file may be MERGEd with a user program to define
100 ' routine offsets and establish the PCLAB segment.
110 '
120 XAV=3     : XADT=6    : XSA=9     : XAS=12    : XBAD=15   : XTAD=18
130 XWAD=21   : XDV=24    : XDDT=27   : XSD=30    : XDS=33    : XBDD=36
140 XTDD=39   : XWDD=42   : XSCD=45   : XSSC=48   : XSCF=51   : XSCP=54
150 XEFI=57   : XEFO=60   : XIDV=63   : XODV=66   : XIDDT=69  : XDDDT=72
160 XSECW=75  : XGEC=78   : XSB=81    : XSBA=84   : XSDC=87   : XSAR=90
170 XSAC=93   : XSDR=96   : XSLF=99   : XSTG=102  : XST=105   : XGDE=108
180 XRD=111   : XGDS=114  : XCWFC=117 : XCWFD=120 : XCWFI=123 : XSAD=126
190 XSDD=129  : XCAD=132  : XCDD=135  : XMV=138   : XMT=141   : XMC=144
200 XATV=147  : XVTD=150  : XDTV=153  : XDLY=156  : XSTB=159  : XWD=162
210 XGC=165   : XCEV=168  : XREV=171  : XGF=174   : XSC=177   : XINIT=180
220 XTERM=183 : XIXR=186  : XIXW=189  : XFDL=192  : XESC=195  : XOSC=198
230 '
240 DEF SEG=&H0  ' get the PCLAB segment
250 PCLSEG = PEEK ( &H4FE ) + 256*PEEK ( &H4FF )
260 DEF SEG=PCLSEG ' REM address the PCLAB segment
270 ERROR.VALUE% = 0
280 CALL XSECW(ERROR.VALUE%)
290 '
300 GAIN% = 8
310 TYPE% = 116
320 CJCHAN% = 0
330 OPTION BASE 1
340 DIM TEMP(4,7)
350 '
360 CLS
370 ON TIMER(20) GOSUB 410
380 TIMER ON
390 GOTO 390
400 '
410 LOCATE 2,1
420 '
430 '
440    FOR BOARD% = 1 TO 4
450    CALL XSB(BOARD%)
460       FOR CHAN% = 1 TO 7
470          CJTOTAL = 0
480          TOTAL = 0
```

```
490         FOR I = 1 TO 16
500            CALL XAV(CJCHANX, GAINX, CJADATAX)
510            CJTOTAL = CJADATAX + CJTOTAL
520            CALL XAV(CHANX, GAINX, ADATAX)
530            TOTAL = ADATAX + TOTAL
540         NEXT I
550         CJADATAX = CINT(CJTOTAL / 16)
560         ADATAX = CINT(TOTAL / 16)
570         CJTEMP = (((CJADATAX * .04) / 4096) - .02) * 2000
580         CALL XDTV(TYPEX, CJTEMP, CJVOLTS)
590         VOLTS = (((ADATAX * .04) / 4096) - .02) + CJVOLTS
600         CALL XVTO(TYPEX, VOLTS, TEMPS)
610       TEMP(BOARDX,CHANX) = TEMPS
620       NEXT CHANX
630    NEXT BOARDX
640 AVER1 = (TEMP(1,1)+TEMP(2,1)+TEMP(3,1)+TEMP(4,1))/4!
650 AVER2 = (TEMP(1,2)+TEMP(2,2)+TEMP(3,2)+TEMP(4,2))/4!
660 AVER3 = (TEMP(1,3)+TEMP(2,3)+TEMP(3,3)+TEMP(4,3))/4!
670 CLS
680 PRINT "Total input power = "; : PRINT USING "##.##";Q;
690 PRINT " Watt            ";
700 PRINT " CC =";CICS
710 PRINT "Cylinder-Right wall spacing, WS/D = "; :PRINT USING "##.###";WSDR
720 PRINT "Cylinder-Left wall spacing, WS/D  = "; :PRINT USING "##.###";WSDL
730 PRINT
740 PRINT "             ( TEMPERATURES IN DEGREE CENTIGRADE ) "
750 PRINT "Thermocouple #    1       2       3       4       5      6"
760 PRINT USING "Cylinder 3     ###.##  ###.##  ###.##  ###.##  ###.##  ###.##";
TEMP(1,3);TEMP(2,3);TEMP(3,3);TEMP(4,3);TEMP(1,5);TEMP(2,5)
770 PRINT USING "Cylinder 2     ###.##  ###.##  ###.##  ###.##  ###.##  ###.##";
TEMP(1,2);TEMP(2,2);TEMP(3,2);TEMP(4,2);TEMP(3,4);TEMP(4,4)
780 PRINT USING "Cylinder 1     ###.##  ###.##  ###.##  ###.##  ###.##  ###.##";
TEMP(1,1);TEMP(2,1);TEMP(3,1);TEMP(4,1);TEMP(1,4);TEMP(2,4)
790 '
800 PRINT
810 PRINT "Average temperature for cylinder # 3 = ";
820 PRINT USING "###.## C";AVER3
830 PRINT "Average temperature for cylinder # 2 = ";
840 PRINT USING "###.## C";AVER2
850 PRINT "Average temperature for cylinder # 1 = ";
860 PRINT USING "###.## C";AVER1
870 PRINT
880 STTEMP=TEMP(1,6)-TEMP(1,7)
890 AMAVR=(TEMP(1,6)+TEMP(1,7))/2!
900 PRINT "Ambient temperature difference = "; : PRINT USING "###.## C";STTEMP
910 PRINT "Ambient temperature    = "; : PRINT USING "###.## C";AMAVR
920 TEND3=TEMP(3,5)-TEMP(3,6)
930 TEND2=TEMP(2,6)-TEMP(2,7)
```

```
940 TEND1=TEMP(4,5)-TEMP(4,6)
950 PRINT "End cap temperature difference for cylinder #3 = ";
960 PRINT USING "###.##";TEND3
970 '
980 PRINT "End cap temperature difference for cylinder #2 = ";
990 PRINT USING "###.##";TEND2
1000 '
1010 PRINT "End cap temperature difference for cylinder #1 = ";
1020 PRINT USING "###.##";TEND1
1030 PRINT
1040 '
1050 ' CHECK FOR STEADY STATE CONDITION:
1060 '
1070 P1=(AVER1-OBL1)*100!/OLD1
1080 P2=(AVER2-OLD2)*100!/OBL2
1090 P3=(AVER3-OLD3)*100!/OLD3
1100 '
1110 IF P1<.2 AND P2<.2 AND P3<.2 AND FLAG1<>1 THEN FLAG1=1 :CTIME=TIMER+600!
1120 OLD1=AVER1 : OLD2=AVER2 : OLD3=AVER3
1130 IF FLAG1=1 AND P1>.2 OR P2>.2 OR P3>.2 THEN FLAG1=0
1140 IF FLAG1=1 AND (CTIME+600)>TIMER THEN GOTO 1190
1150 PRINT "**********"
1160 PRINT "---- STEADY STATE CONDITION WAS REACHED IN THE LAST TEN MINETS ---"
1170 PRINT "--------------- AT TIME = ";CTIME+600;" SEC ----------------"
1180 '
1190    RETURN
1200    STOP
1210    END
```

APPENDIX B

RADIATION CORRECTION

The data reduction procedure, shown in section 3.4.2, illustrates that the accuracy of the natural convection heat transfer coefficient of the cylinders was dependent on the accuracy of the radiation correction. The cylinders were designed to make $Q_{rad} << Q_{convection}$. This was accomplished by polishing the surfaces of the aluminum cylinders to a mirror-like finish.

The procedure to determine the radiation corrections for the cylinder in a free single cylinder, an array of cylinders without a wall, an array of cylinders with a single wall, and an array of cylinders with two walls will be discussed in the following sections.

B.1 Radiation correction from a free single cylinder and an array of cylinders without a wall

The radiation correction for a free single cylinder was calculated from the following equation:

$$Q_r = e\ Sb\ A\ (T_w^4 - T_{inf}^4) \qquad (B.1)$$

where Sb is Stefan-Boltzmann constant and equal to 5.6696×10^{-8} $(w/m^2.K^4)$ and e is the emissivity = 0.05. The radiation

correction for multiple elements depends on the view factors between the surfaces as well as on the surface heating/cooling condition. The surface condition could be at a constant temperature or constant heat flux. Therefore, equation B.1 is no longer valid for a free array.

The view factor between the cylinders with the same diameter was calculated as follows:

$$F_{C-C} = \frac{1}{\pi}\left[(X^2 - 1)^{1/2} + \sin^{-1}\left(\frac{1}{X}\right) - X \right] \qquad (B.2)$$

Where X = 1 + (H/D) and H is the surface-to-surface distance between the cylinders, Howell [B.1]. Marsters [B.2] showed that the radiation corrections for the cylinders of an array at known surface temperature can be calculated from equation B.3 :

$$Q_r = (1 - K\ F_{C-C})\ e\ Sb\ A\ (T_w^4 - T_{inf}^4) \qquad (B.3)$$

where K = 1 if the cylinder is at the edge of the array or K = 2 if the cylinder is in the interior of the array. This procedure was implemented in the data reduction program, Appendix C, to calculate the radiation correction for the cylinders in the no wall cases.

B.2 Radiation correction for an array with a single wall

This case included three heated cylinders (the array) and an adiabatic wall. The wall was made of a poor thermal conductivity material and its back surface was insulated. Owing to the radiation heat transfer from the cylinders and the high temperature of the raised plume from the cylinders by natural convection, the surface of the wall was at a higher temperature than the ambient. Therefore, the wall cannot be considered as an adiabatic wall for radiation heat transfer considerations. Since the wall had poor thermal conductivity, the wall temperature was not uniform and the temperature along the wall was dependent on the elevation from each cylinder of the array and the spacing between the array and the wall (S/D). The closer spacing (S/D) resulted in higher non-uniform temperature along the wall. To account for this non-uniform temperature distribution, the wall was treated as five separate elements. The middle three elements had a length equal to the cylinders' center-to-center spacing, CC. These elements were numbered 5, 6, and 7 as shown in figure B.1. Hereafter these elements will be referred to as a "wall" with a specific number assigned to each. The temperature of each wall was recorded during the experiments. Wall numbers 5, 6, and 7 had the highest average temperature. Wall #8 had the next highest and wall #4 had the lowest temperature. The surfaces of the walls were black and had an emissivity equal to

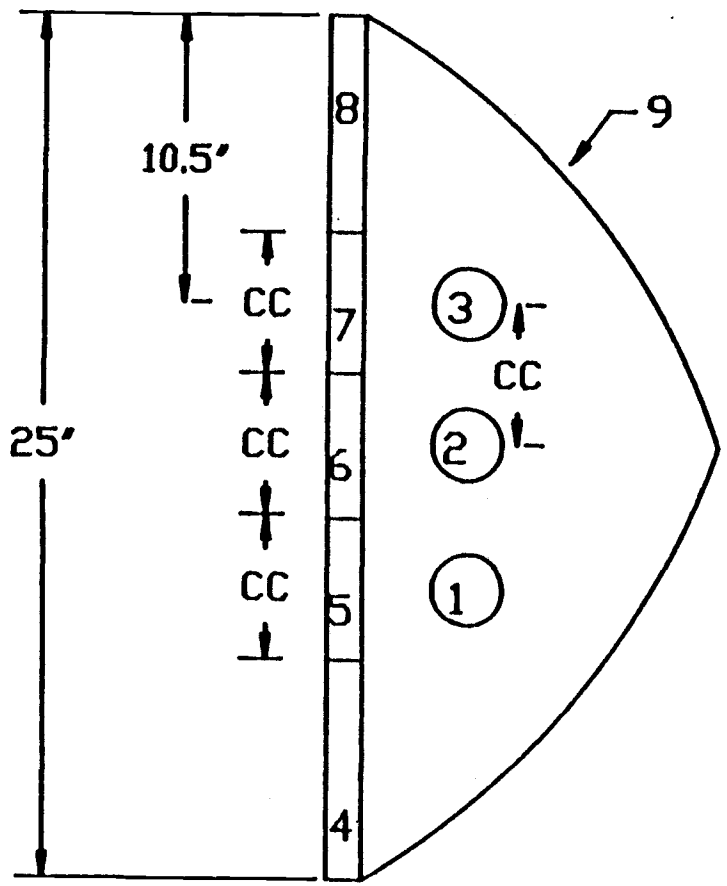

Figure B.1 The wall numbers for the view factors.

unity (i.e e_k=1.0 for k=4,5,. 6, 7, 8).

To further facilitate the analysis, it is convenient to envision an enclosure with black interior surfaces by adding surface #9, as shown in figure B.1. The view factors, which are defined as the fraction of energy leaving one surface that reaches another surface , Seigel and Howell [B.3], were calculated by using three different approaches. Surface shape and position of the surfaces determined which approach was used.

The first approach, equation B.2, determined the view factor between the cylinders, $F_{C\text{-}C}$. The view factors between each cylinder and the walls (walls #4 - 8) were calculated by using the crossed-string method. This method was used when the extended strings between a specific cylinder and a wall element were bent around the neighboring cylinder. In other words, this method was used when the viewing of the wall by the cylinder was obstructed by the cylinder directly above or below the specified cylinder. This condition is shown in figure B.2 and equation B.4 illustrates how the view factor was calculated by using the crossed-string method.

$$F_{3-4} = \frac{(fg+gc+cd+deh+ha) - (ab+bgc+cd+de+ef)}{2(\Pi D)} \qquad (B.4)$$

When the wall could be viewed by the specified cylinder without any obstruction by the other cylinder(s), the view factor was calculated from equation B.5.

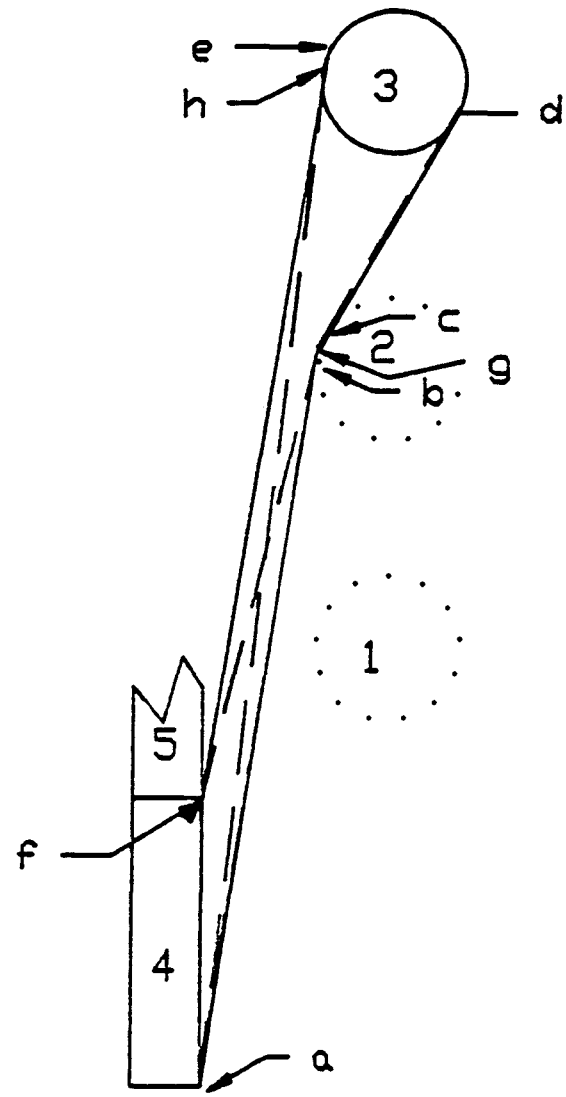

Figure B.2 Crossed-String method to calculate F_{3-4}.

$$F_{1-4} = \frac{1}{2\Pi} [\tan^{-1} B_1 - \tan^{-1} B_2] \qquad \text{where } B_1 = \frac{b_1}{a} \text{ and } B_2 = \frac{b_2}{a} \qquad (B.5)$$

The dimensions in this equation are shown in figure B.3. Equation B.5 yielded the same results as the crossed-string method and it was used for simplicity in the calculations. The reciprocal relations for the view factors were used to determine the view factors from Wall numbers 4, 5, 6, 7, and 8 to the cylinders. This relationship is illustrated as follows:

$$A_i F_{i-j} = A_j F_{j-i}$$

The view factors from the walls numbers 1 through 8 to wall #9 were calculated as follows:

$$F_{i-9} = 1 - \sum_{j=1}^{9} F_{i-j}$$

Table B.1 shows a sample of the view factors for the array with CC = 2D at S/D = 0.5. Once the view factors were determined, the radiosity values (the outgoing radiant energy per unit area), q_o , were determined from equation B.6, Siegel and Howell [B.2], by considering the surfaces as a diffuse-gray enclosure.

$$\sum_{j=1}^{9} [\delta_{kj} - (1-e_k) F_{k-j}] q_{o,j} = e_k Sb T_k^4 \qquad 1 \leq k \leq 9 \qquad (B.6)$$

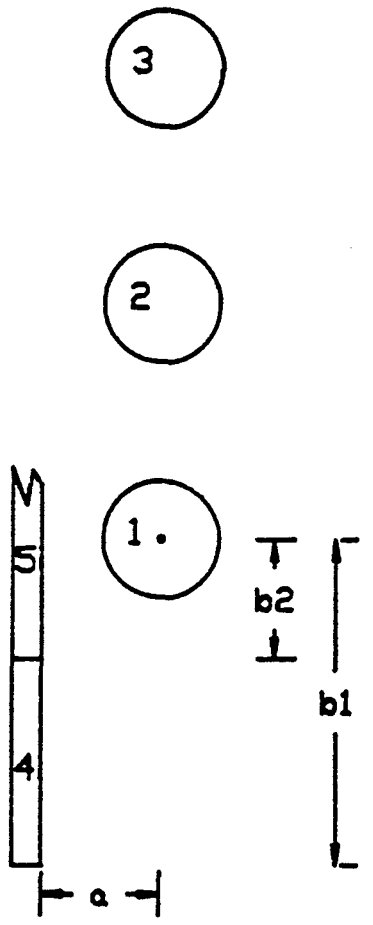

Figure B.3 The dimensions of equation B.5 .

Table B.1 View factors for a single wall case at CC= 2D and S/D= 0.5.

	1	2	3	4	5
1	0.00000E+00	8.13758E-02	0.00000E+00	1.09888E-01	2.50000E-01
2	8.13758E-02	0.00000E+00	8.13758E-02	1.08139E-02	7.37918E-02
3	0.00000E+00	8.13758E-02	0.00000E+00	2.35292E-03	5.19180E-03
4	3.63393E-02	3.57609E-03	7.78096E-04	0.00000E+00	0.00000E+00
5	3.92699E-01	1.15912E-01	8.15526E-03	0.00000E+00	0.00000E+00
6	1.15912E-01	3.92699E-01	1.15912E-01	0.00000E+00	0.00000E+00
7	8.15526E-03	1.15912E-01	3.92699E-01	0.00000E+00	0.00000E+00
8	7.78096E-04	3.57609E-03	3.63393E-02	0.00000E+00	0.00000E+00

	6	7	8	9
1	7.37918E-02	5.19180E-03	2.35292E-03	4.77400E-01
2	2.50000E-01	7.37918E-02	1.08139E-02	4.18037E-01
3	7.37918E-02	2.50000E-01	1.09888E-01	4.77400E-01
4	0.00000E+00	0.00000E+00	0.00000E+00	9.59307E-01
5	0.00000E+00	0.00000E+00	0.00000E+00	4.83234E-01
6	0.00000E+00	0.00000E+00	0.00000E+00	3.75477E-01
7	0.00000E+00	0.00000E+00	0.00000E+00	4.83234E-01
8	0.00000E+00	0.00000E+00	0.00000E+00	9.59307E-01

where $\delta_{kj} = 1$ if $k=j$ or $\delta_{kj} = 0$ if $k \neq j$

Since surfaces #4 to 9 were black surfaces, the radiosity values of these surfaces were known, owing to ($e_k=1$ for k=4 to 9). Hence equation B.6 can be written for $1 \leq k \leq 3$. From this, three equations were obtained which were solved for $q_{o,1}$, $q_{o,2}$, $q_{o,3}$. Then, the radiation heat transfer values from the surfaces were calculated from equation B.7.

$$Q_{r_k} = A_k \left(q_{o,k} - \sum_{j=1}^{9} F_{k-j}\, q_{o,j}\right) \quad 1 \leq k \leq 9 \text{ and } 1 \leq j \leq 8 \quad \text{(B.7)}$$

A computer program to calculate the heat transfer was written. This program is listed at the end of this appendix. A sample of the results of this program is shown in Table B.2.

B.3 Radiation heat transfer for two wall cases

Each of the side walls were considered as a single element. This was based on the following:

a. Owing to a higher flow rate between the two walls than the flow rate for a single wall, the temperature differences between the measured temperatures along the walls and the ambient were less in two wall cases at (S/D)R = 0.5 than that for a single wall at (S/D) = 0.5.

b. The temperature gradients along the wall at S/D $\geq$ 0.5 were less than the temperature gradient at smaller

Table B.2 Radiation corrections for the array at CC= 2D and S/D= 0.5.

TOTAL RADIATION

---	Q= 1 WATT	S/D=	.5
1	4.84352E-02	WATT	
2	5.19953E-02	WATT	
3	5.34983E-02	WATT	
	Q SUM 123 =	.1539288	
---	Q= 3 WATT	S/D=	.5
1	1.17373E-01	WATT	
2	1.26267E-01	WATT	
3	1.28733E-01	WATT	
	Q SUM 123 =	.3723726	
---	Q= 10 WATT	S/D=	.5
1	3.80710E-01	WATT	
2	3.93905E-01	WATT	
3	3.99162E-01	WATT	
	Q SUM 123 =	1.173777	
---	Q= 20 WATT	S/D=	.5
1	7.91351E-01	WATT	
2	8.19280E-01	WATT	
3	8.37882E-01	WATT	
	Q SUM 123 =	2.448513	
---	Q= 30 WATT	S/D=	.5
1	1.27777E+00	WATT	
2	1.32216E+00	WATT	
3	1.34775E+00	WATT	
	Q SUM 123 =	3.947678	

spacings.

c. The calculations of the radiation heat transfer for a single wall at S/D = 0.5 (by considering a single side wall element) were compared to the results of multiple wall elements. This showed that there was less than a 0.5% difference in the radiation correction from the multiple wall results.

Figure B.4 shows the numbers of the walls for two wall cases. Wall #6 was the flow outlet side and its temperature was considered to be the average of the transverse temperature readings between the two walls. Wall #7 was the inlet flow side and its temperature was considered to be the ambient temperature. The average temperatures for walls # 4 and 5 were calculated from the average temperature of the wall elements shown in figure B.1. The temperature of each element was weighted by its area as shown in the following equation:

$$T_{av} = \frac{\sum_{i=4}^{8} (A_i\ T_i)}{A} \qquad \text{where } A = \sum_{i=4}^{8} A_i \text{ and } i = \text{wall numbers in figure B.1.}$$

The view factors between the cylinders were calculated by using equation B.1. The crossed-string method was used to calculate the view factors from cylinders 1, 2, and 3 to the side walls 4 and 5. F_{1-7} and F_{3-6} were determined from equation B.5.

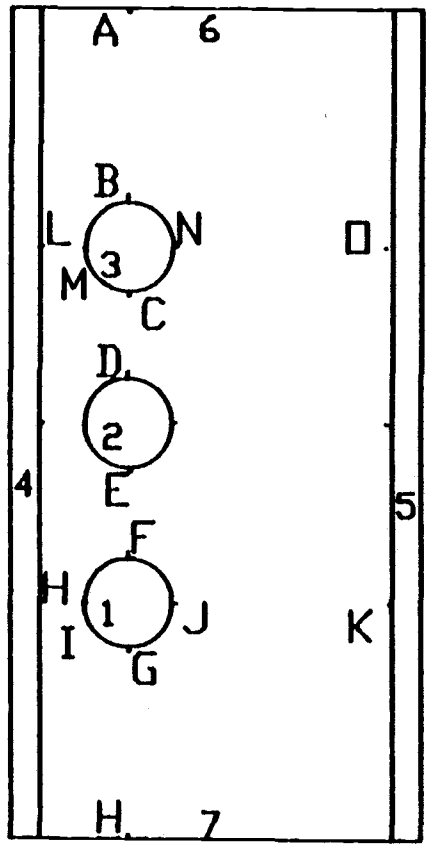

Figure B.4 The numbers of the walls for two walls cases.

The view factors between wall 4 and wall 5 were calculated as follows:

$$F_{4-5} = F_{4-5 \text{ through A-B}} + F_{4-5 \text{ through C-D}} + F_{4-5 \text{ through E-F}} + F_{4-5 \text{ through G-H}} \quad \text{(B.8)}$$

The spacings A-B, C-D, E-F, and G-H are shown in figure B.4. The view factors on the right hand side of equation B.8 were calculated by using the crossed-string method. For walls 6 and 7, the view factors were calculated as follows:

$$F_{6-7} = F_{6-7 \text{ through L-M}} + F_{6-7 \text{ through N-O}} \quad \text{(B.9)}$$

The view factors from cylinder 2 to wall 6 and 7 were determined as follows:

$$F_{2-6} = F_{2-6 \text{ through L-M}} + F_{2-6 \text{ through N-O}}$$

$$F_{2-7} = F_{2-7 \text{ through H-I}} + F_{2-7 \text{ through J-K}}$$

By using the reciprocal relation and by considering the fact that the fraction of energy leaving one surface and reaching the surfaces of the enclosure must equal unity, all the view factors were determined. Table B.3 shows the view factors for CC = 2D at S/D = 0.5 and $(S/D)_R$ = 2.00.

Wall numbers 4 through 7 were considered as black surfaces

Table B.3 View factors for two walls case at CC= 2D with S/D= 0.5 and $(S/D)_R$= 2.0 .

VIEW FACTORS

------- S/D= 0.5 (S/D)R= 2.00

WALL	1	2	3	4
1	0.0000000D+00	8.1375800D-02	0.0000000D+00	4.4398102D-01
2	8.1375800D-02	0.0000000D+00	8.1375800D-02	4.1802030D-01
3	0.0000000D+00	8.1375800D-02	0.0000000D+00	4.4398102D-01
4	5.5792300D-02	5.2599806D-02	5.5792300D-02	0.0000000D+00
5	5.2612187D-02	5.1423069D-02	5.2612187D-02	7.1310886D-01
6	3.2809889D-03	4.4953199D-03	4.6956411D-02	4.3848761D-01
7	4.6956411D-02	4.4953199D-03	3.2809880D-03	4.3848761D-01

WALL	5	6	7
1	4.1867448D-01	3.6552996D-03	5.2313415D-02
2	4.0921179D-01	5.0081660D-03	5.0081660D-03
3	4.1867448D-01	5.2313415D-02	3.6552990D-03
4	7.1310886D-01	6.1388281D-02	6.1388281D-02
5	0.0000000D+00	6.5121850D-02	6.5121850D-02
6	4.6515607D-01	0.0000000D+00	4.1623493D-02
7	4.6515607D-01	4.1623493D-02	0.0000000D+00

(i.e., $e_k = 1$ for k = 4, 5, 6, and 7). Therefore, the radiosity values of these walls were known and equation B.6 was written for $1 \leq K \leq 3$ only. Once the radiosity, q_o, of each surface was known, the radiation heat transfer was calculated from equation B.7 for $1 \leq k \leq 7$ and $1 \leq j \leq 7$. These calculations were performed by modifying the computer program for a single wall by changing the wall numbers. The original single-wall computer program is shown at the end of this appendix. Table B.4 shows the output results of the modified program for CC = 2D at S/D = 0.5 and $(S/D)_R = 2.00$.

B.1 Howell, John R., "A Catalog of Radiation Configuration Factors", McGraw-Hill Book Company, New York.

B.2 Marsters,G.F.; "Arrays of Heated Horizontal Cylinders in Natural Convection"; Int. J. Heat Mass Transfer, vol.15, 1972.

B.3 Siegel, Robert and Howell, John R.; "Thermal Radiation Heat Transfer"; 2nd Edition, Mc Graw-Hill Book Company, New York.

Table B.4 Radiation corrections for the array at CC= 2D and two walls at S/D= 0.5 and $(S/D)_R$ =2.0 .

TOTAL RADIATION

--- Q= 1 WATT S/D= 0.5 (S/D)R= 2.00

1	4.39798D-02	WATT
2	5.21138D-02	WATT
3	5.32893D-02	WATT
4	2.45852D-01	WATT
5	-3.86176D-01	WATT
6	6.20987D-02	WATT
7	-7.63374D-02	WATT

Q SUM 123 = .149382 Q SUM 4-7 = -.154563

--- Q= 3 WATT S/D= 0.5 (S/D)R= 2.00

1	1.05245D-01	WATT
2	1.24548D-01	WATT
3	1.28079D-01	WATT
4	3.44062D-01	WATT
5	-7.10074D-01	WATT
6	1.10993D-01	WATT
7	-1.08110D-01	WATT

Q SUM 123 = .357871 Q SUM 4-7 = -.363129

--- Q= 10 WATT S/D= 0.5 (S/D)R= 2.00

1	3.21437D-01	WATT
2	3.74163D-01	WATT
3	3.80615D-01	WATT
4	8.92923D-01	WATT
5	-1.55482D+00	WATT
6	-2.25960D-02	WATT
7	-3.97262D-01	WATT

Q SUM 123 = 1.076215 Q SUM 4-7 = -1.081759

--- Q= 20 WATT S/D= 0.5 (S/D)R= 2.00

1	6.64789D-01	WATT
2	8.05114D-01	WATT
3	7.98795D-01	WATT
4	1.18983D+00	WATT
5	-2.46210D+00	WATT
6	-2.48190D-01	WATT
7	-7.54242D-01	WATT

Q SUM 123 = 2.268698 Q SUM 4-7 = -2.274709

--- Q= 30 WATT S/D= 0.5 (S/D)R= 2.00

1	1.08727D+00	WATT
2	1.27683D+00	WATT
3	1.29299D+00	WATT
4	1.13367D+00	WATT
5	-3.29260D+00	WATT
6	-4.30315D-01	WATT
7	-1.08430D+00	WATT

Q SUM 123 = 3.657083 Q SUM 4-7 = -3.663547

Appendix C

DATA REDUCTION PROGRAM

```
10 ' ********** Program (CALRONUP.TRA) to calculate the radiation and
20 ' ********** Nuselt number for the three cylinders and printout the results.
30 REM
40                    CORRECT THE FILE NAMES IN LINE 390, 540 AND LINE 940
50 DEFDBL A-Z
60 DEFSNG I,K,J
70 DIM TW(9,9,3),TA(9,9),TR(9,9,3),QR(9,9,3),QCO(9,9,3),QCV(9,9,3),Q(9),WS(9)
80 DIM TEND(9,9,3),PR(9,9,3),GRM(9,9,3),RAM(9,9,3),NUEX(9,9,3)
90 DIM TWAV(9,9,3),AMY(9,9,3)
100 REM
110 REM ********************* INPUT DATA  ********************************
120 REM
130 PRINT "CYLINDER LENGTH, CL=";:INPUT CL
140 PRINT "CYLINDER DIAMETER, D=";:INPUT D
150 PRINT "CYLINDER CENTER-TO-CENTER SPACING, CCS="; : INPUT CCS
160 REM
170 R=D/2! : PI=3.14159265# :  REM R=CYLINDER RADIUS.
180 REM ************************************************************
190 REM
200 ' ****  CALCULATE CYLINDER TO CYLINDER VIEW FACTOR, FCC, FOR NO WALL CASES:
210 REM
220 CCL=CL/R  :  REM CCL= NORMALIZED CYLINDER LENGTH.
230 CR=CCS/R  :  REM CR= NORMALIZED CYLINDER CENTER TO CENTER SPACING.
240 SCR=1!/CR : SSCR=SCR/(1!-SCR^2)^.5 :ASCR=ATN(SSCR)
250 CCX=((((CR^2-1!)^.5 - (PI/2!))/ASCR)+1!)^.5
260 CCY=CCL^2!-CCX^2!+1!
270 CCZ=CCL^2!+CCX^2!-1!
280 REM
290 SCCX=1!/CCX : SSCCX=SCCX/(1!-SCCX^2)^.5 : ASCCX=ATN(SSCCX)
300 YDZ=CCY/CCZ : CYDZ=YDZ/(1!-YDZ^2)^.5 : ACYDZ=(PI/2!)-ATN(CYDZ)
310 CR2=2!/CR : CCR2=CR2/(1!-CR2^2!)^.5 : ACCR=(PI/2!)-ATN(CCR2)
320 CYXZ=CCY/(CCX*CCZ) : CCYXZ=CYXZ/(1!-CYXZ^2!)^.5 : ACYXZ=(PI/2!)-ATN(CCYXZ)
330 CCA=(1!/(2!*PI))*((CR^2-4!)^.5 - CR+ PI- 2!*ACCR)
340 REM
350 CCI=1!-(1!/PI)*( ACYDZ  - (1!/(2!*CCL)) *(((CCY+2!*CCX^2)^2!-(2!*CCX)^2)^.5*
ACYXZ + CCY*ASCCX - (PI/2!)*CCZ) )
360 FCC=CCA*CCI : FCK=1!-FCC   : FCK2=1!-(2!*FCC)
370 ' ************************************************************
380 ' Read the data from the file, RWSCC#.DAT, in drive C:
390 OPEN "RWSCC##.DAT" FOR INPUT  AS #1
400 INPUT #1,INQ,D,L,KWS
410 '
420 FOR KQ=1 TO INQ
430 INPUT #1,Q(KQ)
440 FOR KS=1 TO KWS
450 INPUT #1,WS(KS),TA(KQ,KS)
460 FOR KC=1 TO 3
470 INPUT #1,TW(KQ,KS,KC),TWAV(KQ,KS,KC),TEND(KQ,KS,KC)
480 NEXT KC
```

```
490 NEXT KS
500 NEXT KQ
510 CLOSE#1
520 '
530 ' Read the data from the file, QRWSCC#.DAT, in drive C:
540 OPEN "QRWSCC##.DAT" FOR INPUT  AS #1
550 INPUT #1,INQ,D,L,KWS
560 FOR KQ=1 TO INQ
570 INPUT #1,Q(KQ)
580 FOR KS=1 TO KWS-1
590 INPUT #1,WS(KS),QR(KQ,KS,1),QR(KQ,KS,2),QR(KQ,KS,3)
600 NEXT KS
610 NEXT KQ
620 CLOSE#1
630 '
640 ' ************************************************************************
650 ' Calculate the Nusselt number:
660 G=127000000#  : ' G= gravity in m/hr2
670 A= PI*D*L  :' A=cylinder surface area in sq. meter.
680 AS=(D/2!)^2*PI  : ' AS= Cylinder cross section area in M2 .
690 FOR KQ=1 TO INQ
700 FOR KS=1 TO KWS
710 FOR KC=1 TO 3
720 '
730 IF KS<>KWS THEN GOTO 760
740 IF KC=2 THEN FK=FCK2 ELSE FK=FCK
750 QR(KQ,KS,KC)=7.900001E-02*.00000005699#*FK*A*((TW(KQ,KS,KC)+273.15)^4-(TA(KQ
,KS)+273.15)^4)
760 ' QR() = Radiation from the cylinder.
770 QCD(KQ,KS,KC)=AS*.00055#*418.68*(TEMD(KQ,KS,KC)/.007366)*2!
780 ' QCD()= Condection heat loss in Watt.
790 QCV(KQ,KS,KC)=Q(KQ)-QR(KQ,KS,KC)-QCD(KQ,KS,KC)
800 QPA=QCV(KQ,KS,KC)/A
810 TT=(TW(KQ,KS,KC)+TA(KQ,KS))/2!
820 TR(KQ,KS,KC)=TT
830 TAK=TA(KQ,KS)+273.15
840 ' Go to the subroutine to calculate the air properties at temp.= TAK .
850 GOSUB 1160
860 NUEX(KQ,KS,KC)=QPA*D/(CK*(TW(KQ,KS,KC)-TA(KQ,KS)))
870 GRM(KQ,KS,KC)= RD^2*B*G*QPA*D^4/(CK*M^2)
880 PR(KQ,KS,KC)=CP*M/CK
890 RAM(KQ,KS,KC)=GRM(KQ,KS,KC)*PR(KQ,KS,KC)
900 '
910 NEXT KC
920 NEXT KS
930 NEXT KQ
940 OPEN "RWSCC##.CAL" FOR OUTPUT AS #1
950 WRITE #1,CCS,INQ,D,L,KWS
```

```
960 FOR KQ=1 TO INQ
970 WRITE #1,Q(KQ)
980 FOR KS=1 TO KWS
990 WRITE #1,WS(KS),TR(KQ,KS)
1000 FOR KC=1 TO 3
1010 WRITE #1,TW(KQ,KS,KC),NUEX(KQ,KS,KC),RAM(KQ,KS,KC),GRM(KQ,KS,KC),PR(KQ,KS,K
C)
1020 NEXT KC
1030 NEXT KS
1040 NEXT KQ
1050 CLOSE#1
1060 PRINT : PRINT " ***** What do you want to print:"
1070 PRINT "        1- detailed output. "
1080 PRINT "        2- End the program. "
1090 PRINT "      Put your choise #"; :INPUT PCHO
1100 IF PCHO=1 GOTO GOSUB 1440 : GOTO 1060
1110 IF PCHO<>1 AND PCHO<>2 GOTO 1060
1120 '
1130 END
1140 '
1150 '
1160 REM    ************ AIRPROP.TRA ***********************************
1170 ' This subroutine calculates the air properties at different
1180 ' temperatures, TT .
1190 '
1200 '
1210 ' Define function to calculate the thermal conductivity, FNFK(XK,P1):
1220 DEF FNFCK(XK,P1) =((.000006325#*XK^.5)/(1!+(245!/XK)*10^P1))*(360!/.860421)

1230 ' P1=-12.0/XK ;XK= temp. in K ; FNFK(XR,P1)= WATT/METER.K
1240 '
1250 ' Define function to calculate the specific heat, FNFC(XK):
1260 DEF FNFC(XK) = (.249679 - .0000755179#*XK + .0000001691948*XK^2 - .00000000
0064612#*XK^3)*1.163#
1270 ' FNFC(XK)= specific heat in (W-Hr/Kg.K) for temperature = 260 to 610 k.
1280 '
1290 ' Define function to calculate the viscosity, FNFM(XK):
1300 DEF FNFM(XK)=((145.8*XK^1.5)/((XK+110.4)*10000000#))*360!
1310 ' FNFM(XK)= Viscosity in Kg/M.hr ; XK= Temp. in K
1320 '
1330 'Define function to calculate the density , FNFRD(XK):
1340 DEF FNFRD(XK)= .46458*760!/XK  :' FNFRD(XK)=Density in (Kg/m3) ; XK=Temp.K
1350 '
1360 TK=TT+273.15  : 'TT=Temperature in degree centigrade; XK= Temp. in Kelvin.
1370 P1=-12!/TK    : CK=FNFCK(TK,P1) : ' CK=thermal conductivity (W/m.K)
1380 CP=FNFC(TK)   : ' CP=specific heat (W-hr/Kg.C)
```

```
1390 M=FNFM(TK)    : ' M =viscosity (Kg/m.hr)
1400 RO=FNFRO(TK)  : ' RO=density (Kg/M3)
1410 B=1!/TAK      : ' B =thermal expansion (1/K)
1420 '
1430 RETURN
1440 '******** To print out the results in detailes : ************************
1450 LPRINT "  ------------ WALL TEMPERATURE, TW, (C)             CC/0 = ";CCS;
" --------------"
1460 LPRINT ""
1470 FOR KQ=1 TO INQ
1480 LPRINT "     ******** Q =";Q(KQ);"WATT"
1490 LPRINT "      WS/0      CYLINDER #1     CYLINDER #2     CYLINDER #3 "
1500 FOR KS=1 TO KWS
1510 IF KS=KWS THEN  GOTO 1540
1520 LPRINT USING "     ##.###     #######.####    #######.####    #######.####"
;WS(KS);TW(KQ,KS,1);TW(KQ,KS,2);TW(KQ,KS,3)
1530 GOTO 1550
1540 LPRINT USING "      NO WALL   #######.####    #######.####    #######.####"
;TW(KQ,KS,1);TW(KQ,KS,2);TW(KQ,KS,3)
1550 NEXT KS
1560 LPRINT ""
1570 NEXT KQ
1580 LPRINT CHR$(12)
1590 LPRINT "  --------- REFERENCE TEMPERATURE, TR, (C)          CC/0 = ";CCS;"
 ---------------"
1600 LPRINT ""
1610 FOR KQ=1 TO INQ
1620 LPRINT "     ******** Q =";Q(KQ);"WATT"
1630 LPRINT "      WS/0      CYLINDER #1     CYLINDER #2     CYLINDER #3 "
1640 FOR KS=1 TO KWS
1650 IF KS=KWS THEN  GOTO 1680
1660 LPRINT USING "     ##.###     #######.####    #######.####    #######.####"
;WS(KS);TR(KQ,KS,1);TR(KQ,KS,2);TR(KQ,KS,3)
1670 GOTO 1690
1680 LPRINT USING "      NO WALL   #######.####    #######.####    #######.####"
;TR(KQ,KS,1);TR(KQ,KS,2);TR(KQ,KS,3)
1690 NEXT KS
1700 LPRINT ""
1710 NEXT KQ
1720 LPRINT CHR$(12)
1730 LPRINT "  ------------ AMBIENT TEMPERATURE, TA, (C)          CC/0 = ";CCS;"
 ---------------"
1740 LPRINT ""
1750 FOR KQ=1 TO INQ
1760 LPRINT "     ******** Q =";Q(KQ);"WATT"
1770 LPRINT "      WS/0      CYLINDER #1     CYLINDER #2     CYLINDER #3 "
1780 FOR KS=1 TO KWS
1790 IF KS=KWS THEN  GOTO 1820
1800 LPRINT USING "     ##.###     #######.####    #######.####    #######.####"
;WS(KS);TA(KQ,KS);TA(KQ,KS);TA(KQ,KS)
1810 GOTO 1830
```

```
1820 LPRINT USING "     NO WALL   #######.####    #######.####    #######.####"
:TA(KQ,KS);TA(KQ,KS):TA(KQ,KS)
1830 NEXT KS
1840 LPRINT ""
1850 NEXT KQ
1860 LPRINT CHR$(12)
1870 LPRINT "  --------- RADIATION HEAT LOSS, QR, (WATT)         CC/D = ";CCS;"
 ---------------"
1880 LPRINT ""
1890 FOR KQ=1 TO INQ
1900 LPRINT "     ******** Q =";Q(KQ);"WATT"
1910 LPRINT "      WS/D      CYLINDER #1     CYLINDER #2     CYLINDER #3 "
1920 FOR KS=1 TO KWS
1930 IF KS=KWS THEN  GOTO 1960
1940 LPRINT USING "     ##.###     #######.####    #######.####    #######.####"
;WS(KS);QR(KQ,KS,1);QR(KQ,KS,2);QR(KQ,KS,3)
1950 GOTO 1970
1960 LPRINT USING "     NO WALL   #######.####    #######.####    #######.####"
;QR(KQ,KS,1);QR(KQ,KS,2);QR(KQ,KS,3)
1970 NEXT KS
1980 LPRINT ""
1990 NEXT KQ
2000 LPRINT CHR$(12)
2010 LPRINT "  --------- CONDECTION HEAT LOSS, QCD, (WATT)        CC/D = ";CCS;"
 ---------------"
2020 LPRINT ""
2030 FOR KQ=1 TO INQ
2040 LPRINT "     ******** Q =";Q(KQ);"WATT"
2050 LPRINT "      WS/D      CYLINDER #1     CYLINDER #2     CYLINDER #3 "
2060 FOR KS=1 TO KWS
2070 IF KS=KWS THEN  GOTO 2100
2080 LPRINT USING "     ##.###     #######.####    #######.####    #######.####"
;WS(KS);QCD(KQ,KS,1);QCD(KQ,KS,2);QCD(KQ,KS,3)
2090 GOTO 2110
2100 LPRINT USING "     NO WALL   #######.####    #######.####    #######.####"
;QCD(KQ,KS,1);QCD(KQ,KS,2);QCD(KQ,KS,3)
2110 NEXT KS
2120 LPRINT ""
2130 NEXT KQ
2140 LPRINT CHR$(12)
2150 LPRINT "  --------- NET CONVECTION HEAT TRANSFER, QCV, (WATT)   CC/D = ";CC
S;" ------------"
2160 LPRINT ""
2170 FOR KQ=1 TO INQ
2180 LPRINT "     ******** Q =";Q(KQ);"WATT"
2190 LPRINT "      WS/D      CYLINDER #1     CYLINDER #2     CYLINDER #3 "
2200 FOR KS=1 TO KWS
2210 IF KS=KWS THEN  GOTO 2240
2220 LPRINT USING "     ##.###     #######.####    #######.####    #######.####"
;WS(KS);QCV(KQ,KS,1);QCV(KQ,KS,2);QCV(KQ,KS,3)
2230 GOTO 2250
2240 LPRINT USING "     NO WALL   #######.####    #######.####    #######.####"
;QCV(KQ,KS,1);QCV(KQ,KS,2);QCV(KQ,KS,3)
```

```
2250 NEXT KS
2260 LPRINT ""
2270 NEXT KQ
2280 LPRINT CHR$(12)
2290 LPRINT "  --------- PRANDTL NUMBER, PR                    CC/D = ";CCS;"
 ---------------"
2300 LPRINT ""
2310 FOR KQ=1 TO INQ
2320 LPRINT "     ******** Q =";Q(KQ);"WATT"
2330 LPRINT "      WS/D      CYLINDER #1     CYLINDER #2     CYLINDER #3 "
2340 FOR KS=1 TO KWS
2350 IF KS=KWS THEN  GOTO 2380
2360 LPRINT USING "     ##.###     #######.####    #######.####    #######.####"
;WS(KS);PR(KQ,KS,1);PR(KQ,KS,2);PR(KQ,KS,3)
2370 GOTO 2390
2380 LPRINT USING "      NO WALL   #######.####    #######.####    #######.####"
;PR(KQ,KS,1);PR(KQ,KS,2);PR(KQ,KS,3)
2390 NEXT KS
2400 LPRINT ""
2410 NEXT KQ
2420 LPRINT CHR$(12)
2430 LPRINT "  --------- MODEFIED GRASHOF NUMBER, GRM           CC/D = ";CCS;"
 ---------------"
2440 LPRINT ""
2450 FOR KQ=1 TO INQ
2460 LPRINT "     ******** Q =";Q(KQ);"WATT"
2470 LPRINT "      WS/D      CYLINDER #1     CYLINDER #2     CYLINDER #3 "
2480 FOR KS=1 TO KWS
2490 IF KS=KWS THEN  GOTO 2520
2500 LPRINT USING "     ##.###     #######.####    #######.####    #######.####"
;WS(KS);GRM(KQ,KS,1);GRM(KQ,KS,2);GRM(KQ,KS,3)
2510 GOTO 2530
2520 LPRINT USING "      NO WALL   #######.####    #######.####    #######.####"
;GRM(KQ,KS,1);GRM(KQ,KS,2);GRM(KQ,KS,3)
2530 NEXT KS
2540 LPRINT ""
2550 NEXT KQ
2560 LPRINT CHR$(12)
2570 LPRINT "  --------- MODEFIED RAYLEIGH NUMBER, RAM          CC/D = ";CCS;"
 ---------------"
2580 LPRINT ""
2590 FOR KQ=1 TO INQ
2600 LPRINT "     ******** Q =";Q(KQ);"WATT"
2610 LPRINT "      WS/D      CYLINDER #1     CYLINDER #2     CYLINDER #3 "
2620 FOR KS=1 TO KWS
2630 IF KS=KWS THEN  GOTO 2660
2640 LPRINT USING "     ##.###     #######.####    #######.####    #######.####"
;WS(KS);RAM(KQ,KS,1);RAM(KQ,KS,2);RAM(KQ,KS,3)
2650 GOTO 2670
2660 LPRINT USING "      NO WALL   #######.####    #######.####    #######.####"
;RAM(KQ,KS,1);RAM(KQ,KS,2);RAM(KQ,KS,3)
2670 NEXT KS
```

```
2680 LPRINT ""
2690 NEXT KQ
2700 LPRINT CHR$(12)
2710 LPRINT "  --------- CALCULATED NUSSELT NUMBER, NUEX=QCV.D/(A.K.DT),  CC/D =
 ";CCS;" -------"
2720 LPRINT ""
2730 FOR KQ=1 TO INQ
2740 LPRINT "     ******** Q =";Q(KQ);"WATT"
2750 LPRINT "      WS/D      CYLINDER #1     CYLINDER #2     CYLINDER #3 "
2760 FOR KS=1 TO KWS
2770 IF KS=KWS THEN  GOTO 2800
2780 LPRINT USING "     ##.###     #######.####    #######.####    #######.####"
;WS(KS);NUEX(KQ,KS,1);NUEX(KQ,KS,2);NUEX(KQ,KS,3)
2790 GOTO 2810
2800 LPRINT USING "      NO WALL   #######.####    #######.####    #######.####"
;NUEX(KQ,KS,1);NUEX(KQ,KS,2);NUEX(KQ,KS,3)
2810 NEXT KS
2820 LPRINT ""
2830 NEXT KQ
2840 LPRINT CHR$(12)
2850 RETURN
```

APPENDIX D

UNCERTAINTY ANALYSIS

This section will address the uncertainty in the experimental values of the average Nusselt number for the cylinders. The uncertainty in an experimental result, $\Re$, where $\Re = f(X_1, X_2, \ldots, X_n)$, was evaluated by using the following equation, Holman [D.1]:

$$\omega_{\Re} = \left\{ \left[\frac{\delta \Re}{\delta X_1} \omega_1 \right]^2 + \left[\frac{\delta \Re}{\delta X_2} \omega_2 \right]^2 + \ldots . + \left[\frac{\delta \Re}{\delta X_n} \omega_n \right]^2 \right\}^{1/2} \qquad (D.1)$$

where $X_1, X_2, \ldots, X_n$ are the independent variables of the experimental result $\Re$, and $\omega_1, \omega_2, \ldots, \omega_n$ are their uncertainty values, respectively.

To calculate the uncertainty in the average Nusselt number, Nu, of the cylinders, the definition of Nu , as shown in equation 3.2, should be considered.

$$Nu = \frac{Q \; D}{A \; K \; (T_w - T_{inf})}$$

Where $A = \Pi \; D \; L$ and $Q = I \; V = \frac{V^2}{RI}$.

By assuming $\Delta T = T_w - T_{inf}$, The average Nusselt number becomes

$$Nu = \frac{V^2}{(R1\ L\ \Pi\ \Delta T\ K)} = f(V,R1,L,\Delta T,K) \qquad (D.2)$$

Therfore, the uncertainty in the average Nusselt number, ω_{Nu} , can be calculated from equation (D.1) as follows

$$\omega_{Nu} = \left\{ \left[\frac{\delta Nu}{\delta V}\omega_V\right]^2 + \left[\frac{\delta Nu}{\delta R1}\omega_{R1}\right]^2 + \left[\frac{\delta Nu}{\delta L}\omega_L\right]^2 + \left[\frac{\delta Nu}{\delta \Delta T}\omega_{\Delta T}\right]^2 + \left[\frac{\delta Nu}{\delta K}\omega_K\right]^2 \right\}^{1/2} \qquad (D.3)$$

The partial derivative terms in this equation were evaluated from equation (D.2) as shown below :

$$\frac{\delta Nu}{\delta V} = \frac{2\ V}{R1\ L\ \Pi\ \Delta T\ K}$$

$$\frac{\delta Nu}{\delta R1} = \frac{-\ V^2}{R1^2\ L\ \Pi\ \Delta T\ K}$$

$$\frac{\delta Nu}{\delta L} = \frac{-\ V^2}{R1\ L^2\ \Pi\ \Delta T\ K}$$

$$\frac{\delta Nu}{\delta \Delta T} = \frac{-\ V^2}{R1\ L\ \Pi\ \Delta T^2\ K}$$

$$\frac{\delta Nu}{\delta K} = \frac{-\ V^2}{R1\ L\ \Pi\ \Delta T\ K^2}$$

Substituting these terms in equation (D.3), the uncertainty in Nu is

$$\omega_{Nu} = \left[\frac{V^2}{R1\ L\ \Pi\ \Delta T\ k} \right] \left\{ \left[\frac{2}{V} \omega_V \right]^2 + \left[\frac{-1}{R1} \omega_{R1} \right]^2 + \left[\frac{-1}{L} \omega_L \right]^2 + \left[\frac{-1}{\Delta T} \omega_{\Delta T} \right]^2 + \left[\frac{-1}{k} \omega_K \right]^2 \right\}^{1/2}$$

or

$$\frac{\omega_{Nu}}{Nu} = \left\{ \left[\frac{2}{V} \omega_V \right]^2 + \left[\frac{-1}{R1} \omega_{R1} \right]^2 + \left[\frac{-1}{L} \omega_L \right]^2 + \left[\frac{-1}{\Delta T} \omega_{\Delta T} \right]^2 + \left[\frac{-1}{k} \omega_K \right]^2 \right\}^{1/2} \quad \text{(D.4)}$$

Considering the following conditions :

V	=23.0 Volts	± 0.01%
R1	= 1.0 Ohm	± 5.00%
ΔT	= 100.0 °C	± 0.5%
K	= 0.029181 W/m.k	± 0.5%
L	=0.254 m	± 0.01%

the uncertainties in these independent variables were,

ω_V = 0.023 Volt

ω_{R1} = 0.05 Ohm

$\omega_{\Delta T}$ = 0.5 °C

ω_K = 0.0001459 W/m.K

ω_L = 0.000025 m

Substituting for V, R1, L, , and K and their uncertainty values in equation (D.4), the uncertainty percentage was

$$\frac{\omega_{Nu}}{Nu} = 5.0\ \%$$

D.1 Holman, J. P., " Experimental Methods for Engineers", 4th Edition, McGraw-Hill Book Company, New York.